

# TECHNICAL REPORT

Naval Facilities Engineering Service Center, Port Hueneme, CA 93043-4328

**TR-2020-SHR**

**August 1994**

## **FEASIBILITY FOR USE OF MICROSEISMS AS AN AID TO NAVY BASE MICROZONATION**

by

**John Ferritto**

**Sponsored by:**

**19960126 068 Office of Naval Research  
Arlington, VA**

**Abstract** The U.S. Navy has a number of bases in seismically active areas. Mission requirements dictate that these bases be located at the waterfront, often on marginal soils. Since the seismic exposure is high, the Navy has had an active research program to mitigate the risk to waterfront structures. The dynamic response of saturated cohesionless soils results in a loss of strength; liquefaction and the potential for associated damage is a major problem. The 1989 Loma Prieta earthquake caused over \$125 million in damages primarily from liquefaction. In 1993 the Guam earthquake caused an additional \$120 million loss.

The Navy has developed automated procedures for conducting site seismicity studies that use an epi-

center data base and available geologic data to predict the recurrence of seismic events and compute the probability distribution of site acceleration ground motion. A set of response spectra matched to the site conditions can be assembled from a data base of records. To further define local site response, research was conducted on using microseisms as a means of predicting site amplification. Procedures were developed to measure microseisms on rock and soil sites and compute amplification spectra. These procedures are easily and rapidly accomplished and offer the potential to map the relative seismic amplification at a Navy base. This is a tool to define locations on a base where greatest amplification would be expected.

# METRIC CONVERSION FACTORS

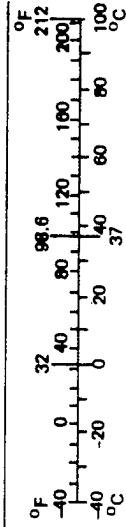
## Approximate Conversions to Metric Measures

Symbol	When You Know	Multiply by	To Find	Symbol
in ft yd mi	inches	<b>LENGTH</b> *2.5 30 0.9 1.6	centimeters	cm
	feet		centimeters	cm
	yards		meters	m
	miles		kilometers	km
in <sup>2</sup> ft <sup>2</sup> yd <sup>2</sup> mi <sup>2</sup>	square inches	<b>AREA</b> 6.5 0.09 0.8 2.6 0.4	square centimeters	cm <sup>2</sup>
	square feet		square meters	m <sup>2</sup>
	square yards		square meters	m <sup>2</sup>
	square miles		square kilometers	km <sup>2</sup>
oz lb	ounces	<b>MASS (weight)</b> 28 0.45 0.9	grams	g
	pounds		kilograms	kg
	short tons		tonnes	t
	(2,000 lb)			
tsp Tbsp fl oz c pt qt gal ft <sup>3</sup> yd <sup>3</sup>	teaspoons	<b>VOLUME</b> 5 15 30 0.24 0.47 0.95 3.8 0.03 0.76	milliliters	ml
	tablespoons		milliliters	ml
	fluid ounces		milliliters	ml
	cups		liters	l
	pints		liters	l
	quarts		liters	l
	gallons		liters	l
	cubic feet		cubic meters	m <sup>3</sup>
°F	cubic yards	<b>TEMPERATURE (exact)</b> 5/9 (after subtracting 32)	cubic meters	m <sup>3</sup>
	Fahrenheit temperature		Celsius temperature	°C

\* 1 in = 2.54 (exactly). For other exact conversions and more detailed tables, see NBS Misc. Publ. 286, Units of Weights and Measures, Price \$2.25, SD Catalog No. C13.10:286.

## Approximate Conversions from Metric Measures

Symbol	When You Know	Multiply by	To Find	Symbol
mm cm m km	millimeters	<b>LENGTH</b> 0.04 0.4 3.3 1.1 0.6	inches	in
	centimeters		inches	in
	meters		feet	ft
	kilometers		yards	yd
cm <sup>2</sup> m <sup>2</sup> km <sup>2</sup> ha	square centimeters	<b>AREA</b> 0.16 1.2 0.4 2.5	miles	mi
	square meters		square inches	in <sup>2</sup>
	square kilometers		square yards	yd <sup>2</sup>
	hectares (10,000 m <sup>2</sup> )		square miles	mi <sup>2</sup>
g kg t	grams	<b>MASS (weight)</b> 0.035 2.2 1.1	ounces	oz
	kilograms		pounds	lb
	tonnes (1,000 kg)		short tons	
ml l l l m <sup>3</sup> m <sup>3</sup>	milliliters	<b>VOLUME</b> 0.03 2.1 1.06 0.26 35 1.3	fluid ounces	fl oz
	liters		pints	pt
	liters		quarts	qt
	liters		gallons	gal
	cubic meters		cubic feet	ft <sup>3</sup>
	cubic meters		cubic yards	yd <sup>3</sup>
°C	Celsius temperature	<b>TEMPERATURE (exact)</b> 9/5 (then add 32)	Fahrenheit temperature	°F



## **PREFACE**

On 1 October 1993, the Naval Civil Engineering Laboratory (NCEL) and the Naval Energy and Environmental Support Activity (NEESA) were consolidated with four other Naval Facilities Engineering Command (NAVFAC) components into the Naval Facilities Engineering Service Center (NFESC).

REPORT DOCUMENTATION PAGE			Form Approved OMB No. 0704-018	
Public reporting burden for this collection of information is estimated to average 1 hour per response, including the time for reviewing instructions, searching existing data sources, gathering and maintaining the data needed, and completing and reviewing the collection of information. Send comments regarding this burden estimate or any other aspect of this collection information, including suggestions for reducing this burden, to Washington Headquarters Services, Directorate for Information and Reports, 1215 Jefferson Davis Highway, Suite 1204, Arlington, VA 22202-4302, and to the Office of Management and Budget, Paperwork Reduction Project (0704-0188), Washington, DC 20503.				
1. AGENCY USE ONLY (Leave blank)	2. REPORT DATE August 1994	3. REPORT TYPE AND DATES COVERED Final; October 1993 - September 1994		
4. TITLE AND SUBTITLE <b>FEASIBILITY FOR USE OF MICROSEISMS AS AN AID TO NAVY BASE MICROZONATION</b>		5. FUNDING NUMBERS PR - Rm33F60, Task A16 WU - DN387338		
6. AUTHOR(S) John M. Ferritto				
7. PERFORMING ORGANIZATION NAME(S) AND ADDRESS(ES) Naval Facilities Engineering Service Center 560 Center Drive Port Hueneme, CA 93043-4328		8. PERFORMING ORGANIZATION REPORT NUMBER <b>TR-2020</b>		
9. SPONSORING/MONITORING AGENCY NAME(S) AND ADDRESSES Office of Naval Research Arlington, VA 22217-5000		10. SPONSORING/MONITORING AGENCY REPORT NUMBER		
11. SUPPLEMENTARY NOTES				
12a. DISTRIBUTION/AVAILABILITY STATEMENT Approved for public release; distribution is unlimited.		12b. DISTRIBUTION CODE		
13. ABSTRACT (Maximum 200 words)  The U.S. Navy has a number of bases in seismically active areas. Mission requirements dictate that these bases be located at the waterfront, often on marginal soils. Since the seismic exposure is high, the Navy has had an active research program to mitigate the risk to waterfront structures. The dynamic response of saturated cohesionless soils results in a loss of strength; liquefaction and the potential for associated damage is a major problem. The 1989 Loma Prieta earthquake caused over \$125 million in damages primarily from liquefaction. In 1993 the Guam earthquake caused an additional \$120 million loss.  The Navy has developed automated procedures for conducting site seismicity studies which utilize an epicenter data base and available geologic data to predict the recurrence of seismic events and compute the probability distribution of site acceleration ground motion. A set of response spectra matched to the site conditions can be assembled from a data base of records. To further define local site response, research was conducted on using microseisms as a means of predicting site amplification. Procedures were developed to measure microseisms on rock and soil sites and compute amplification spectra. These procedures are easily and rapidly accomplished and offer the potential to map the relative seismic amplification at a Navy base. This is a tool to define locations on a base where greatest amplification would be expected.				
14. SUBJECT TERMS Earthquake, microseisms, amplification		DTIC QUALITY INSPECTED 2		15. NUMBER OF PAGES 216
				16. PRICE CODE
17. SECURITY CLASSIFICATION OF REPORT Unclassified	18. SECURITY CLASSIFICATION OF THIS PAGE Unclassified	19. SECURITY CLASSIFICATION OF ABSTRACT Unclassified	20. LIMITATION OF ABSTRACT UL	

## Executive Summary

The Navy has numerous bases situated on marginal soft soils and located in seismically active areas. Ground motion amplification at these sites is high. Recent Navy experience during the 1989 Loma Prieta earthquake and the 1993 Guam earthquake demonstrate that Navy sites sustain high levels of ground shaking which produces damage. For this reason the study of waterfront amplification of motion is of Navy significance.

This report demonstrates the feasibility of using microseism measurements as tool to gain additional insight into the response of waterfront sites. The report shows that the technique can be used as an extension of analytical techniques to augment geophysical site properties to improve the accuracy of estimating local site response. A typical Navy application would involve soft marginal soils at the waterfront. These site exhibit significant spatial variation. Existing boring logs are may not be available over wide areas and may lack data at depth. It is often difficult to define bedrock. Often shear wave velocity is not available and must be estimated from standard penetration blowcount data which has its level of associated error. Measuring shear wave velocity at a site can costly and is limited to projects of large size to warrant such a detailed investigation. Strain effects on damping and shear modulus require laboratory testing and are usually not performed; several standard type curves for sand and clay are routinely used as substitutes. With these limitations in gathering data for analysis, it can be seen that there is a strong need for an inexpensive field test to quantify site behavior. Microseisms seems to offer that potential.

- The report has presented microseism measurements which show for soft soil sites high levels of amplification at the low levels of excitation. Data was presented showing such a response is expected and that a relationship exists such that spectral ratio amplification is inversely related to the level of excitation.
- Traditional wave propagation analysis techniques for local site response were seen to be applicable to microseism measurements.
- Because spectral ratio obtained from microseism measurements are higher than those of strong motion shaking, normalized results can be used to provide information of the spatial variation relative to a site of known response.
- Microseism measurements at a soil site can be used to estimate fundamental period and damping of the site and save as a means for improving the reliability of material property data used in the wave propagation computation. A systems analysis procedure was shown to lend insight to the process.

It is concluded that microseism measurements can be used on a relative normalized basis to extend the information from a known local response to areas where additional data is lacking. A systems analysis procedure applied to the microseism data can be used to extend the knowledge of site material properties such as shear velocity and damping. Long term measurements describe overall site stability and are essential. Microseism measurements can be conducted during windows of stability A generalized procedure should consist of the following steps:

1. Careful review of site geology
2. Investigation of rock reference site and its variability
3. Selection of rock reference site
4. Selection of soil reference site having extensive borehole data
5. Long term measurements between rock and soil reference site to establish stability
6. Selection of a array plan to cover region of interest
7. Conducting measurements at rock reference site, soil reference site and at each array site.
8. Reduction of data using appropriate spectral processing.
9. Repeat steps 7 and 8 based on local site variability to obtain best estimate.

It should be noted that it is recommended that closely spaced measurements be made both at the rock and soil reference site throughout the array measurements to monitor overall stability.

# CONTENTS

	Page
CHAPTER 1. INTRODUCTION .....	1
Background .....	1
Construction Design Ground Motion Determination .....	2
Site Ground Motion Amplification .....	3
Liquefaction .....	4
Microzonation .....	4
References .....	5
CHAPTER 2. EARTHQUAKE MECHANISM .....	9
Earthquake Ground Motion .....	9
Elastic Layered Deposit Over Bedrock .....	10
The Earthquake System Model .....	11
System Identification .....	13
Application of Model to Study Site Amplification .....	15
Acceptability of General Model .....	15
Nakamura Method .....	17
References .....	19
CHAPTER 3. MICROSEISMS .....	25
Composition and Source .....	25
Coastal Sources .....	26
Use of Microseisms in Earthquake Engineering .....	28
Noise and Microseism Measurements .....	29
References .....	30
CHAPTER 4. AMPLIFICATION OF GROUND MOTION .....	35
Introduction .....	35
Rock Site Geology .....	35
Topography .....	36
Geology Effects on Spectra .....	37
Level of Excitation .....	38
Site Response Effects .....	41
References .....	43

	Page
CHAPTER 5. PORT HUENEME PROGRAM OF INVESTIGATION . . . . .	67
Introduction . . . . .	67
Geology of the Oxnard Plain . . . . .	67
Soil Conditions . . . . .	68
Microseism Measurements . . . . .	68
Rock - Soil Transfer Function . . . . .	69
Topography Effects . . . . .	70
Array Measurements NFESC Site . . . . .	70
Site Analysis . . . . .	70
Array Measurements NCBC Site . . . . .	72
Nakamura Method . . . . .	72
References . . . . .	73
CHAPTER 6. TREASURE ISLAND CASE STUDY . . . . .	147
Introduction . . . . .	147
Geology of Treasure Island and Yerba Buena Island . . . . .	147
Yerba Buena Measurements . . . . .	148
Treasure Island Measurements . . . . .	148
Treasure Island Array Measurements . . . . .	148
Treasure Island Response to Loma Prieta Earthquake . . . . .	150
Nakamura Method . . . . .	151
References . . . . .	152
CHAPTER 7. INVESTIGATION ON NONLINEAR AMPLIFICATION . . . . .	191
Introduction . . . . .	191
Earthquake Data Treasure Island . . . . .	191
Earthquake Data Gilroy . . . . .	191
Earthquake Data Coalinga . . . . .	191
Discussion . . . . .	192
References . . . . .	193
CHAPTER 8. SUMMARY . . . . .	199
Feasibility of Microseism Measurements . . . . .	199
Development of Procedure . . . . .	199
Need for Additional Study . . . . .	200
Acknowledgment . . . . .	201
APPENDIX	
A - Instrumentation and Procedures for Microseism Measurements . . . . .	A-1



## CHAPTER 1 INTRODUCTION

### Background

This report will discuss the Navy's research program to reduce the vulnerability to damaging earthquakes by developing better procedures to compute ground motion amplification. The Navy has numerous bases located in seismically active regions throughout the world. Safe effective design of waterfront structures requires calculation of the expected site specific earthquake ground motion and effective design of complex waterfront structures. The Navy's problem is further complicated by the presence of soft saturated marginal soils which can significantly amplify the levels of seismic shaking as evidenced in the 1989 Loma Prieta earthquake and again in the 1993 Guam earthquake. The Navy began its seismic program in response to the 1977 Earthquake Hazards Reduction Act. Executive Order 12699 reinforces that mandate for earthquake safety.

The prediction of seismic ground motion amplification at sites with marginal soil properties is of great importance to the Navy since those sites are so prevalent at the waterfront. Most of the naval facilities were constructed on such type soils before their earthquake damage potential was recognized. Current procedure for estimating ground motion at a Navy site involve performing a site seismicity study in which historical and geological data are used to estimate seismic ground motion levels for use in design of structures. Site specific spectra are then generated to account for local soil conditions using historical earthquake records. The data base of response records do not account for the response of soft marginal sites. An option for a more detailed analysis of local site response of marginal soils involves wave propagation analysis. This approach requires an insitu shear wave velocity profile to determine the site's shear properties. A one dimensional wave propagation analysis is performed to determine ground motion amplification. This approach is complex, requires field data measurement and may result in significant underestimation of ground motion amplification for sites with marginal soils. This is not surprising since the approach is characterized by several problems.

The geological process of creating the marginal deposits such as bay muds found in harbors and bays involves ocean currents or river erosion. This often results in dipping layers. Such basin structures violate the assumption of parallel layers assumed in one-dimensional analysis. The problem must be addressed from a two-dimensional or three-dimensional resonance point of view. Two- and three-dimensional resonance characteristics may be significantly different from the one dimensional ones (Bard and Bouchon, 1984; Tiao and Dravinski, 1993). In addition, the wave analysis procedure currently in use requires material properties from field measurement or laboratory soil tests which are difficult to perform accurately. Field tests can be performed only at a limited number of boreholes since the drilling and testing is expensive. This can significantly limit the understanding of the spatial variation of the soil deposits. There is a need for a new approach for facilitating estimating ground motion amplification at such sites. One of such techniques involves measurements of long period microtremors.

Even in the absence of earthquakes the ground is continuously vibrating. The amplitude of such vibrations may be less than several microns with periods ranging from tenths of seconds to several seconds (Kanai, 1983). The motion of this type is called microtremors. It is common to distinguish two types of microtremors: (i) Long period microtremors or microseisms (with periods  $T > 1$  sec) and (ii) short period microtremors ( $T < 1$  sec). Usually, microseisms are defined as oscillations of the ground with periods 2 - 20 sec not caused by earthquakes or local causes such as traffic or gusts of wind (Longuet-Higgins, 1950; Hasselman, 1963). In this paper long period microtremors are considered with periods ranging between 0.5 - 10 sec.

### **Construction Design Ground Motion Determination**

The Naval Facilities Engineering Command's seismic design manual, NAVFAC P355.1, requires a probabilistic assessment of ground motion for design of essential structures. Ferritto (1993a) presents the basis for the Navy's Seismic Hazard Analysis procedure which was developed and is intended to be used with the Seismic Hazard Analysis computer program and user's manual, Ferritto (1993b). The procedure utilizes the historical epicenter data base and available geologic data, together with source models, recurrence models and attenuation relationships to compute the probability distribution of site acceleration and an appropriate site specific spectra.

A number of theoretical mathematical models have been postulated to express earthquake recurrence. Geologic stress builds up along a fault and earthquakes occur when the accumulated stress reaches a threshold value at some location on the fault. The rupture which occurs reduces the stress buildup. The size of the earthquake is measured by the change in stress level with larger events producing larger stress changes. After an earthquake, the amount of time required for stress to build up to the threshold determines the time to the next earthquake. This time is related to the size of the recent earthquake and the rate of stress accumulation. A critical evaluation of seismic recurrence models includes evaluation of the accuracy of forecasts, evaluation of general applicability of the model to a variety of sites worldwide and availability of data. While it is beyond the Navy's mission to conduct fundamental research on earthquake mechanisms and developing earthquake prediction theories, it is crucial that the Navy select and use those models developed by seismologists which are appropriate for Navy waterfront design problems and are consistent with levels of fault data available and economically obtainable during the construction project design.

Consideration of the temporal and spatial dependence between occurrences of earthquakes is an important aspect of seismic hazard analysis. The choice of recurrence model and the dependence between occurrences of earthquakes directly affects the design accelerations at a site and impacts significantly on cost-effective structural design. Recent research indicates a correlation between an earthquake recurrence interval and the size of the preceding event. A characteristic model has been implemented into the current procedure.

## Site Ground Motion Amplification

To better understand the problem of ground motion amplification, it is important to look at an example of recent Navy experience. The Loma Prieta earthquake occurred when a segment of the San Andreas fault northeast of Santa Cruz, California ruptured over a length of 28 miles producing a Richter local magnitude,  $M_L$ , of 7.0 and an average surface wave magnitude,  $M_S$ , of 7.1, Seed et. al. 1990. The epicenter was 10 miles (16 km) northeast of Santa Cruz and 20 miles (32 km) south of San Jose. The initial rupture length was estimated to be 24 miles (38 km). The main rupture began at a depth of 11 miles (17.5 km) below the earth's surface and near the center of what would be the rupture plane. Over the next 7 to 10 seconds the rupture spread approximately 12 miles to the north and 12 miles (19 km) to the south. The unusual middle location of the hypocenter within the rupture location contributed to the unusually short duration of the event. Approximately 8 to 10 seconds of strong shaking was observed which is considerably less than would be expected from an event of this size. The rupture propagated towards the earth's surface but during the main event appears to have stopped at a depth of 3 to 4 miles (5 to 6 km).

Strong ground motion was recorded on the Naval Station, Treasure Island; the peak horizontal ground acceleration components from the main shock were 0.16g and 0.10g, Hryciw et. al. (1991). A significant factor in the Loma Prieta earthquake was the amplification of ground motion in areas underlain by thick deposits of Bay sediments. Treasure Island falls within this observation especially in comparison with recordings on nearby Yerba Buena Island where the peak horizontal accelerations recorded on a rock site were about three times less than those on Treasure Island. Yerba Buena Island, a large rocky outcrop, had horizontal components of motion from this event equal to 0.068g and 0.031g, both significantly less than those on Treasure Island.

Of considerable interest is the strain dependent properties for the Bay Mud. Rollins uses data by Lodde (1992) to define the strain dependent shear modulus ratio. Figure 1.1 shows a plot of the Bay Mud curve compared with the more normal values based on data provided by Vucetic 1991. It can be seen that the Bay Mud has a significantly stiffer modulus with strain. Figure 1.1 also contains data from Mexico City, Seed et al. 1987 which is very similar to the Bay Mud behavior. The Mexico City clays were noted to be rather stiff at low strain. Note that distant earthquakes are relatively low strain events. The stiffer soils such as Bay Muds and Mexico City clays respond more elastically and contribute significantly to the observed increases in response.

A one-dimensional soil column analysis using SHAKE, Schnabel 1972, was performed on the site using the actual properties for the Bay Mud as well as properties more typical of a softer clay, Ferritto (1992). Strains in the analysis using the Bay Mud properties are in the range of 0.03 to 0.08 percent in the Bay Mud layers; this results in an effective shear modulus of about 60 percent of maximum with damping in the range of 0.06 to 0.12 of critical. However when typical clay data is used the shear modulus drops

to about 10 percent of maximum and damping increases to 0.08 to 0.15 of critical. This explains the difference in response between the stiffer Bay Mud soil and a typical clay.

The San Francisco site and the Mexico City site both have clays that are substantially stiffer than would be expected. Sharma (1991) shows that the Plasticity Index for Bay Muds is in the range of 20 to 40 between 38 and 75 feet (11.5 and 23 m). The Plasticity Index for Mexico City clays was 30. Vucetic (1991) shows data documenting that the shear modulus is stiffer with shear strain as the Plasticity Index increases. This data indicates that the stiffness of clay under cyclic loading should be increased to account for the Plasticity Ratio. The Plasticity Index is based on the amount of water required to transform a remolded soil from semisolid to a liquid state. It is a function only of the size shape and mineralogy of the soil particles and the pore water. Engineers should be alert to the presence of high plasticity clay deposits as a potential source of ground motion amplification. The high amplification results in significant damage especially when it is coupled with liquefaction. Amplification of motion at the waterfront where marginal soils are prevalent is a major Navy problem.

### **Liquefaction**

Again to better understand the amplification problem, we must also look at a frequently occurring associated problem of liquefaction of loose saturated cohesionless deposits which the Navy faces at most of its waterfront sites. Observation of the Naval Station, Treasure Island record from the 1989 Loma Prieta earthquake shows that at about 15 seconds after the start of recording, the ground motion changed indicating the occurrence of subsurface liquefaction. Liquefaction occurred after about 4 or 5 "cycles" of shaking after about 5 seconds of strong motion. Sand boils were observed at numerous locations and bayward lateral spreading occurred with associated settlements. Ground cracking was visible with individual cracks as wide as 6 inches (15 cm). Overall lateral spreading of 1 foot (30 cm) was estimated. Ground survey measurements indicate that settlements of 2 to 6 inches (3 to 15 cm) occurred variably across the island and that some areas had as much as 10 to 12 inches (25 to 30 cm) of settlement. The liquefaction related deformations resulted in damage to several structures and numerous broken underground utility lines, Egan et al. 1991.

The above paragraphs were intended to explain the significance of amplification and liquefaction to Navy facilities. To put this problem in perspective the Navy suffered \$245 million in damages almost entirely from amplification and liquefaction during the 1989 Loma Prieta and 1993 Guam earthquakes.

### **Microzonation**

Having identified the Navy problems from marginal soil, there is a strong need for a solution such as microzonation, the identification mapping of local site response which considers the specific local soil profile at a Navy base. The use of microseisms will be shown as a tool capable of adding considerable insight on the variation of site conditions,

amplification of motion and fundamental period of site response. Procedures will be presented which will allow the user to measure site response. These techniques require a set of instrumentation composed of seismometers and amplifier recorders which the Naval Facilities Engineering Service Center owns and operates. The basic measurements can be accomplished relatively easily.

Current procedures for computing seismic ground motion amplification require definition of the site soil profile at each location of interest and determination of the material properties for each layer in the site profile as discussed above. This involves an expensive program of borings which are required to define the site. It is very costly to perform these tests at numerous sites around a Navy base. Use of microseisms can serve as a means of extending the boring log data providing relative variations and reducing the need for sampling..

## References

- Bard, P-Y., and Bouchon, M., 1985. The two-dimensional resonance of sediment-filled valleys, Bulletin Seismological Society of America,, No 75, 519-541.
- Egan, John A. and Zih-Liang Wang, (1991) " Liquefaction Related Ground Deformation And Effects On Facilities At Treasure Island, San Francisco, During the 17 October 1989 Loma Prieta Earthquake", Proceedings from the Third Japan-US. Workshop on Earthquake Resistant Design of Lifeline facilities and Countermeasures for Soil liquefaction, National Center for Earthquake Engineering Research, State University of New York at Buffalo Feb. 1991
- Ferritto, J. M. (1993a) N-1855 "Development of Procedures For Computing Site Seismicity", Naval Civil Engineering Laboratory, Port Hueneme, CA Feb 1993
- Ferritto, J. M. (1993b) UG0027 "User's Guide Seismic Hazard Analysis", Naval Civil Engineering Laboratory, Port Hueneme, CA Feb 1993
- Ferritto, J. M. (1992) N-1844 "Ground Motion Amplification and Seismic Liquefaction: A Study of treasure Island and the Loma Prieta Earthquake", Naval Civil Engineering Laboratory, Port Hueneme, CA June 1992
- Hasselman, K., 1963. A statistical analysis of the generation of microseisms, Review Geophysics, 1, No. 2, 177-210.
- Hryciw, Roman D. et al. (1991) "Soil Amplification at treasure Island During The Loma Prieta Earthquake", Proceedings Second International Conference on Recent Advances in Geotechnical Earthquake Engineering and Soil Dynamics, March 11-15 1991, St. Louis, Missouri

Kanai, K., 1983. "Engineering Seismology", Univsity Tokyo Press, Tokyo.

Lodde, P.F. (1992) Dynamic Response of San Francisco Bay Mud" MS Thesis, University of Texas at Austin 1982.

Longuet-Higgins, M.S., 1950. "A theory of the origin of microseisms," Philosophical Transactions Royal Society London A 243, 1-35.

Naval Facilities Engineering Command, NAVFAC P-355 "Seismic Design for Buildings.", Oct. 1992.

Rollins, Kyle et al. "Soil Amplification at Treasure Island During The Loma Prieta Earthquake" in publication

Schnabel Per B., et. al. (1972) "SHAKE, A Computer Program For Earthquake Response Analysis Of Horizontally Layered Sites", EERC 72-12 University of California, Berkeley, Ca Dec. 1972.

Seed H. B. et al. (1987) Relationships Between Soil Conditions and earthquake Ground Motions in Mexico City In The Earthquake of Sept. 19, 1985" EERC 87-15 University of California, Berkeley Ca Oct. 1987

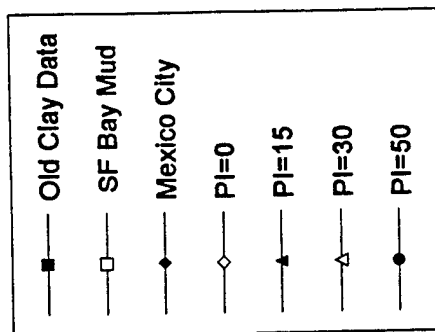
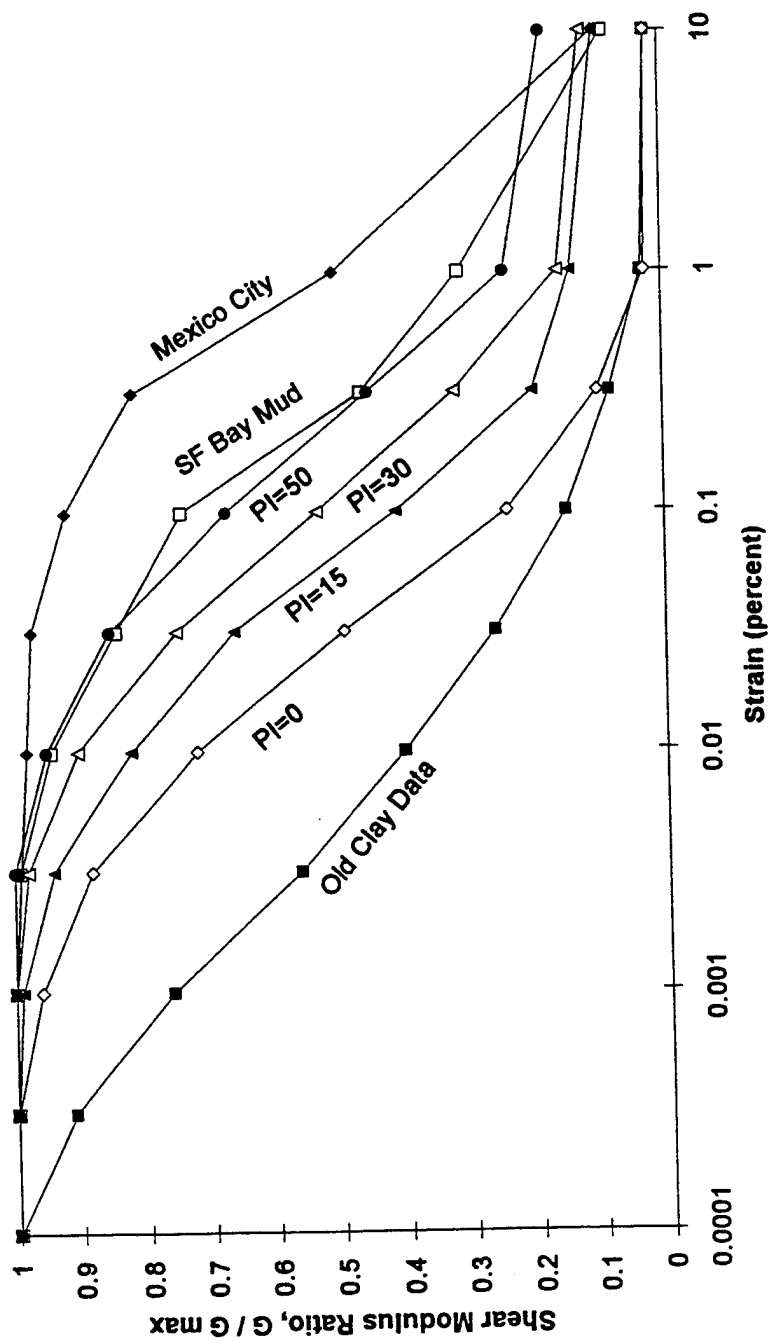
Seed R. B. et. al. (1990) EERC 90-05 "Preliminary Report On The Principal Geotechnical Aspects Of The October 17, 1989 Loma Prieta Earthquake" College of Engineering University of California, Berkeley, California April 1990

Sharma H. D. (1991) "Performance of a hazardous Waste and Sanitary Landfill subjected to Loma Prieta Earthquake", Proceedings Second International Conference on Recent Advances in Geotechnical Earthquake Engineering and Soil Dynamics, March 1991, St. Louis Missouri

Tiao, Z., and Dravinski, M., 1993. "Resonance of sediment valleys and its prediction through an eigenvalue method", Geophysical Journal International, submitted. for publication.

Vucetic M. et al. (1991) " Effect of Soil Plasticity on Cyclic Response" Journal of Geotechnical Engineering Vol. 117 No. 1. January 1991.

Figure 1.1 Shear modulus ratio.



## CHAPTER 2 EARTHQUAKE MECHANISM

### Earthquake Ground Motion

An earthquake occurs when the buildup of stress along a fault exceeds the rupture strength of the rock. This rupture process begins from the weakest location and then propagates for some distance. During the rupture process earthquake induced ground shaking occurs radiating outward. The extent of the rupture and the amount of energy released are proportional to the event magnitude. Earthquake ground shaking is composed of body waves which radiate in three directions and surface waves which radiate in only two directions. Body waves are composed of primary waves, dilational longitudinal vibration compression waves, and secondary waves, distortional transverse vibration shear waves. Surface waves are composed Love waves, horizontal transverse shear type vibration, and Rayleigh waves, surface vertical longitudinal vibration. There are different wave propagation velocities for each type of wave and each attenuates differently with distance. Since attenuation through the near surface alluvial material is greatest, propagation is generally controlled by bedrock transmission. Waves traveling through bedrock tend to refract toward the vertical because shallower layers have lower propagation velocities. Generally vertically propagating horizontal shear waves are the dominant energy source affecting most structures at sites of interest.

Compressional wave velocity is computed from

$$C_p = \sqrt{\frac{(\lambda + 2 G)}{\rho}}$$

where

$\lambda$	Lame's constant
$G$	Shear modulus
$\rho$	Mass density

$$\lambda = \frac{\nu E}{(1 + \nu)(1 - 2\nu)}$$

where

$\nu$	Poisson's ratio
$E$	Young's modulus

$$G = \frac{E}{2(1 + \nu)}$$



Shear wave velocity can be estimated from data on compressional wave velocity:

$$C = C_p ((1 - 2\nu) / (2(1 - \nu)))^{1/2}$$

or

$$C = (G / \rho)^{1/2}$$

The fundamental period of a soil deposit may be estimated by

$$T = 4H / (C(2n - 1))$$

where

$\omega$	natural frequency
$H$	Depth of deposit
$n$	mode of response 1, 2, ....

From the above it is interesting to note that a site may have constant period if the ratio of depth of the deposit,  $H$ , to shear wave velocity,  $C$ , remains constant. Sites with constant shear wave velocity will have spatial variation of period affected only by depth of the deposit.

### Elastic Layered Deposit Over Bedrock

For the case of a soft soil layer over bedrock, the amplification factor of surface displacement from vertically propagating horizontal shear (SH) waves is given by

$$|U(\omega)| = 2 [ \cos^2(\omega H / C_1) + (\rho_1 C_1 / \rho_2 C_2)^2 \sin^2(\omega H / C_1) ]^{-1/2}$$

where the incident wave is harmonic with unit amplitude and frequency  $\omega$ , and

$C_1$	Shear wave velocity of soil layer
$\rho_1$	Mass density of soil
$C_2$	Shear wave velocity of bedrock
$\rho_2$	Mass density of bedrock

The above equation predicts an amplification of 2 for the familiar free surface effect of incident waves with wave length much longer than the thickness. The amplification response reaches peaks at incident wave lengths of  $4H$ ,  $4/3H$ ,  $4/5H$ , ... at which points the factor is equal to twice the impedance ratio between the bedrock and the

layer,  $2(\rho_1 C_1 / \rho_2 C_2)$ . The above equation can be extended for multiple layers over bedrock. Note that since the system is elastic the amplification ratio depends only on frequency content for a given impedance ratio and is not affected by the amplitude of the input motion.

Peak amplification of SH waves decreases with increasing wave incidence angle; however the process becomes more complicated by the coupling of P and SV which may produce sharp peaked amplification much beyond the impedance ratio, Aki (1988). For sites of comparable thickness and geology, amplification of ground motion increases with decreasing shear wave velocity.

Blakeslee et. al. (1991) installed seismometers at the surface and at depth for two sites in Parkfield, California. They recorded data for micro earthquakes and computed amplification using the above formulation. The computed and measured results showed significant amplification and satisfactory agreement.

### **The Earthquake System Model**

In the 1960's and 1970's seismologists began to analyze the earthquake process in terms of an assemblage of components. This procedure is still in use today as a tool to better understand the elements which affect the response of a structure at a site. The system model consists of:

- Source model of fault mechanism
- Path model of transmission
- Local site model from bedrock to surface
- Structure model

This process allows for the development of component models which can not only be studied in the time domain but also in the frequency domain. Using linear system theory it is possible to establish a series of transfer functions to represent each of the components.

In 1961 Kanai (1961) proposed the idea upon which much recent work is based. In 1972 Lastrico (1972) developed the following model:

$$G = E W X = I X$$

and as

$$|G| = |E| |W| |X| = |I| |X|$$

where all factors are complex functions of frequency and

G	is the surface motion at the site of interest
E	is the equivalent source motion
W	is the crustal bedrock path transfer function
X	is the subsurface site transfer function
I	is the incident motion at bedrock at the site

and the brackets symbolize the Fourier transform. Use of the above model allows the investigator to analyze a series of sites where accelerograms were recorded from a single earthquake event. In this case two sites equally distant from the source can be assumed to have the same source and path functions and local site conditions studied. Additionally a single site can be studied for several different earthquakes investigating source and path effects.

The assumptions inherent in this model are that the surface motion is primarily vertically traveling plane shear waves and the subsurface model is composed of elastic horizontal layers overlying bedrock

Fourier analysis will form a main analytical tool. The use of the Fourier spectra provides a measure of the system response. The motion at a given point as a function of time,  $g(t)$ , may be written as an informationally equivalent Fourier transform,  $G(\omega)$ , a function of the frequency

$$G(\omega) = \int_{-\infty}^{\infty} g(t) e^{-i\omega t} dt$$

$$G(\omega) = \int_{-\infty}^{\infty} g(t) \cos \omega t dt - i \int_{-\infty}^{\infty} g(t) \sin \omega t dt$$

$$G(\omega) = P(\omega) - i Q(\omega)$$

The Fourier transform can be written in an alternative form which will be used here.

$$G(\omega) = |G(\omega)| e^{i\phi(\omega)}$$

in which

$$|G(\omega)| = [(P(\omega))^2 + (Q(\omega))^2]^{1/2}$$

$$\phi(\omega) = \tan^{-1} [-Q(\omega) / P(\omega)]$$

where the first expression represents the amplitude of the transform and the second expression represents the phase angle. The site amplification can be represented as

$$X = \frac{G(\omega)}{I(\omega)}$$

An alternative measure of site amplification can be represented as the ratio of the cross-spectral density between the reference site and the site of interest to the spectral density of the reference site.

$$H(\omega) = \frac{S_{GI}(\omega)}{S_{II}(\omega)}$$

where

$S_{GI}(\omega)$  cross spectral density of surface to bedrock

$S_{II}(\omega)$  spectral density of bedrock

The coherence function is given by the following

$$\gamma_{GI}(\omega) = \frac{|S_{GI}(\omega)|^2}{S_{II}(\omega) S_{GG}(\omega)}$$

The determination of spectral ratios based on the cross spectral density is fundamentally more exact than the simple division of the soil site spectra divided by the reference site spectra. However, Field et al. (1992) reports some difficulty in using the cross spectrum approach from noise. They also note that the cross-spectrum approach gives an estimation of amplification of about twice the direct ratio method for several sites studied, perhaps from the noise problem. Most papers tend to report results in terms of the direct ratio of the spectra.

### System Identification

The system identification process is a powerful tool which can enhance the usage of microseism measurements to confirm fundamental site properties. To illustrate the

concept we will focus on representation of a simple system composed of a single degree of freedom oscillator. The Fourier transform can be used to assist in quantification of system properties. The general equation of motion of the system can be expressed as:

$$m \ddot{y}(t) + c \dot{y}(t) + k y(t) = x(t)$$

where

$m, c, k$  scalar coefficients for mass, damping and stiffness  
 $x(t)$  excitation  
 $y(t)$  response

The transfer function can be shown to be:

$$|H(f)| = \left( \frac{1 + (2\zeta f / f_n)^2}{(1 - (f / f_n)^2)^2 + (2\zeta f / f_n)^2} \right)^{1/2}$$

where

$\xi$  percent critical damping

This for low levels of damping can be approximated by the following at peak response frequency  $f = f_n$ :

$$|H(f)| = 1 / (2\zeta)$$

The system parameters can be estimated from the best fit of the response function as illustrated in Figure 2.1. Figure 2.1 illustrates how the system mass and stiffness control the fundamental period of response and how the peak amplitude of response at the fundamental period is controlled by the system damping. In the specifics of the site response problem, the site is usually analyzed in an engineering analysis using wave propagation techniques. This technique requires a site profile to be modelled by a series of horizontal layers, each having density, shear modulus or shear wave velocity, and damping identified. The simplest boring log data usually reports density data, standard penetration blow counts and soil classification. Often the blow count data is used to estimate shear wave velocity; however the relationship between blowcount and shear wave velocity is imprecise and has a high level of uncertainty. The density of data is usually more easily defined. The relation of modulus and damping with strain is obtained from laboratory tests and is usually approximated by graphs reported in the literature. Depending on the depth of the boring log, the depth to firm ground or bedrock may or may not be well established. So while under ideal circumstances, we can calculate the site response using wave propagation techniques, we are often limited by lack of data. The systems identification process allows us to use the measured microseism data such as fundamental period of response and amplification to quantify the possible range of parameters. For example, if the computed period differs from the measured consideration

can be given to adjusting either the depth to bedrock or the initial modulus of the soil which affects the stiffness. If for example the depth to bedrock were well established by the boring log, emphasis could be placed on the shear modulus, since density is usually defined. The amount of damping can be adjusted to converge on the appropriate level of amplification. In this way the measured response to microseisms can be used to confirm low level site response and associated material properties. This allows us to converge on an acceptable site model especially when site response strong motion data are lacking. The process helps reduce the levels of uncertainty and establishes the bounds of material properties and site response.

Figure 2.2 illustrates how the coherence function can be used as a measure of statistical confidence in a spectral transfer function estimate. The imaginary part of the transfer function can give an indication of the system damping. Figure 2.3 illustrates two cases (after Palo 1994). The first case indicates a frequency independent damping while the second illustrates frequency dependent damping. The case of frequency dependent damping results in an integro-differential equation in the form of:

$$m \ddot{y}(t) + \int c(\tau) \dot{y}(t - \tau) d\tau + k y(t) = x(t)$$

### Application of Model to Study Site Amplification

A specific application of the general system model can be made to study site amplification. For the case where the source and path are shown to be the same as will be discussed in the next chapter, two sites may be directly compared. One of those sites is chosen as a *reference* rock outcrop site such that that site has a transfer function from surface to bedrock of essentially unity. The accelerogram recordings made on the reference rock outcrop can then be directly used as the bedrock motion at the second site, the site of interest. It is important to note that in the procedures for doing this to be discussed in later chapters involve measurement of ground motion but do not require quantification of the material properties.

### Acceptability of General Model

There are several elements to the problem which must be noted:

- Acceptability of linear transfer function concept using rock outcrop and soil site;
- Use of ocean induced microseism as excitation;
- Establishing a frequency range of interest for building structure response.

The general concept of combination of source path and site effects has been widely used by seismologists. Hutchings (1991) demonstrated that empirical Green's function method can be used to capture the propagation and linear site response effects for frequencies from 0.02 to 0.5 Hz ( periods from 2 to 50 sec). He predicted actual recorded ground motion from the Loma Prieta earthquake at 5 San Francisco sites using recordings

of Loma Prieta aftershocks. He presented 25 source models that spanned the range of uncertainty. Nonlinear material properties such as the variation of shear modulus and damping with strain level are widely accepted, and use of equivalent linear strain dependent material properties for transient wave propagation analysis in the frequency domain is common. Program SHAKE for example has been in use for twenty years and has been shown to accurately predict site amplification. It is recognized that as the level of ground shaking increases there is a reduction in shear modulus and an increase in damping. Jarpe et al. (1993) shows that although there is evidence that some soft sites respond nonlinearly, linear predictions do a surprisingly good job of estimating earthquake level site response. Aki (1988) notes that nonlinearities were evident only in the case of liquefaction such as in the Niigata 1964 earthquake records. He states "As a matter of fact, seismologists tend to find a good correlation between weak and strong motions at a given site, namely similar amplification factors for both, implying that non-linearities are not important as the first order effect in most cases." However he also notes that for the SMART-1 ground motion array in Taiwan that the standard deviation of ground motion acceleration is less for large events than small indicating a magnitude dependence which may be attributed to non-linear soil effects.

For low levels of strain associated with microseisms, linear approximations are quite appropriate. Seale and Archuleta (1989) report results of an instrumented hole at McGee Creek, California. Instruments were placed at depths of 0, 35 and 166 m and two earthquakes recorded, the 5.8 1984 Round Valley event and the 6.4 1986 Chalfant Valley event. Surface amplification compared with depth was 5.7. They conclude that the impedance contrast of the materials does not account for all of the amplification. Resonances of the layer system below 10 Hz ( above 0.1 sec) contribute significantly. They state that a linear model can predict the soil response to 10 Hz.

Seismologists tend to analyze problems at a regional level and have rarely found nonlinearities in assessment of site conditions as evidenced by the largely elastic response of soil sites during the 1985 earthquake in Mexico City, Finn (1991).

The process of using microseisms as a predictor of amplification seems viable. The mechanism of combination of source, path and site models is feasible since the first two components, source and path are fundamentally appropriate for linearization. The site transfer function may incorporate nonlinearities, but these nonlinearities do not preclude the use of microseisms as long as they are recognized. If this is done the fundamental concept of microseisms usage requires linearity only in source and path. The subject of nonlinearity of site transfer function is a main topic of this research and will be discussed in detail in following chapters. It is most important to note that *long period microseisms* will be used for this study. High frequency noise such as traffic and other man made signals are minimized by this selection. For this study the frequency band of 0.1 to 2 Hz (0.5 to 10 second period ) is used and is a region chosen because it is applicable to building response. While it may have academic interest, ground response at 50 Hz does not affect building response significantly. It is important to keep this fact in mind, since in reading research papers by others many elements of system response are reported. In

sorting out data it is essential to consider the frequency range of the data, the source of the excitation and the applicability to structures. The microseism research area has not progressed to a state where there is common acceptance of results and development of standardized procedures. There are reported papers showing unsuccessful results. These are important as a learning tool.

Udwadia and Trifunac (1973) report 15 events recorded in El Centro, California and compare results to microtremor excitations. They conclude that local soil conditions are overshadowed by source mechanism and transmission path. They found that the microtremor and earthquake processes vary widely in character and have little correlation in ground response. On first appearance the results seem to negate the feasibility of use of microseisms. The paper presents a study based only on spectra not spectral ratio. It does not use a rock reference site but simply analyzes response at the site of interest. It presents results over a wide range of frequency. The microtremors were high frequency short period measurements. *The procedures suggested as part of this study will use lower frequency long period measurements at both a rock reference site and a soil site to eliminate source and path effects. Further this study will use the systems identification process to tie measured microseism data to computations for earthquake response.*

Gutierrez and Singh (1992) report on another study where microtremor and earthquake response agreement was only fair. They studied a location in Accapulco, Mexico using a rock reference site and several sites on sand and clay deposits, alluvium, and a sand, lime and clay bar. They use a seismometer with a period of 5 seconds and report results from 0.5 Hz to 50 Hz. Measurements were made during high traffic times and at night. They found that the traffic noise affected both the shape and amplitude of the spectra. For structural response applications the region of interest would be much narrower than the high frequency reported and would cover only the lower end of 0.5 to 2 Hz. Their results are shown in Figure 2.4. To better cover the long period - lower frequency segment, this study will use a seismometer with a 20 second period and flat bandwidth from 0.05 to 20 Hz. It is hoped this will give better response in the region most affecting structures.

### **Nakamura Method**

Nakamura (1989) performed a series of microtremor studies in Japan, recording data hourly for 30 hours at several sites. In this study he proposed a procedure for removing source effects from microtremor records based on a modification of the transfer function. He assumes that the surface source of microtremors generates Rayleigh waves affect both horizontal and vertical motions in the surface layer. Under these conditions:

$$E_s = S_{vs} / S_{vb}$$

where



$E_s$	Amplitude effect of source
$S_{vs}$	Spectral vertical motion at surface
$S_{vb}$	Spectral vertical motion of base

The transfer function of a site is defined by

$$S_T = S_{HS} / S_{HB}$$

where

$S_T$	Site transfer function
$S_{HS}$	Spectral horizontal motion at surface
$S_{HB}$	Spectral horizontal motion at base

The source effects are compensated for by dividing  $S_T$  by  $E_s$  as follows:

$$S_{TT} = S_T / E_s$$

This can be written as

$$S_{TT} = R_s / R_B$$

where

$R_s$	is defined by	$S_{HS} / S_{VS}$
$R_B$	is defined by	$S_{HB} / S_{VB}$

Nakamura assumes that  $R_B = 1.0$  over the range of engineering interest based on his extensive studies and field experience. Thus the transfer function is given by  $R_s$  alone, the ratio of horizontal to vertical surface motions. This approach replaces the traditional rock reference site response with the vertical response. The base or bedrock motion fluctuates over a much narrower range than surface motions. This approach has been tried by several researchers and results tend to show agreement of spectral ratios from microtremors and strong motion at least in the long period range. Seekins (1994) applied this technique to sites in San Francisco at which the 1989 Loma Prieta event was measured with good results over a narrow frequency band at two stations.

## References

- Aki, Keliti (1988) "Local site effects on strong ground motion" Earthquake Engineering and Soil Dynamics - Recent Advances in Ground-Motion Evaluation, ASCE Geotechnical Special Publication 20, New York NY
- Blakeslee S. and Peter Malin. (1991) "High frequency site effects at two Parkfield downhole and surface stations." University of California, Institute for Crustal Studies, Santa Barbara CA July 1991
- Field E. H. et al. (1992) "Earthquake site response estimation: a weak-motion case study" Bulletin of the Seismological Society of America, Vol 82 No 6 pp 2283-2307 Dec 1992
- Finn, W. D. Liam (1991) "Geotechnical Engineering Aspects of Microzonation"
- Gutierrez, G and S. K. Singh, (1992) "Site Effects in Acapulco, Mexico" Bulletin of the Seismological Society of America, Vol 82 No 2 pp 642-659 April 1992
- Hutchings, L J. (1991) "Prediction of strong ground motion for the 1989 Loma Prieta earthquake using empirical Green's functions", Bulletin Seismological Society of America, 81, 1813-1837
- Jarpe, S. and P. Kasameyer, (1993) "Validation of a methodology for predicting broadband kinematic strong motion time histories from empirical Green's functions", UCRL-JC-102465 Lawrence Livermore National Laboratory, Livermore CA May 1993
- Kanai, K. (1961) An empirical formula for the spectrum of strong earthquake motions, Bulletin Earthquake Research Institute, Tokyo University, 39 pp 85-96
- Lastrico, R. et al. (1972) Effects of site and propagation path on recorded strong earthquake motions. Bulletin of the Seismological Society of America, Vol. 62 No 4 pp 933-954 Aug. 1972.
- Palo, P. (1994) Oral communication
- Nakamura, Y (1989) "A method for dynamic characteristics estimation of subsurface using microtremor on the ground surface" QR or RTR1, Vol 30, No 1, February 1989
- Seekins (1994) Oral communication
- Udwadia, F.E. and M.D. Trifunac (1973), "Comparison of earthquake and Microtremor Ground Motions in el Centro, California" Bulletin of the Seismological Society of America, Vol 63 No 4 pp 1227-1263 August 1973

• = numerical | H(f) | estimate

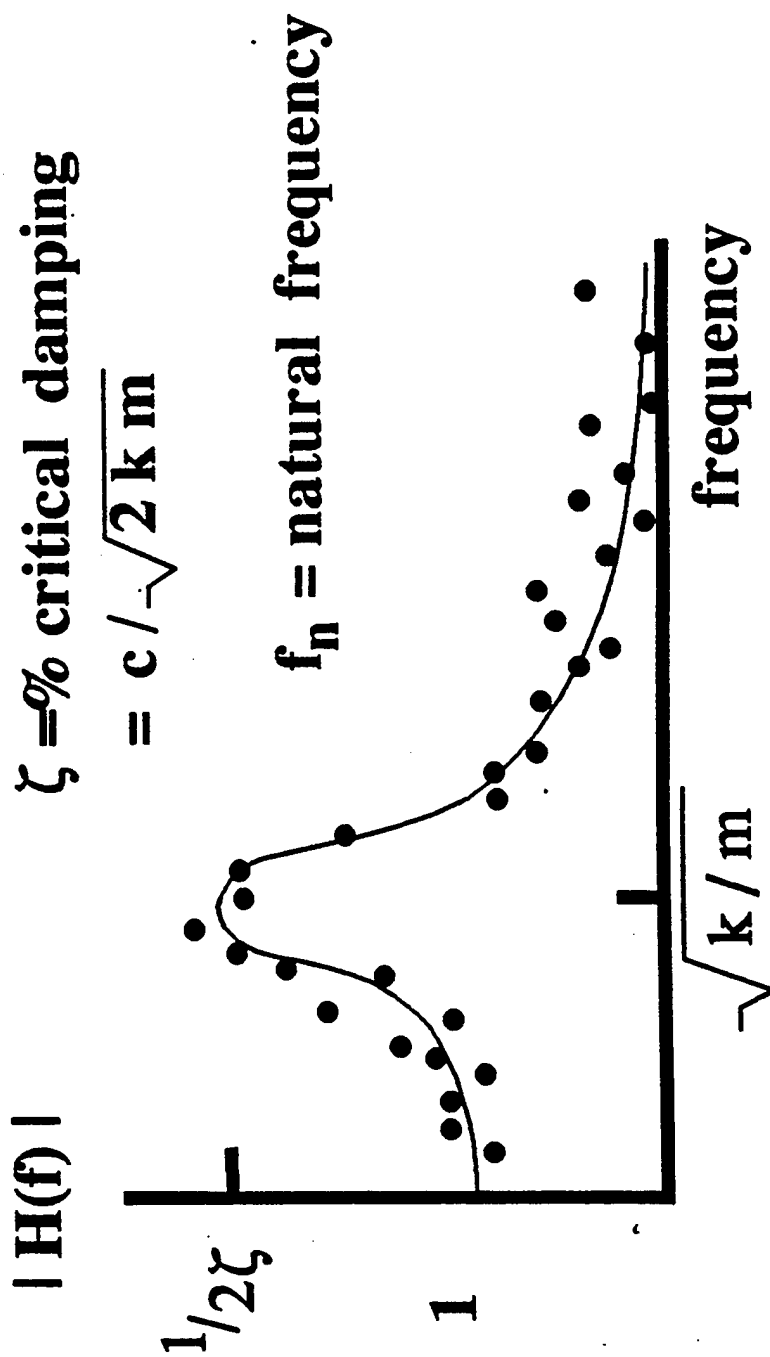


Figure 2.1 System identification, after Palo, 1994

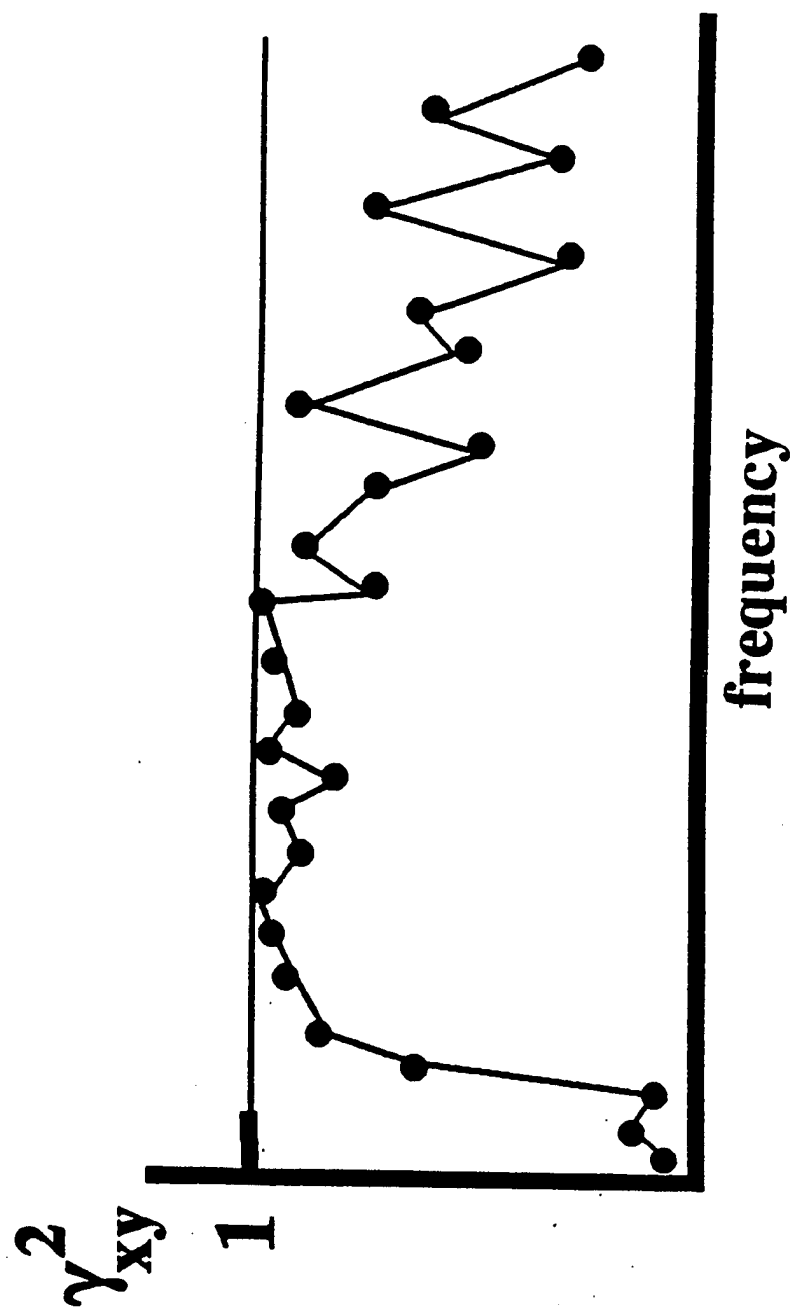


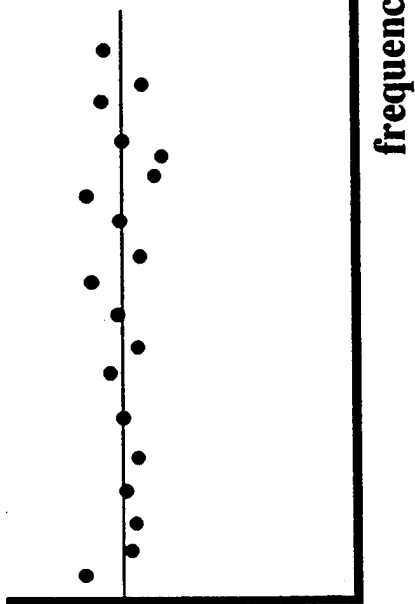
Figure 2.2 Coherence function, after Palo, 1994

• = numerical |  $H(f)$  | estimate — = best analytical fit

$H_{Imag}(f) / (2\pi f)$

Case #1: estimated damping is independent of frequency, so:

- $c = \text{constant}$ ,
- equation of motion is *differential*.



$H_{Imag}(f) / (2\pi f)$

Case #2: estimated damping is NOT constant versus frequency, so:

- equation of motion is integro-differential;

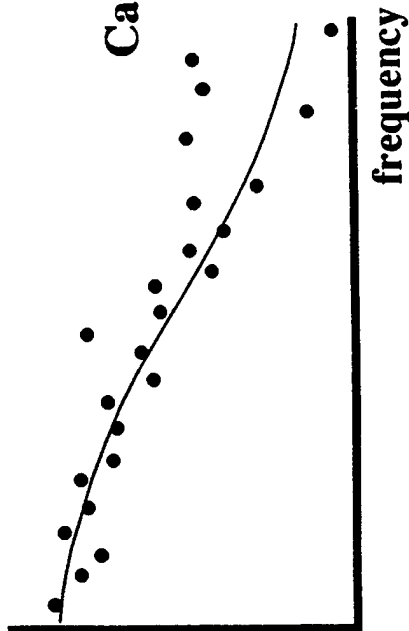


Figure 2.3 Imaginary part of transfer function,  
after Palo 1994

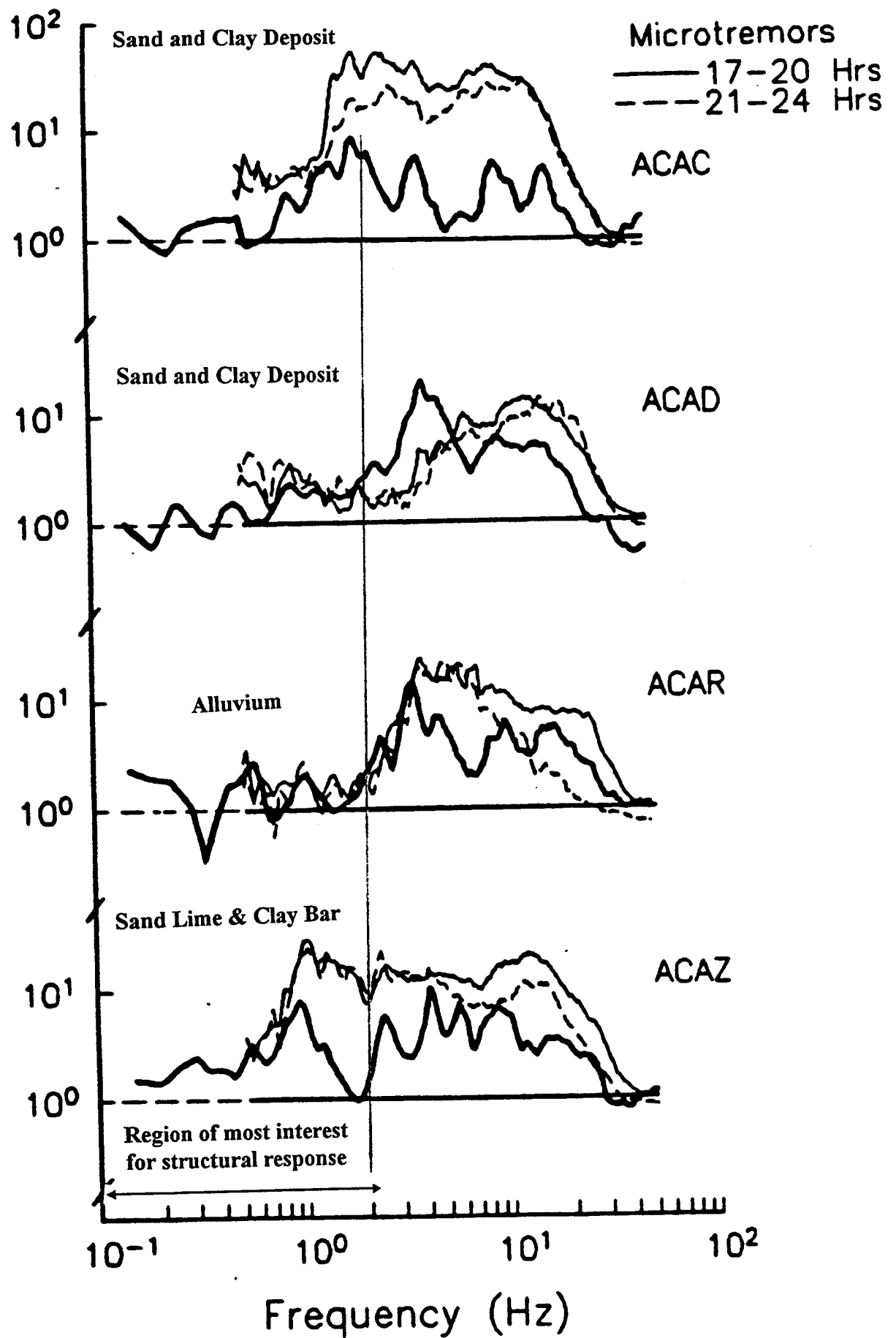


Figure 2.4. Acapulco Mexico From Gutierrez and Singh (1992)

## CHAPTER 3 MICROSEISMS

### Composition and Source

Microseisms along coastal areas consist of persistent oscillation of seismic waves characterized by long periods which are for the most part generated by ocean wave action. Several studies have shown that the ocean-bottom microseism spectrum is similar to the shape of the continental microseism spectrum but with greater amplitude and can be shown to correlate with known storm activity. Haubrich et al. (1963) identified microseisms as primary and double frequency covering two distinctly different frequency bands .08 Hz (12.5 sec) and .15 Hz (6.66 sec) respectively. The primary microseisms observed on land are between 0.04 and 0.08 Hz and have spectral peaks equal to the wavelength of the dominant ocean waves which appear to form in shallow water by interaction of ocean swells with a shoaling ocean bottom. The double frequency microseisms have a dominant period between 6 to 10 seconds. They are believed to result from an interplay amongst ocean waves of equal frequency traveling in opposite directions resulting in a nonlinear, second-order pressure perturbation on the ocean bottom, Cessaro (1989).

It is interesting to note that microseisms recorded on land and ocean bottom arrays can be used to track storms by applying frequency wave number analysis. Microseism source azimuths exhibited sufficient stability over periods of one hour to permit determination of reliable source locations by triangulation with two arrays. In these cases the microseism noise source is associated with the near shore process. Cessaro notes that spectral power from primary microseisms associated with major storm activity fluctuates significantly over a matter of minutes. Use of spectral averaging and moving window analysis are used for azimuth determination. Variation in source with time is not as significant for amplification computation as long as the rock reference site and the soil site are recorded simultaneously since the ratio of the two sites will be used.

Microseisms are generated essentially in three ways (Hasselman, 1963): (i) Action of ocean waves on coast, (ii) atmospheric pressure variations over the ocean, and (iii) nonlinear interactions between ocean waves. Long period microtremors have been observed for quite some time. However, most of the studies have been limited to their origins and wave characteristics (Longuet-Higgins, 1950; Hasselman, 1963) while only few investigations studied them to explain the ground dynamics of earthquake motion (Ohta, 1978). Until recently, the latter problem has been considered only in the short period range (Tanaka et al., 1968). Iida and Ohta (1964) investigated relationships between the amplitude of microtremors and soil structures and proposed correlation for the observations on Nagoya, Japan. Kubotera and Otsuka (1970) observed microtremors in the period range of 1 to 3 sec in Aso Caldera area, Japan. They suggested that the microtremors are mainly Love waves with predominant period which correlates well with the thickness of the soil deposits. Earthquake engineering application of microtremors can be found in the papers by Toriumi et al. (1972) and Ohta and Nagouchi (1972).

Kagami et al. (1982) observed long period microtremors in deep sedimentary basins of the Niigata Plain and Los Angeles. These locations were selected because strong ground motion records obtained during the 1964 Niigata earthquake and 1971 San Fernando Earthquake contain large long period amplitudes. Understanding of these predominant long-period motions is very important for evaluation of seismic motion of large scale structures. The results show that the amplitude of long period microtremors increases systematically from basement rock sites compared to deep sediment sites. This coincides with the observations obtained through studies of strong ground motion records. Therefore, Kagami et al. (1982) concluded that simultaneous observation of long period microtremors at multiple stations can provide insight into deep soil amplification effects and therefore, permit an estimate of input motions for large-scale structures.

In another study Kagami et al. (1986) measured long period microtremors in the San Fernando Valley, California. A complete two-dimensional study of the influence of soil deposits on seismic motions was carried out. It was shown that the spectral amplitude of microtremors correlates with the thickness of the sediments and that the site dependency of amplification is consistent with available geological and strong ground motion data.

The Michoacan earthquake of September 19, 1985 which devastated Mexico City prompted Kobayashi et al. (1986) to measure the long period microtremors within the Mexico Valley shortly after the earthquake. The measurements were performed at 95 sites in and around of Mexico City. For sites in the downtown area (area of many damaged buildings) microtremor measurements indicate predominant periods from 1 to 2.5 seconds which correspond to the natural periods of the collapsed buildings in this region. (Predominant period is defined as a period of the peak spectral amplitude of the predominant component of motion.) At sites where strong ground motion was measured, the acceleration response spectra of the main shock compare well (with a few notable exceptions) with the Fourier velocity spectra of microtremors at the corresponding locations.

Lermo et al. (1988) extended the microtremor measurements of Kobayashi et al. (1986) to a total of 181 sites. In the transition and the lake bed zones of the Valley of Mexico these measurements show that the period at which peak in microtremor Fourier velocity spectra occurs corresponds to the natural period of the sites. Excellent agreement was obtained between natural period estimates using microtremor spectra and from strong ground motion records.

### **Coastal Sources**

Cessaro (1992) has performed research using data from three land based long period seismic arrays. Reliable microseism source locations were determined by wide-angle triangulation using azimuths of approach obtained from frequency wave-number analysis of the records of microseisms propagating across these arrays. He found that there were two near shore sources of both primary and secondary microseisms which are



persistent and associated with essentially constant locations. Further he noted that secondary microseisms were observed to emanate from wide ranging pelagic locations in addition to the same near shore locations.

In Cessaro's work (Cessaro, 1992) he notes:

" that primary microseisms emanate from persistent near-shore locations that do not correlate well with their associated pelagic storm locations. During the time period sampled for this study, three major storms were active in the North Pacific and Atlantic oceans and two primary microseism source locations are identified: (1) A wide ranging North Pacific storm correlates with a microseism source near the west coast of Queen Charlotte Islands, BC and (2) Two North Atlantic storms correlate well with a source near the coast of Newfoundland. While the North Pacific storm trajectory subtends an arc greater than 90 degrees from the LASA array, the associated primary microseism source appears to be stable. The microseism near Newfoundland exhibits similar stability"

Cessaro concludes:

Although pelagic storms provide the source of microseismic wave energy, it is the interplay between (1) the pelagic storm parameters, such as tracking velocity, peak wind speed, location, effective area, and the ocean surface pressure variation, (2) the resulting storm waves and their wave number distribution, (3) the direction of the storm wave propagation, and (4) the near-shore and deep-ocean processes that control the production of microseisms. It is apparent that only a fraction of the total storm-related noise field is coherent. From the perspective of a seismic array, at any given moment only the most energetic coherent portion of the noise field is detected by FK analysis, i.e. a peak in the FK power represents the most energetic coherent portion of the microseismic wave field at that instant. ... It is also noted that both primary and secondary microseism source locations do not appear to follow the storm locations directly.

He further notes that there are local areas where near shore locations radiate strong coherent primary and secondary microseisms perhaps as a result of local resonance.

Orcutt (1992) notes that for secondary microseisms with peaks around 0.15 Hz there is no apparent correlation with increases in local wind speed and wave height. He suggests they are controlled by surface gravity waves from large distant storms. Akamatsu (1984) studied the Kyoto basin under different sea conditions noting that the spectra were influenced by the sea waves around Japan in particular during the winter and by typhoons, cold fronts, and monsoons. Although the amplitude and peak frequency varied with meteorological conditions,

he noted the spectral ratios were nearly constant in frequency and amplitude. This further emphasizes the fact that microseisms are quite variable and their use is only possible by use of pair of reference site to site of interest response, and not through a single station response.

### **Use of Microseisms in Earthquake Engineering**

The Japanese have been using microtremors as a means of site soil classification, Kanai (1961). They note the period distribution curve of microtremors shows a correlation to soil conditions. The presence of a single sharp peak is indicative of a simple stratified layer. The presence of two or more peaks indicates more complex layering. They note the following correlations:

- Mountain peak      Sharp peak at period 0.1 to 0.2 sec
- Diluvial soil        Peak at 0.2 to 0.4 sec
- Soft alluvial soil    Number of peaks 0.4 to 0.8 sec
- Thick soft site      Relatively flat curve from .05 to 2 sec

They note the period is often influenced by the properties of the first layer of the site. Rock sites tend to have flat curves. When the microtremor spectra exhibits a single peak, that peak correlates well to peaks from earthquake strong ground motion. However when there are more than one peak, the dominant peak can be influenced by the frequency content of the input source motion.

Kanai (1961) developed procedures for classification of sites which are used in the Japanese Building Code. They define four types of site soil conditions.

- Type I      Ground consisting of rock, hard sandy gravel, etc. classified as tertiary or older strata.
- Type II     Ground consisting of sandy gravel, sandy hard clay, loam etc. classified as diluvial, or gravelly alluvium, about 5 meters or more in thickness.
- Type III    Ground consisting of alluvium 5 meters or more in thickness which can be distinguished from the Type II site by a bluff formation.
- Type IV    Alluvium consisting of soft delta deposits, topsoil, mud or the like with a depth of 30 meters or more. Reclaimed land.

Japanese lateral force coefficients are influenced by the above classifications. Kanai (1961) developed two rules for site classification. The first rule assigns classification by using the largest period peak and the mean period peak as shown in Figure 3.1 They note

this rule to be in error for very thick soft deposits when the predominant period is short because the top layer controls the resonance and its influence predominates. Also Figure 3.1 is not to be used for rock and "sand hills" which have flat spectra. For cases where the first rule is in error a second rule is to be used based on the amplitude of the spectra, as shown in Figure 3.2. This is a marked deviation since it is based on microtremor absolute spectral values and not ratios.

### Shear Wave Velocity

Tanaka et al (1988) developed an empirical equation to predict the shear wave velocity of the top 30 meters of a deposit based on microtremor measurements

$$V_s = 160 \alpha T_m^{-0.668} + 200 \beta \text{ Amp}^{-0.348}$$

where

$V_s$  Shear wave velocity m/sec

$T_m$  Mean Period

Amp Largest amplitude in microns

The values of  $\alpha$  and  $\beta$  are based on the range of uncertainty of selecting the type band defined on the previous page and are obtained from Figures 3.1 and 3.2. The uncertainty associated with the soil type band in Figure 3.1 is defined as A and the uncertainty associated with the soil type band in Figure 3.2 is defined as B. The following table is used based on the difference in A-B.

A-B	$\alpha$	$\beta$
0.0	1.000	0.000
0.5	0.833	0.167
1.0	0.666	0.334
1.5	0.500	0.500
2.0	0.334	0.666
2.5	0.167	0.833
3.0	0.000	1.000

### Noise and Microseism Measurements

The ability to actually measure microseisms and distinguish the results from local noise is of critical importance to their use in any engineering measurement. Nakamura (1989) made extensive measurements. He reports Fourier amplification for a site during a quiet interval and for an interval having the passage of a train. The spectra have close agreement in the frequency range of 0.1 hz (10 sec period) to 3 hz (0.33 sec period). Above 3 hz (below 0.33 sec period) the effect of the train is noted as substantially higher

peaks. It is important to note that for engineering applications to structures the range of interest in period is from 0.5 sec to 5 sec. Most noise is exhibited as low period/high frequency outside the range of engineering interest. Filtering is performed to eliminate these components by high and low pass filters.

In reporting results comparing microseism data to weak or strong motion data, many researchers make comparisons over a wide range of frequency. For engineering applications it is essential to focus on the range of interest. Generally agreement is better for periods greater than 1 sec. When interpreting the conclusion drawn by researchers attention must be paid to the frequency range being reported. It is also critical to understand the frequency range of the instrument being used. Instruments intended for high frequency measurements will be noise sensitive and are not well suited for measurement of long period microseisms.

## References

- Akamatsu J. (1984) "Seismic amplification by soil deposits inferred from vibrational characteristics of microseisms" Bulletin Disaster Prevention Research Institute, Kyoto University, Vol 34 Part 3 No 306 Sept 1984
- Cessaro R and W. Chan, (1989) " Wide-angle triangulation array study of simultaneous primary microseism sources." Journal of Geophysical Research, Vol 94, No B11 pp. 15.555-15.563 Nov. 1989.
- Cessaro R. (1992) TGA 92-13 " Land-based seismic array studies of low frequency ambient oceanic noise." Teledyne Geotech, Alexandria VA., Feb. 1992
- Hasselman, K., (1963) "A statistical analysis of the generation of microseisms", Review Geophysics, 1, No. 2, 177-210.
- Haubrich R. et al. (1963) "Comparative spectra of microseisms and swells", Bulletin of Seismological Society of America, 53 , pp 27-37
- Iida, K., and Ohta, Y., (1964) "A study of microtremors observed in Nagoya and its vicinity", Journal Earth. Sciences, Nagoya University, Vol. 12, 192-221.
- Kagami, H., Duke, C. M., Liang, G. C. and Ohta, Y., (1982) "Observation of 1- to 5-second microtremors and their application to earthquake engineering. Part II. Evaluation of site effect upon seismic wave amplification due to extremely deep soil deposits", Bulletin Seismological Society of America 72, pp. 987-998 (1982).
- Kagami, H., Okada, S., Shiono, K., Oner, M., Dravinski, M., and Mal, A.K., (1986) Observation of 1- to 5-second microtremors and their application to earthquake engineering. Part III. A two dimensional study of site effect in the San Fernando

valley, Bulletin Seismological Society of America, bf 76, 1801-1812.

Kanai K and T. Tanaka, (1961) On Microtremors, VIII" Bulletin of the Earthquake Research Institute, University of Tokyo, Vol 39 1961

Kubotera, A., and Otsuka, M., (1970) "Nature of non-volcanic microtremor observed in Aso-caldera", Journal of Physical Earth}, 115-124.

Lermo, J., Singh, S. K., Dominguez, T., Ordaz, M., Espinoza, J.M., Mena, E. and Quaas, R., (1988) "A study of amplification of seismic waves in the Valley of Mexico with respect to a hill zone site", Earthquake Spectra, No. 4, 653-674.

Longuet-Higgins, M.S., (1950) "A theory of the origin of microseisms", Philisophical Transaction Royal Society London, A 243, 1-35.

Nakamura, Y (1989) " A method for dynamic characteristics estimation of subsurface using microtremor on the ground surface" QR or RTR1, Vol 30, No 1, February 1989

Ohta, Y., Kagami, H., Goto, N., and Kudo, K., (1978) "Observation of 1- to 5-second microtremors and their application to earthquake engineering. Part I: comparison with long-period accelerations at the Tokachi-oki earthquake of 1968, Bulletin Seismological Society of America, bf 68, pp. 767-779.

Ohta, Y., and Nogouchi, S., (1972) Observation of 1- to 5-sec microtremors and their application to earthquake engineering, (in Japanese), Proceedings Symposium Disaster Science, bf 9, 247-248.

Orcutt John A.(1992) "Seafloor pressure array studies at ultra low frequencies." California University, San Diego AD A247663

Tanaka, T., Kanai, K., and Osada, K., (1968) Observation of Microtremors. XII, Bulletin Earthquake Research Institute, bf 46, 1127-1147.

Tanaka A and K Migata (1988) "Estimation of shear wave velocity based on the results of microtremor observation" Geophysical Exploration Vol 41 No1 Feb. 1988

Toriumi, I., Takeuchi, I., and Ohba, S., (1972) Observation of microtremors with a 10 sec. pickup in Nagoya (in Japanese), Proceedings. Symposium Disaster Science, bf 9, 249-252.

# Kanai Rule 1

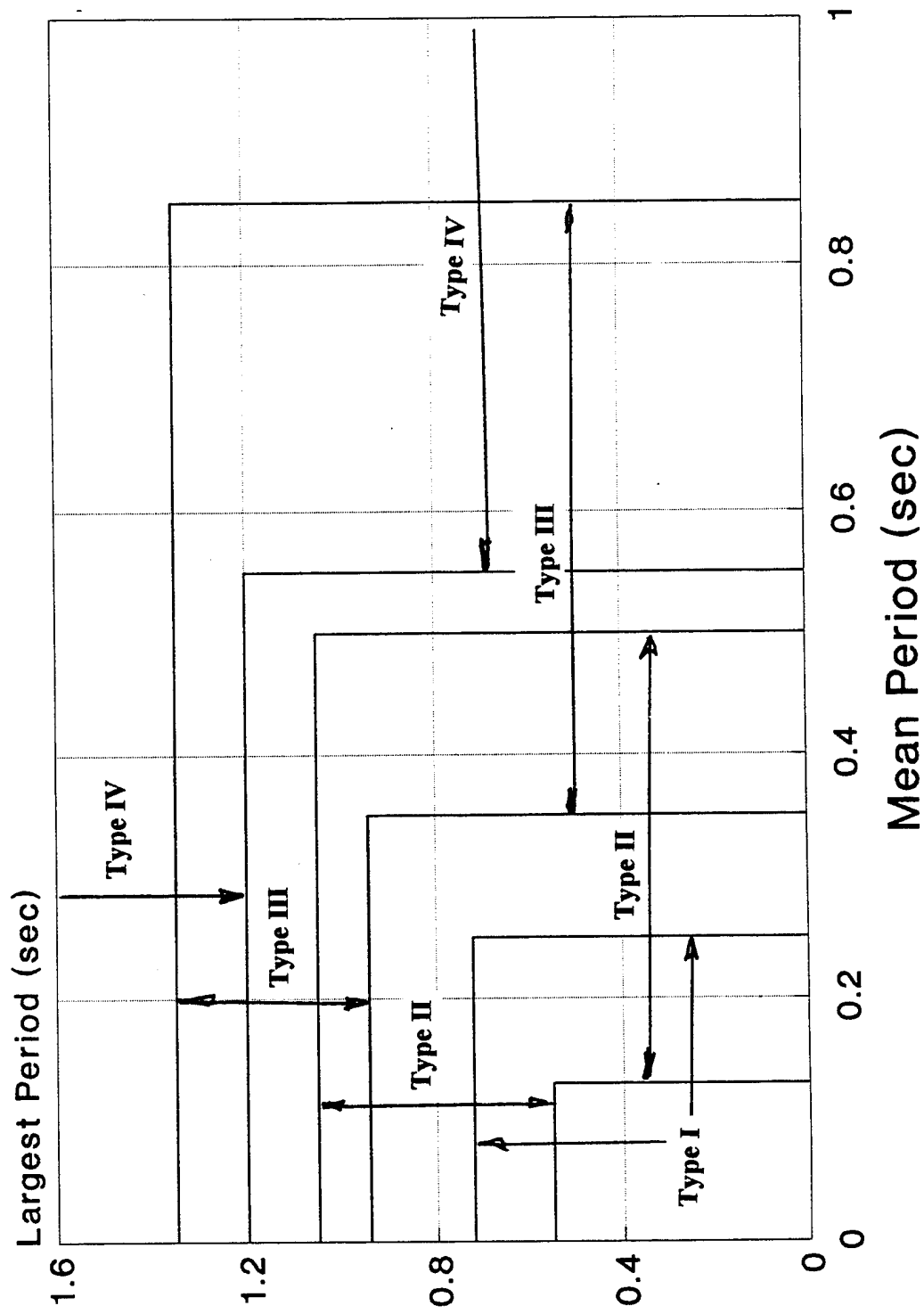


Figure 3.1 Kanai rule 1, based on Kanai (1961)

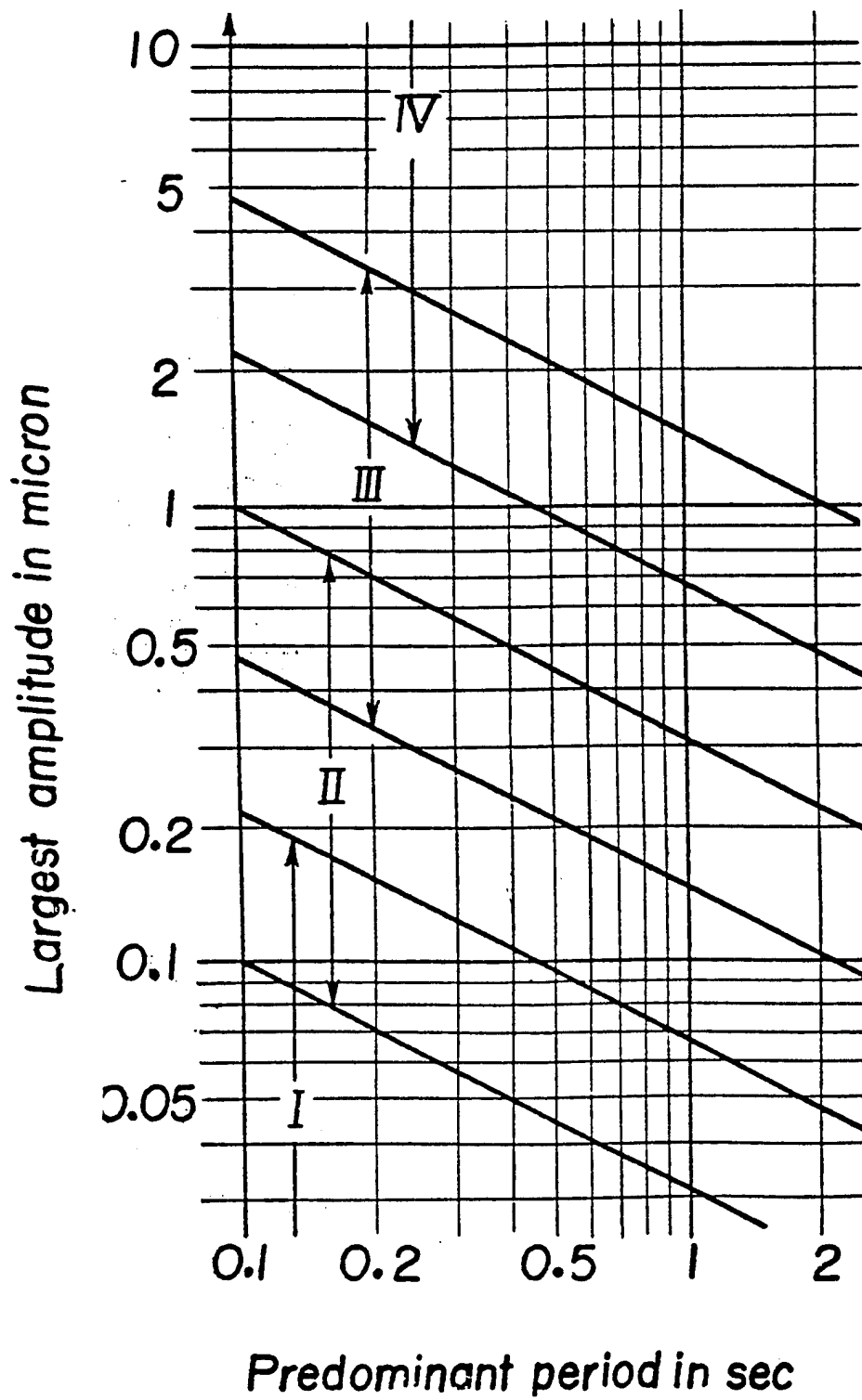


Figure 3.2 Kanai rule 2, based on Kanai (1961)

## CHAPTER 4 AMPLIFICATION OF GROUND MOTION

### Introduction

Spatial variation of ground motion amplification is a critical component of microzonation. In Chapter 2 elastic layer response was shown to predict an amplification of 2. It was noted that that level could be increased significantly when inclined SV waves are included. There exists a critical angle based on the ratio of S wave velocity to P wave velocity such that a strong coupling of S and P waves occur. The following sections will report on the effects of geology, topography and site conditions on amplification.

### Rock Site Geology

Lindley and Archuleta (1993) made recordings of the Loma Prieta aftershocks in the Santa Cruz Mountains. After studying a large number of records they conclude that site effects were controlled by geology. Of significance is that all the sites would be effectively classified as rock sites.

"The relative amplification between sites was measured from the low-frequency spectral asymptotes of the Fourier spectra corrected for geometric spreading and attenuation.. The lowest amplification sites were located on the Franciscan Complex, the highest-amplification sites on latest Tertiary (Miocene and Pliocene) sedimentary rocks. The average amplification at these Miocene and Pliocene sedimentary rock sites exceeded that at the Franciscan Complex sites by a factor of 3.3 for P waves and 3.9 for S waves. Amplification was less at ridge tops relative to valley sites, probably because most ridge top sites were on the Franciscan Complex.

From Lindley and Archuleta's data the following table is constructed.

Relative Amplification			
Geology	Age million years ago	P wave Amplification	S wave Amplification
Miocene & Pliocene	9-13 m yr	3.3	3.9
Eocene & Oligocene	15-20 m yr	2.0	1.8
Cretaceous & Jurassic	45-65 m yr	1	1

The above illustrates the significance in selection of an appropriate reference site since amplification occurs among rock sites based on their geology. Akamatsu et al. (1991) report that horizontal microtremor amplitudes exceed vertical and that amplitude increase in proportion to depth of soil above bedrock. It is important to restate a key assumption that the rock outcrop reference site and the soil site of interest be located nearby such that



the source and path effects are the same and that other than the free-surface amplification the reference site does not have any amplification of motion. If the rock reference site exhibits amplification its effects must be included to produce a bedrock reference. It is essential to capture an accurate reference spectra. This can be more easily accomplished by averaging spectra from several locations at the reference site to capture the variation, Field et al (1992). Archuleta (1992) instrumented a downhole array at Garner Valley in southern California. The site consisted of 19 m of soil ( fine alluvial and granular silty sands, silts and some clay layers) over 24 m of weathered granite over granite. They found that a site mean amplification from a depth of 220 m to the surface of 10 for a range of magnitudes from 1.2 to 4.7. Resonance peaks exist at about 1.7, 3.0 and 12 Hz with spectral ratios of nearly 40. The impedance of soil layer relative to the weathered granite amplifies all frequencies by a factor of about 3. "The effect of the weathered granite layer can be examined by examining the spectral ratios 22m / 220m. The average level of the spectral ratio between 2.0 and 30 Hz is around 3." Archuleta (1992) points out the desirability of having the rock outcrop reference be of the same geologic structure as the bedrock below the soil site of interest and extend much deeper than the depth of soil above. Abrahamson (1993) reports that the rock site strong motion variability based on arrays and multiple events is much higher than soil sites perhaps caused by shifts in resonance caused by variations in frequency content of the earthquake waves. It must be noted that while rock sites generally have shear wave velocities greater than 2000 ft/sec (600 m/sec) weathered rock can have shear wave velocities as low as 800 ft/sec (240 m/sec). Such a site composed of a zone of weathered rock can produce considerable amplification.

### **Topography**

Aki (1988) reports on several studies of ridges and mountains. Amplification at a ridge crest can be expected to be 50 percent higher based on analytical studies. From an elastic model of a ridge and valley, amplification may be expected to vary with the ratio of the angle of the valley to the angle of the ridge; thus, a ridge with a summit angle twice that of the valley would double the motion.

Lindley and Archuleta (1993) measured aftershock from the 1989 Loma Prieta earthquake in the Santa Cruz Mountains. The recording sites were at ridge top and valley sites. They could not discern a correlation between simple topography and amplification. While they expected amplification at ridge tops they actually observed reduced response controlled by site geology as discussed in the preceding section.

Celebi reports on the 1985 Chile earthquake where damage was observed largely on a "hilltop crowned by ridges and canyons". He reports work of others observing amplification at ridges. Site conditions consisted of alluvial deposits and a rock reference site on decomposed granite. Transfer functions were constructed from which he concludes that transfer functions were higher at sites where topography and geology were both prevalent as opposed to sites where only topography was a factor. Campbell (1983) reports on a study where rock sites were classified by topography of the region and notes

that recordings on tops or sides of hills or slopes were higher than those at the bottoms or on relatively flat ground.

Bard (1983) reports on an analytical study supported by observation which shows amplification at the top of a mountain and deamplification at the bottom. The effects were noted to be larger on the horizontal motion compared with the vertical. He also analyzes shallow and deep sediment filled valleys and notes that amplification from 2-dimensional analysis indicates results substantially higher (2 to 4 times) than those from 1-dimensional analysis. Additionally the frequencies are also different. He observes large differential motion and very strong propagation of motion and duration of motion. Jibson (1987) reports on an instrumented 20 degree embankment of about 150 m height which experienced 0.4 g at the base and 1 g at the top.

Bard and Gabriel (1986) calculated the amplification transfer function for a wide shallow sediment filled valley with bedrock outcrops at both edges. Their results show that 1-dimensional and 2-dimensional solutions agree reasonably over the middle half of the valley. However results deviated at the outer zones. Deep narrow valleys showed a different kind of response with 2-dimensional analysis having multiple spectral peaks compared with one or two associated with 1-dimensional analysis.

### **Geology Effects On Spectra**

Kanai (1961) measured microtremors at 5000 locations in Japan and developed a method for classification of the sites. This method involved measuring the interval between successive zeros on the horizontal component of a 2 minute microtremor record, thus established the wave periods by multiplying each time interval by 2. A frequency period histogram was generated by tabulating the number of occurrences of each period of the record. They assume that microtremor spectra are flat and broad band before they enter the region of interest which shapes the spectra. The subsequent spectra represents the effects of various geologies found.

Nogoshi conducted studies after the 1983 Central Coast earthquake in Japan, Immediately after the earthquake the responses were calculated using aftershocks in Akita City, and seismic amplification response transfer functions were correlated with site geology. Microtremors were also measured at 153 sites in Noshiro City. Three of those sites were studied in detail where the occurrence of liquefaction was correlated to microtremor spectral shape. The spectra were divided into four types (A, B, C, and D) for about 1 to 10 Hz. See Figure 4.1

- Type A had a single peak below 1.5 Hz.
- Type B had a single peak below 1.5 Hz and a peak from 2.0 to 3.0 Hz
- Type C had a peak from 2.0 to 3.0 Hz

- Type D had plural peaks from 1 to 10 Hz.

It was noted that average amplitudes of microtremors were particularly small at terrace deposits and slightly larger at a natural levee. Type A microtremor spectra were found mostly at terrace deposits and Type B were found on older alluvial soil.

For the purposes of investigating liquefaction an additional two sets were identified (a and b). Type a had a peak above 4 Hz and Type b did not. Type a microtremor spectra were observed in areas with high water table damaged by liquefaction where the spectra peaks above 4 Hz were found to be related to large shear wave velocity contrast between soil layers, Figure 4.2. Kagami et al (1986) noted that microseism amplitudes correlated with the thickness of the sedimentary layers forecasting amplification increases with thicker deposits. Their work validated prediction of fundamental period for such deposits using quarter wave theory.

Kamiyama et al. (1992) compiled data showing site effects. They note for earthquakes that the level of amplification for acceleration differs from that of velocity and displacement. The later two tend to be at the same levels. They present data which has been recompiled by the authors to show correlation to site condition. The data is at periods of engineering significance since most structures have first mode response between 0.5 and 2 sec. Figure 4.3 shows spectral amplification from earthquakes for stiff or rock sites. Amplification tends to be low and relatively flat over the period range shown. Figure 4.4 shows amplification for a relatively soft layer over a stiff layer or rock. The spectra shows at least one large peak reflecting the soft layer- rock impedance contrast whose amplitude depends on the degree of softness. Figure 4.5 shows amplification spectra for deep sites. The sites shown have moderate stiffness so amplification is moderate relative to softer sites. The more uniform and homogeneous the deposit, the flatter the amplification spectra. Any peaks which occur reflect the impedance contrast between layers. Figure 4.6 shows amplification spectra for soft sites which show high amplification and distinct peaks based on the impedance contrast to more competent layers. Note the location of the peak is influenced both by the softness of the upper layer and depth to a stiffer zone.

In general site amplification decreases with increasing age of the deposit. This is explained by increases in density and decreases in void ratio normally associated with increasing geologic age. This will be demonstrated in following sections.

### **Level Of Excitation**

The ground motion reaching a site is a function of the causative rupture. There are differences in the frequency content of two ground motion records both at the same nominal peak acceleration one caused by a distant large event, the other caused by a local small event. Site response depends in part on the frequency content of the driving ground motion. Rogers et al. (1983) present an interesting discussion of nonlinear site effects.

"Although laboratory data suggest that soils behave in a nonlinear fashion when strain exceeds  $10^{-5}$  ... field data have been collected suggesting that high- and low-amplitude soil response are perhaps linear for strains up to  $10^{-3}$ ." They report experience using distant nuclear explosions and the data from the 1971 San Fernando earthquake to illustrate that transfer functions from both are similar over a wide range of strain. They postulate that nonlinear soil behavior may be limited to a small area around the fault. " For instance, a magnitude 7-7.5 earthquake develops velocities on soil sites exceeding 100 cm/sec at distances less than 7-13 km.... For soil sites with 200 m/sec shear velocities, strains of  $5 \times 10^{-3}$  will be developed within this zone. Based on the observations discussed above, this strain level may still be below the level of significant non-linear behavior. Because damaging motions on soils (with intensity)  $III > VI$  occur to distances of 60-100 km (50 percentile) for a 30 km rupture, the area of damage susceptible to non-linear soil response is about 2-9 percent of the total area of damage." They note that the zone of nonlinear behavior may produce the greatest life loss but also note that a high percentage of total damage occurs outside this zone. Murphy (1983) also confirms that over a wide range of strain consistency has been observed for spectral ratios from earthquakes and nuclear explosions. Boore et al. (1983) reports on measurements taken in a sediment valley in the Garm region of what was the Soviet Union. The measurements covered a range of ground motion from  $10^{-5}$  to 0.2 g with high agreement of the amplification ratio over the wide range in levels of motion supporting linearity of response. Table 4.1 summarizes some of the observations which support the concept that response is independent of the level of excitation and linear theories are adequate.

Darragh and Shakal (1991) measured the site response at Treasure Island, California to weak and strong ground motion using the Yerba Buena Island site as a rock reference. The data included strong shaking from Loma Prieta and its aftershocks. They note that the amplitude, shape and frequency distribution of the spectral ratios for the soft Treasure Island site on Bay Mud varies with local magnitude. Figure 4.7 shows peak ground velocity and amplification. Figure 4.8 shows event magnitude and amplification. These results may be interpreted to show a clear trend that amplification increases as the size of the event decreases giving the implication of a nonlinear process. They conclude " that weak ground motion may be amplified to a greater extent than strong ground motion especially at sites similar to Treasure Island where nonlinear effects are observed at peak acceleration and velocity levels as low as 0.16g and 33 cm/sec, respectively. The corresponding rock motion near this soft site is only 0.07g and 15 cm/sec." It is important to note that the Treasure Island site liquefied during the Loma Prieta event and significantly affected at least part of the response record. The liquefaction occurrence obviously introduced nonlinearities into the site. Absent the occurrence of liquefaction it is not clear whether the site response would have been higher and of an amplification level comparable to that measured by aftershocks which did not liquefy the site. Darragh and Shakal (1991) also report on another site at Gilroy with a stiff site response. They report that the stiff site had an amplification of 2 for the 7.1 Loma Prieta earthquake, and an amplification of 4 for the 6.1 Morgan Hill and 5.6 Coyote Lake earthquakes. The same data is presented by Jarpe et al. (1989) suggesting the nonlinear response at high strain. They report additional data for two sites (one composed of thin alluvium over sandstone ,

the other thick dry alluvium) in Livermore, California where weak ground motion spectral ratios are essentially at the same levels as main shock data and they cite similar observations from the Coalinga California earthquake from a dry site having strong motion accelerations of up to 0.7g where weak motion spectral ratios were of the same levels. Field et al (1990) reports on a microtremor evaluation of a site in Flushing Meadows New York where significant amplification was observed in the spectral ratios over 50. The site had a 10 to 15 meter layer of soft Holocene organic clay and a thin layer of man made fill to cover the previous marsh environment.

Kameda et al (1991) reports on six sets of sites using Loma Prieta data and microtremor data. Four of the sites on bay mud exhibited much larger microtremor spectral ratio amplification than corresponding strong motion data. Two sites of thick Quaternary deposits exhibited the same order of magnitude for both Loma Prieta and microtremor data. Akamatsu (1991) presents similar data in a very constructive manner. Note on the map in Figure 4.9, the location of the site. The geology is noted on the map. Figure 4.10 shows the spectral amplification ratios. By noting the location of the three letter sites on Figure 4.9 the reader can see how the site spectral amplification ratios increase with proximity to the San Francisco Bay and Holocene estuarine Bay Mud soils. Clearly waterfront deposits are affecting response. Okada et al. (1991) studied the Sapporo region conducting microtremor readings from the Ishikara Bay inland. They noted that microtremor spectral ratio data increased from 10 to 25 with proximity to the coastline. Celebi (1987) notes in his study of the 1985 Chile earthquake that spectral ratio amplification transfer functions (on the order of 40 to 60 at 2 Hz) computed from weak ground motion aftershocks substantially exceeded transfer functions computed from strong-ground motion of the main shock. The sites were coastal areas composed of estuarine terrace deposits, sands, and alluvial deposits. The fact that the same phenomenon occurs with weak ground motion from earthquakes suggest process is controlled by the geology rather than the excitation source.

Sato (1991) measured microtremors at Ashigara Field, a site a few kilometers from Sagami Bay having upper layer shear wave velocities of 110 m/sec. This site produced peak spectral ratios of 50 at a frequency of 2 Hz. Sato notes that the site response is controlled by the upper 10 m soft surface layer. This implies that saturated waterfront marginal site would be expected to have amplification from microseisms greater than that from main shocks of large earthquakes, but dry alluvial sites may not exhibit these differences. The Table 4.2 summarizes some cases which indicate marginal waterfront soils experience a nonlinear amplification effect as a inverse function of level of excitation.

Tazoh et al. (1988) reports on two sites in Japan where the site period based on transfer functions of depth to surface varied from 0.25 sec for small local earthquakes to 1.35 for a large event. This phenomenon may depend more on the frequency content of the source than a fundamental shift of site properties. It is well known that local events producing the same site acceleration as distant large events have lower energy in the 1 to 10 second period range, Figure 4.11

## Site Response Effects

Rogers et al. (1983) present observations based on data from ground shaking induced by nuclear explosions which they note to correlate well to earthquake data. Their work is based on an assemblage of large amounts of data for numerous events. They note that maximum amplitude of motion recorded on alluvial sites are several times larger than on sedimentary or crystalline sites. The amplification at long periods is greatest at sites underlain by the thickest sediments. Amplification of horizontal ground motion is generally larger than amplification of vertical ground motion. Rogers et al. (1983) noted amplifications in the range of 2 to 7 for long period horizontal ground motion for sites of thick alluvium, with lower amplification for sites underlain by thin alluvium. Resonance was not noted to be a factor at the thick alluvium sites; they displayed flat spectra. They draw some interesting associations from their data. "Sites underlain by Holocene and Pleistocene sedimentary deposits undergo levels of shaking 2.6 to 3.4 times greater than those underlain by crystalline rock for all period bands. The void ratio (of the upper 8 m soil) has a strong influence on short-period response, with void ratios in the 0.8 -0.9 range indicating a mean response on soil 6 times greater than on crystalline rock and 3 times greater than on low-void ratio soils. Amplitudes in the long-period band generally increase with increasing thickness of Quaternary deposits and/or depth to basement."

The following table shows the influence of age of the material for three period ranges on relative spectral amplification:

Age	0.3-0.5 sec	0.5-3.3 sec	3.3-10.0 sec
Holocene	3.4	3.3	2.6
Pleistocene	3.2	3.1	2.6
Pliocene	1.4	1.6	2.0
Miocene	2.5	2.2	1.4
Mesozoic	1.7	1.1	0.8

The following table shows the influence of void ratio in the uppermost 8 meters of soil for short period amplification.

Void Ratio	Period 0.3-0.5 sec
0.2 - 0.4	2.3
0.4 - 0.6	3.1
0.6 - 0.7	3.0
0.7 - 0.8	4.2
0.8 - 0.9	6.2

The following table shows the influence of thickness of Quaternary deposits on intermediate and long-period amplification.

Thickness	0.5 - 3.3 sec	3.3 - 10.0 sec
0	1.6	1.3
0 - 75	2.3	1.4
75 - 200	3.6	2.9
200 - 500	3.6	3.1
500 - 1000	4.1	5.9
>1000	3.4	3.1

The following table illustrates the influence of depth to basement rock of intermediate- and long-period amplification.

Depth	0.5 - 3.3 sec	3.3 -10.0 sec
0	1.1	0.8
0-2	2.6	1.3
2-4	2.8	2.5
4-6	3.8	4.1
>6	3.8	3.9

Donovan (1983) reports on the ratio of earthquake ground motion velocity to acceleration ratio. Figure 4.12 shows his data and derived equation. There is a difference in velocity-acceleration ratio for soil and rock sites with soil having higher levels of velocity per given level of acceleration.

## References

Abrahamson N. A. (1993) in publication

Akamatsu et al (1991) "Long period (1-10s) microtremor measurement in the areas affected by the 1989 Loma Prieta earthquake", Fourth International Conference on Seismic Zonation, Stanford California

Aki, Keliti (1988) "Local site effects on strong ground motion" Earthquake Engineering and Soil Dynamics - Recent Advances in Ground-Motion Evaluation, ASCE Geotechnical Special Publication 20, New York NY

Archuleta R. J. et al (1992) Garner Valley Downhole array of accelerometers: Instrumentation and preliminary data analysis." Bulletin of the Seismological Society of America, Vol 82No 4, pp1592-1621, August 1987

Bard, P (1983) " Site effects: Two dimensional modelling and earthquake engineering", Proceedings of Conference XXII, A Workshop on "Site-specific Effects of Soil and Rock on Ground Motion and the Implications for Earthquake-resistant Design" USGS, Reston VA

Bard, P. and J. C. Gabriel (1986) "The seismic response of two-dimensional sedimentary deposits with large vertical velocity gradients." Bulletin of the Seismological Society of America, No 76, pp 343-346

Boore D. (1983) "Some studies concerning site response." Proceedings of Conference XXII, A Workshop on "Site-specific Effects of Soil and Rock on Ground Motion and the Implications for Earthquake-resistant Design" USGS, Reston VA

Campbell K. (1983) "The effects of site characteristics on near-source recordings of strong ground motion", Proceedings of Conference XXII, A Workshop on "Site-specific Effects of Soil and Rock on Ground Motion and the Implications for Earthquake-resistant Design" USGS, Reston VA

Celebi, M. (1987) "Topographical and geological amplifications determined from strong-motion and aftershock records of the 3 March 1985 Chile earthquake", Bulletin of the Seismological Society of America, Vol 77 No 4, pp1147-1167, August 1987

Darragh R and A. Shakal (1991) " The site response of two rock and soil station pairs to strong and weak ground motion." Bulletin of Seimological Society of America Vol 81 pp 1885-1899



- Donovan, N. (1983) " A practitioners view of site effects on strong ground motion" Proceedings of Conference XXII, A Workshop on "Site-specific Effects of Soil and Rock on Ground Motion and the Implications for Earthquake-resistant Design" USGS, Reston VA
- Field E. H. et al. (1990)" Using microtremors to assess potential earthquake site response: A case study in Flushing Meadows, New York City" Bulletin of the Seismological Society of America, Vol 80 No 6 pp 1456-1480 Dec 1990
- Field E. H. et al. (1992)" Earthquake site response estimation: a weak-motion case study" Bulletin of the Seismological Society of America, Vol 82 No 6 pp 2283-2307 Dec 1992
- Jarpe S. P. et al. (1989) " Selected strong and weak motion data from the Loma Prieta earthquake sequence." Seismological Research Letters, Vol 60, No 4 Oct-Dec 1989
- Jibson, R. (1987) "Summary of research on the effects of topographic amplification of earthquake shaking on slope stability" US Geological Survey Open File Report 87-268 Meno Park CA
- Kagami H. et al. (1986) "Observation of 1 to 5 second microtremors and their application to earthquake engineering" Bulletin of the Seismological Society of America, Vol 76, No 6, pp 1801-1812 Dec 1986
- Kameda H. et al (1991) "Comparative observation of soil amplification from long period microtremor and earthquake recordings for seismic microzonation.", Fourth International Conference on Seismic Zonation, Stanford California
- Kamiyama, M et al (1992) Technical Report NCEER-92-0023 "A semi-empirical analysis of strong motion peaks in terms of seismic source, propagation path and local site conditions." National Center for Earthquake Engineering Research, State University of New York at Buffalo, NY Sept 1992
- Kanai, K. (1961) "On Microtremors. VIII", Bulletin of Earthquake Research Institute, 39: 97-114
- Lindley and Archuleta (1993) "Variation of seismic site effect in the Santa Cruz Mountains, California" in publication
- Murphy J. (1983) "Site effects on strong ground motion observed from underground nuclear explosions." Proceedings of Conference XXII, A Workshop on "Site-specific Effects of Soil and Rock on Ground Motion and the Implications for Earthquake-resistant Design" USGS, Reston VA

Nogoshi, M. "Site Characterization by detailed seismic intensities, aftershocks, and microtremors." Seismological Laboratory, California Institute of Technology, Pasadena CA

Okada S. et al " Two dimensional analysis on site effects in the Sapporo urban region, Japan, based on observation of 1 to 10 second microtremors." Fourth International Conference on Seismic Zonation, Stanford California

Rogers A. et al, (1983) "The issues surrounding the effects of geologic conditions on the intensity of ground shaking", Proceedings of Conference XXII, A Workshop on "Site-specific Effects of Soil and Rock on Ground Motion and the Implications for Earthquake-resistant Design" USGS, Reston VA

Sato K., et al (1991) " Estimation of Surface Ground Motion at Ashigara Field using microtremors." Fourth International Conference on Seismic Zonation, Stanford California

Seo K., et. al (1991) "Microtremor measurements in the San Francisco Bay Area." Fourth International Conference on Seismic Zonation, Stanford California

Table 4.1  
Cases showing response independent of level of excitation.

Site	Soil	Effect	Reference
various Japan	various Alluvium - rock	Period same eq and microtremor	Kanai & Tanaka (1961)
San Francisco, CA	Various sites at distances from Bay	Normal amplification Peninsula sites (AP6,MTR,SVL etc.) Santa Clara Valley ARP, PAH rock Santa Cruz (BAR, KPL, SHE,etc)	Akamatsu (1991)
San Francisco, CA	Alluvium	Period same earthquake & microtremor	Seo(1987)
McGee Creek, CA	Glacial moraine over hornfels	linear response range magnitudes M 6.4, 5.8	Seale and Archuleta (1989)
Garm, Chusal & Yasman	sediment valley	Acceleration range $10^{-5}$ to 0.2 g no difference in site response	Tucker and King (1984)

Table 4.2  
Cases showing high amplification of microtremors or weak motion  
compared with strong ground motion

Site	Soil	Amplification	Reference
Ashigara Field near Sagami Bay Japan	$V_s = 110$ m/sec thick sediment deposit S7/R7	50 at 2 Hz	Sato (1991)
San Francisco, CA	Various sites at different distances from Bay	6 to 18 waterfront Holocene Bay Mud 1 to 2 at distance from waterfront on Quaternary alluvium	Akamatsu (1991)
Canal Beagle, Vina del Mar Chile	CBA estuarine terrace TRA sand EAC sand MUN alluvial REN sand	40 to 60 for weak ground motion	Celebi (1987)
San Francisco, CA	Treasure Island Bay Mud	Loma Prieta peak amp. 1-4 Hz = 4 Aftershocks peak amp. 1-4 Hz = 12	Jarpe (1989)
San Francisco, CA	Treasure island AP2 Bay Mud RSH/RWS Bay Mud MAL Bay Mud SVL/SH4 alluvium ASH/AOH alluvium	L P* - Microtremor 3.35 4.62 4.32 17.93 2.42 13.59 3.43 5.34 1.81 5.04 *LP - Loma Prieta	Kameda (1991)

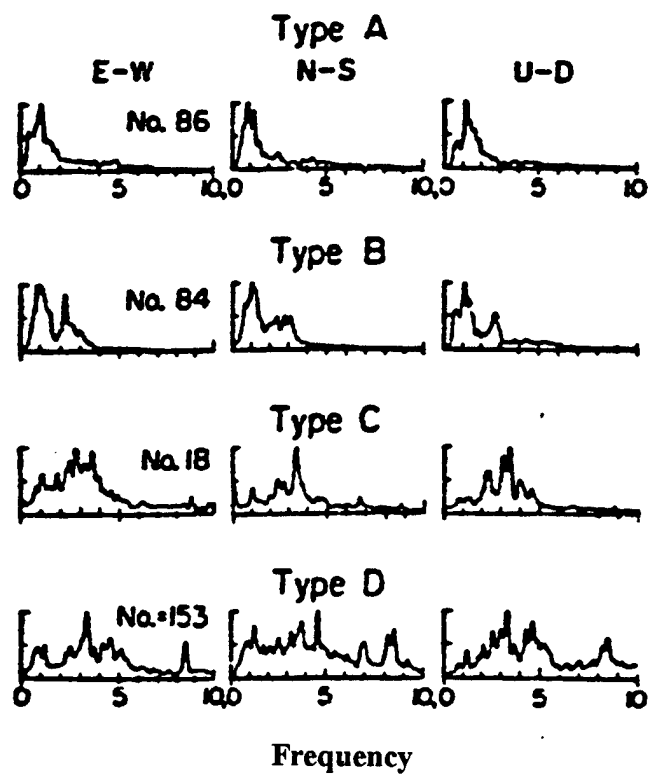


Figure 4.1 Spectra types after Nogoshi.

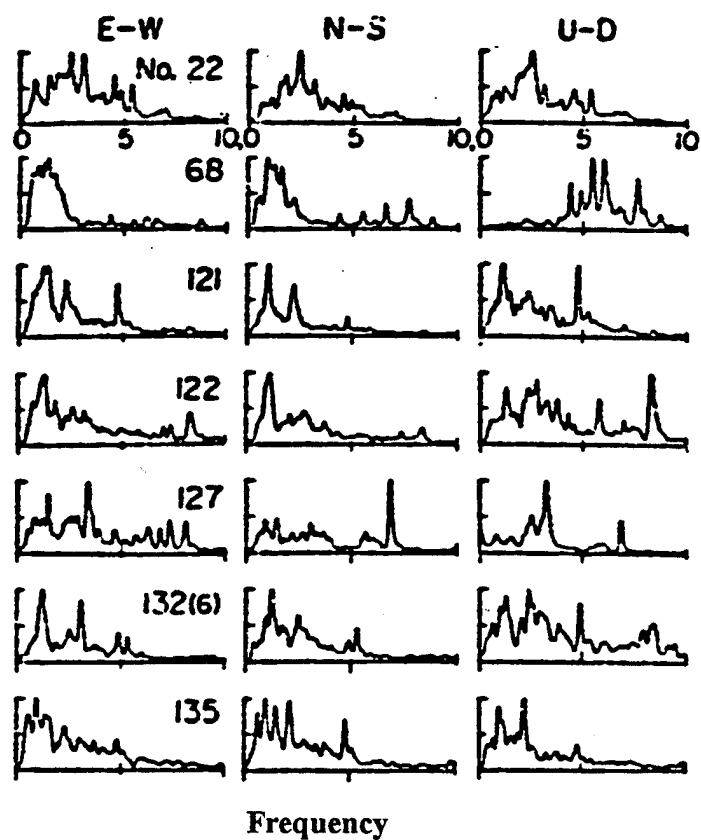


Figure 4.2 Type a spectra after Nogoshi

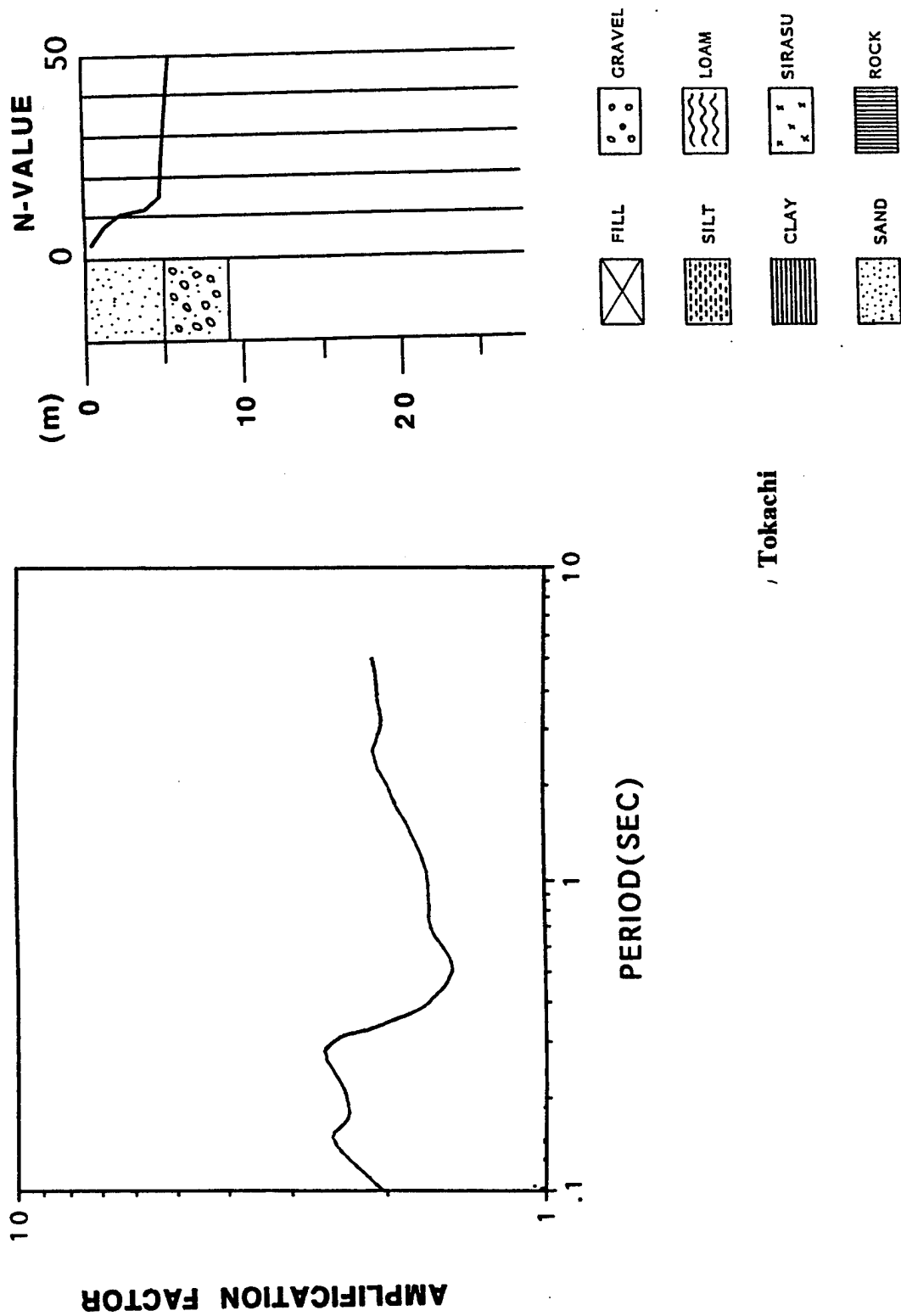


Figure 4.3a Amplification spectra, very stiff soil of rock site, Tokachi

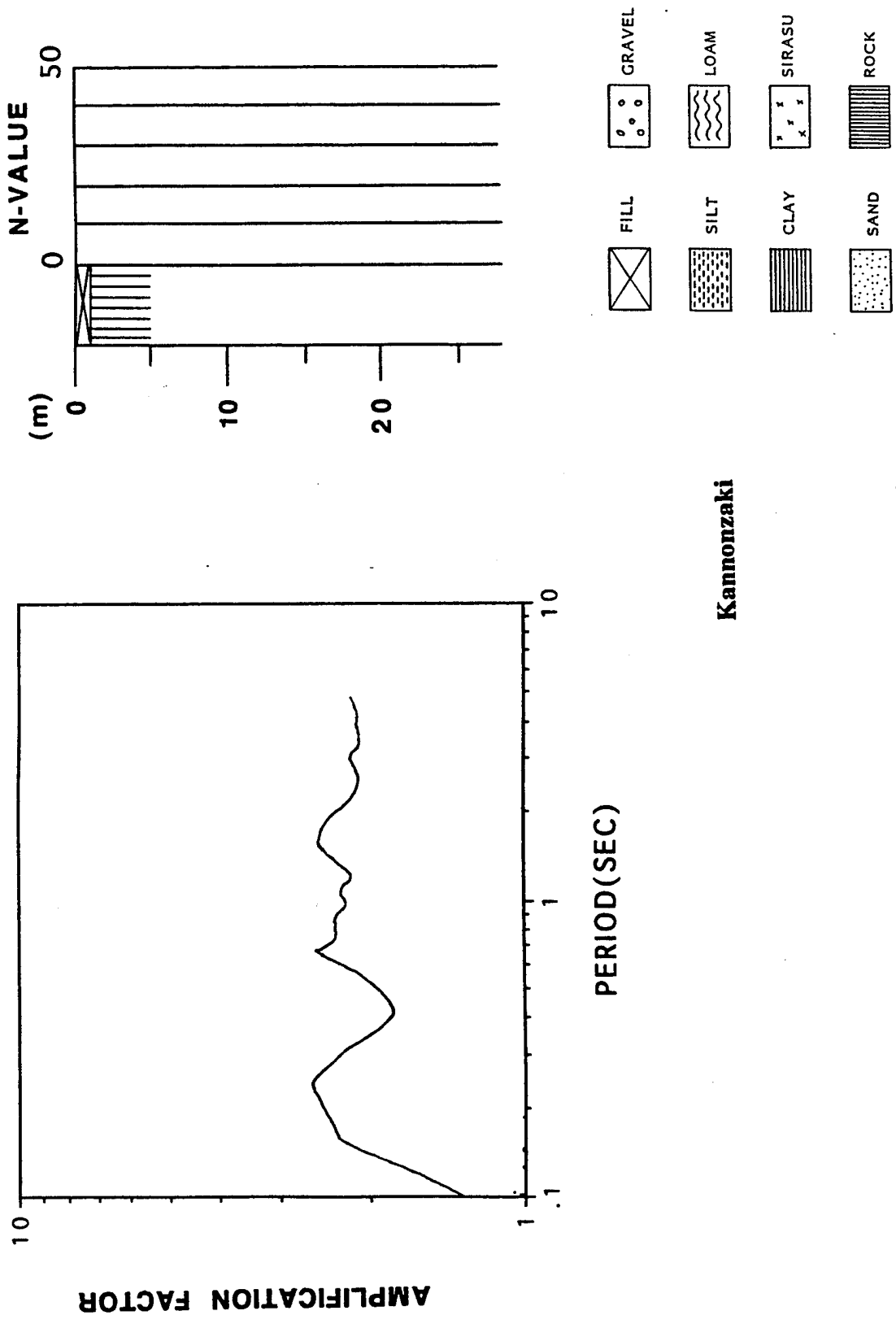
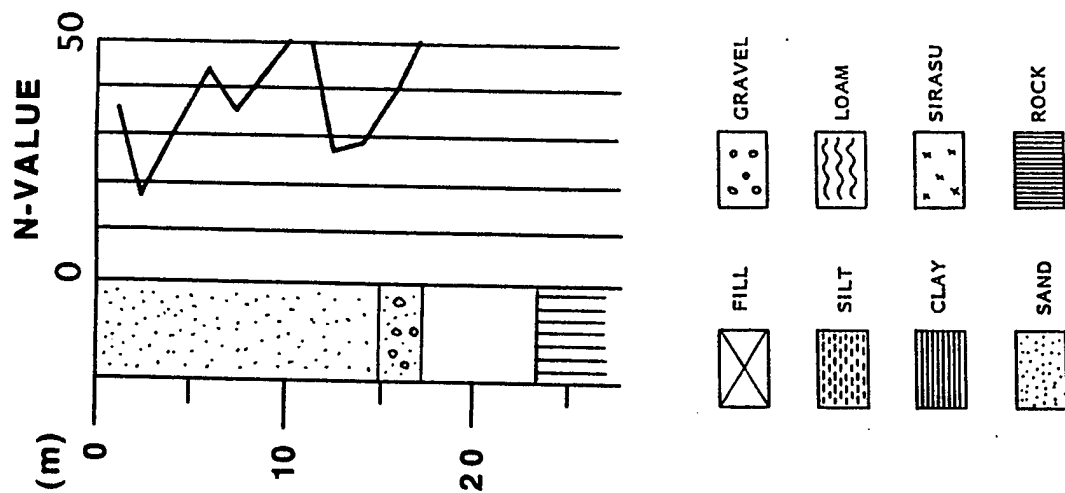
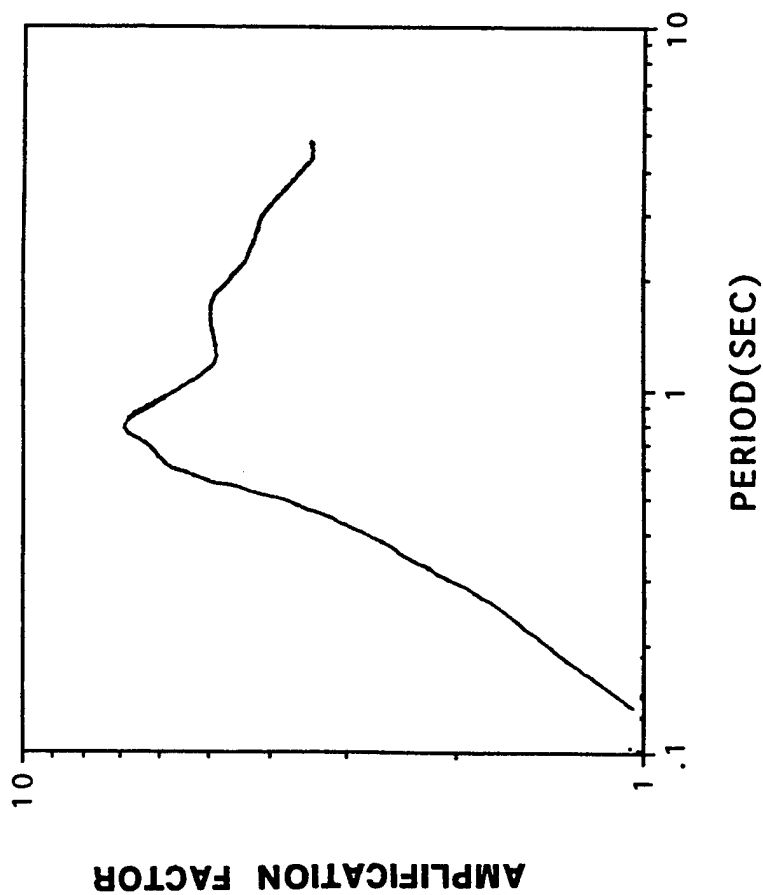


Figure 4.3b Amplification spectra, very stiff soil of rock site, Kannonzaki



Kashima Jimu

LEGEND

Figure 4.4a Amplification spectra, soft layer over stiff soil or rock, Kashima Jimu



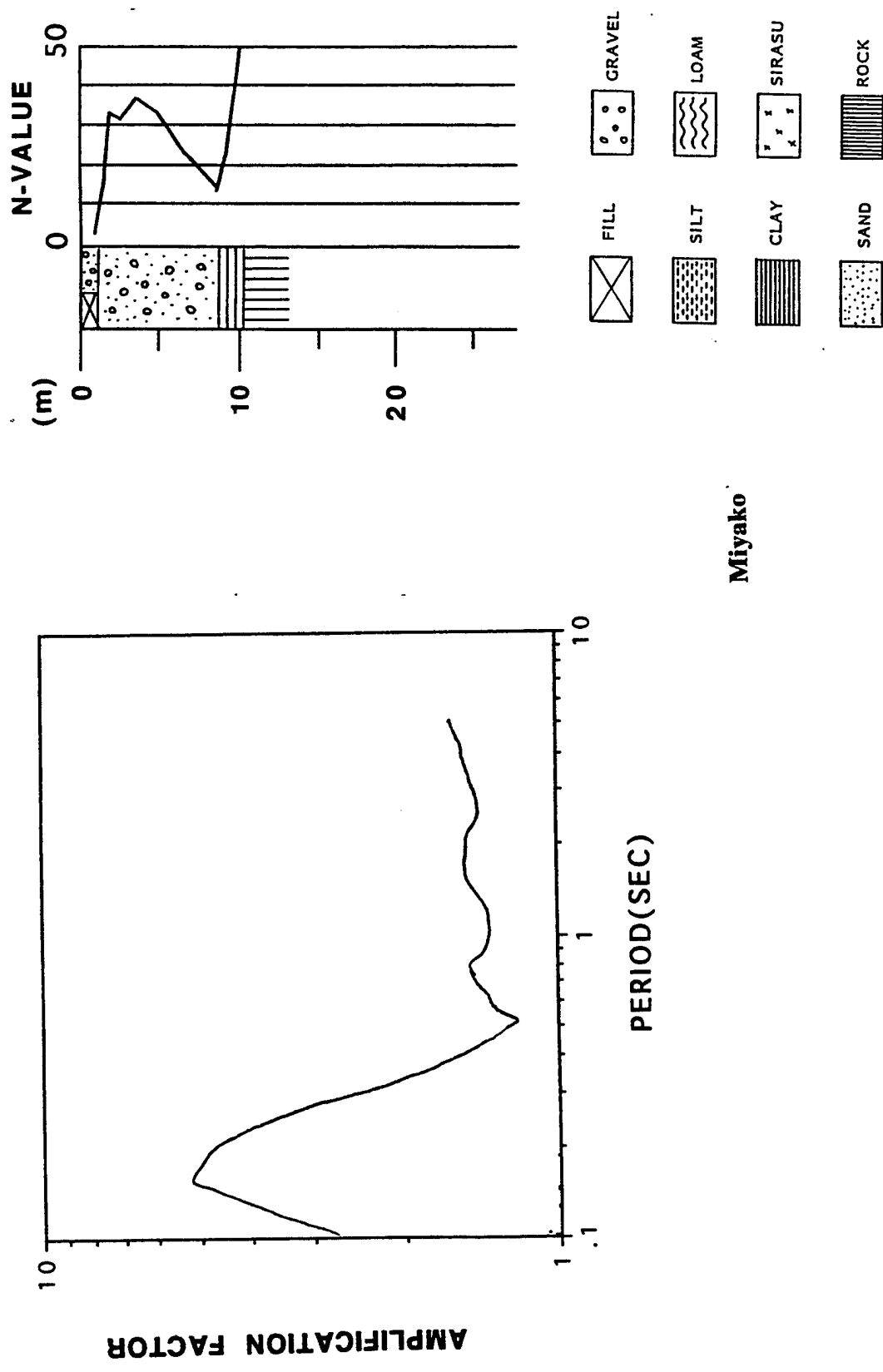
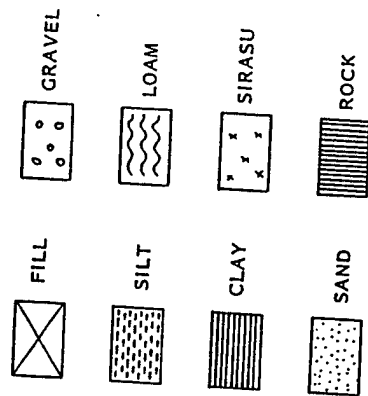
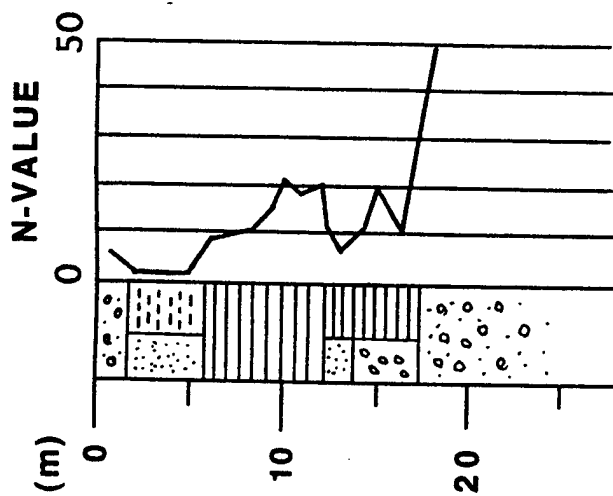
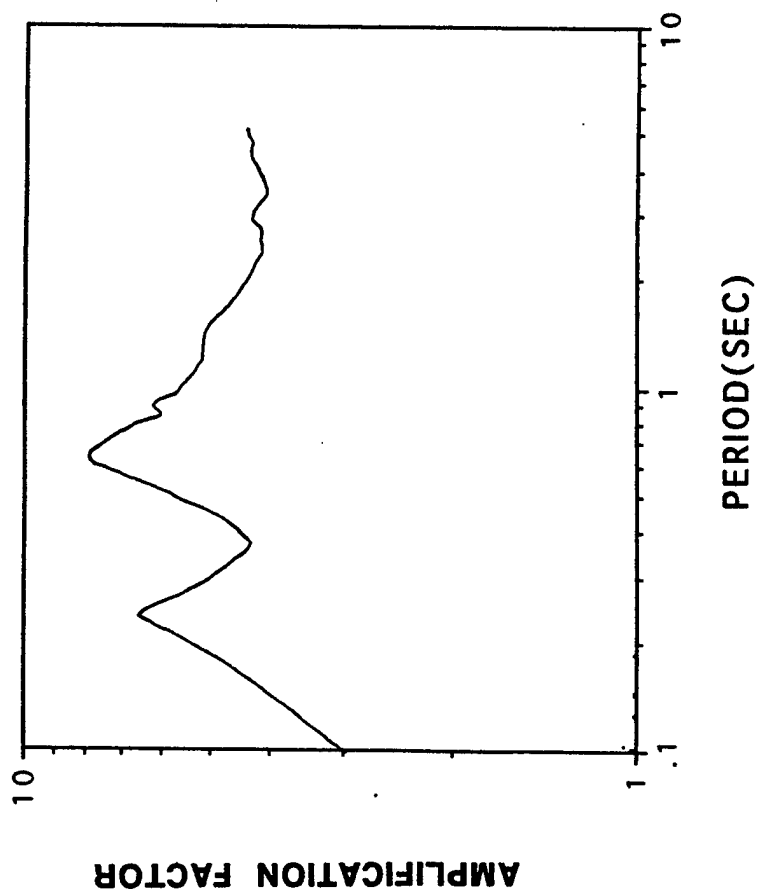


Figure 4.4b Amplification spectra, soft layer over stiff soil or rock, Miyako



LEGEND



Itajima

Figure 4.4c Amplification spectra, soft layer over stiff soil or rock, Itajima

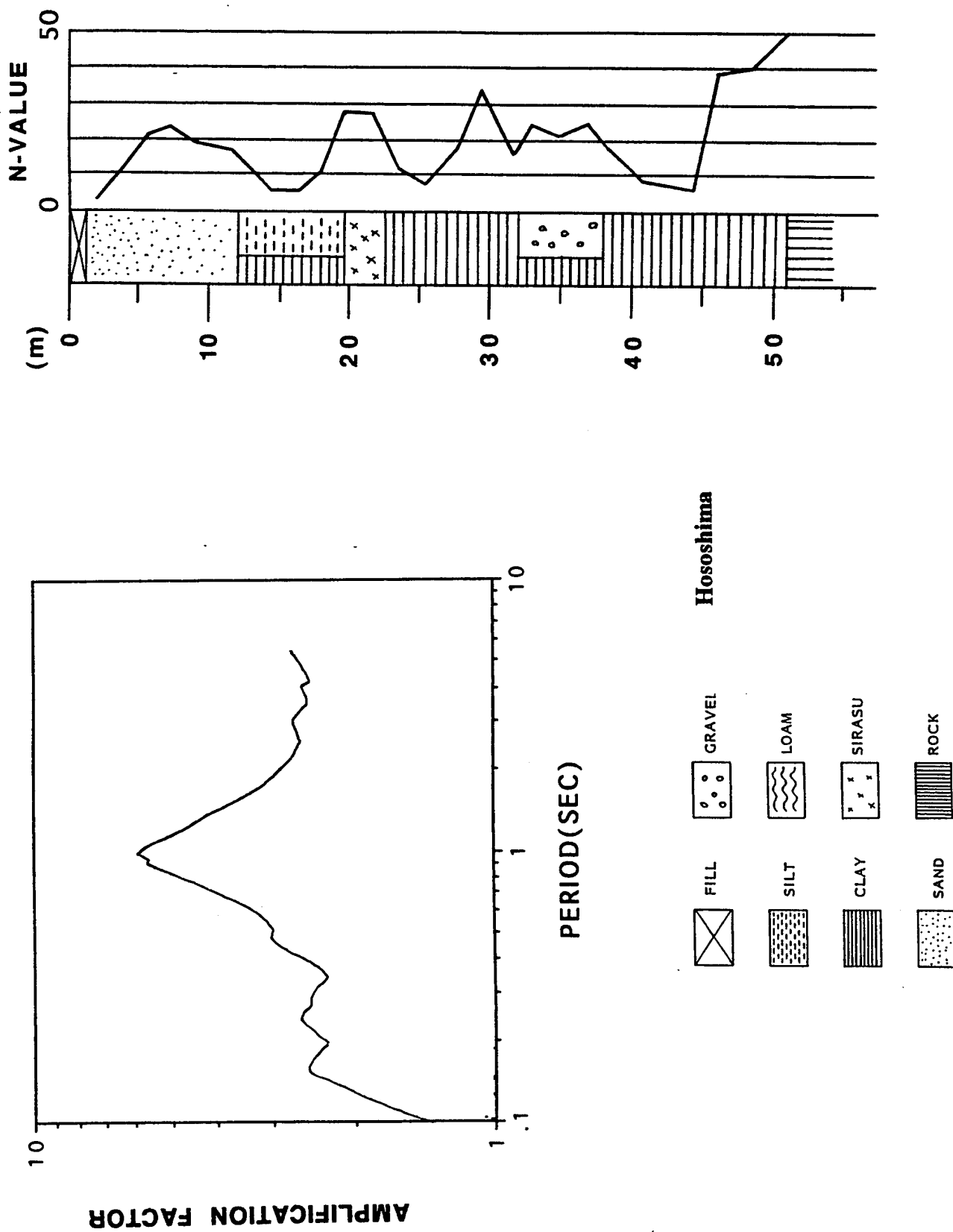
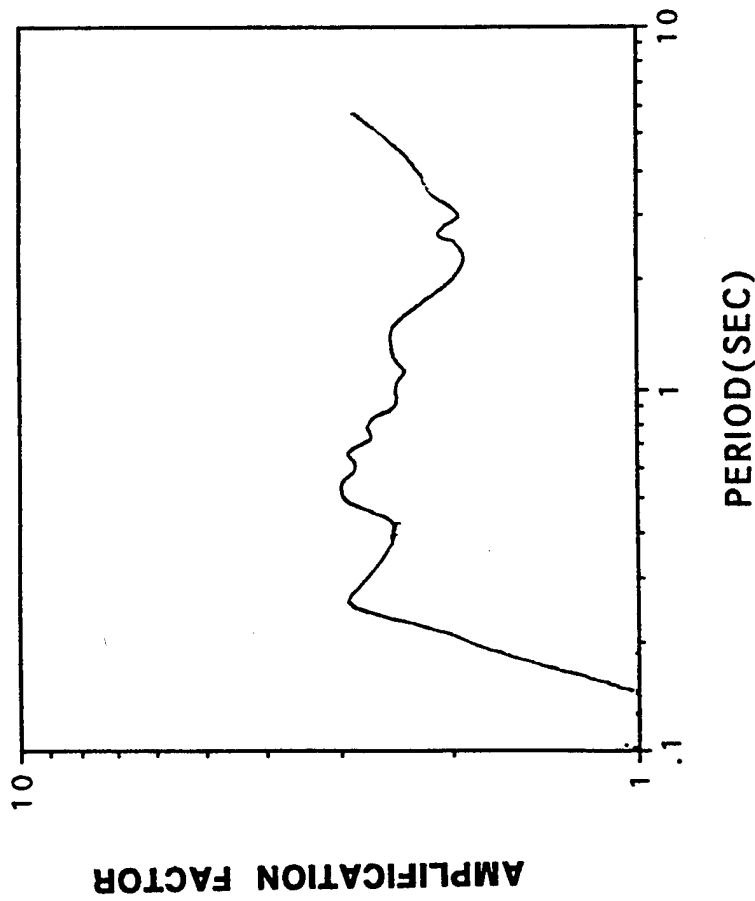
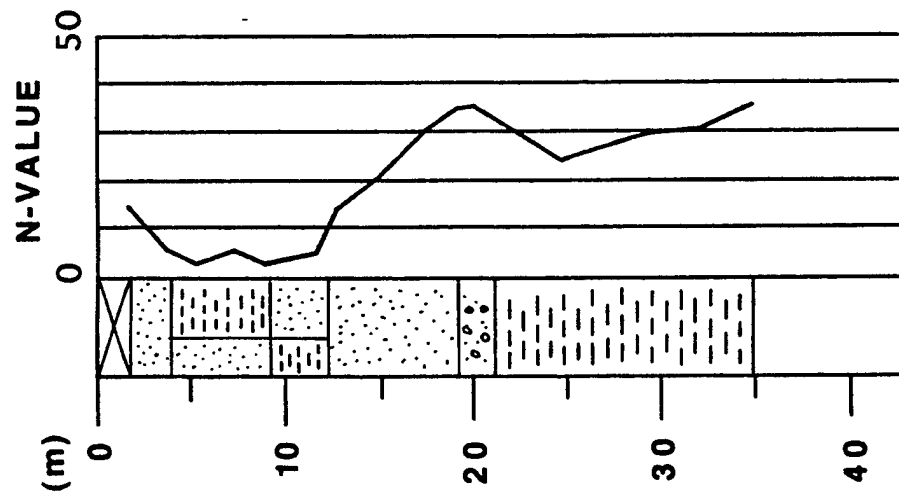


Figure 4.5a Amplification spectra, deep site, N 10 to 50, Hososhima



### Yamashita Hen

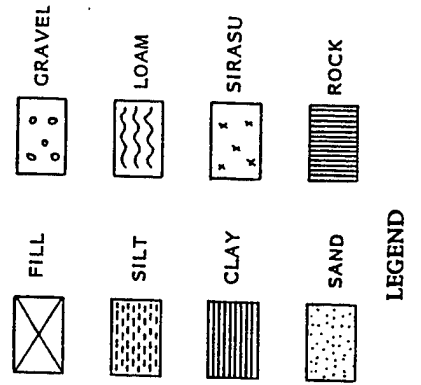
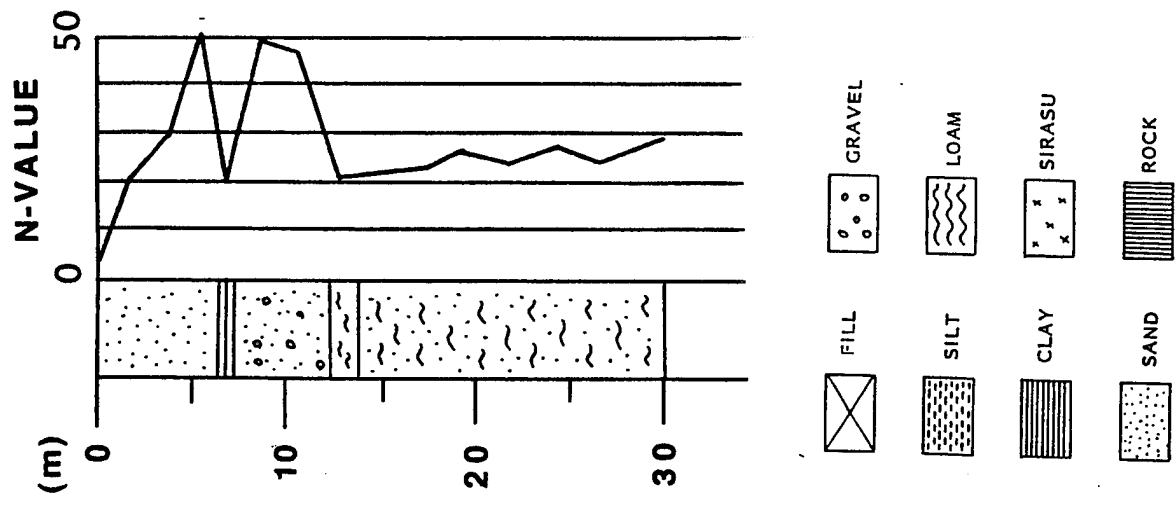
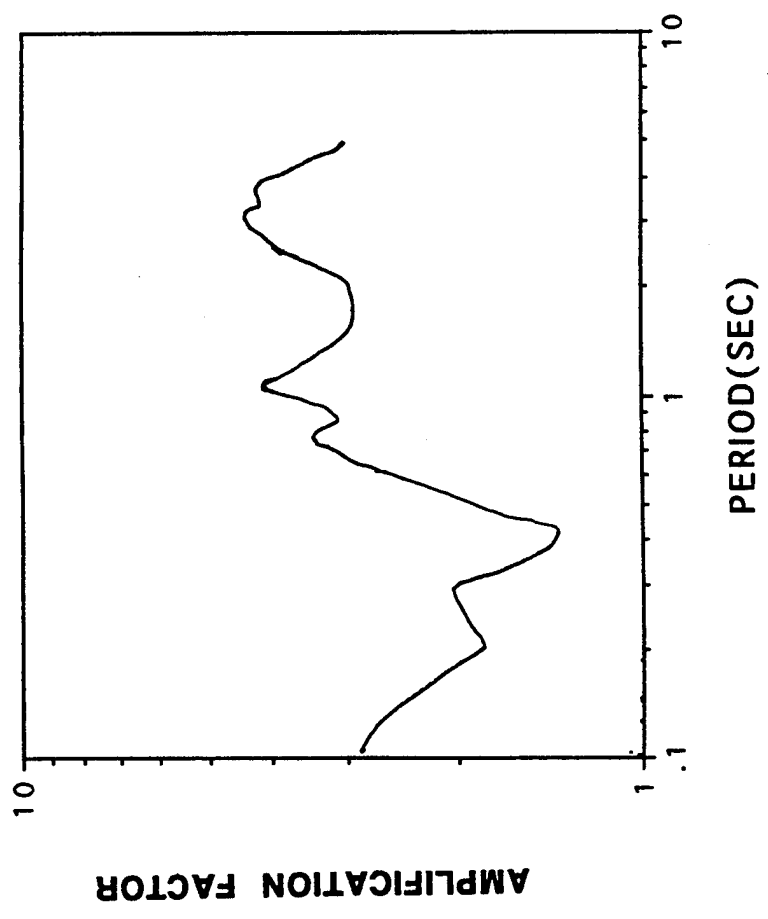


Figure 4.5b Amplification spectra, deep site, N 10 to 50, Yamashita Hen

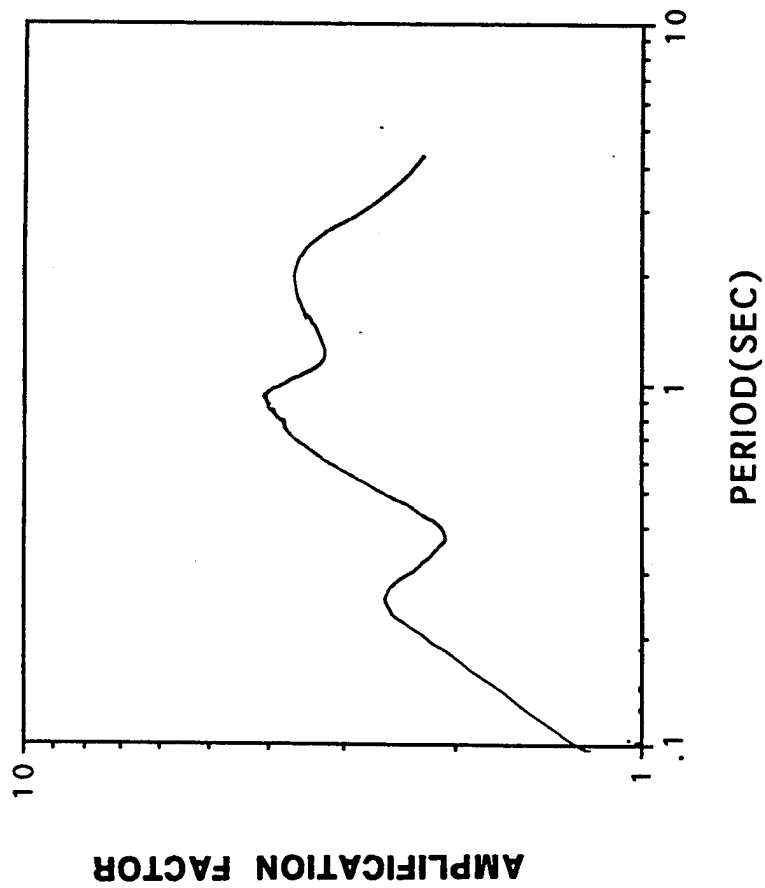


LEGEND

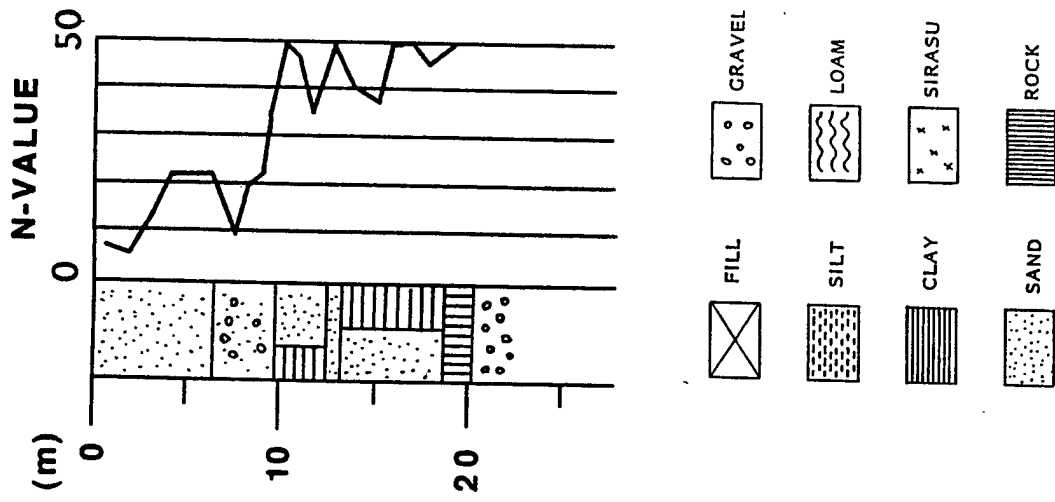


Tomakomai

Figure 4.5c Amplification spectra, deep site, N 10 to 50, Tomakomai

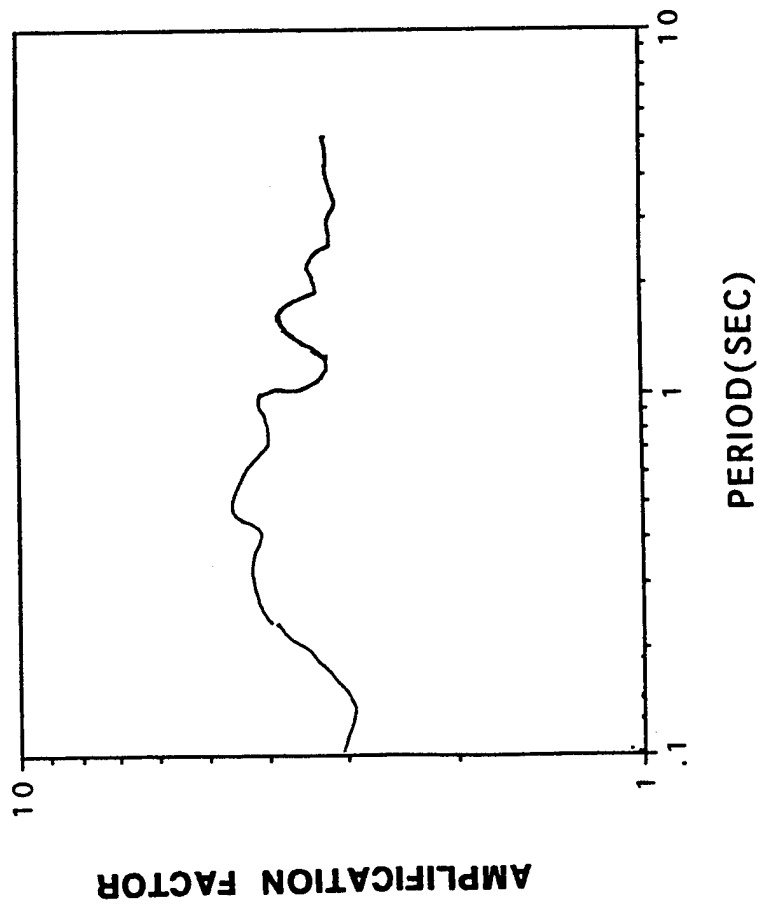


**Hachinohe**



**LEGEND**

**Figure 4.5d Amplification spectra, deep site, N 10 to 50, Hachinohe**



**Murooran**

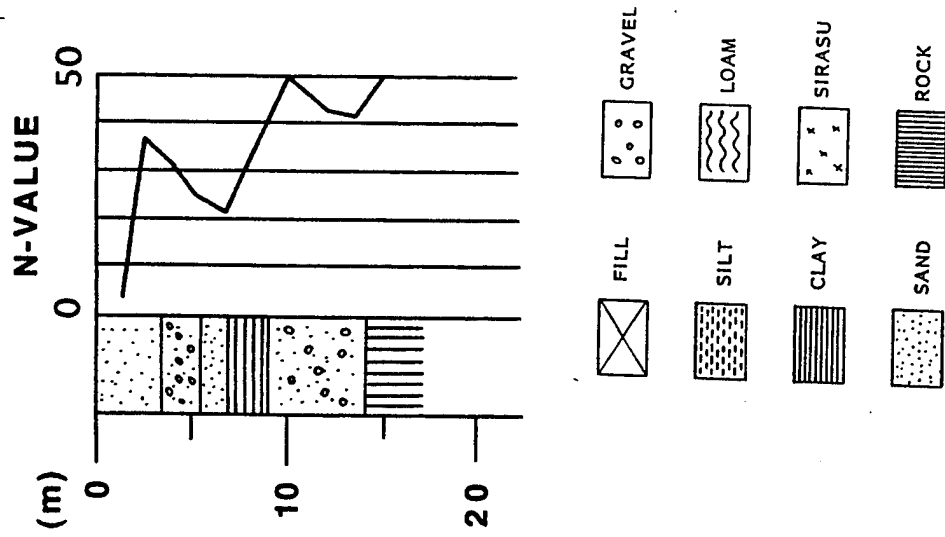
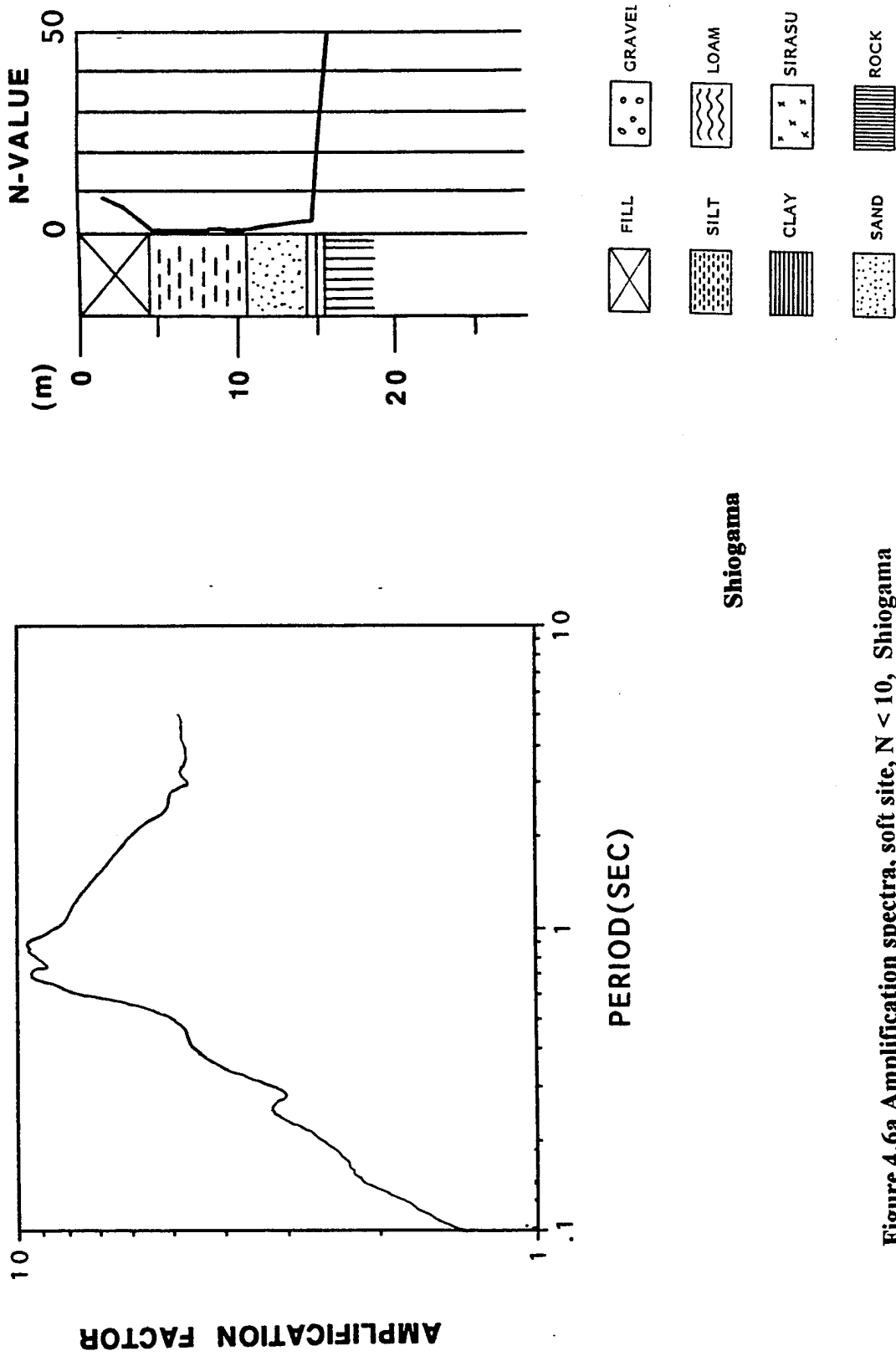


**Figure 4.5e Amplification spectra, deep site, N 10 to 50, Murooran**

**LEGEND**



Shiogama

Figure 4.6a Amplification spectra, soft site,  $N < 10$ , Shiogama



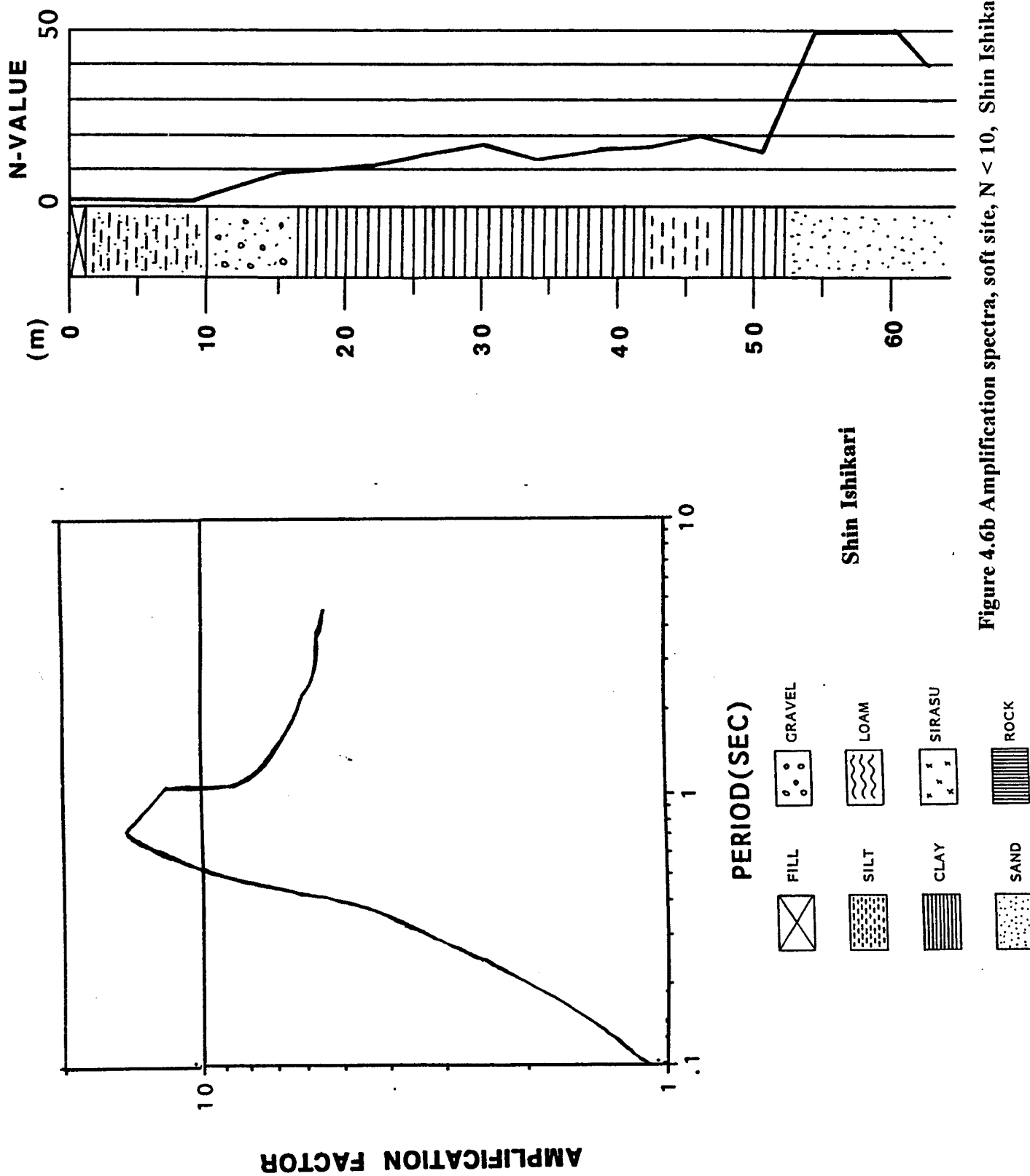
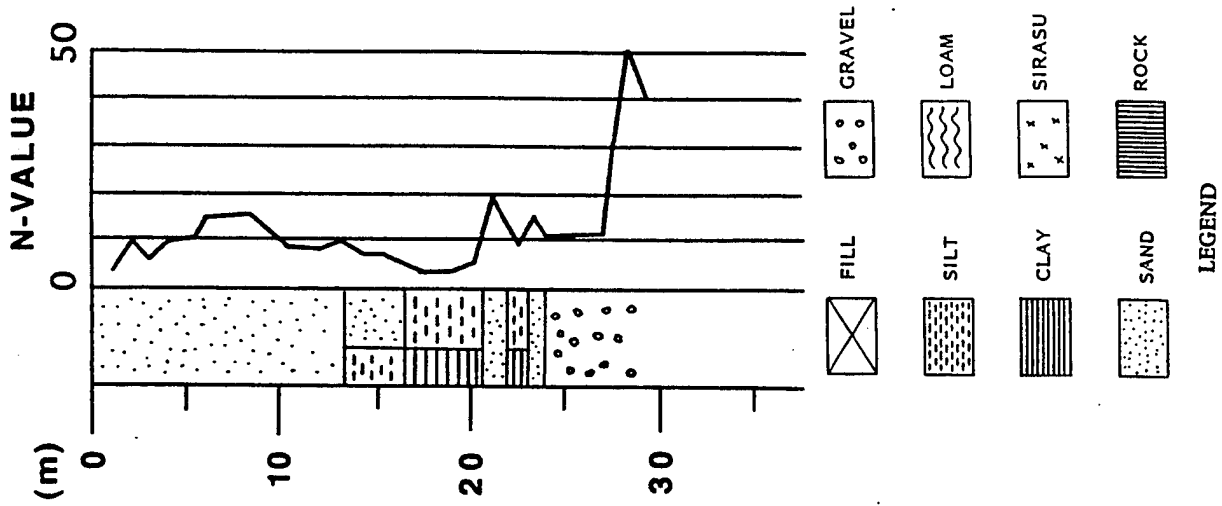
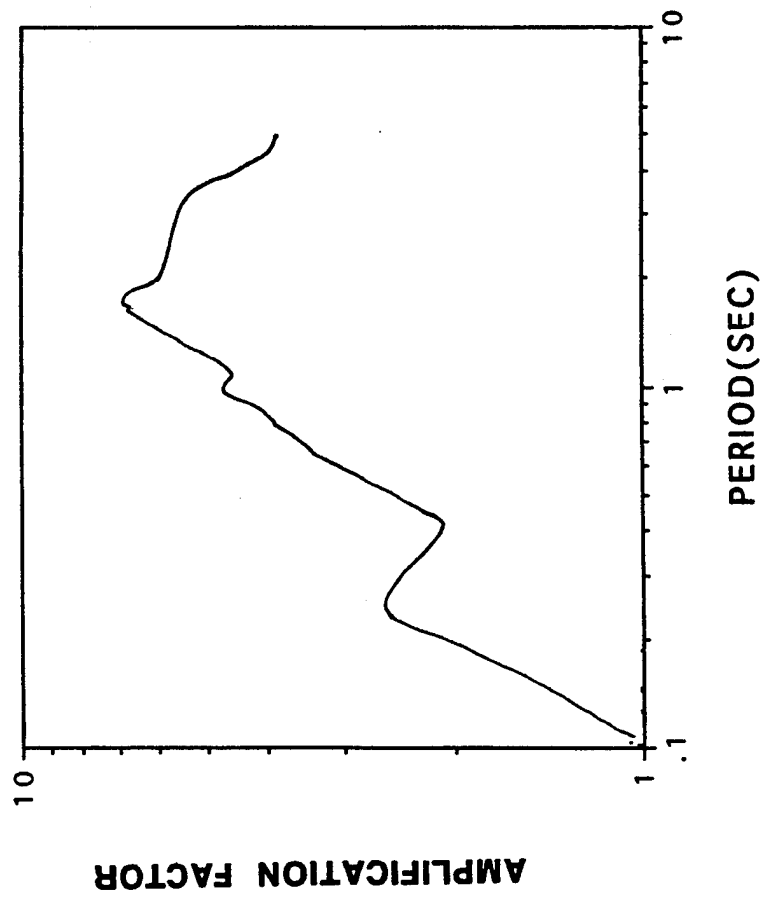


Figure 4.6b Amplification spectra, soft site,  $N < 10$ , Shin Ishikari



Aomori

Figure 4.6c Amplification spectra, soft site,  $N < 10$ , Aomori

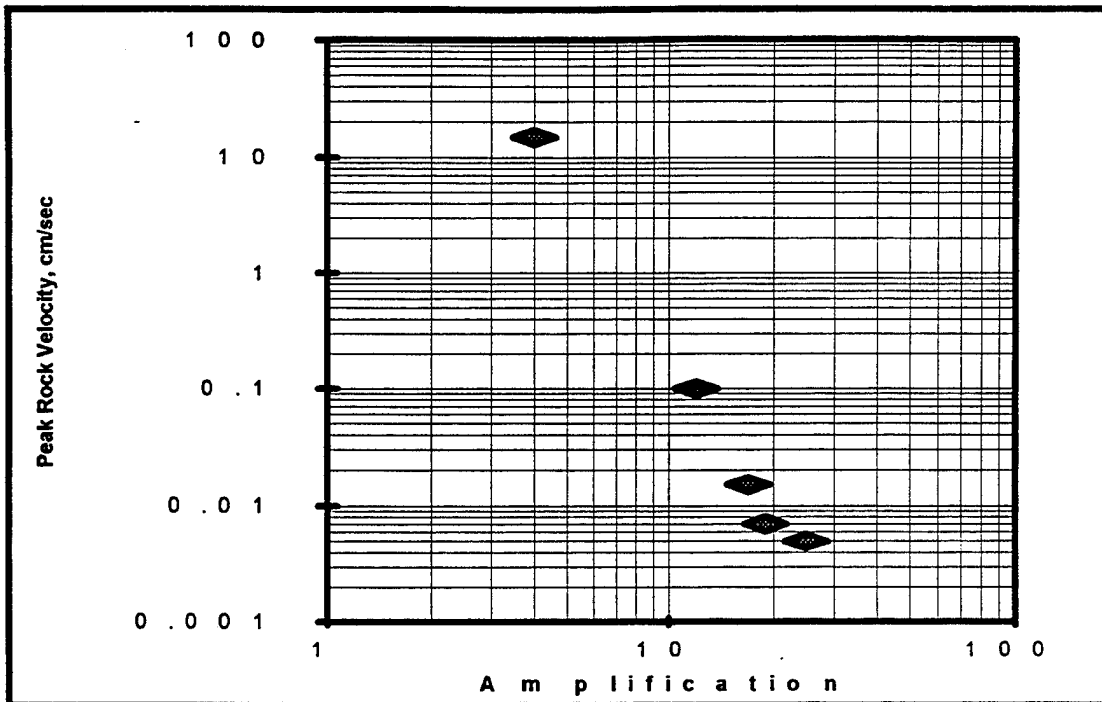


Figure 4.7 Amplification as function of peak velocity  
For Treasure Island Site

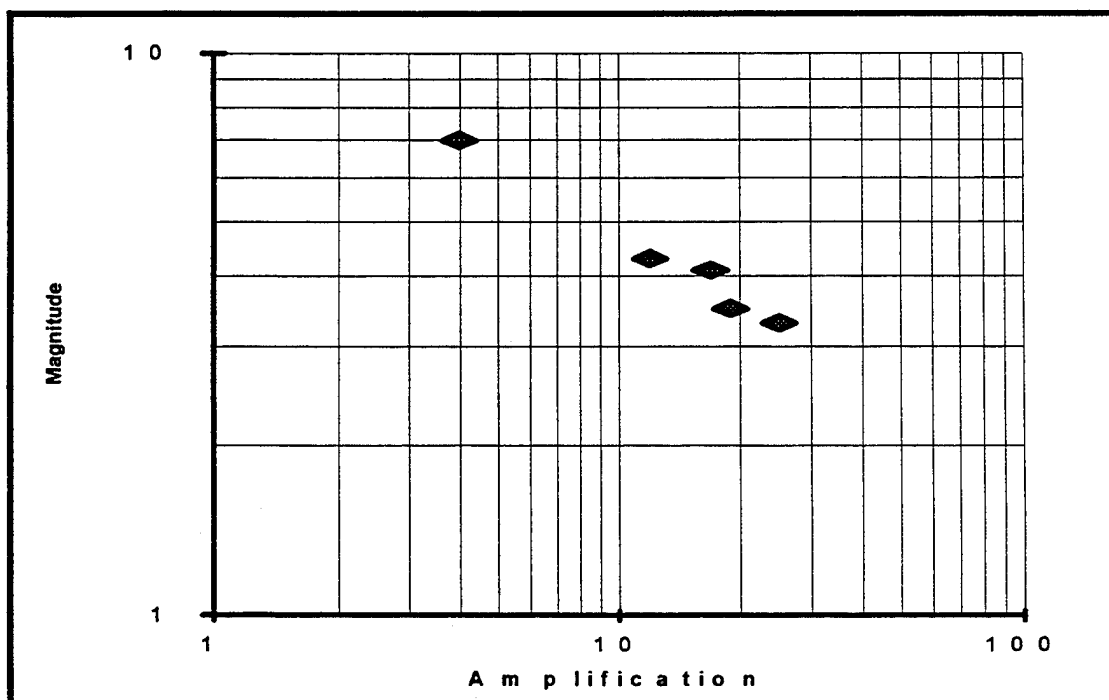


Figure 4.8 Amplification as function of magnitude  
for Treasure island Site.

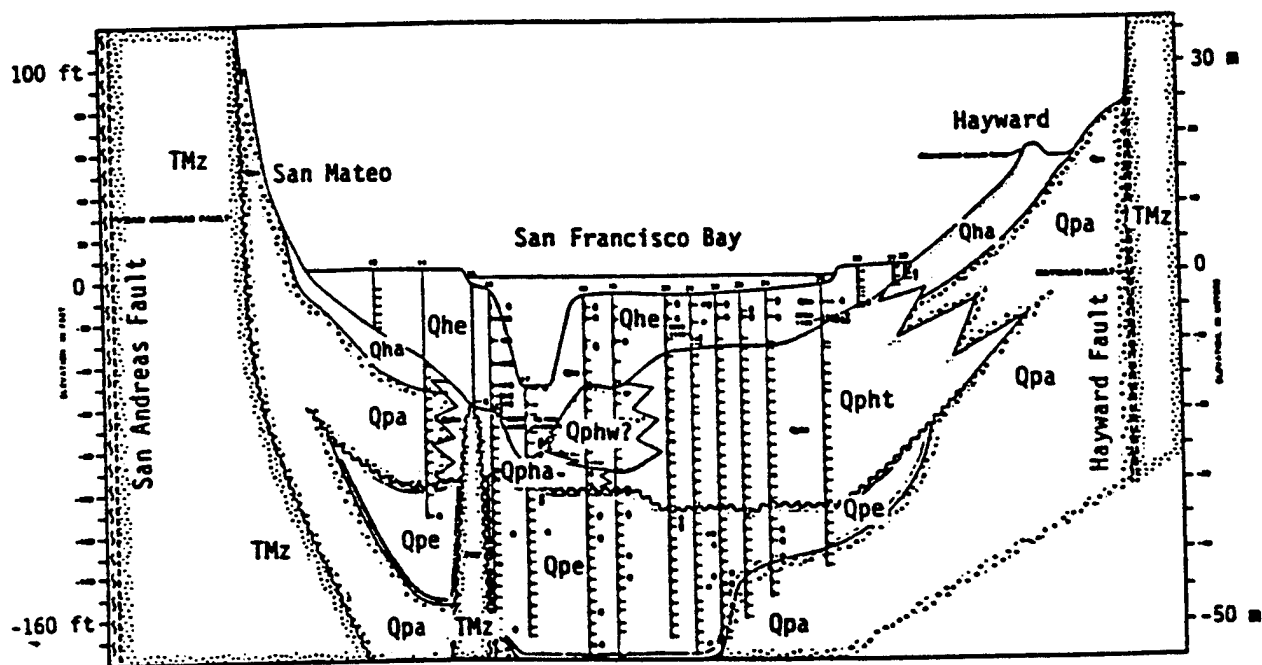
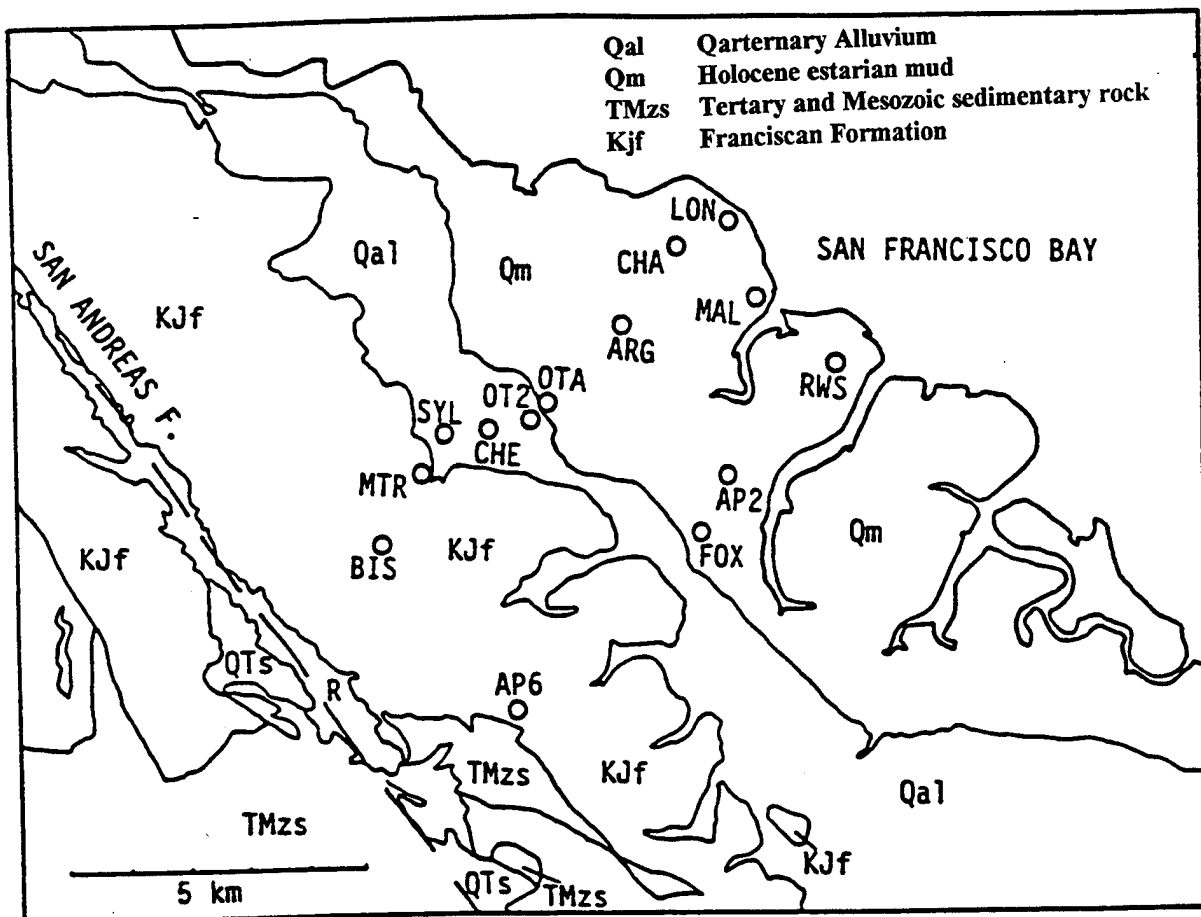


Figure 4.9 San Francisco Bay geology, after Akamatsu

Spectral Amplification Ratio

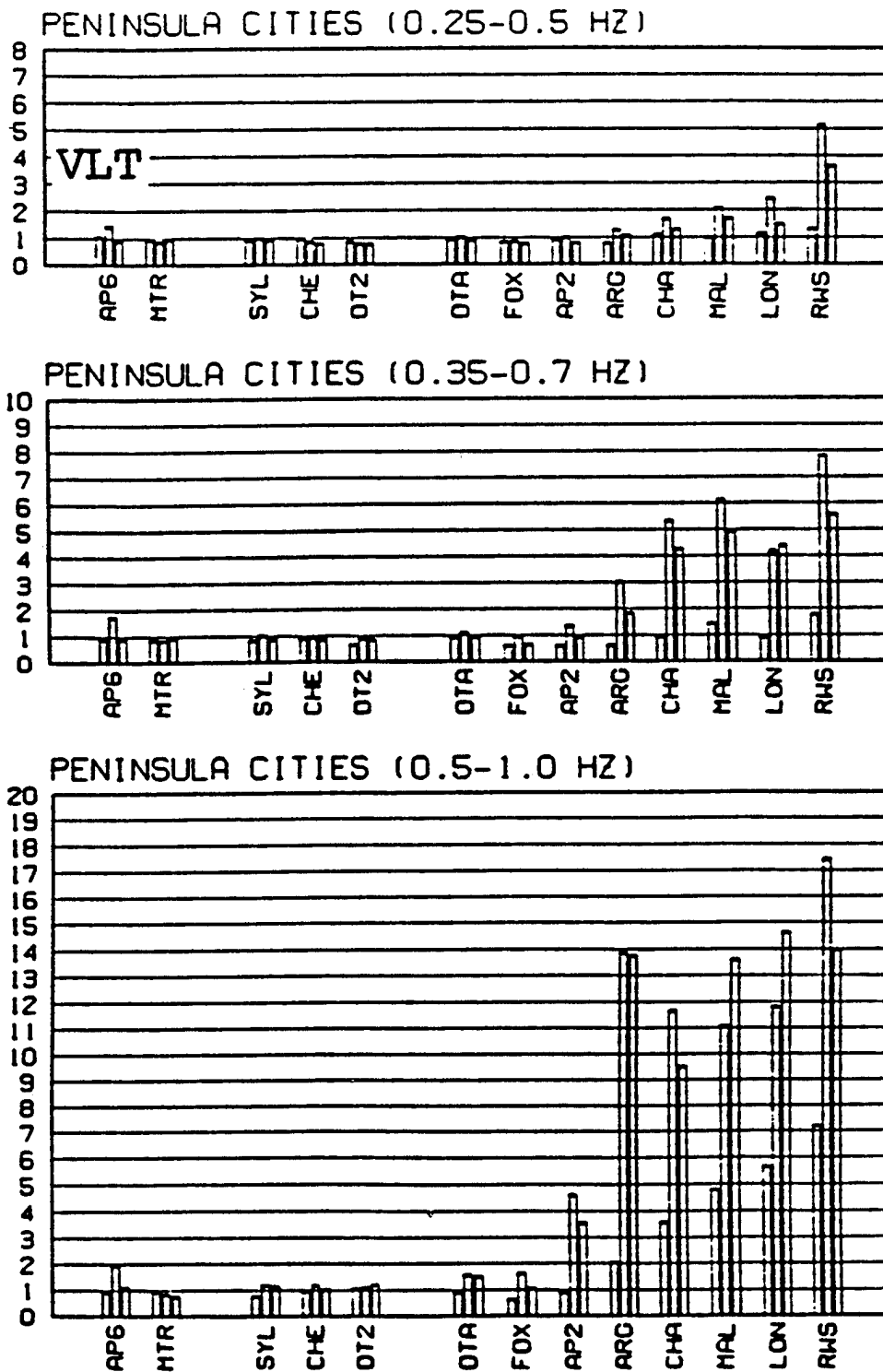


Figure 4.10 Spectral ratios for various sites, after Akamatsu

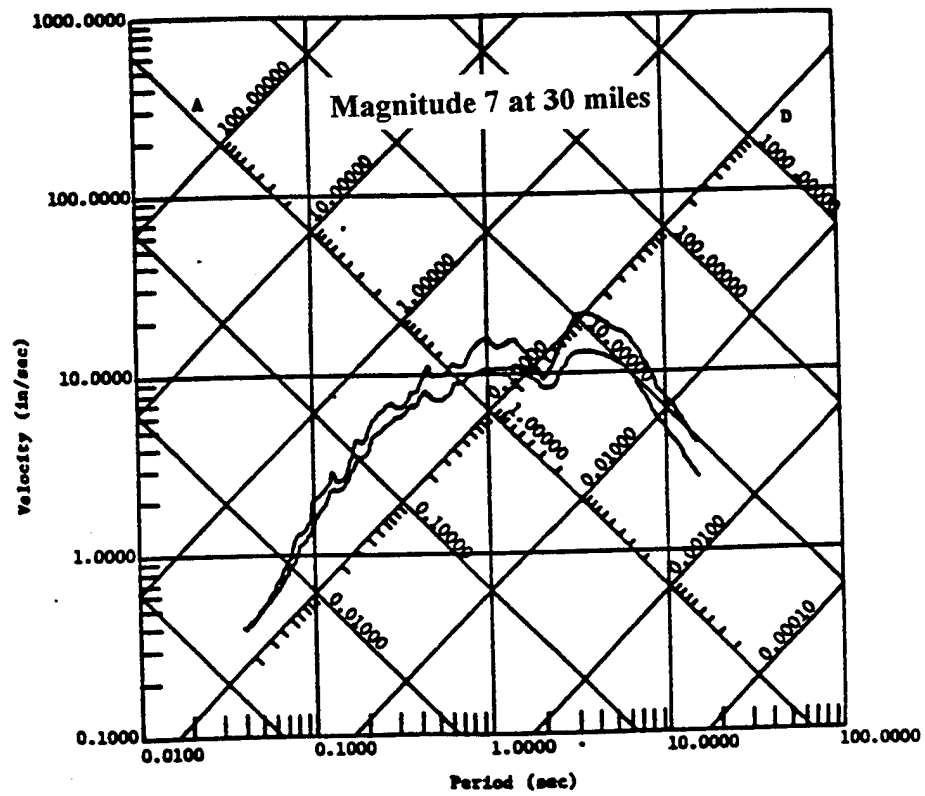
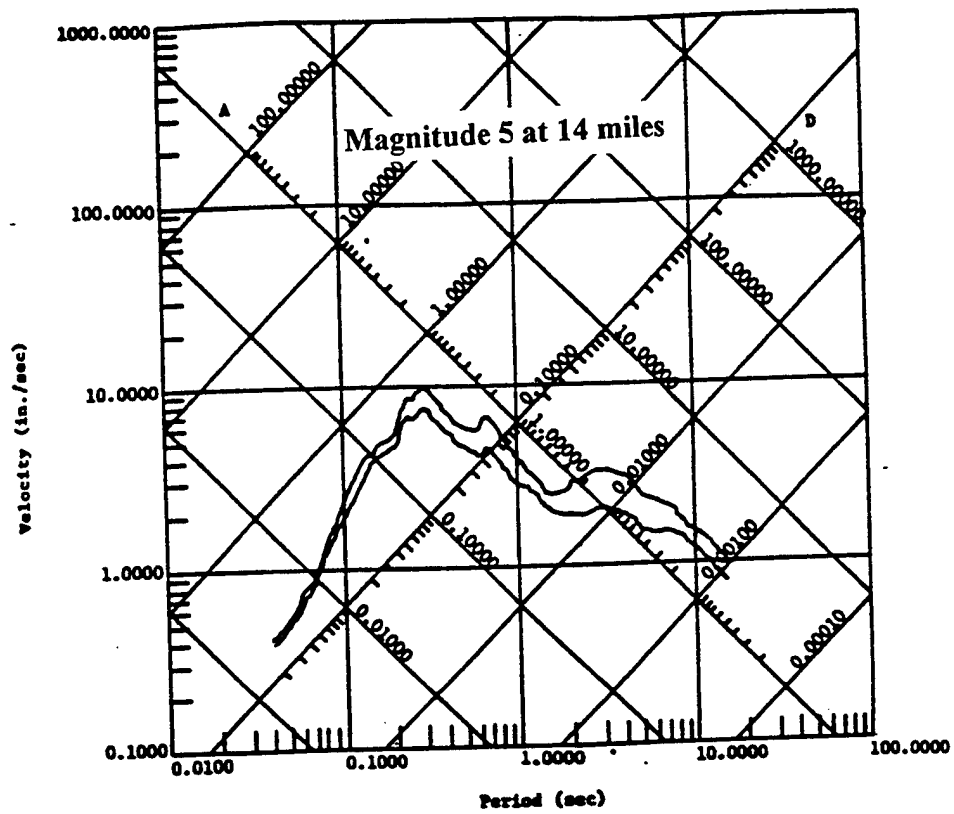


Figure 4.11. Comparison of spectra for Magnitude 5 event at 14 miles with a magnitude 7 event at 30 miles, both producing 0.15 g site acceleration.

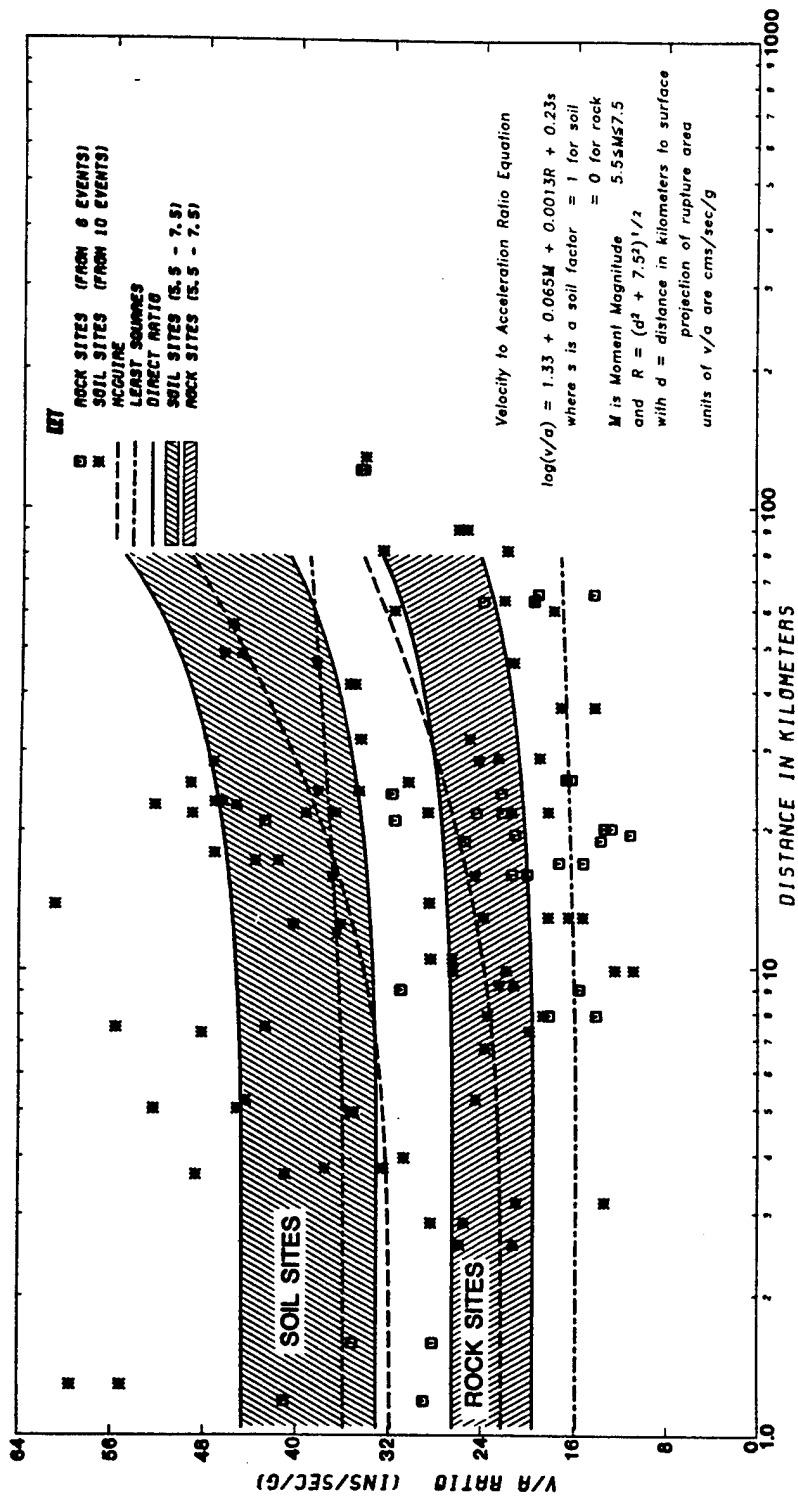


Figure 4.12. Velocity acceleration ratio, after Donovan (1983).

## **CHAPTER 5 PORT HUENEME PROGRAM OF INVESTIGATION**

### **Introduction**

Previous chapters discussed the use of microtremors as a tool to assist in prediction of ground motion amplification and microzonation. This chapter will discuss tests conducted in the Port Hueneme area to investigate the effects of geology, reference site selection and nonlinearity of response. Understanding the regional geology is fundamental to selection of an appropriate reference site and correct interpretation of the microseism results. The following sections will discuss the region and the series of microseism measurements performed.

### **Geology of the Oxnard Plain**

The following section is based directly on California Mines and Geology Open File report 76-5 and Majors Engineering (1993). The Oxnard Plain is in the southwest portion of the Ventura Basin, a part of the Transverse Range Geomorphic Province. The area is a structural feature formed by tectonic compression and consists of a synclinal basin with a substantial depth of recent alluvium overlying older rock. It extends inland from the coast along the northwestern edge of the Santa Monica Mountains, merging into the Las Posas and Pleasant valleys, and abuts the Camarillo Hills and South Mountain. It is a flat alluvial area rising in elevation from sea level to about 100 feet (30 m). "The geology underlying the Oxnard Plain are nearly 45,000 feet (14,000 m) thick consisting of Upper Cretaceous, Tertiary and Quaternary age components which have been deposited on a pre-Upper Cretaceous base of igneous and/or metamorphic rocks. The sedimentary measures are largely of marine origin with locally abundant volcanic and continental deposits." Figure 5.1 shows the geologic time scale, CDMG (1969). The Oxnard Plain represents an ancient delta of the Santa Clara River and was formed at the end of the last glacial epoch which resulted in the surface sediments being interlayered sands, silts and clays. The San Pedro Formation of Lower Pleistocene age is encountered at a depth of approximately 400 feet (120 m). Igneous and metamorphic rock are believed to be at depths of 6000 feet (1800 m) or more.

The Quaternary sediments underlying the Oxnard Plain are about 3,400 feet (1,000 m) thick in the area near the Naval Construction Battalion Center (NCBC), Port Hueneme. The youngest of the Quaternary sediments are composed of loosely to poorly consolidated Holocene (recent less than 10,000 years old) materials deposited during the post-glacial period of rising sea level and include marine, lagoonal, lacustrine, fluvial-flood plain, deltaic and eolian environments. These materials consist of sand, gravel silt, clay, mudstone, local regions of cobbles and boulders, and occasional regions of lenses of peat, carbonaceous material and sea shells. Figure 5.2 shows the southern end of the Oxnard Plain showing contours of depth of Holocene sediments and areas where peat or similar vegetal material may exist. Figure 5.3 shows the NCBC and a geologic description. Figure 5.4 shows surface soil classification. Figure 5.5 shows the geologic cross section through Port Hueneme.



As a sedimentary rock becomes older and more deeply buried it becomes more dense and less subject to ground motion amplification. Figure 5.6 shows the local geology for the closest rock outcrop area. The CDMG (1976) categorized the geology in terms of age of deposit. Category A consists of landslides, Category B represents younger alluvium, Category C older alluvium, Category D includes poorly lithified and slightly older formations, Category E includes moderately lithified slightly older formations and Category F represents the firmest or most dense rock. Within this region it includes volcanic rocks, igneous-metamorphic rock and usually the oldest and firmest and densest sedimentary rocks.

### **Soil Conditions**

CDMG (1976) developed boring logs shown in Figure 5.7. The soils at the Naval Construction Battalion Center are composed of fill over mostly sand with clay interbeds and is interpreted as alluvium of Holocene age deposited at sea level in a stream channel or lagoonal setting. The water table is at a depth of about 6 feet. Figure 5.8 shows one site used as part of this investigation, the proposed location of a new Naval Facility Engineering Service Center (NFESC) building; Figure 5.9 shows locations of boring logs supporting that project and Figure 5.10 shows a typical log. Figure 5.11 shows an idealized soil profile constructed from the boring log data. Figures 5.8, 5.9, and 5.10 are adapted from Majors Engineering (1993). Figure 5.12 shows the NFESC Building 560 site and Figure 5.13 presents a typical boring log from T.K Engineering (1986).

### **Microseism Measurements**

Several rock reference sites were available as follows:

- Mugu Rock A sea level site on the coast shown in Figure 5.6 having lower Miocene Vaqueros Formation sandstone, claystone and siltstone overlain by a very thin layer of fill. The site is classified a DE transition zone
- Laguna Peak A mountain top location shown in Figure 5.6 having middle Miocene Topanga Formation sandstone siltstone and conglomerate overlain by a thin layer of alluvial deposit. The site is classified a DE transition zone
- Camarillo Hospital A low level site shown on Figure 5.6 having middle Miocene Conejo Volcanics and classified as F overlain by a shallow alluvial deposit.

All of these reference sites qualify for designation as rock sites with the first two having a composition similar to the San Pedro Formation beneath the Oxnard Plain.

A number of soil sites were selected in the NFESC compound and at the Naval Construction Battalion Center for array measurements, the results of which will be presented in following sections.. Building 582, a one story prefabricated metal building was selected as the location for (relatively) long term reference measurements.

To evaluate the fluctuation of microseism activity over a period of time, instruments were installed at Laguna Peak and at NFESC Building 582. Laguna Peak is a Navy controlled site with accessibility to facilitate long term measurements. The appendix discusses the instrumentation and data recording procedures. The instruments were set to record the East-West component at a sampling rate of 20 Hz sampling frequency for a period of 5 minutes every 2 hours for a several day period. A typical time history record is shown in Figure 5.14. Figures 5.15 and 16 show the fluctuation of the record with time for Fourier spectra averaged between the period ranges of 0.5 to 0.7 seconds, Figure 5.15 and 2.0 to 4.0 seconds, Figure 5.16. The data reduction procedures are covered in the appendix. The data in Figures 5.15 and 16 show that there is daily fluctuation in the level of signal as would be expected. It is important to note that the spectral amplitude of both sites increases and decreases in unison. This demonstrates the concept of stability of the spectral ratio between both sites. It should be noted that the fluctuation in signal amplitude is gradual. It is reasonable to assume stationarity of the process over a period of minutes to perhaps as much as several hours, but there are significant fluctuations over longer periods.

### **Rock - Soil Transfer Function**

To evaluate the three possible reference sites a series of pairs of measurements were made between NFESC Building 582, a soil site shown in Figure 5.12 and each of the three above cited rock sites. Five sets of three component measurements were made at hourly intervals to evaluate the transfer functions between the following pairs of soil site to rock reference site:

NFESC Bldg. 582 - Mugu Rock

NFESC Bldg. 582 - Laguna Peak

NFESC Bldg. 582 - Camarillo Hospital

Figures 5.17, 5.18 and 5.19 give the average Fourier spectra for each location pair and the spectral ratio. All of the records exhibit the strong predominance of ocean induced components at periods of 7 and 14 seconds. The North - South component tends to be larger than the East - West component which is larger than the vertical. Since the measurements were made on different days and the source activity level fluctuates, conclusions should not be drawn directly from the Fourier spectra in terms of relative levels of activity but rather from spectral ratios. Spectral ratios are greatest for the Mugu Rock site with the other two about the same indicating that relative to NFESC Building 582 Mugu Rock shows lowest signal level. One might have expected the volcanic rock at the Camarillo Hospital site to have been denser than the other two sites and have produced the highest spectral ratios. The NFESC soil site relative to each rock site exhibits high values of spectral amplification. These high levels of amplification are much higher than typical strong motion amplification levels and suggest nonlinear scaling effects.

## Topography Effects

The Laguna Peak site was chosen for further study as the main rock reference site. To evaluate the effect of the topography the Mugu Rock - Laguna Peak transfer function was evaluated. This would allow the soil site data to be reference to both Mugu Rock and Laguna Peak. Figure 5.20 give the Fourier spectra and spectral ratio between Laguna Peak and Mugu Rock. As noted in Chapter 4, a ratio of about 2 is to be expected for the effect of mountain topography based on the geometry. The horizontal component spectral ratios are on the order of 2 in the period range of 0.5 to 1 second and then approach 1 at higher periods. Both rock sites had relatively narrow bands of signal; computation of spectral ratios outside this band results in division of small numbers by small numbers and hence the spectral ratio in the region of low signal is prone to error. It may be concluded that the topographic effect of the mountain topography is relatively small and is quantified per Figure 5.20

## Array Measurements NFESC Site

To determine the spatial variation of amplification at the NFESC site, a series of measurements were made using Laguna Peak as the reference site. Figure 5.21 shows the 12 stations used in the measurement. Measurements were made for 5 minute duration at each station and all measurements were completed in about 4 hours. Figure 5.22 shows the Fourier spectra for each station; Figure 5.23 shows the Fourier spectra for the Laguna Peak reference site. Figure 5.24 gives the spectral ratios. Figure 5.25 shows contours of spectral ratio. It must be recognized that contour plots are an attempt to give a spatial representation of the variation of spectral ratio. The spectral ratio is a function of period and must be divided into bands for representation. There is subjectivity involved in the presentation of the data using contour plots. First the division of spectral ratio into bands is judgmental and second the representation of the data in each band varies in amplitude. One might choose to average the data within the band as shown in Figure 5.25 or perhaps to plot maxima for each period band. The reader should be aware that the contour plots have limitations and are only expressions of the data. Each spectral ratio is a unique complete transfer function which shows how one site responds relative to another. The spectral ratio contours are intended to facilitate location of soft spots where amplification is greatest.

From the contours it is noted that the NFESC site does have variation of  $\pm 15$  percent. This is not a major variation and would be expected at a waterfront site.

## Site Analysis

A one-dimensional wave propagation analysis was performed using the data from the boring logs which consisted of soil classification, dry density and blow count. The blow count data were used to estimate shear wave velocity. Figure 5.26 shows data point

from the US Army Waterways Experiment Station data base, Sykora (1989), relating blow counts to shear wave velocity for Holocene sands. Also plotted is the relationship derived by Ohta and Goto (1978) shown in solid line and a lower bound estimate of similar shape to the relationship. As the reader can see there is considerable uncertainty to estimating shear wave velocity from blow count data. Since laboratory test data is not available standard relationships correlating modulus attenuation with strain and damping with strain had to be used. The deepest boring logs available for the site and neighboring areas are less than 100 feet. It was initially estimated that the shear wave velocity reaches 2500 ft/sec (760 m/sec) at a depth of 250 feet (76 m). With all the assumptions made the analysis can be only an approximate calculation, but is typical of actual field investigation conditions. The soil profile based on boring log number 2 was used as the basis for a one-dimensional wave propagation analysis. The damping was estimated to be about 0.014 (1.4%) of critical based on the A3 station shown in Figure 5.24.a using the systems identification process discussed in Chapter 2 and shown in Figure 2.1. Material property-strain level iteration to produce material properties at earthquake effective strains was omitted since the low level of excitation effectively represented initial values. A microseism acceleration record recorded at site A3 was used as the input motion and assigned at the surface. The results are shown in Figure 5.27 and are noted to reproduce both the level of amplification and the fundamental period shown in Figure 5.24 for station A3.

The same profile was used for a nominal earthquake at 0.1g bedrock motion. Figure 5.28 shows the amplification a nominal 0.1g acceleration introduced at a depth of 250 feet. The site is seen to increase surface acceleration significantly. Figure 5.29 shows the spectral amplification from 250 feet (76 m) to the surface. Using lower bound estimates of shear wave velocity reduces the spectral amplification shown in Figure 5.28 by about 15 percent with only minor reduction in surface acceleration. Variation of the depth of the soil profile results in shifts in the location of the spectral peaks. It is noted that the effect of higher strain levels causes a slight shift of the fundamental period of the site from about 0.5 to about 0.66 and a reduction in amplification from about 48 to about 12. It is again noted that nonlinear scaling effects exist at soft sites between microseism levels of excitation and strong motion levels from earthquakes.

The nonlinear effects noted will be discussed in depth in Chapter 7. For engineering application the contours shown in Figure 5.25 are normalized and used in conjunction with the 1-dimensional analysis. Figure 5.30 shows the normalized contours, normalized with respect to site A3. This procedure allows the microseism measurements to be used to extend the calculations to augment the lack of spatial data. We are able using the systems identification process to adjust site profile characteristics to agree with measured period of response and then extend the range of that data to cover the measured stations. The computed surface acceleration from the full scale earthquake serves as the basis motion to be used with the normalized contours. The procedure extends data from the single boring log location across the whole site and calibrates the computed response to measured data. A transfer function can be constructed by dividing the spectral ratio of any site by that of site A3 chosen as the reference because it had boring log data and was

used for the calculation. Figure 5.31 shows the transfer function of site A4 relative to Laguna Peak divided by the spectral ratio of site A3 relative to Laguna Peak to produce a transfer function of A4/A3. Figure 5.31 also illustrates how the earthquake motion  $x(\tau)$  of  $x(f)$  computed at site A3 by the one-dimensional wave propagation analysis can be used to produce earthquake motion,  $y(\tau)$  or  $y(f)$ , at site A4.

### **Array Measurements NCBC Site**

A series of measurements were made at the NCBC base as a demonstration of the microzonation concept. The measurements were made over a period of 2 days. The first day the outer stations D, E, and F were measured and the second day the inner stations A, B, and C were measured. Figure 5.32 shows a map of NCBC and the location of measurement stations. Figure 5.33 shows the spectral ratios measured at each station using Laguna Peak as the reference site. Figure 5.34 shows the computed results of a 1-dimensional analysis of the site using the boring log at station A1 in Figure 5.32 with a microseism acceleration as the acceleration record. Comparison of the peak spectra ratio in Figure 5.34 with the measured spectral ratio for station A1 in Figure 5.33 shows close agreement. Again as noted above, nonlinear effects cause the microseism amplification for the soft site to be high. Figure 5.35 gives the results of excitation of the profile by an earthquake record of 0.1g nominal bedrock acceleration. Figure 5.36 shows the computed site response with a surface acceleration of 0.46 and a 0.1g base motion. There is a small increase in the site natural period caused by strain dependent material properties and the higher excitation levels of strong motion. The upper 50 feet exhibits significant amplification with motions here slightly higher than at the NFESC site discussed above and the NCBC site exhibits a deeper alluvial profile.

Contours of spectral ratio are shown in Figure 5.37 and are presented again normalized to station A1 or E1 in Figure 5.38. Note the previous discussion on the subjective nature of contour results. For engineering applications Figure 5.36 used in conjunction with Figure 5.38 gives a significant extension of information.

### **Nakamura Method**

The Nakamura procedure discussed in Chapter 2 was tried at the NFESC site. Vertical measurements were made at the same time as horizontal measurements. The vertical measurements were used as the reference measurement. Figure 5.39 shows the results. The procedure produces amplification ratios between 1 and 4. The procedure fails to cancel the source input and exhibits large components in the 7 second range. It would appear that the procedure has limited value and is not applicable to soft waterfront sites.

## References

California Division of Mines and Geology (1969) Special Report 97 " Geologic and engineering aspects of San Francisco Bay fill."

California Division of Mines and Geology (1976) DMG Open File Report 76-5 " Seismic hazards study of Ventura County, California".

Majors Engineering (1993) "Site investigation for Environmental Research Services Center FY1994 BRAC Project P-012 at Naval Construction Battalion Center, Port Hueneme, California" for Western Division Naval Facilities Engineering Command, San Bruno.

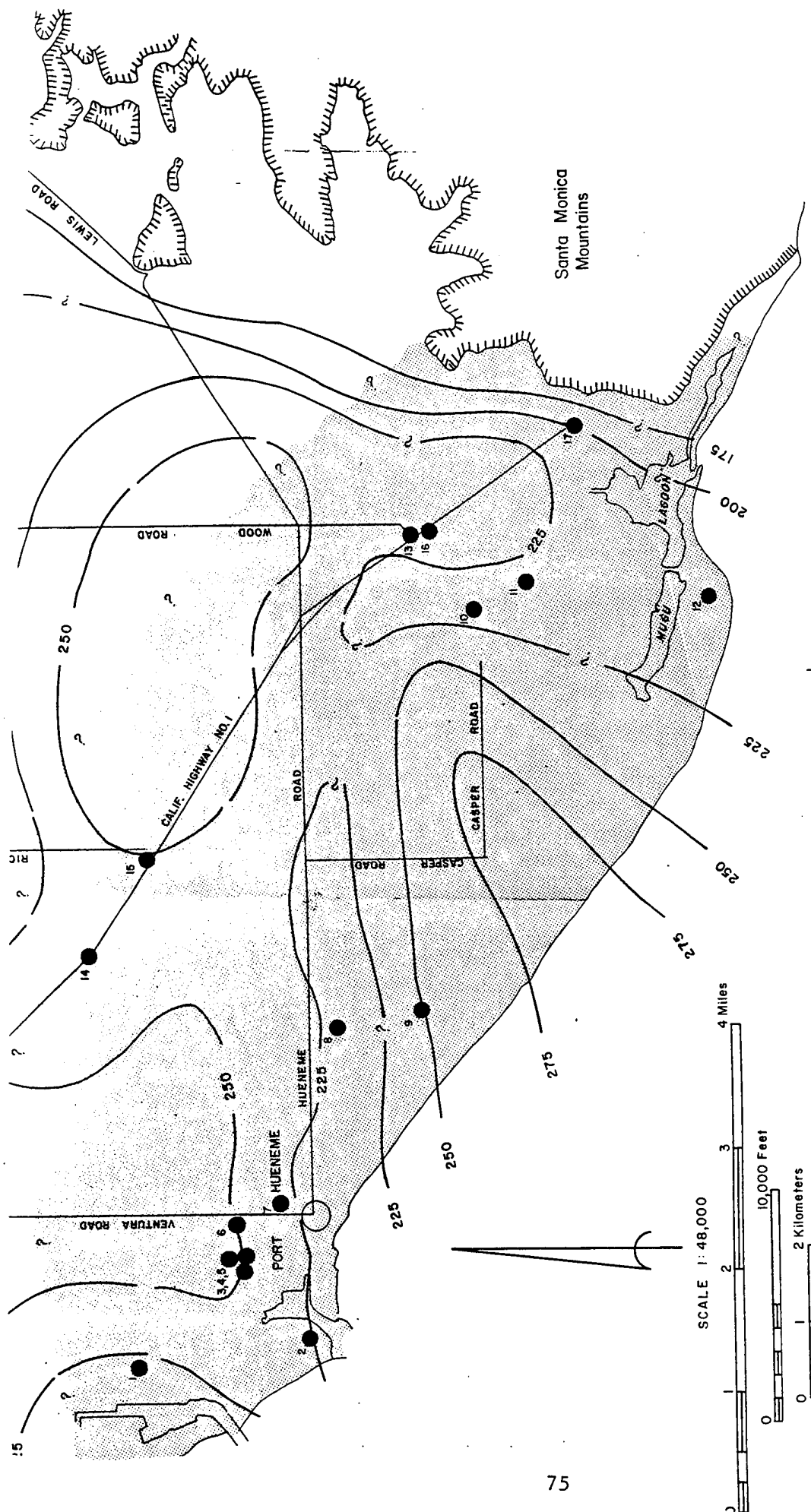
Ohata, Y and N. Goto (1978) "Estimates of S wave velocity in terms of characteristic indices of soil" Butsuri-Tanku, 29:34-41

Sykoa, David (1989) "Evaluation of a method to estimate the soil modulus coefficient,  $K_2$  and shear modulus" Proceedings 25th Symposium on Engineering Geology and Geotechnical Engineering, Reno Nevada, March 1989.

T. K. Engineering (1986) Preliminary Soils Engineering Investigation, unpublished report.

Eras	Approximate age (in millions of years)	Subdivisions	Approximate duration (in millions of years)
Quaternary	.01	Recent	.01
		Pleistocene	3
		Pliocene	9
Tertiary	12	Miocene	13
	25	Oligocene	15
	40	Eocene	20
	60	Paleocene	10
	70	Cretaceous	65
	135	Jurassic	45
	180	Triassic	45
Mesozoic	225	Permian	45
	270	Carboniferous	80
	350	Devonian	50
	400	Silurian	40
	440	Ordovician	60
	500	Cambrian	100
	600		
Paleozoic			
Precambrian		Worldwide subdivisions not well established	2800 +
Oldest rock dated 3.5 billion Age of the earth 4.5 billion			

**Figure 5.1 Geologic Time, from CDMG (1969)**



# LEGEND

- Approximate area indicated to contain peat or similar vegetal material within Holocene sediments.
- Approximate location of water well or highway bridge
- Approximate thickness, in feet, of Holocene sediments.
- Areas of exposure of pre-Holocene rocks including Pleistocene sediments.

Figure 5.2 Contours of Holocene sediments from CDMG (1976)





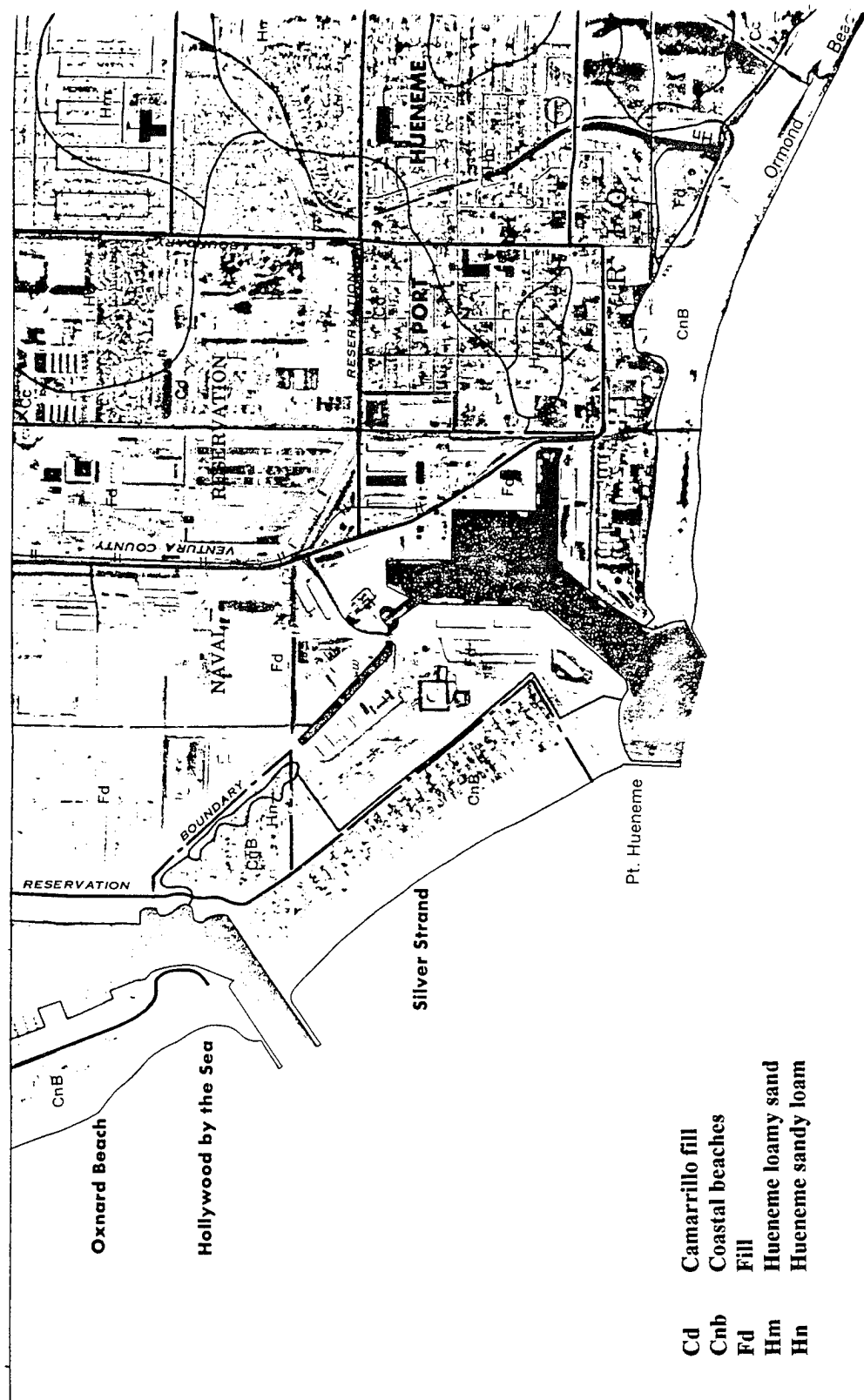


Figure 5.4 Port Hueneme surface soils from CDMG (1969)



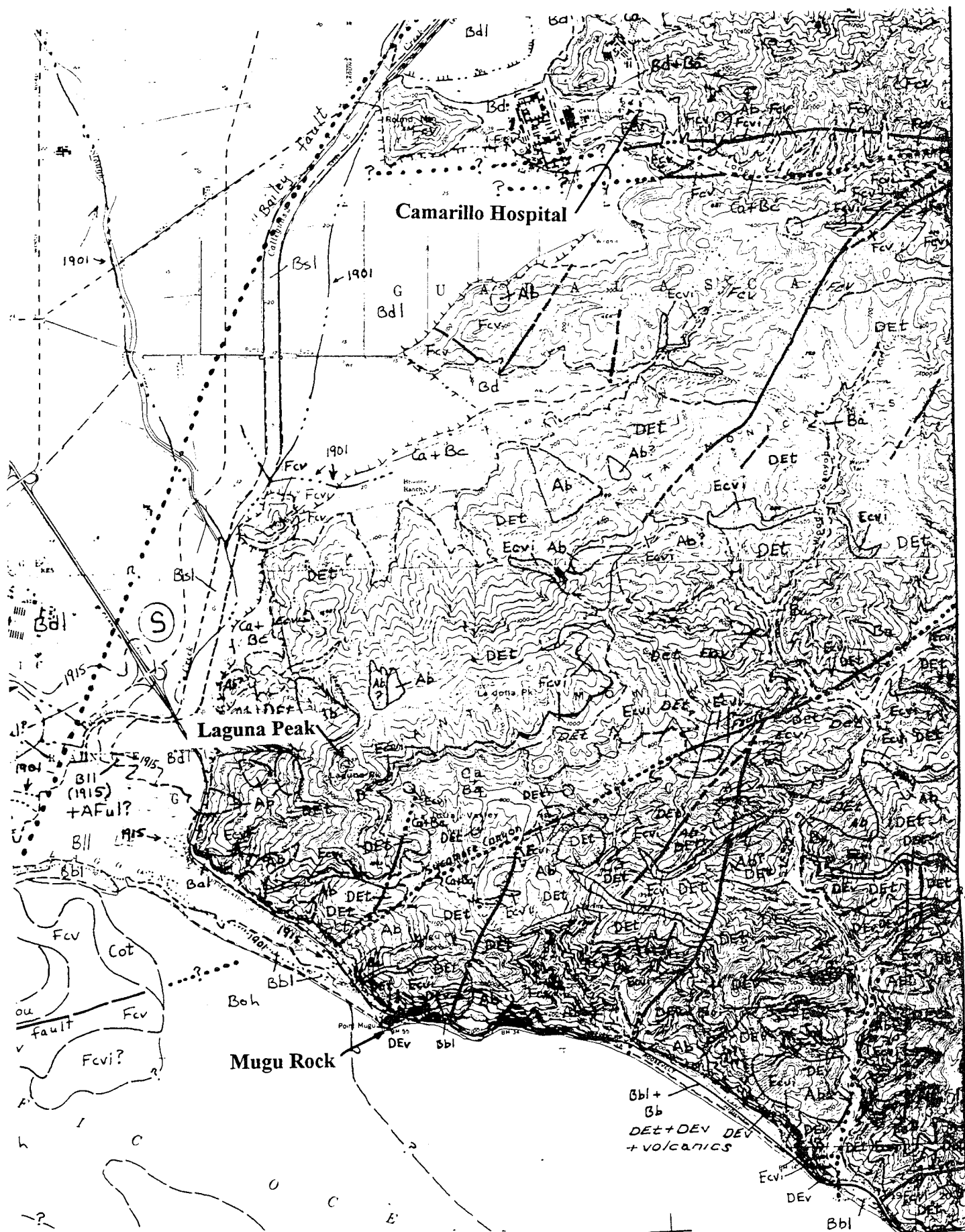


Figure 5.6 Reference site geology from CDMG (1976)

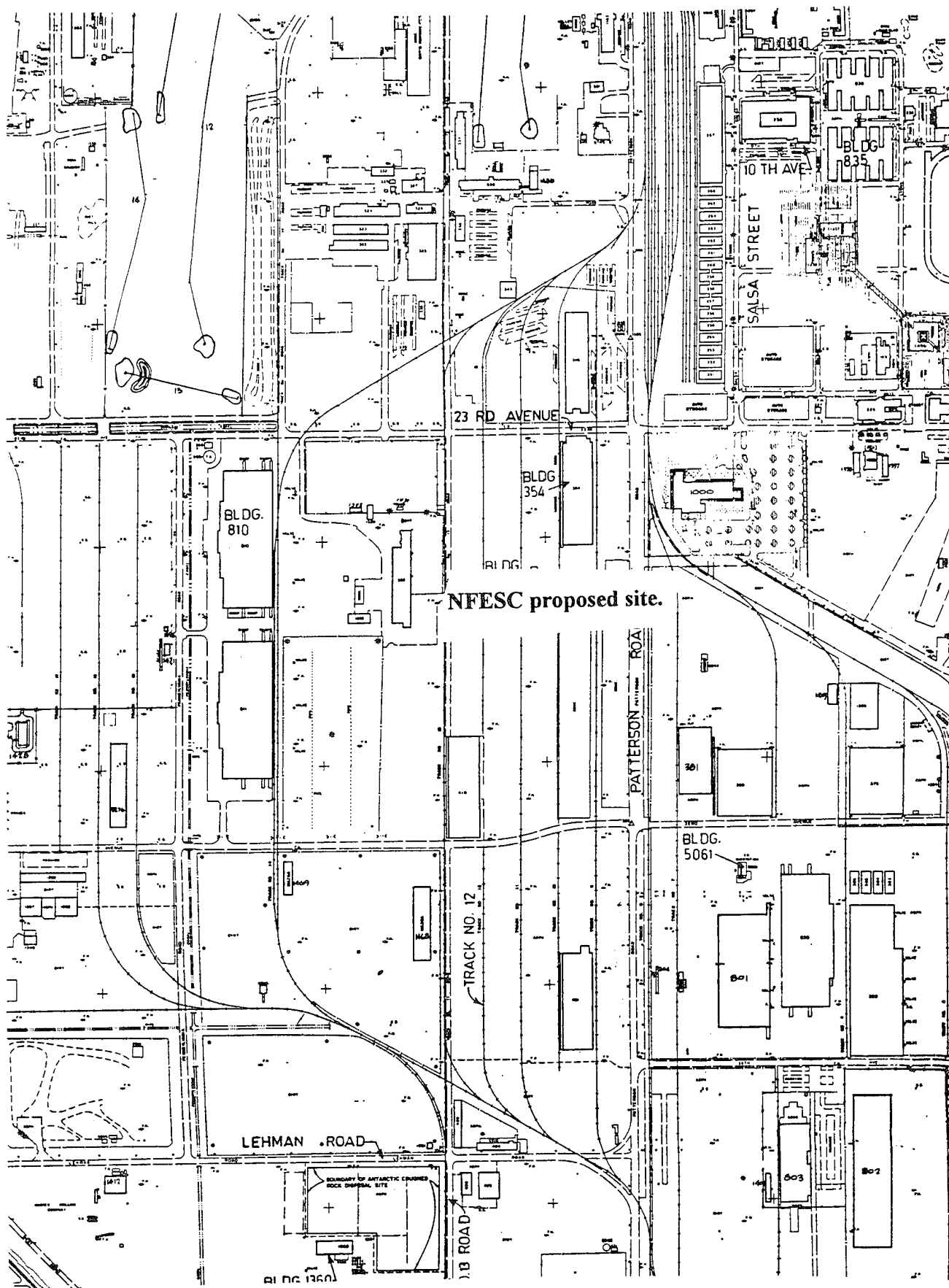


Figure 5.8 Naval Construction Battalion Center and NFESC proposed site.

**Figure 5.7 Boring logs, see Figure 5.2 for location  
From CDMG(1976)**

MAP INDEX NUMBER	STATE WELL NUMBER OR BRIDGE NUMBER	GROUND ELEVATION, IN FEET ABOVE SEA LEVEL	MEASURED WELL DEPTH IN FEET AND LITHOLOGIC DESCRIPTION
1	1N-22W-17M3	9'	2' to 10', Fine to coarse sand with some carbonaceous matter.  96' to 100', Medium to very coarse sand and gray clay with wood fragments.  110' to 125', Medium to coarse sandy clay with a few wood fragments.  145' to 172', Medium to coarse sandy clay with a few wood fragments.
2	1N-22W-20N2	5'	8' to 28', Interbedded brown clay with wood fragments, broken shells and fine to coarse sand.  28' to 32', Coarse sand and gravel with some clay, wood and shell fragments.  32' to 38', Fine sand and some coarse sand, clay and wood fragments.  38' to 52', Brown clay with sand, gravel and wood fragments.  72' to 85', Gray to black clay with some gravel and wood.  100' to 120', Medium to very coarse sand and granules and dark gray organic silty clay.  120' to 125', Sand and clay, as above, with 10 to 15 percent wood and peat seams.  245' to 255', Gray to black clay and one-half inch gravel. Occasional thin beds of peat. (This interval probably in Upper Pleistocene - E.C.S.)
3	1N-22W-20H1	10'	106' to 117', Sandy silt: Gray-black color with fine sand, also black organic particles - wood?
4	1N-22W-20H2	10'	8' to 12', Organic debris with medium grained sand and silt.
5	1N-22W-20H4	10'	87' to 91', Medium to coarse, angular to subangular arkosic sand and gravel, 50 percent gray to green silty clay with some fibers of wood found throughout.

A	Ab	Landslides. "Bedrock" slides - with components of slump and block glide.	F	Well lithified formations: very well cemented and lithified sandstone and conglomerate; well indurated and lithified shale and siltstone; most volcanic rocks.	
	Ad	Debris flows and other surficial slides.		Fc	Coldwater Formation- sandstone.
	As	Offshore landslides.		Fcv	Conejo Volcanics- undivided.
D		Poorly lithified formations: very well consolidated to poorly cemented sand(friable) sandstone) and gravel (rav- elly conglomerate); poorly to moderately indurated clay and silt (mudstone, shale and siltstone).		Fcvi	Conejo Volcanics- resistant intrusive rocks.
	Dc	Casitas Formation- conglomerate.		Fcva	Conejo Volcanics- andesite to dacite.
	Dp	Pico Formation(Western facies): sandstone, shale and mudstone.		Fku	Upper Cretaceous sandstone and shale.
	Ds	Saugus Formation-conglom- erate, sandstone and siltstone.		Fm	Matilija Formation- sandstone.
	Dsb	Santa Barbara Formation-mud- stone, siltstone, sandstone and conglomerate.		Fsc	Santa Susana Formation (lower part): Simi conglomerate.
	Dsp	San Pedro Formation-sand- stone, conglomerate and mudstone.			
DE		Transition zone-units contain major portions of rocks of both "D" and "E" zones.	AF	Man emplaced fill.	
	DEm	Monterey/Modelo Formations (DEmb-"burnt shale"): clay to silicified shale, silt- stone and sandstone.		AFu	Artificial fill- uncompacted.
	DEp	Pico Formation(Eastern facies): sandstone and siltstone.	AFc	AFul	Artificial fill- compacted, "engineered."
	DEr	Rincon Formation-siltstone, mudstone and shale.		AFcl	
	DEs	Sespe Formation-sandstone, siltstone and conglomerate.			
	DEsm	Santa Margarita Formation- mudstone, siltstone and sandstone.			
	DEt	Topanga Formation-sandstone, siltstone and conglomerate.			
	DEv	Vaqueros Formation-sandstone, claystone and siltstone.			
E		Moderately well lithified forma- tions: well cemented sand- stone and conglomerate; well indurated to silicified shale and siltstone; unweathered basalt.			
	Ed	Cozy Dell Formation- shale and siltstone.			
	Evb	Conejo Volcanics- layered basalt.			
	Ecvi	Conejo Volcanics- intrusive basalt.			
	Ej	Juncal Formation- shale and siltstone.			
	El	Lajas Formation- conglomerate, sandstone, siltstone and shale.			
	Ess	Santa Susana Formation (upper part): sandstone.			
	Et	Towsley Formation- sandstone and siltstone.			

**Figure 5.6. Reference site  
geology from CDMG (1976)  
Continued**

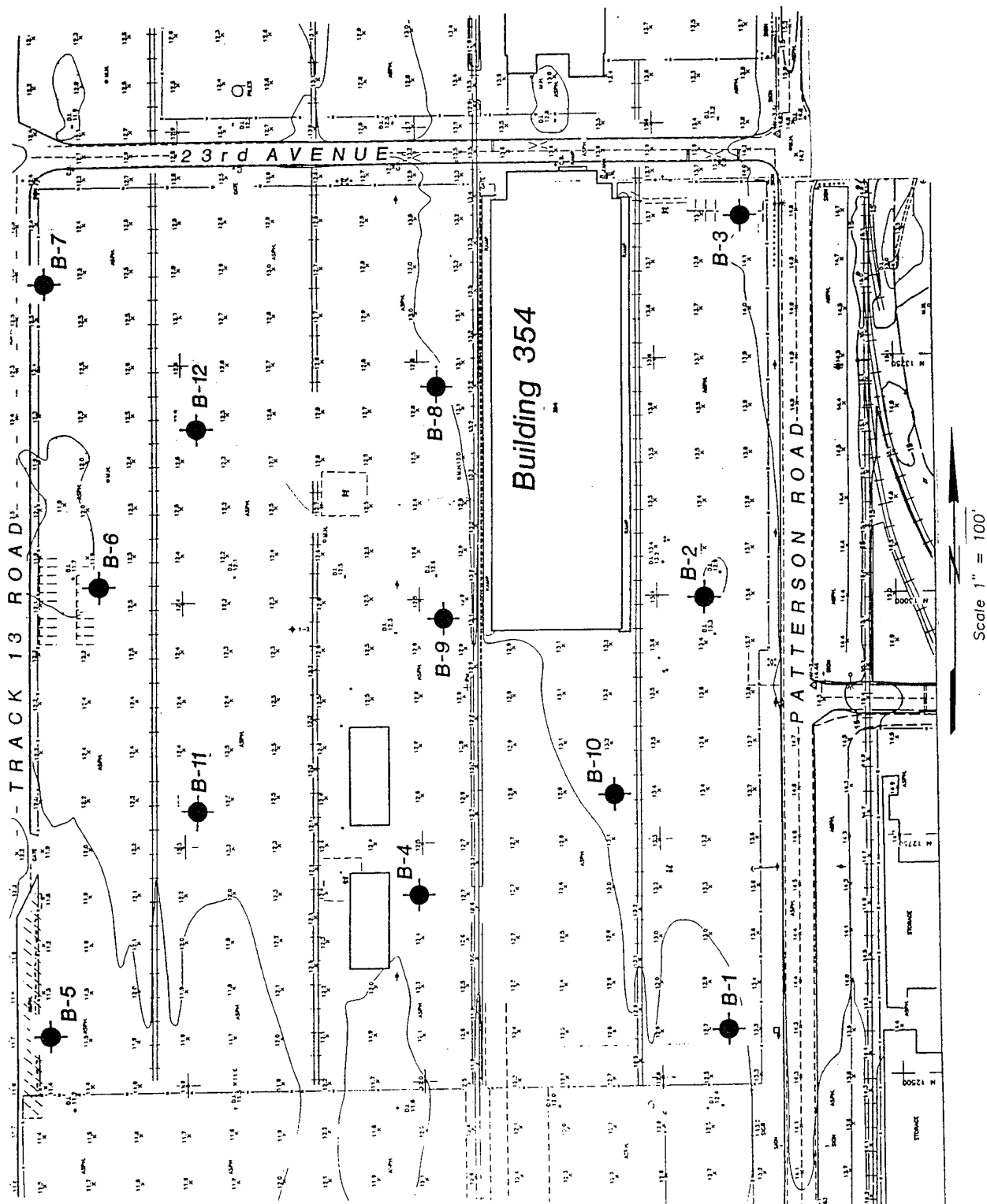


Figure 5.9 NFESC site and boring locations



**Figure 5.10 Typical boring log at NFESC site**

**Figure 5.10 Typical boring log at NFESC site, continued**

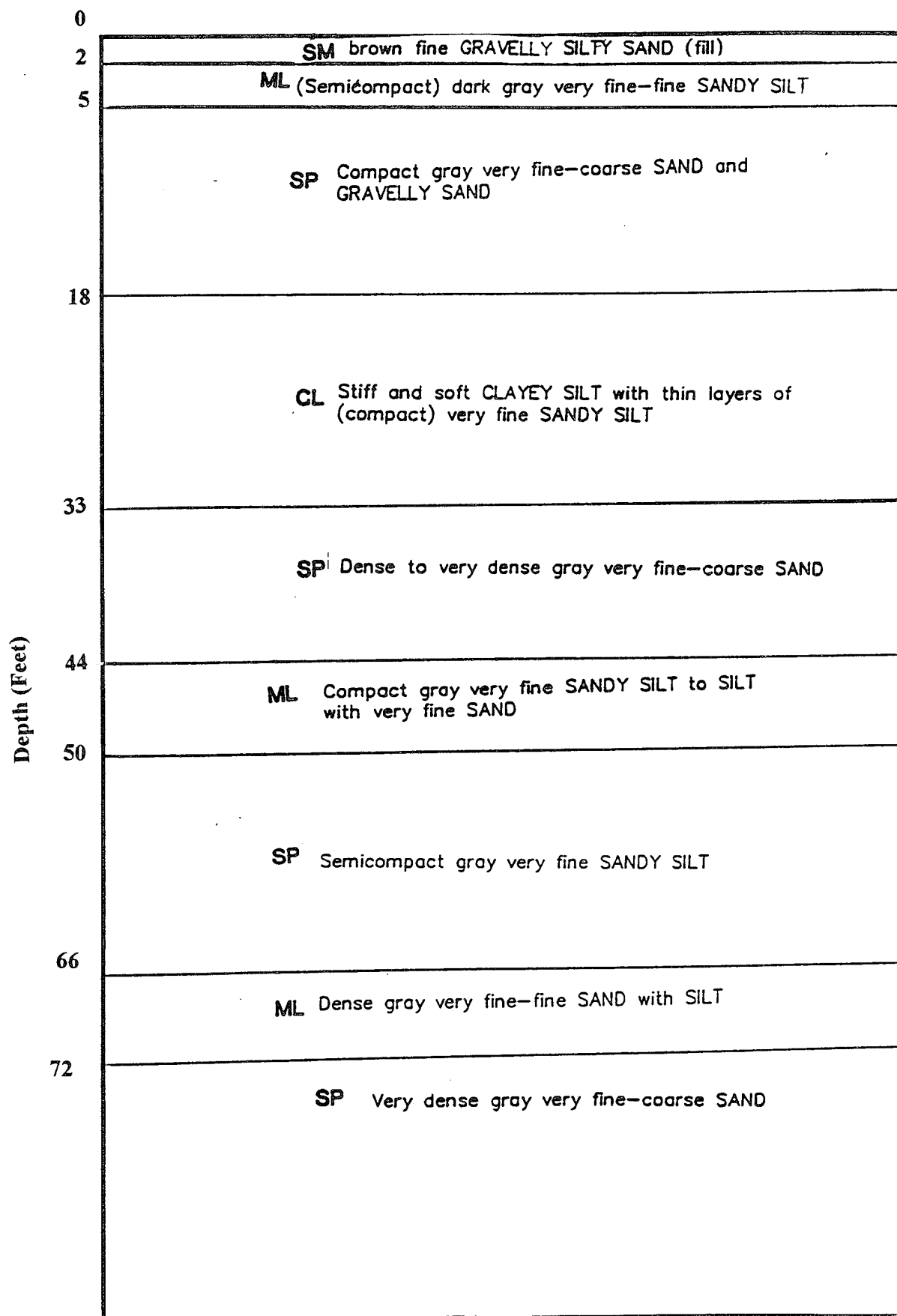


Figure 5.11. Idealized profile, NFESC site.

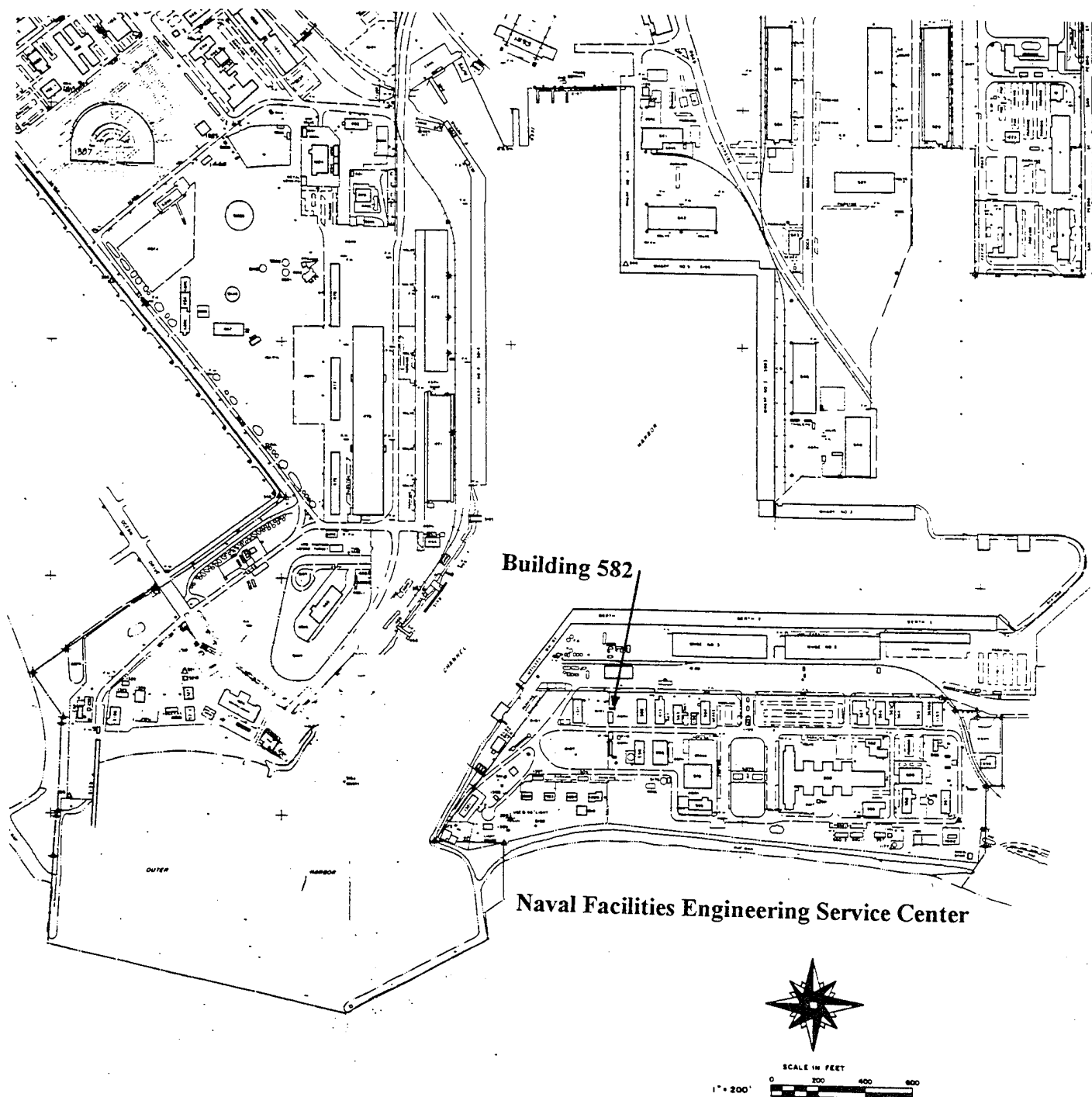


Figure 5.12 NFESC Building 560 site.


BORING LOG NO. 1					
Project Ventilation Improvements			Job No. 85-221E-2		
Driving Weight 140 lbs.			Height of drop: 30 inches		
Depth (feet)	Samples	Blows/foot	DESCRIPTION OF SOILS	Dry Density pcf	Moisture Content, %
1			2" A.C., 6" Base		
2			FILL: Silty & gravelly sand, brown to tan, moist & loose to moderate dense.		
3		19		106.3	8.7
4			SAND: Some gravel, brown, moist & medium dense to dense		
5					
6					
7					
8		21	Increase gravel & cobbles below 5'	104.8	4.7
9					
10					
11		40		116.9	11.0
12					
13					
14					
15					
16		34	End of Boring at 15'	105.3	22.0
17			Water Table at 12'		
18					
19					
20					
21					
22					
23					
24					
25					
26					
27					
28					
29					
30					
31					
32					
33					
34					
35					

Figure 5.13 Boring log, NFESC compound.

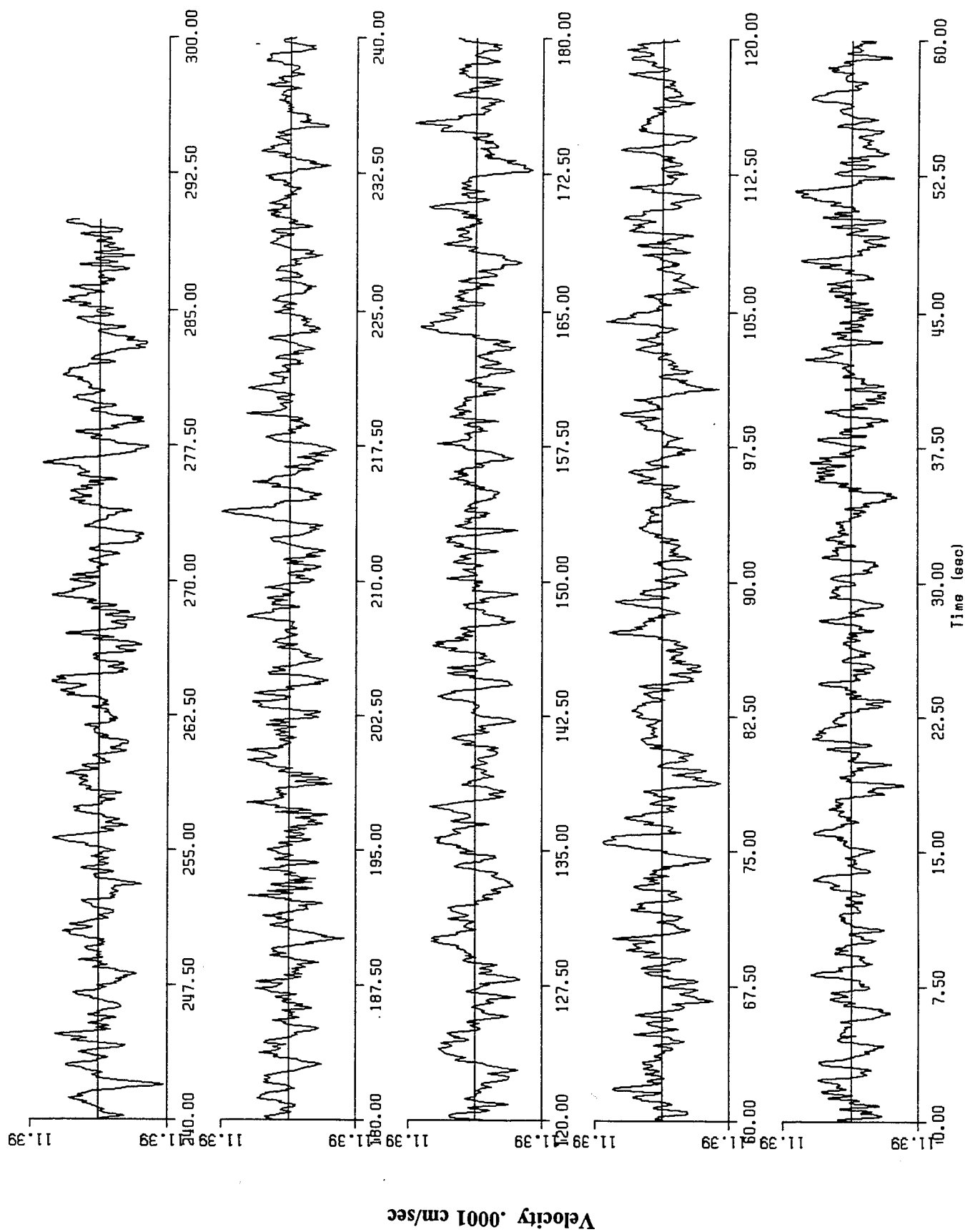


Figure 5.14 Typical time history record of microseism.

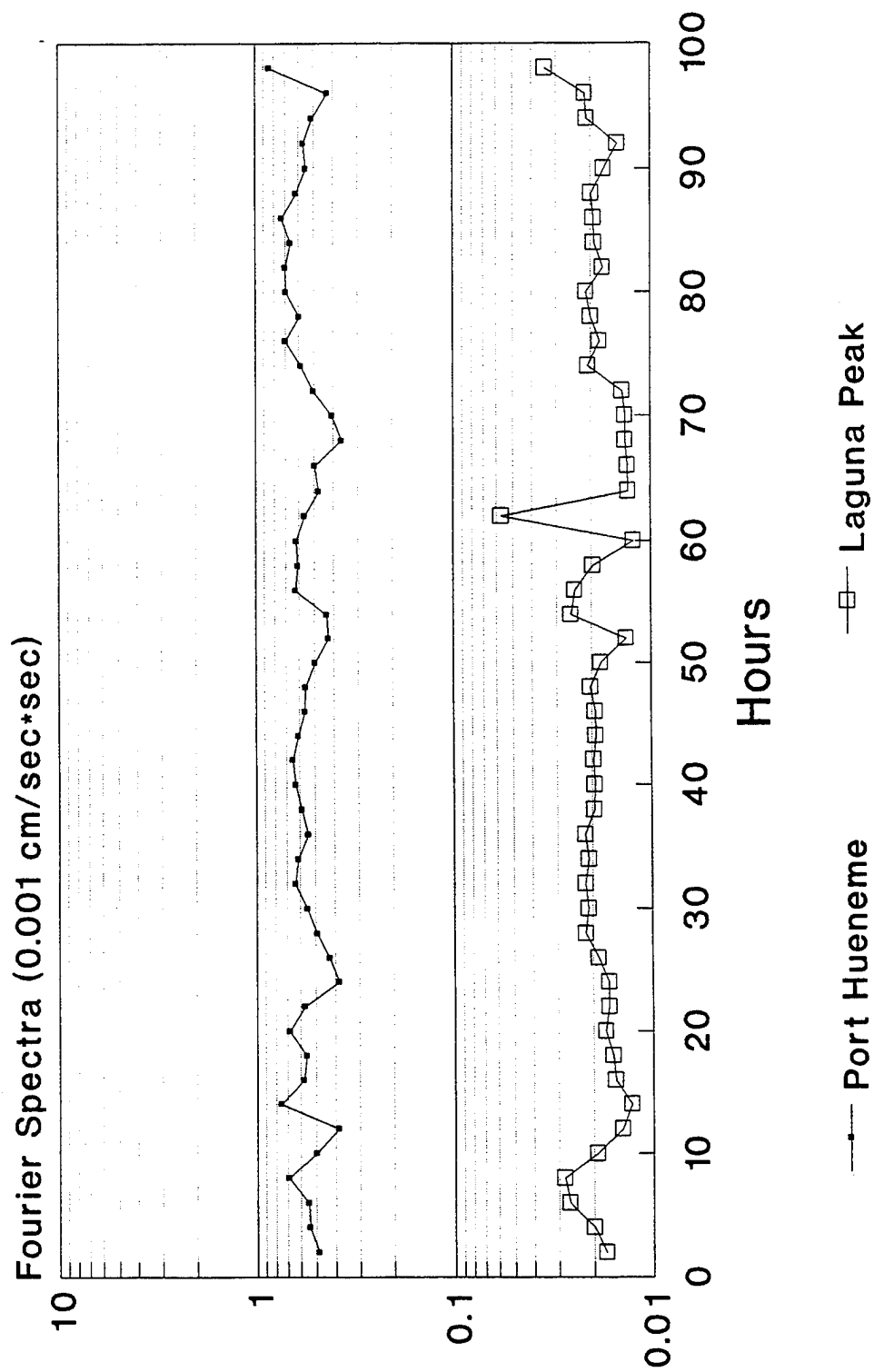


Figure 5.15. Long term measurements, period range 0.5 to 0.7 seconds.

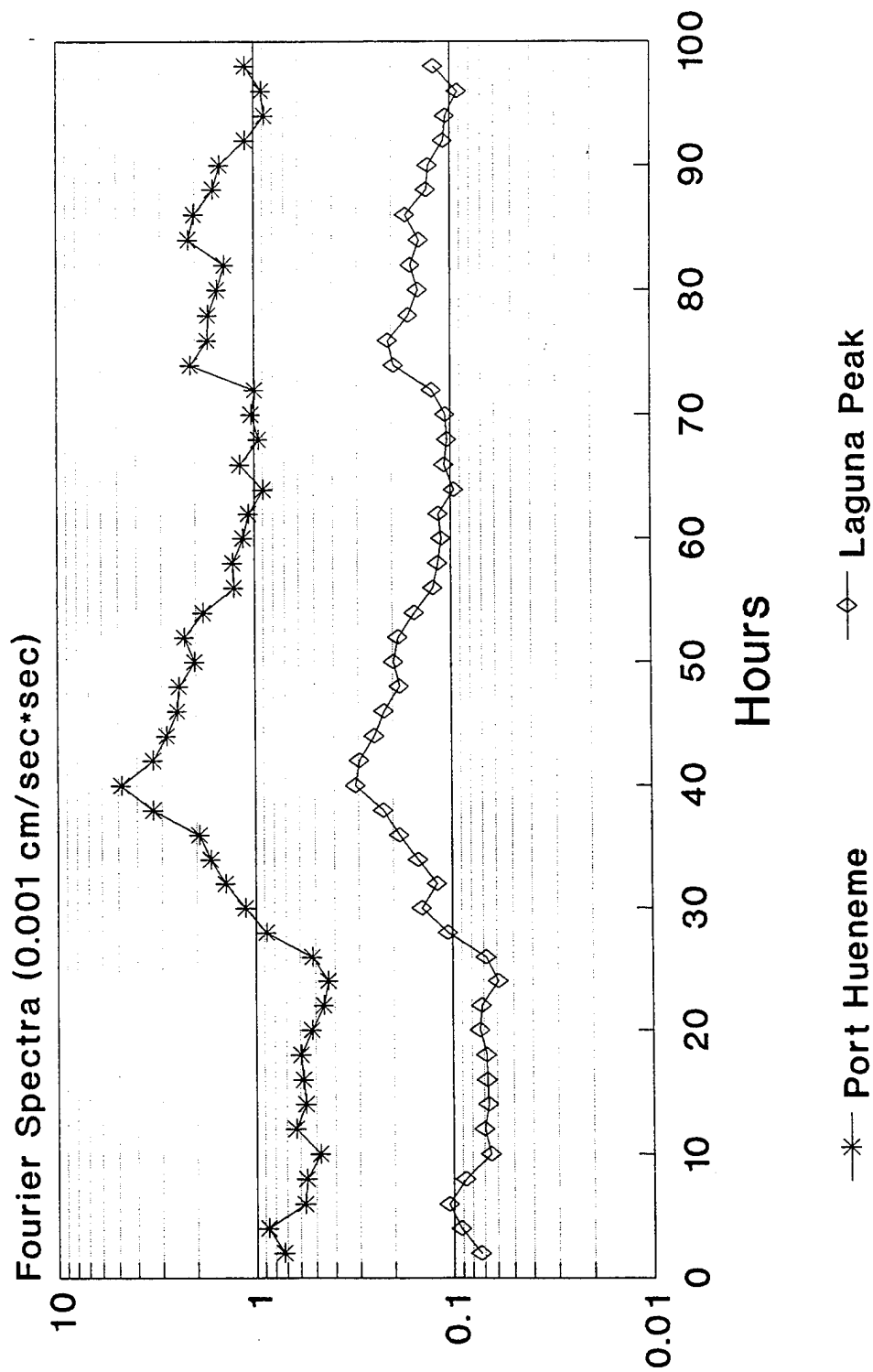


Figure 5.16. Long term measurements, period range 2.0 to 4.0 seconds.



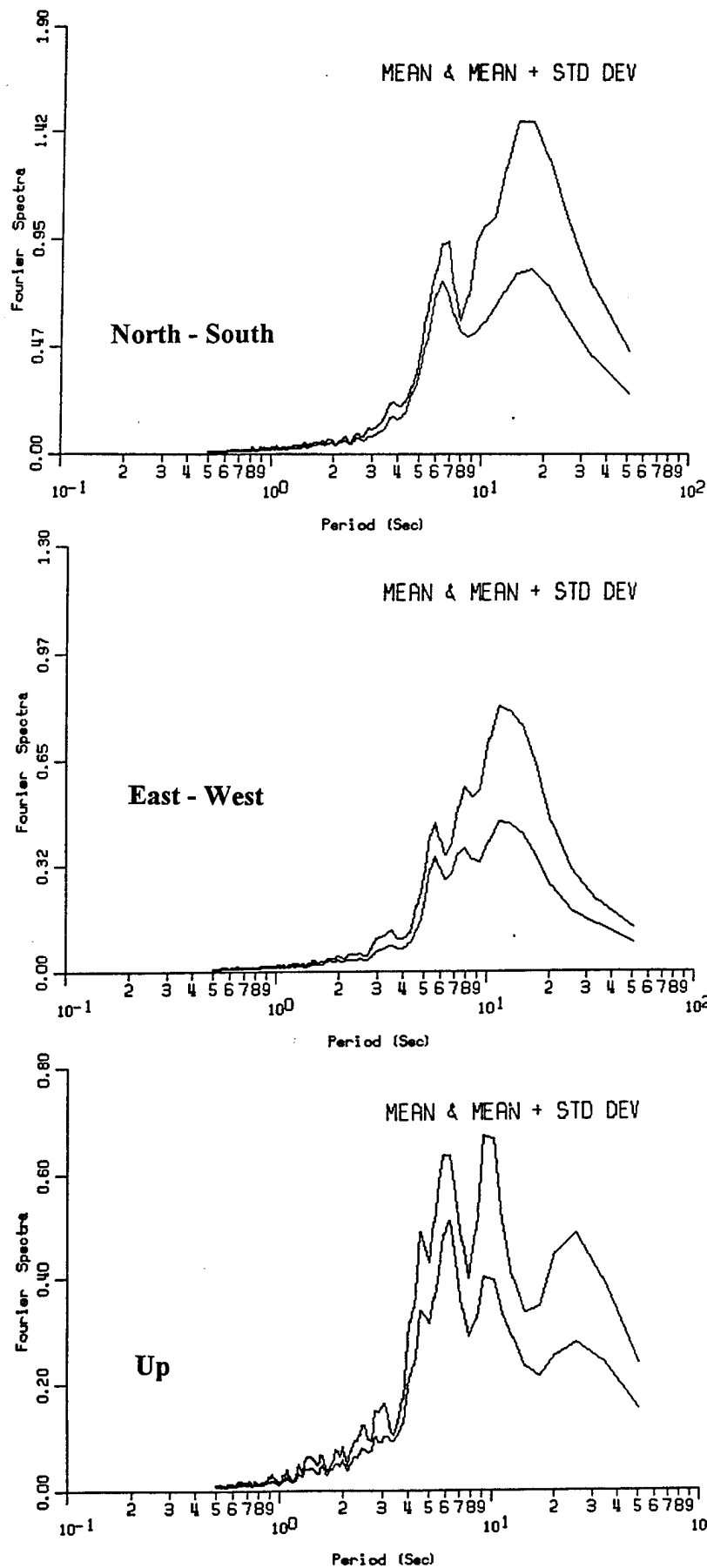


Figure 5.17a Fourier spectra Mugu Rock.

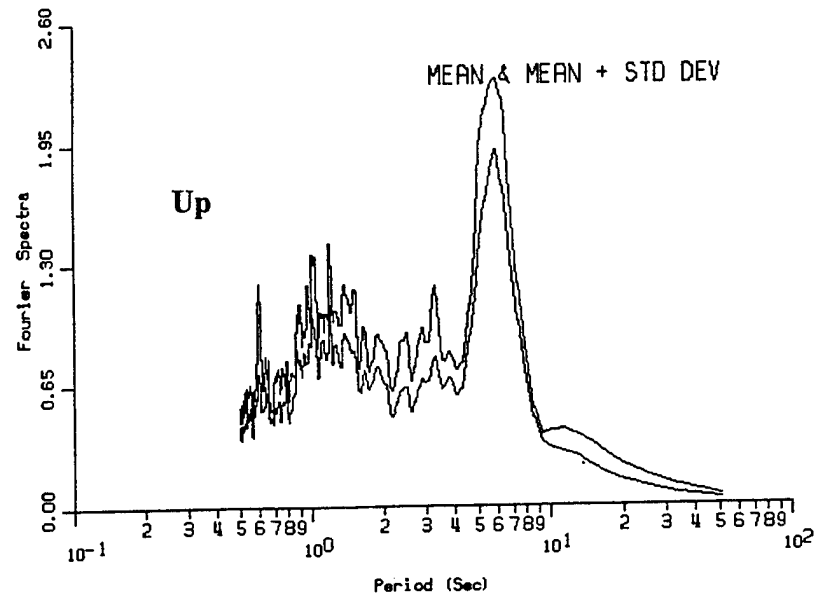
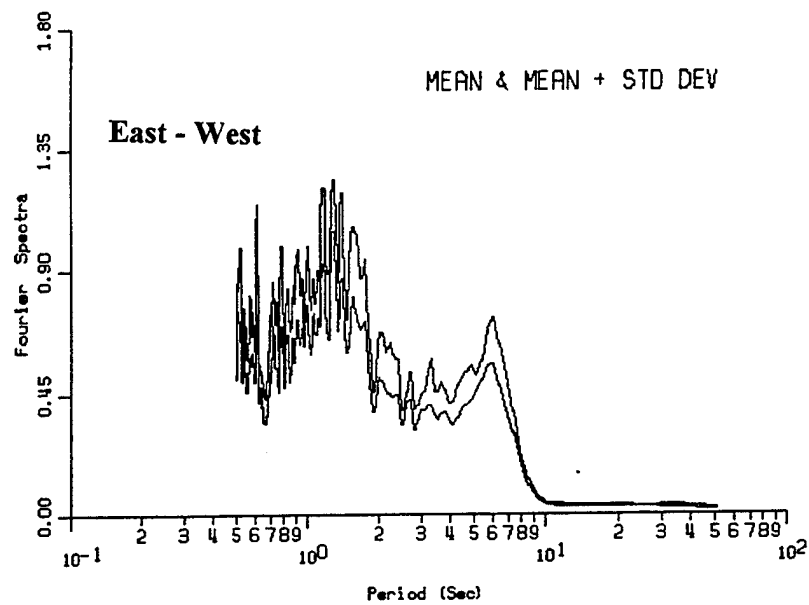
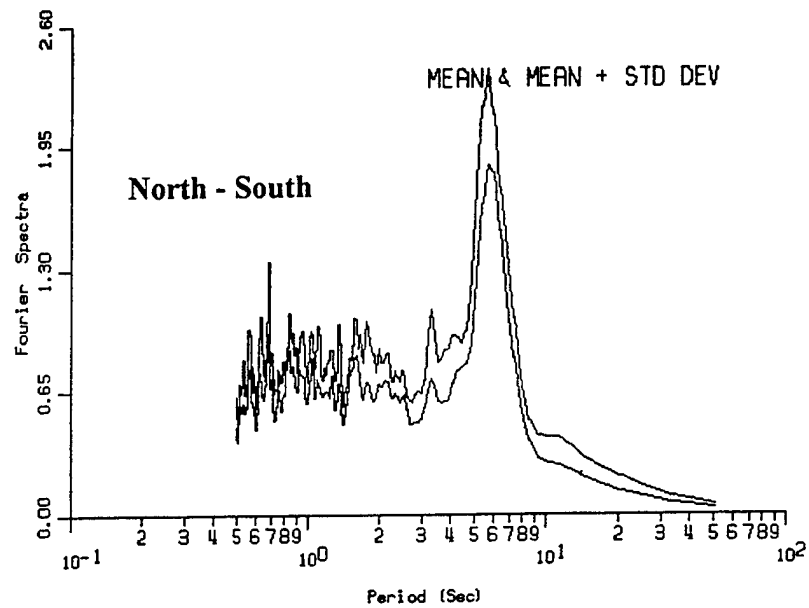
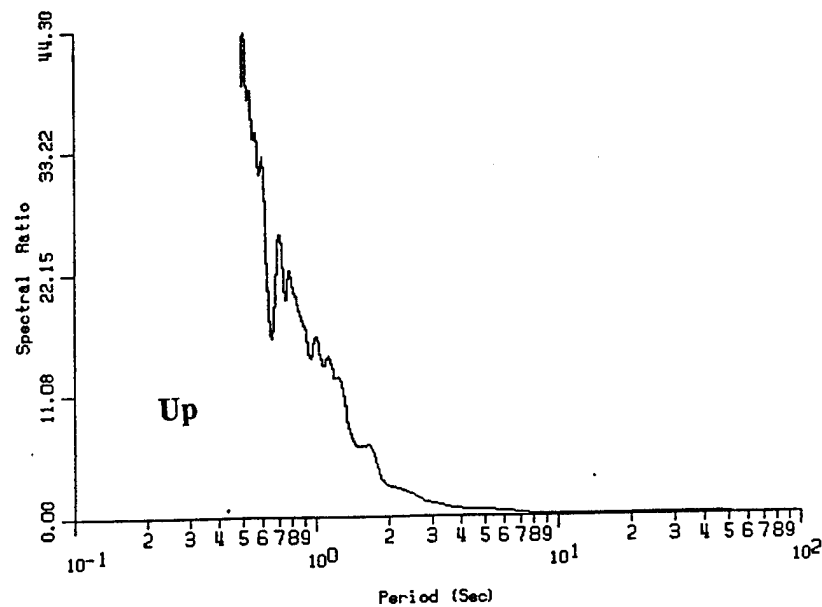
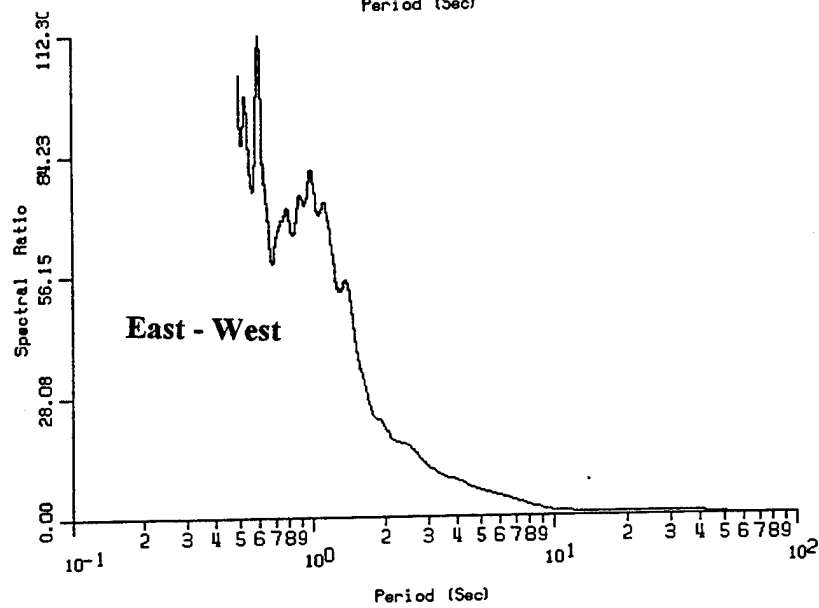
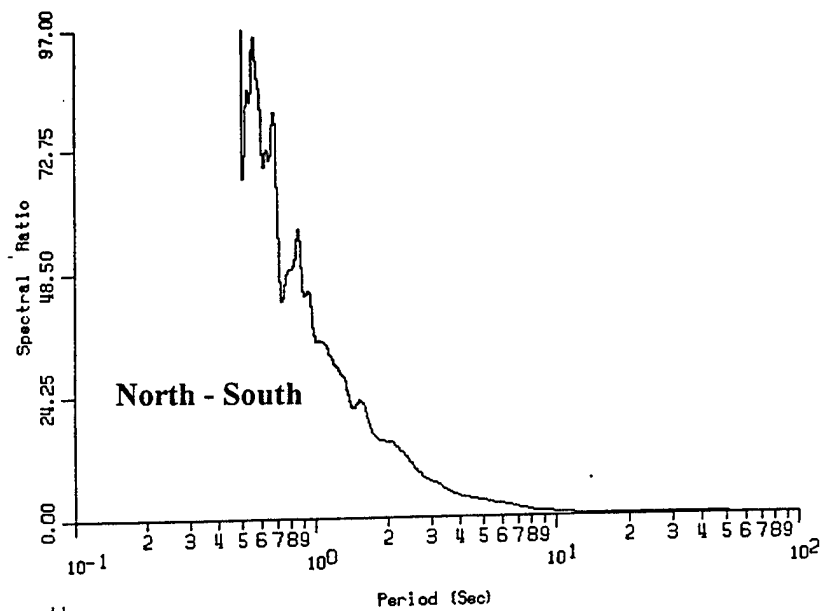


Figure 5.17b Fourier spectra NFESC Building 582, Port Hueneme.



**Figure 5.17c Spectral ratios NFESC/ Mugu Rock.**

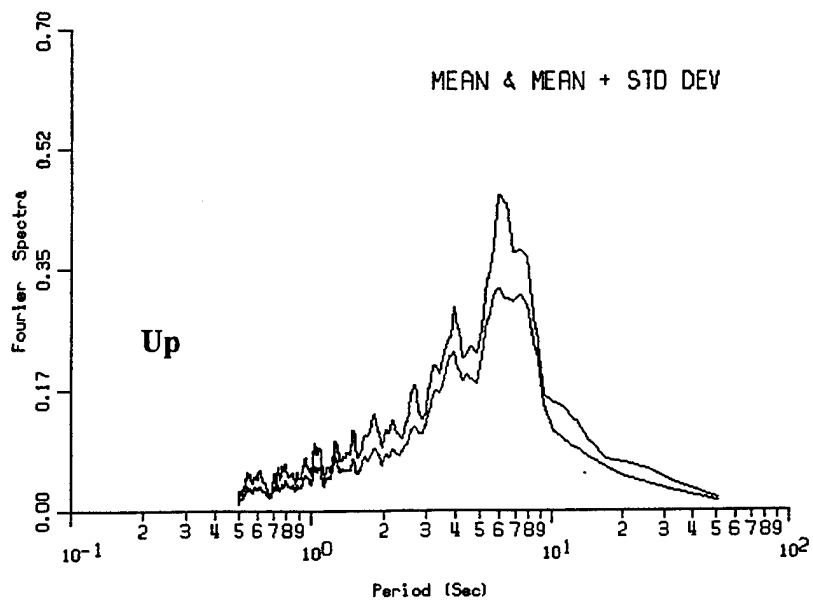
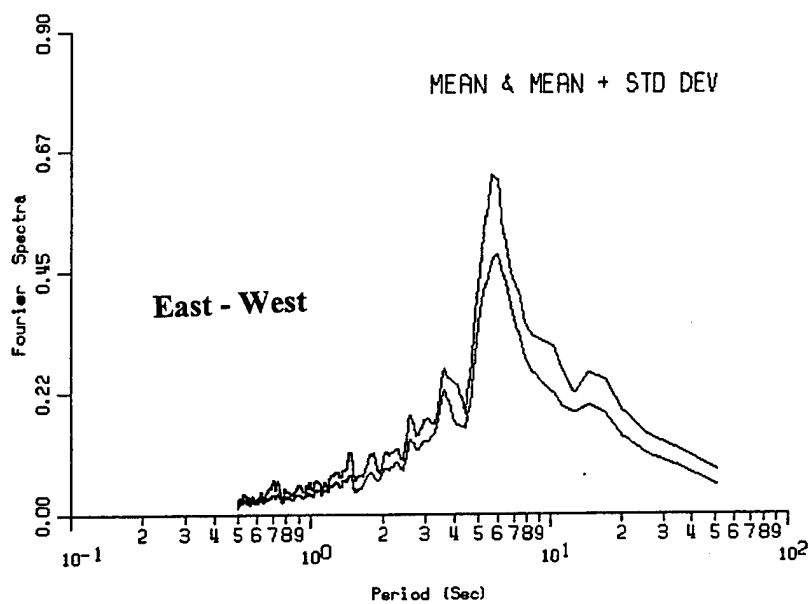
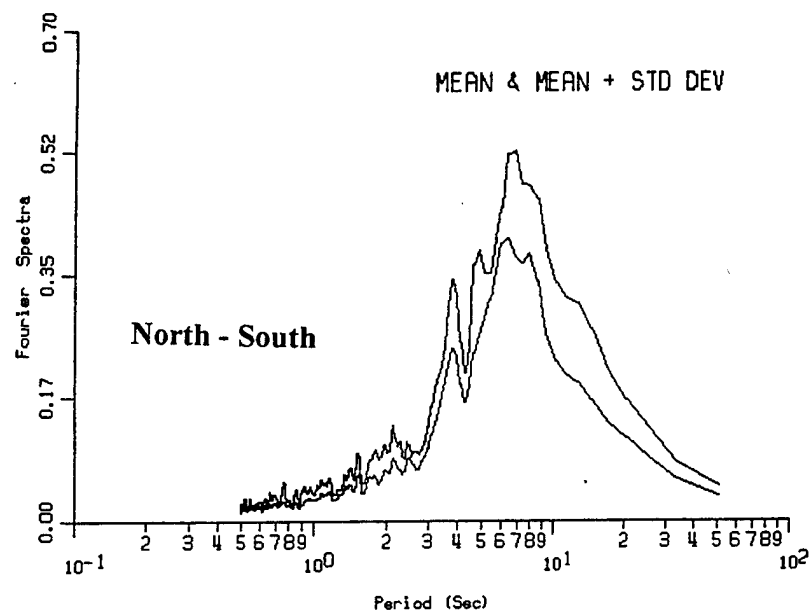
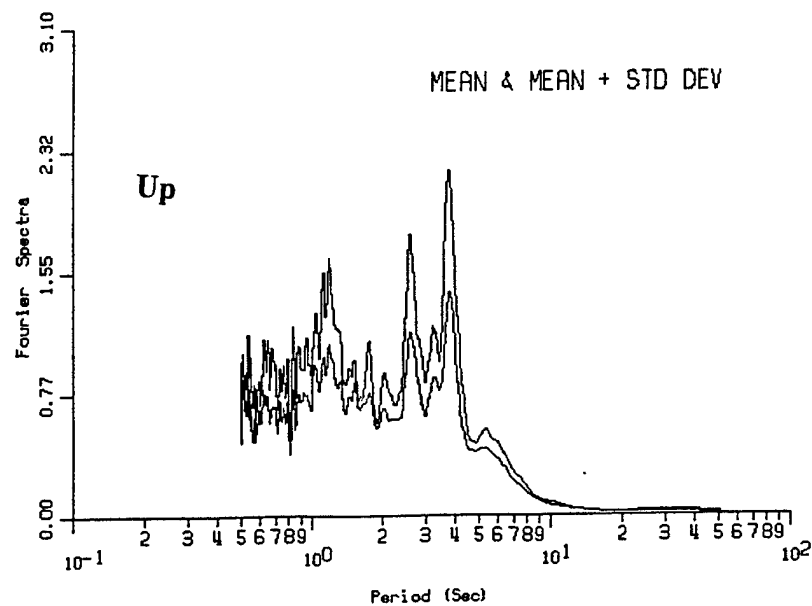
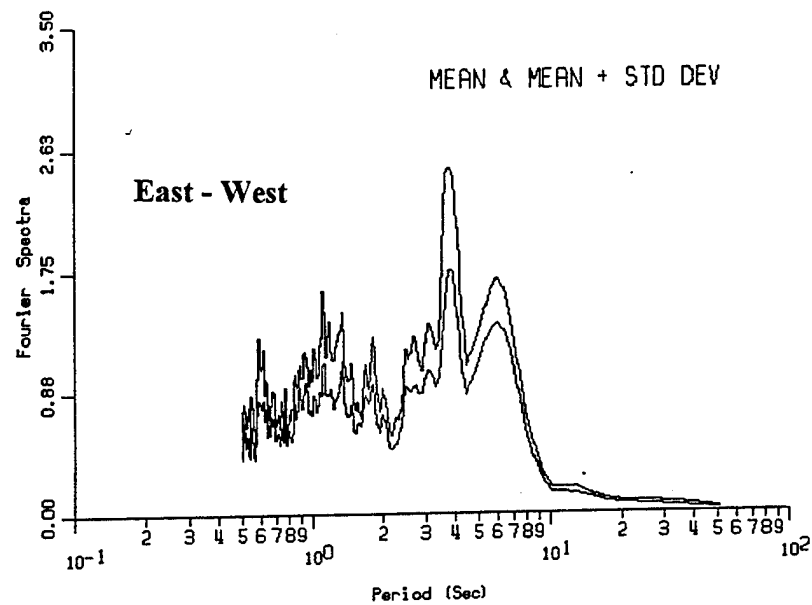
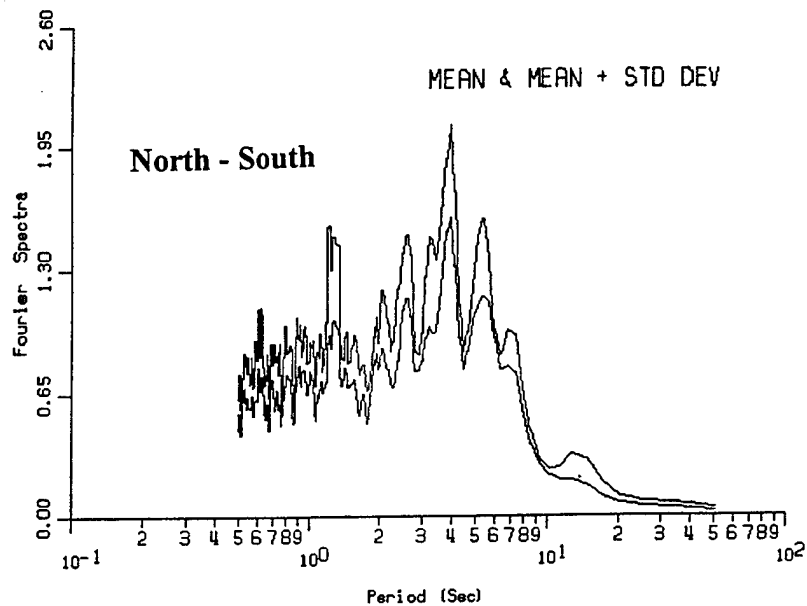
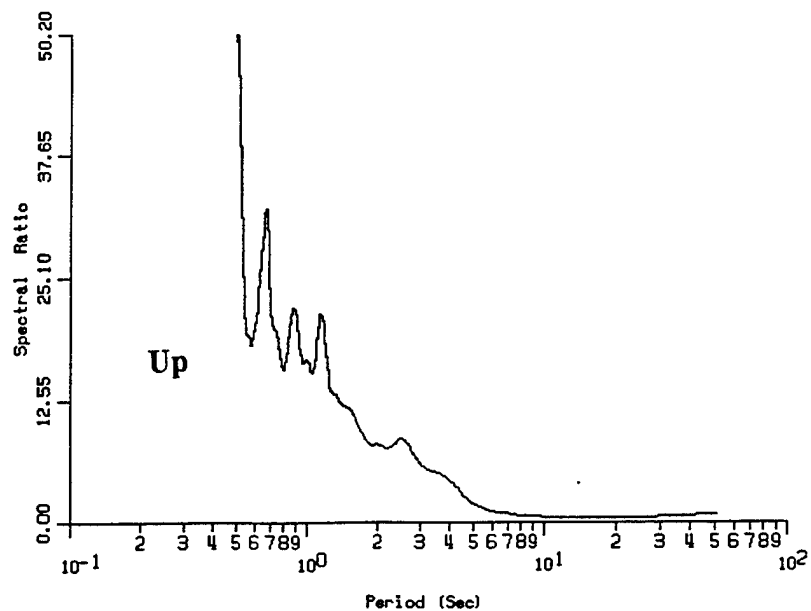
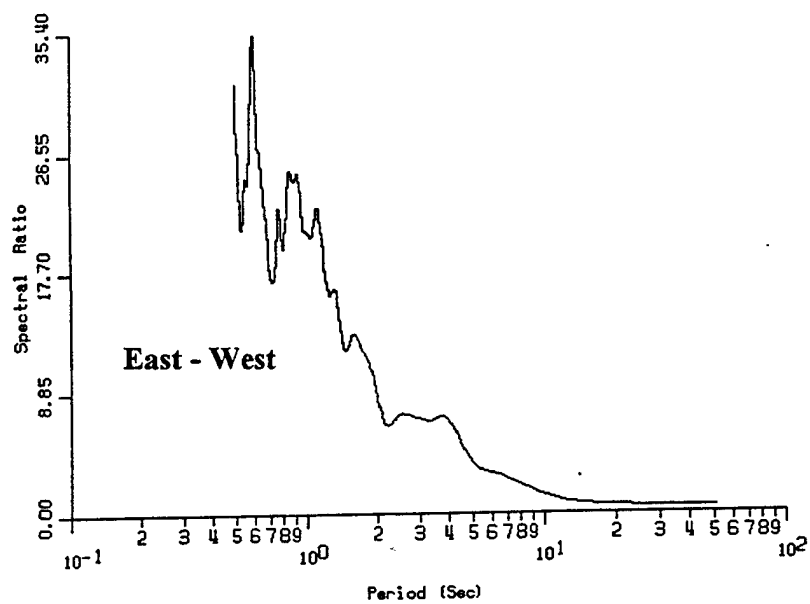
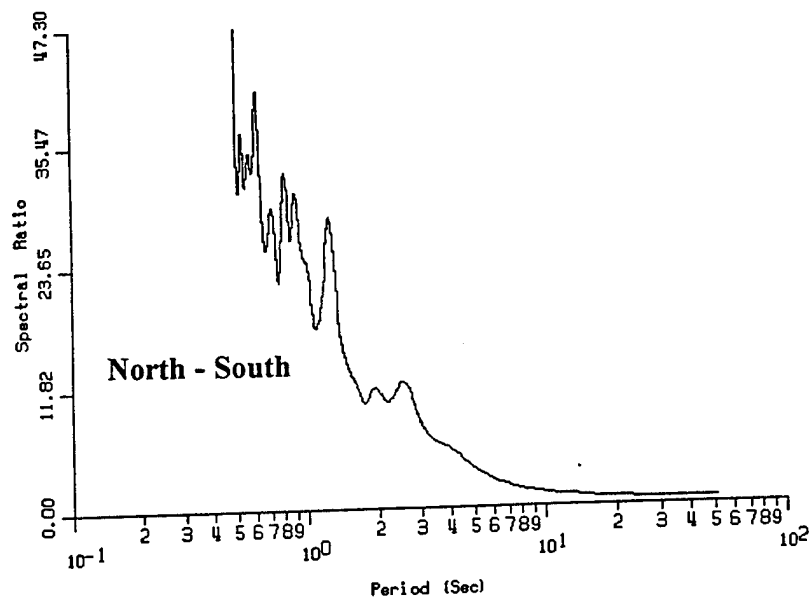


Figure 5.18a Fourier spectra Laguna Peak.



**Figure 5.18b** Fourier spectra NFESC Building 582, Port Hueneme.



**Figure 5.18c Spectral ratios NFESC/ Laguna Peak.**

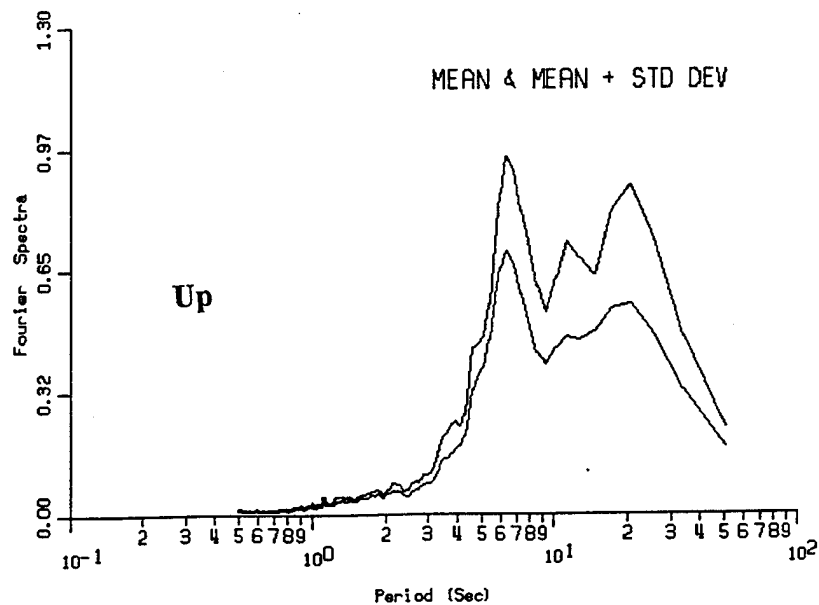
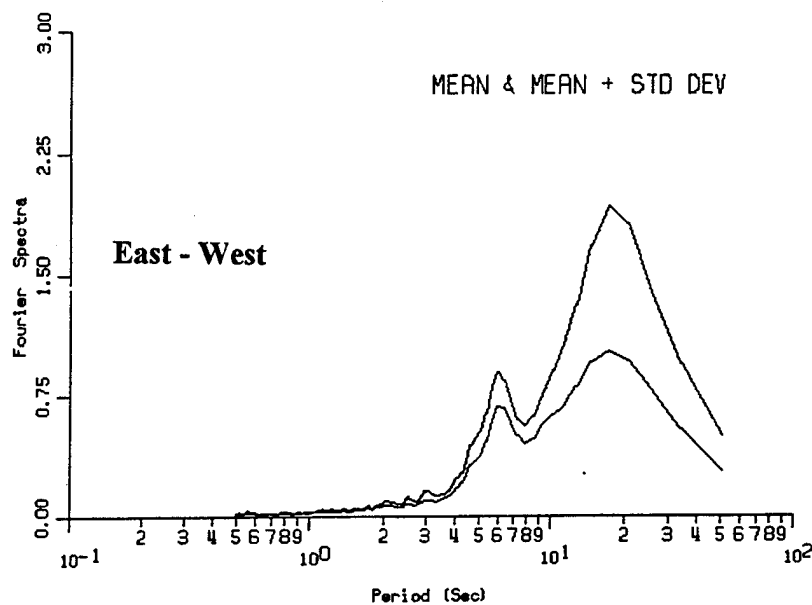
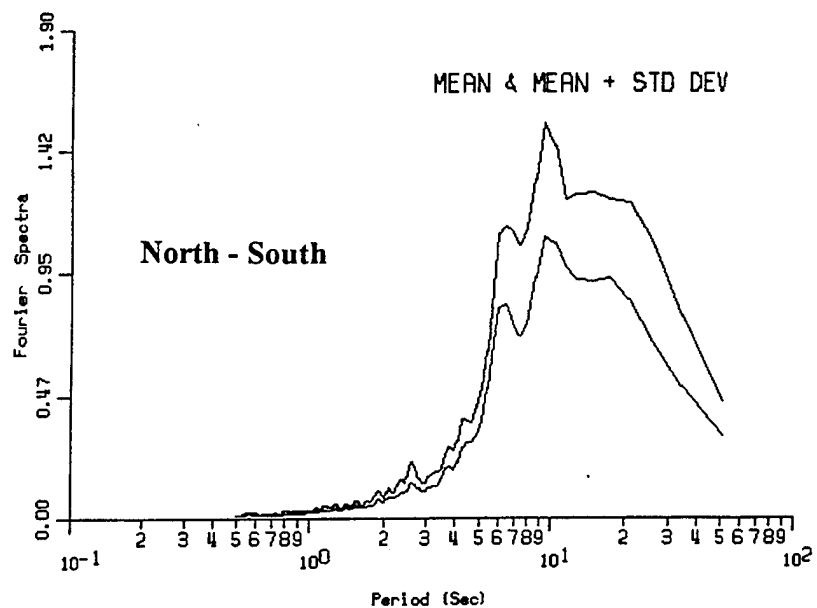


Figure 5.19a. Fourier spectra Camarillo Hospital.

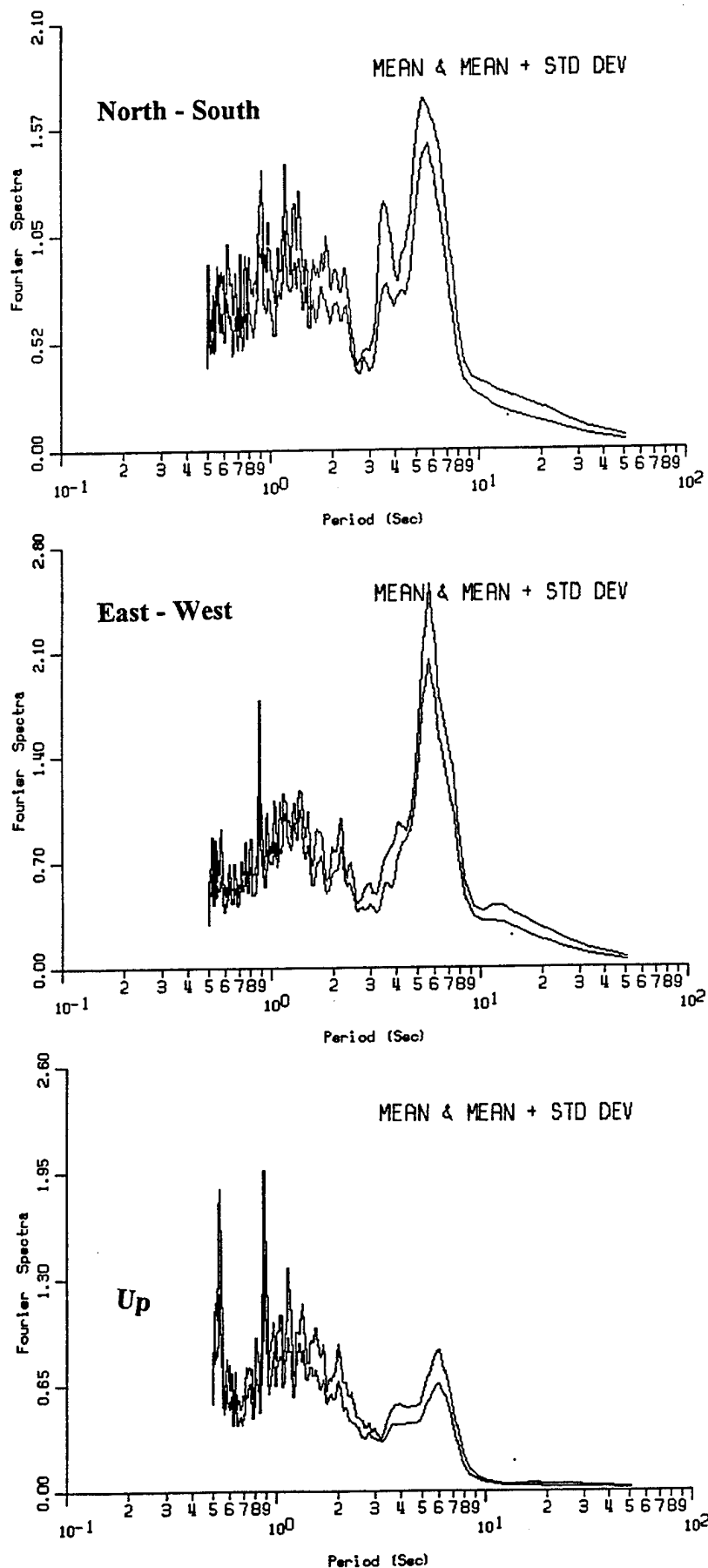
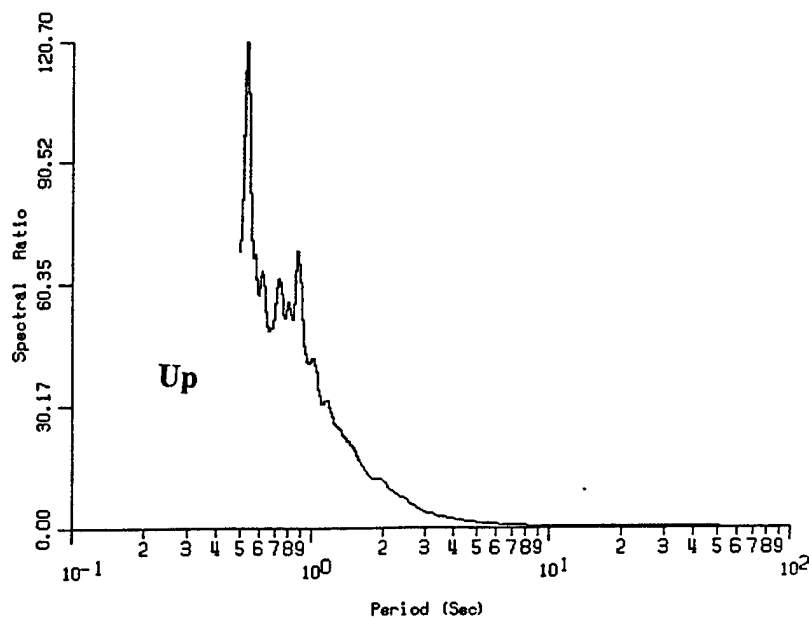
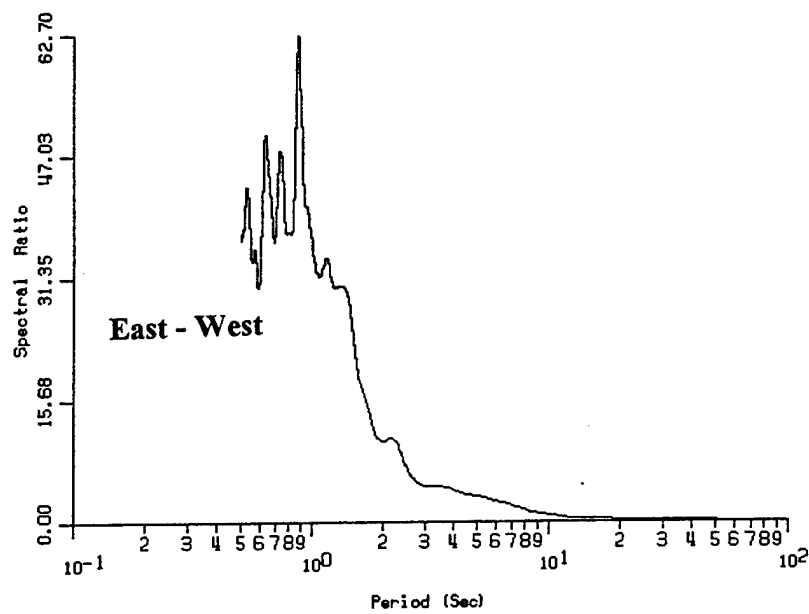
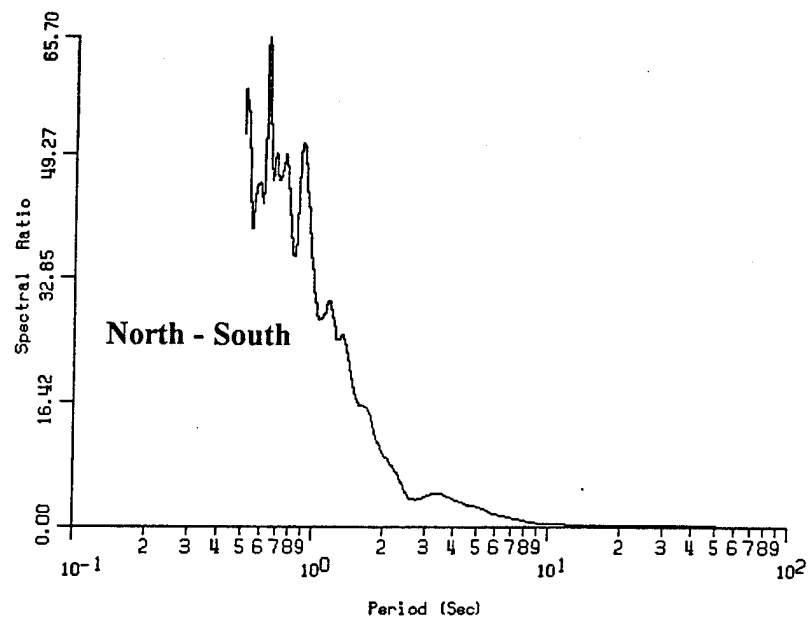


Figure 5.19b. Fourier spectra NFESC Building 582, Port Hueneme.





**Figure 5.19c. Spectral ratios NFESC/ Camarillo Hospital.**

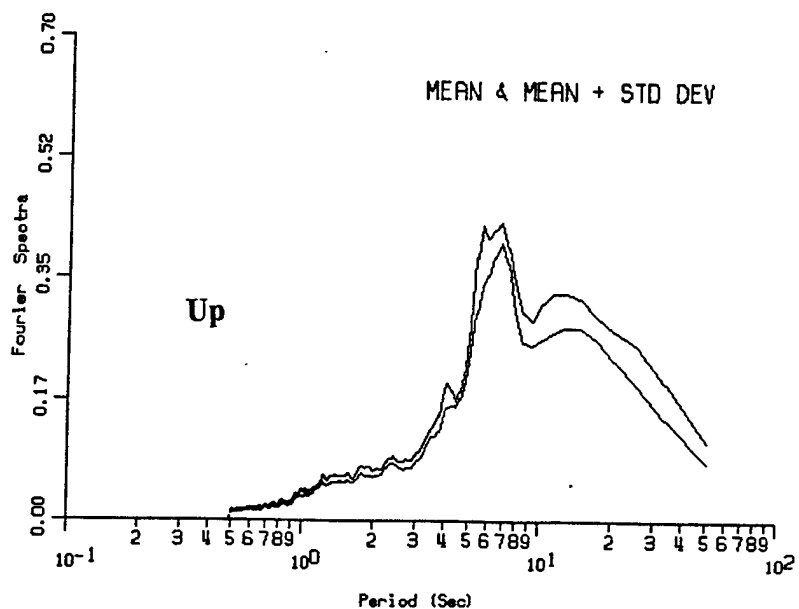
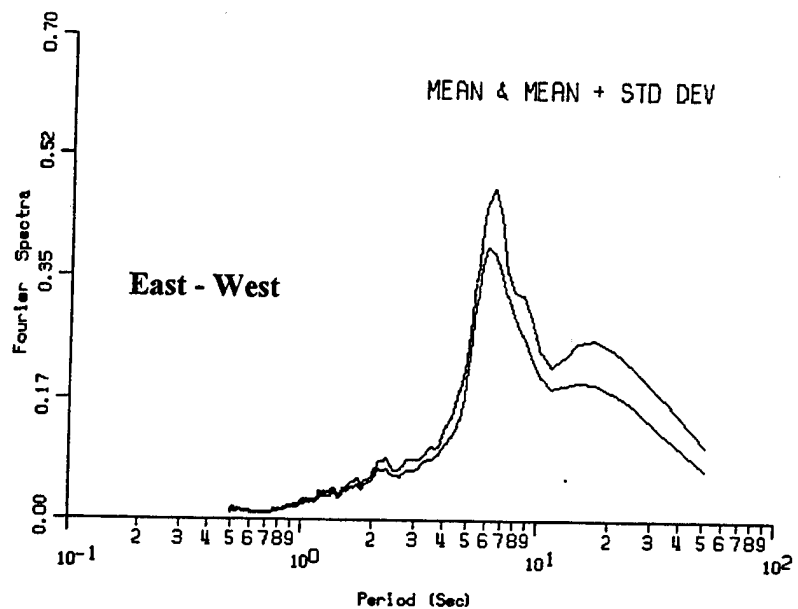
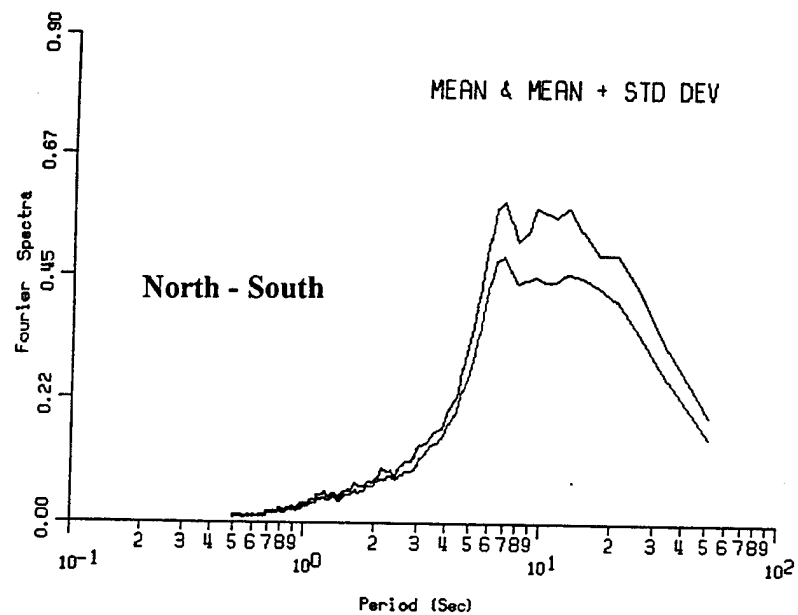


Figure 5.20a. Fourier spectra Mugu Rock.

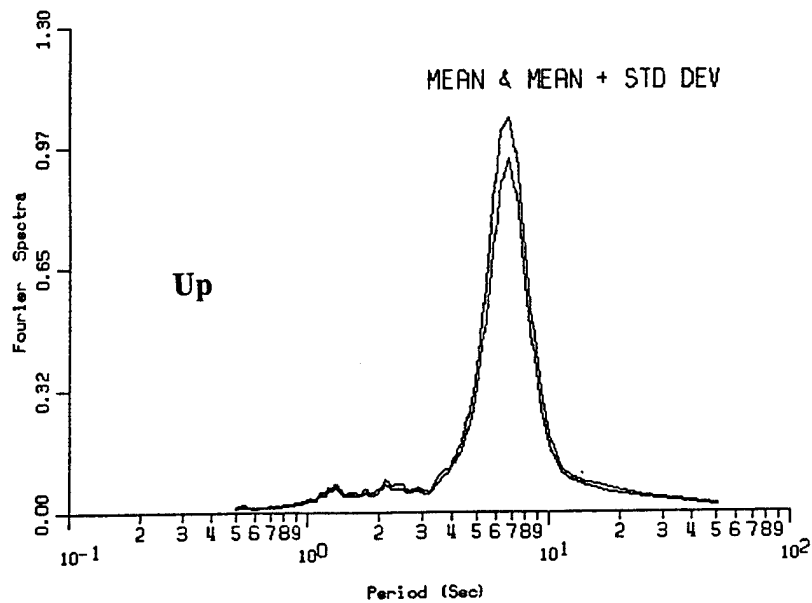
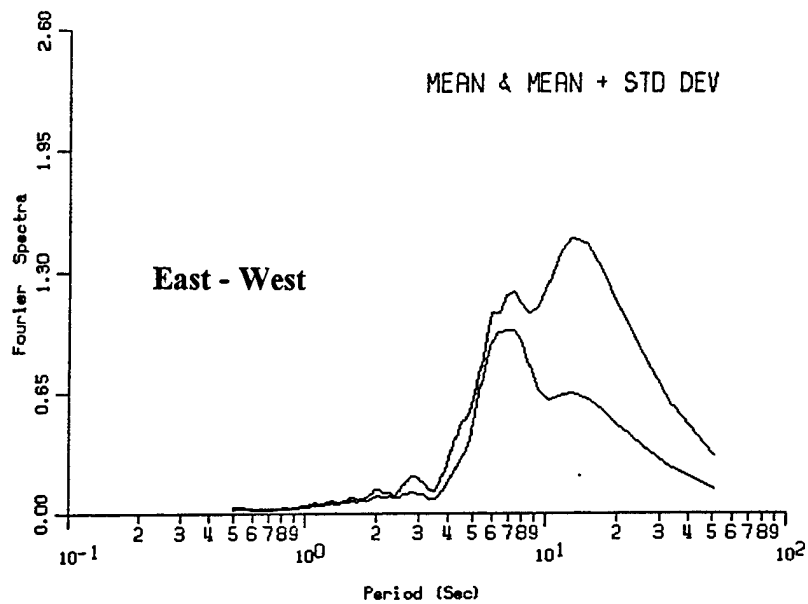
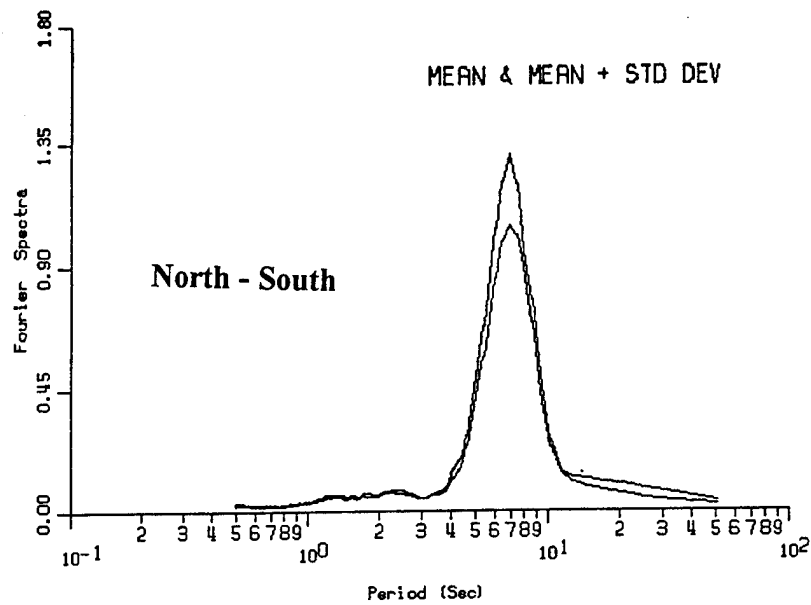
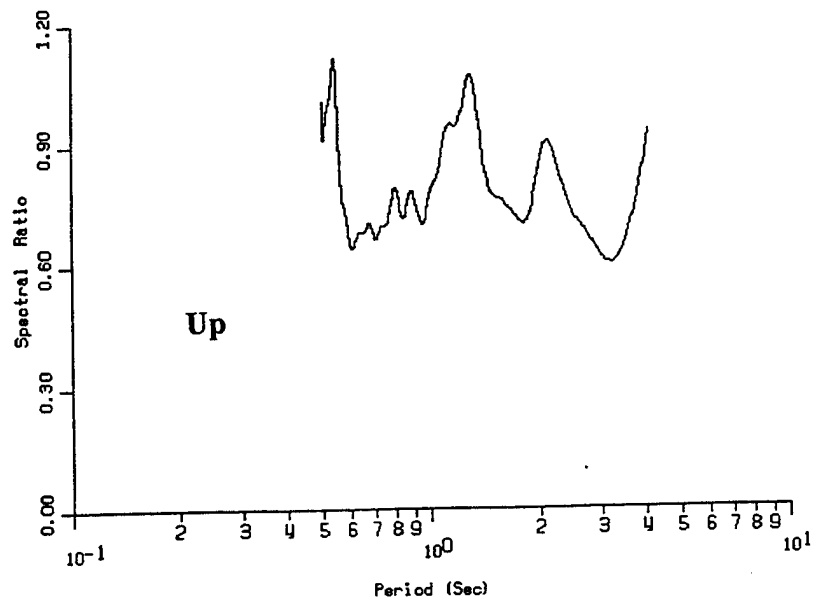
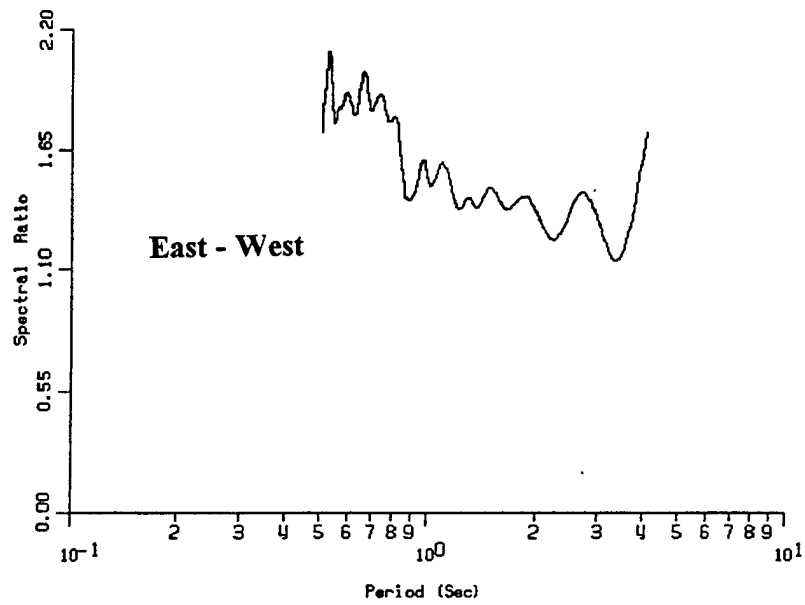
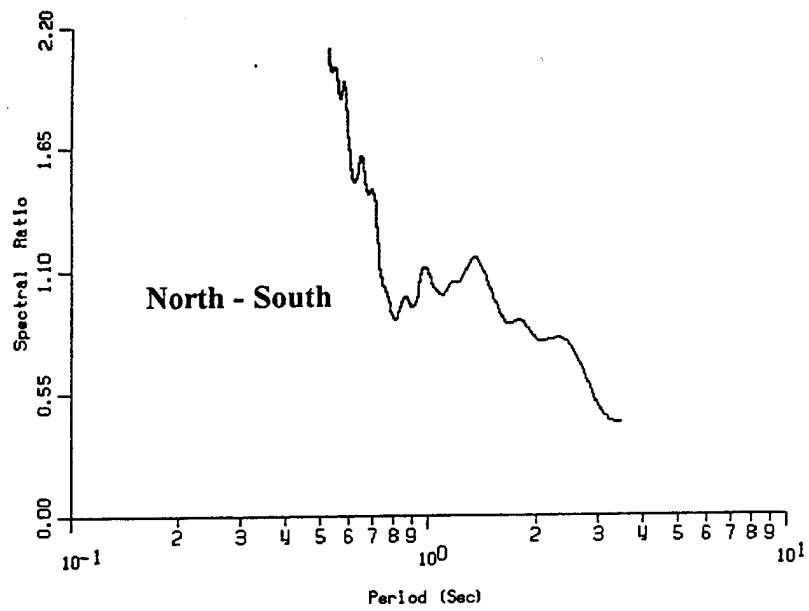


Figure 5.20b. Fourier spectra Laguna Peak.



**Figure 5.20c. Spectral ratios Laguna Peak/Mugu Rock.**

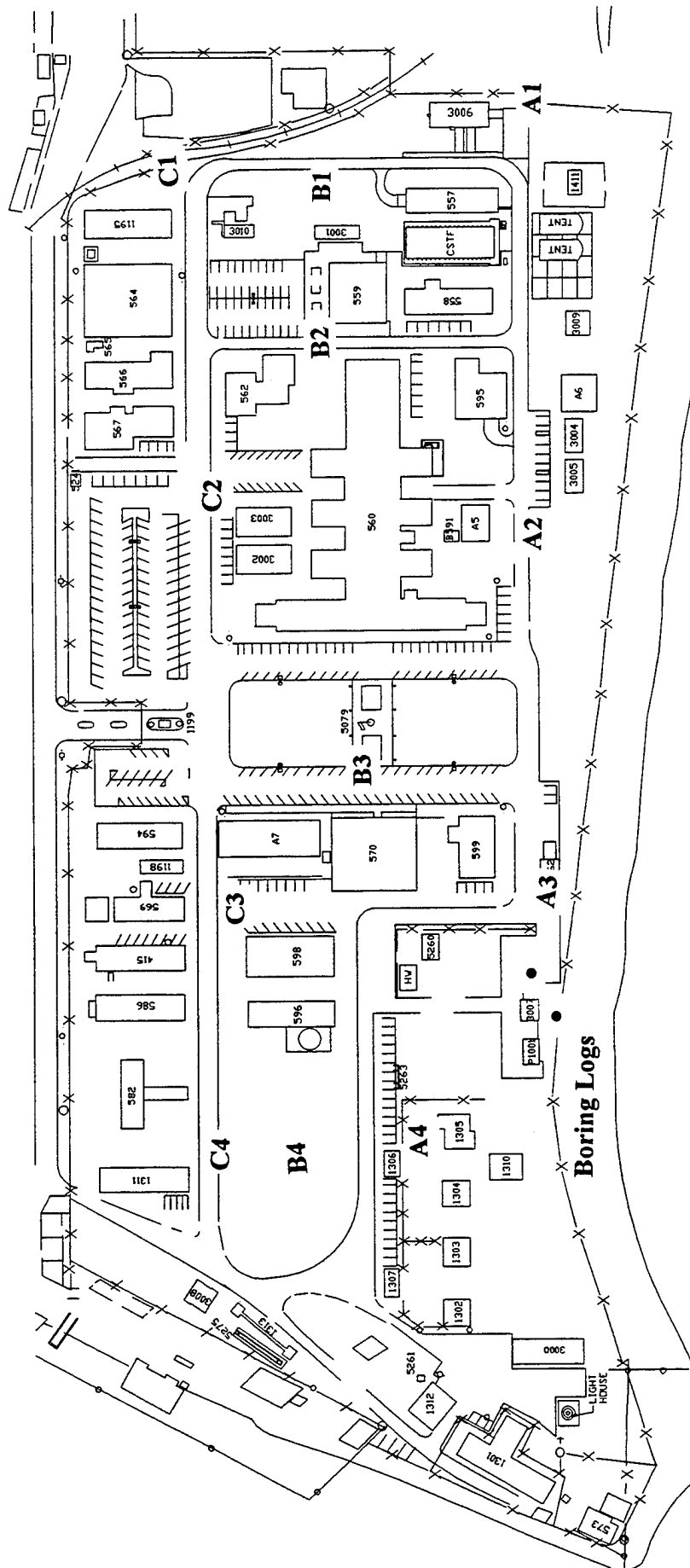


Figure 5.21. NFESC site showing measurement stations.

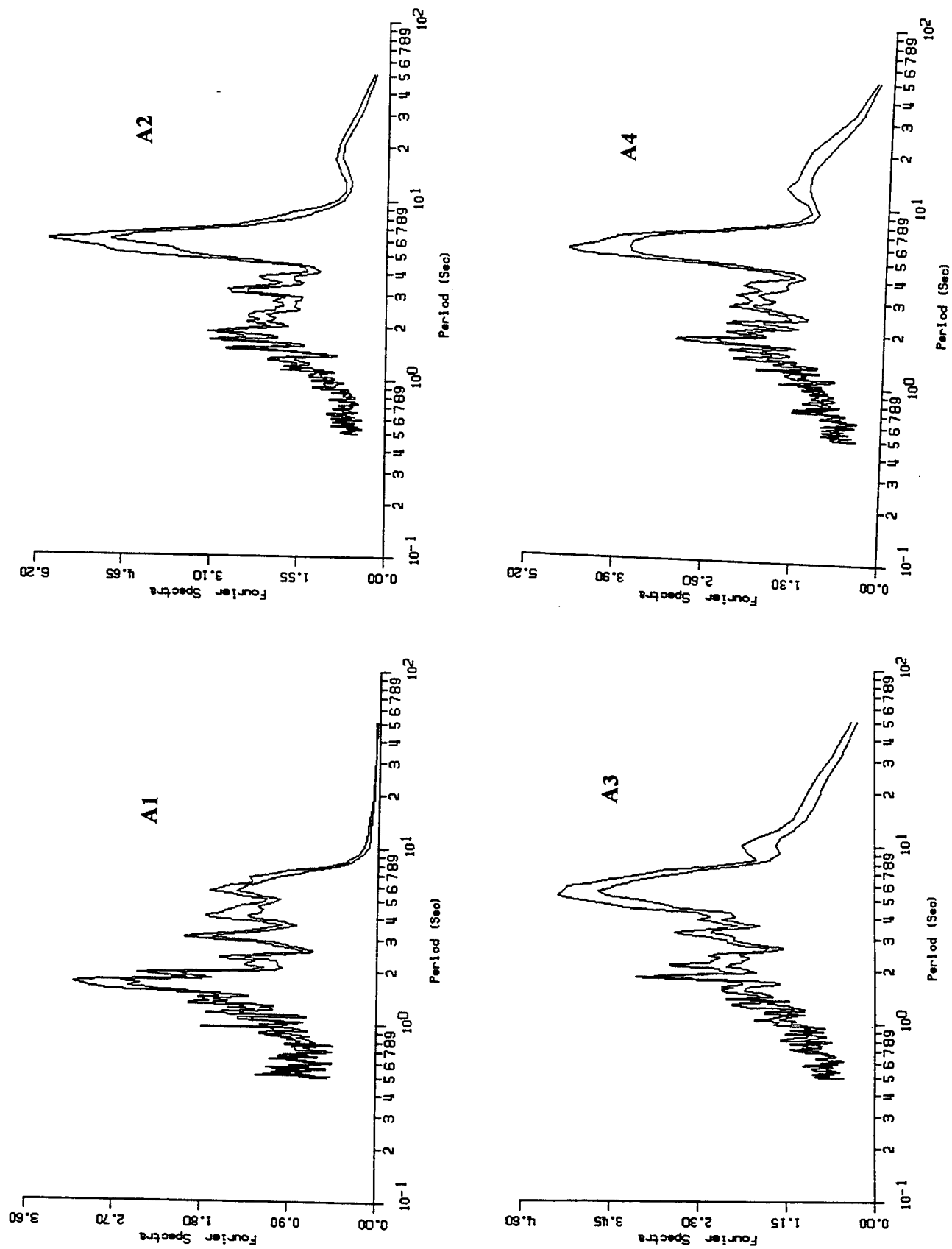


Figure 5.22.a. Fourier spectra NFESC site, stations A1, A2, A3 and A4.

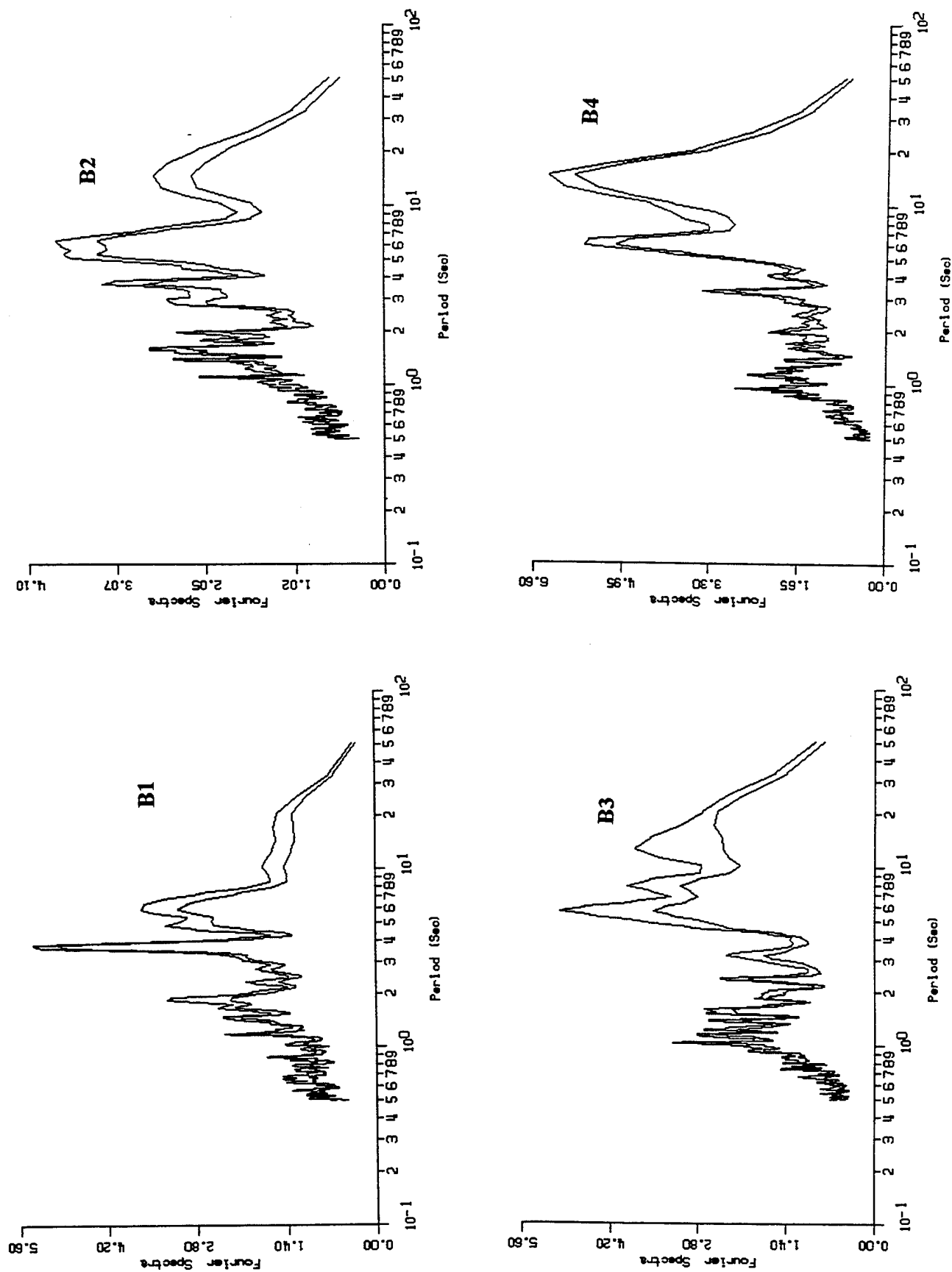


Figure 5.22.b. Fourier spectra NFESC site, stations B1, B2, B3 and B4.

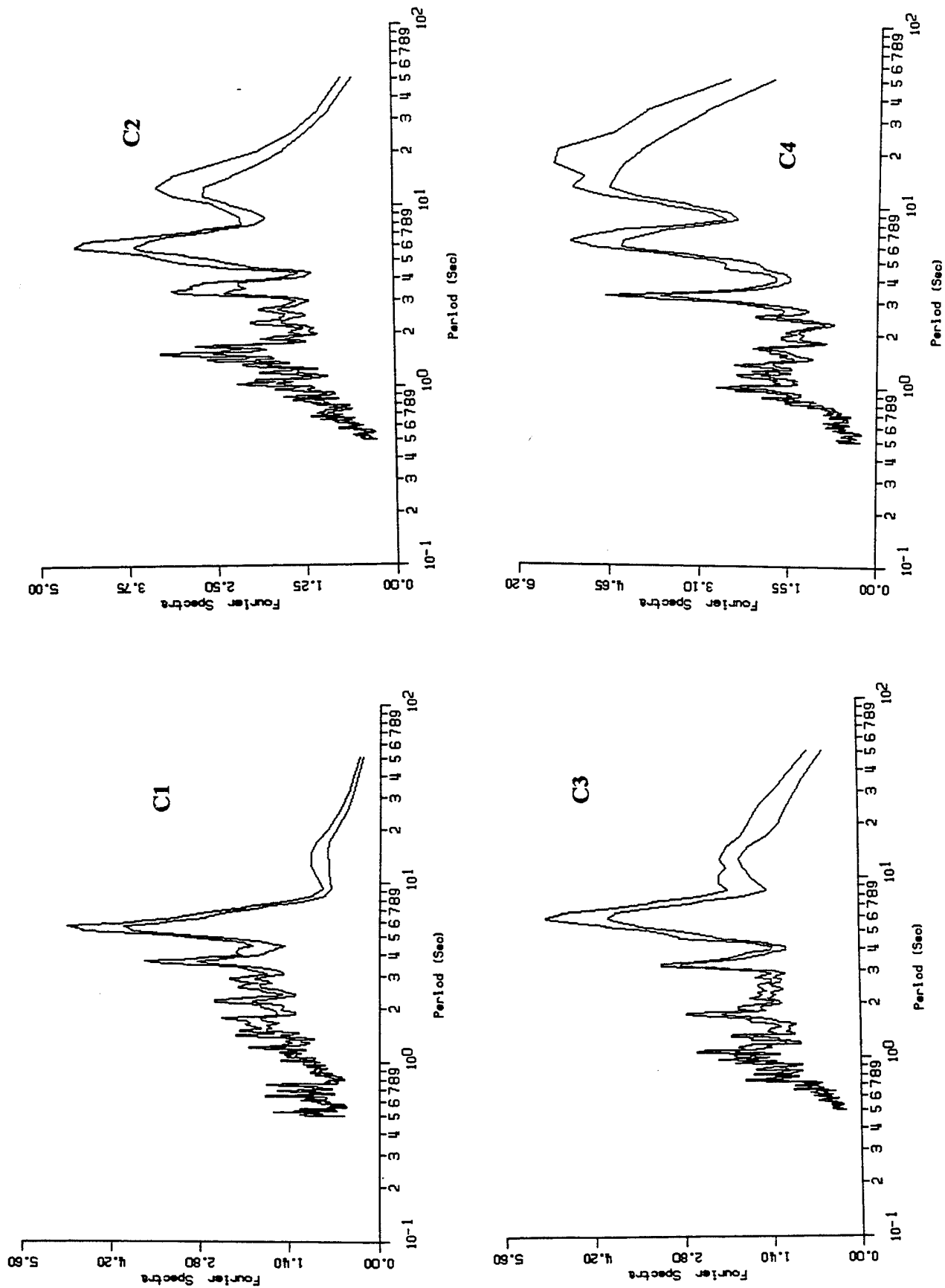


Figure 5.22.c. Fourier spectra NFESC site, stations C1, C2, C3 and C4.



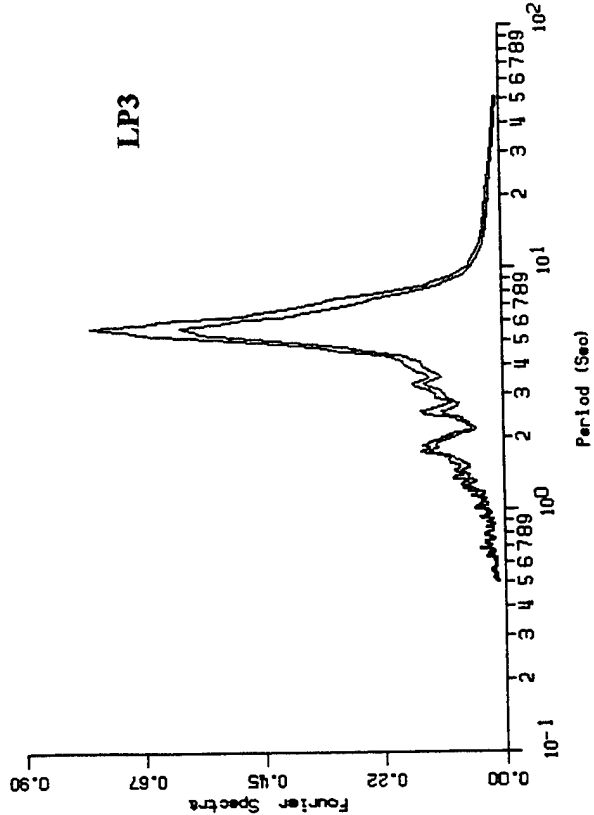
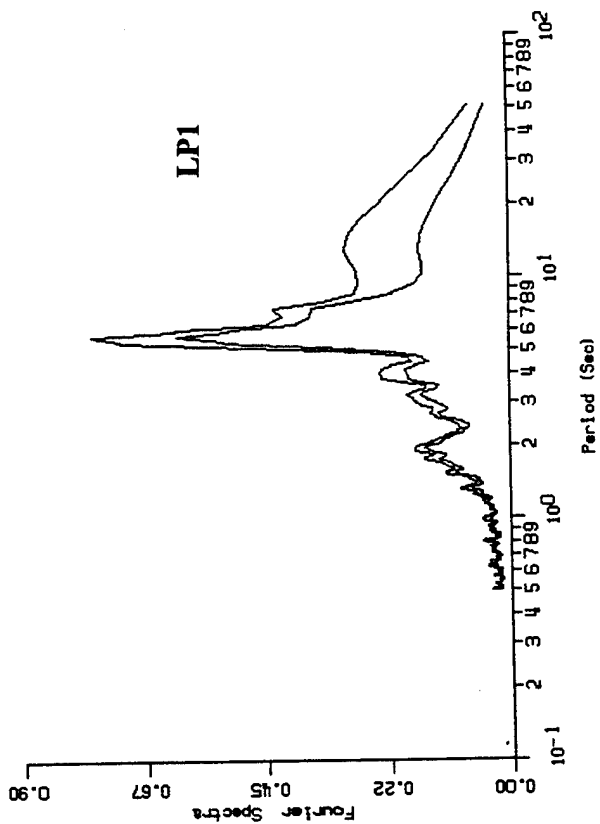
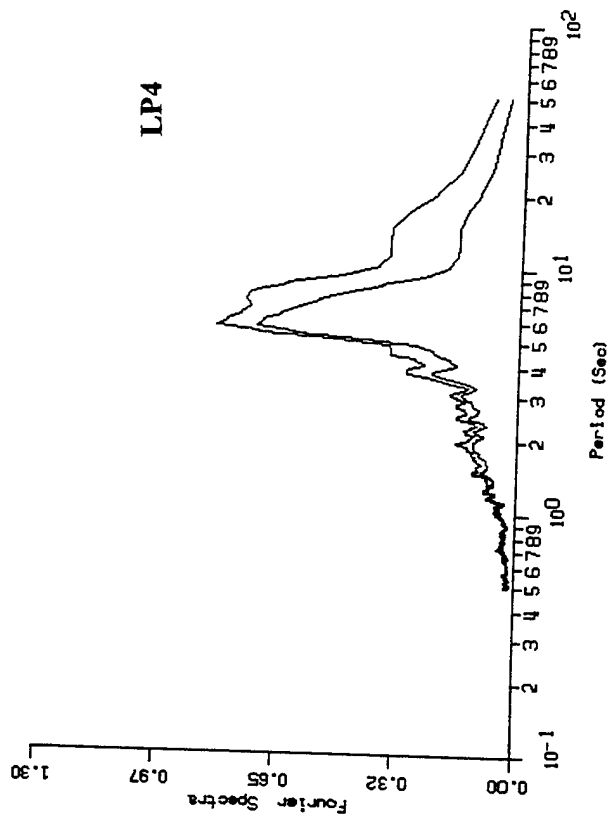
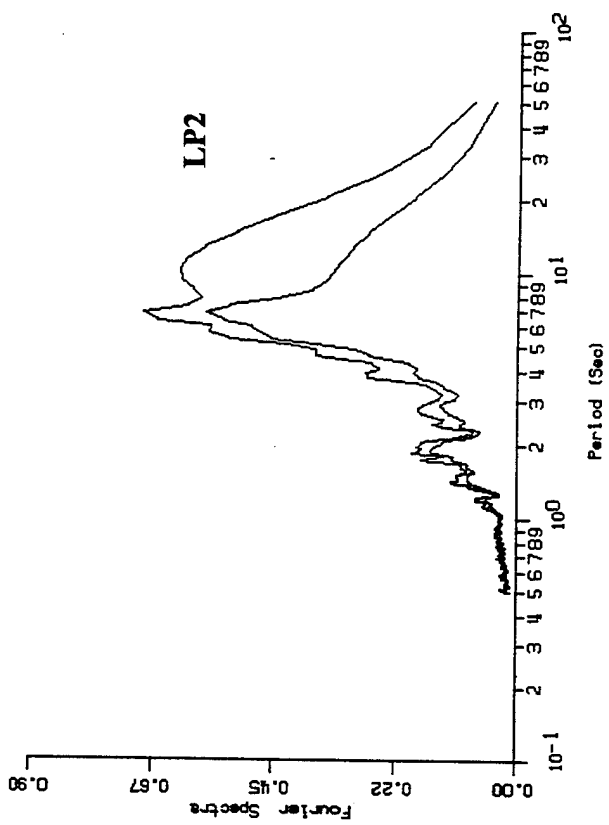


Figure 5.23a. Fourier Spectra Laguna Peak, measurements 1 to 4.

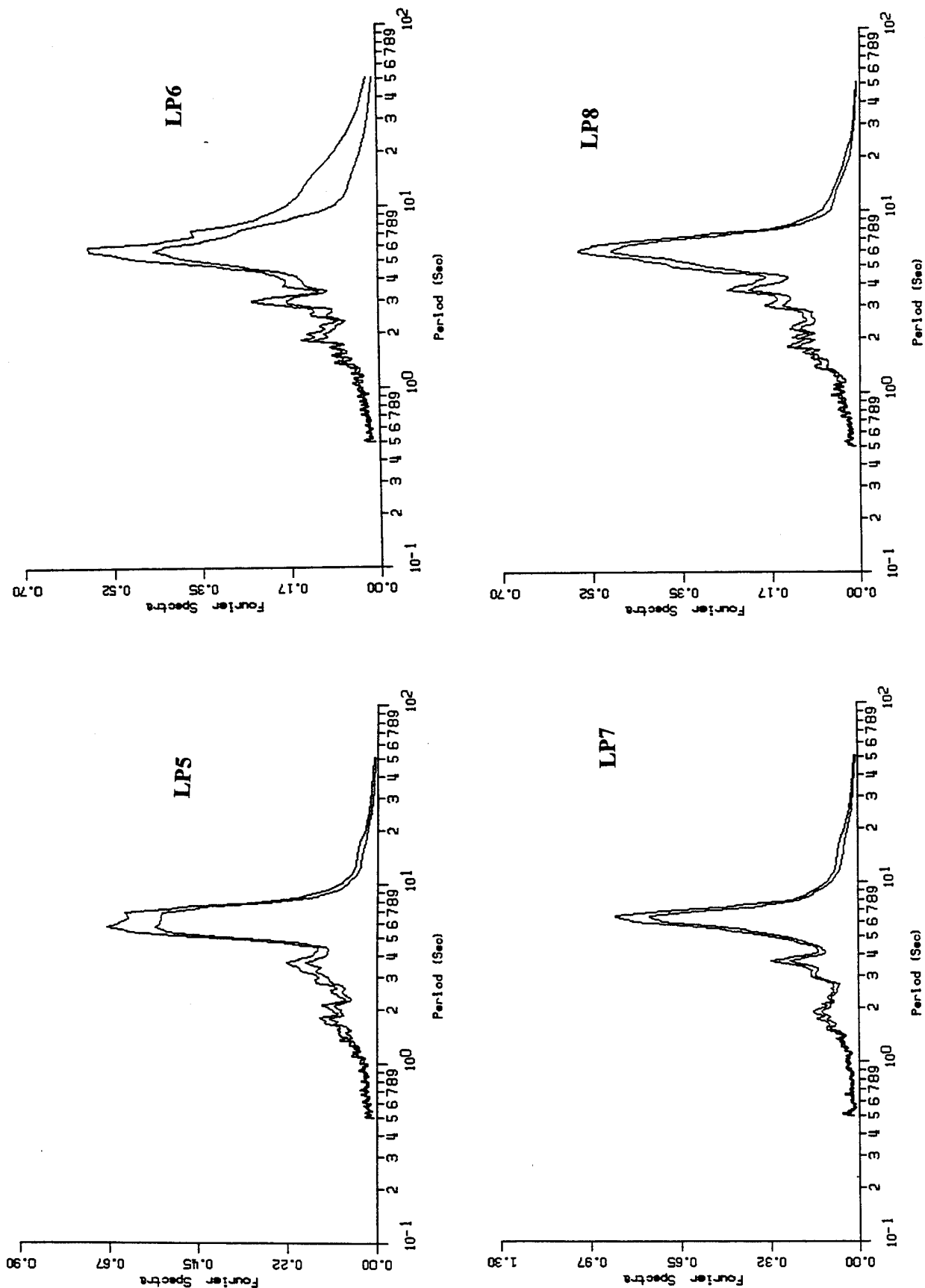


Figure 5.23b. Fourier Spectra Laguna Peak, measurements 5 to 8.

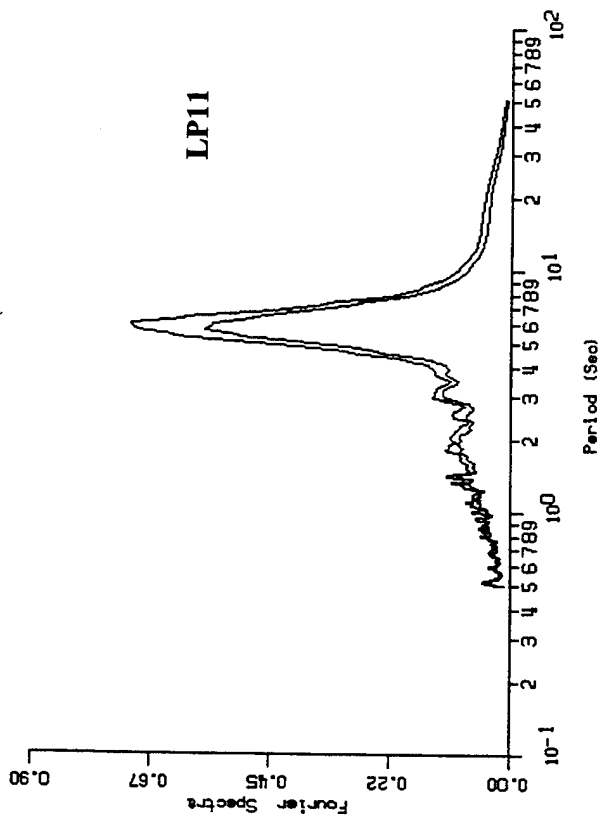
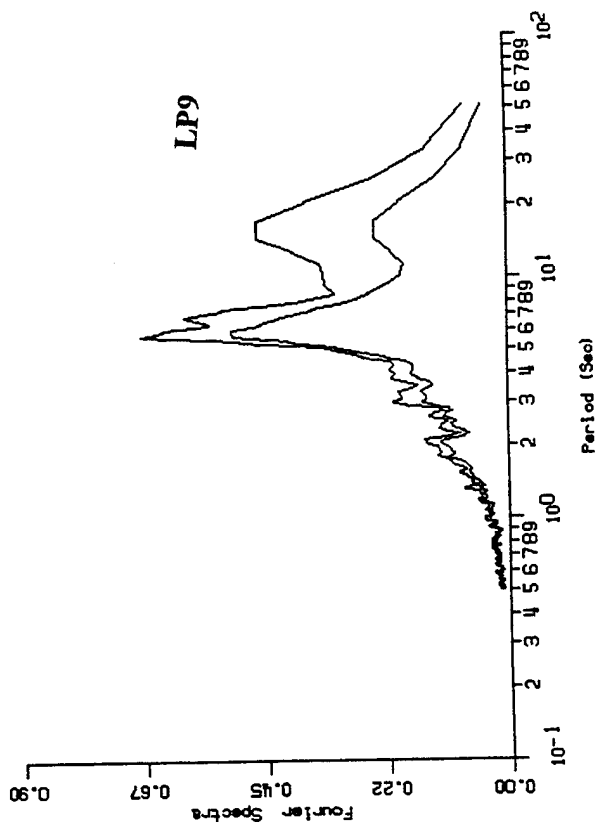
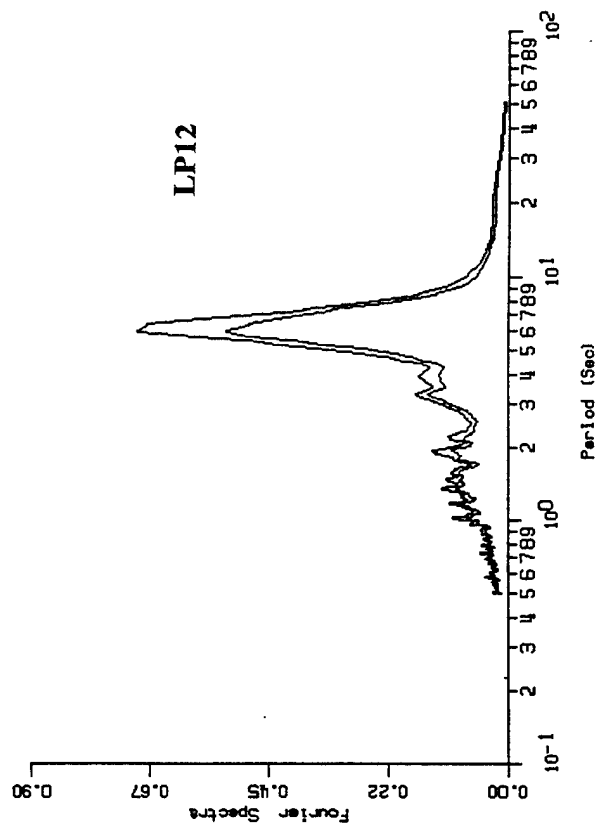
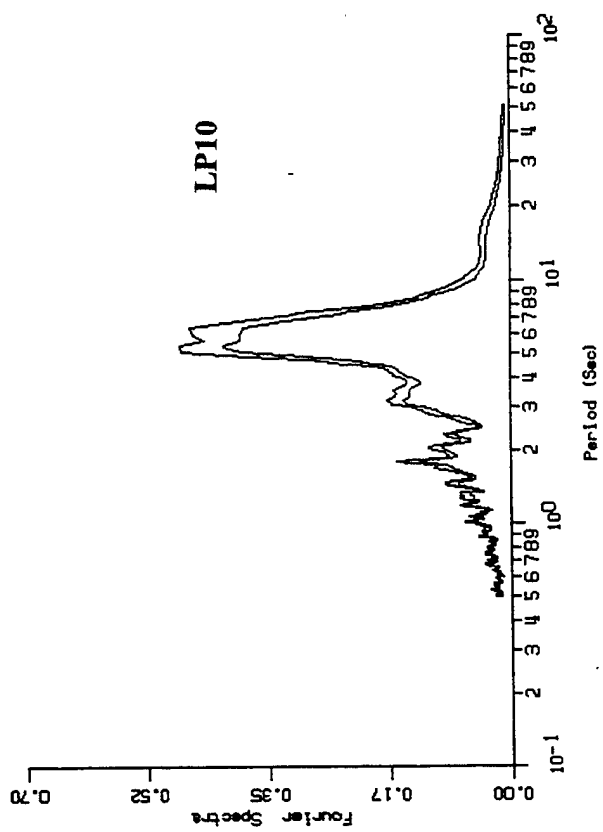


Figure 5.23c. Fourier Spectra Laguna Peak, measurements 9 to 12.

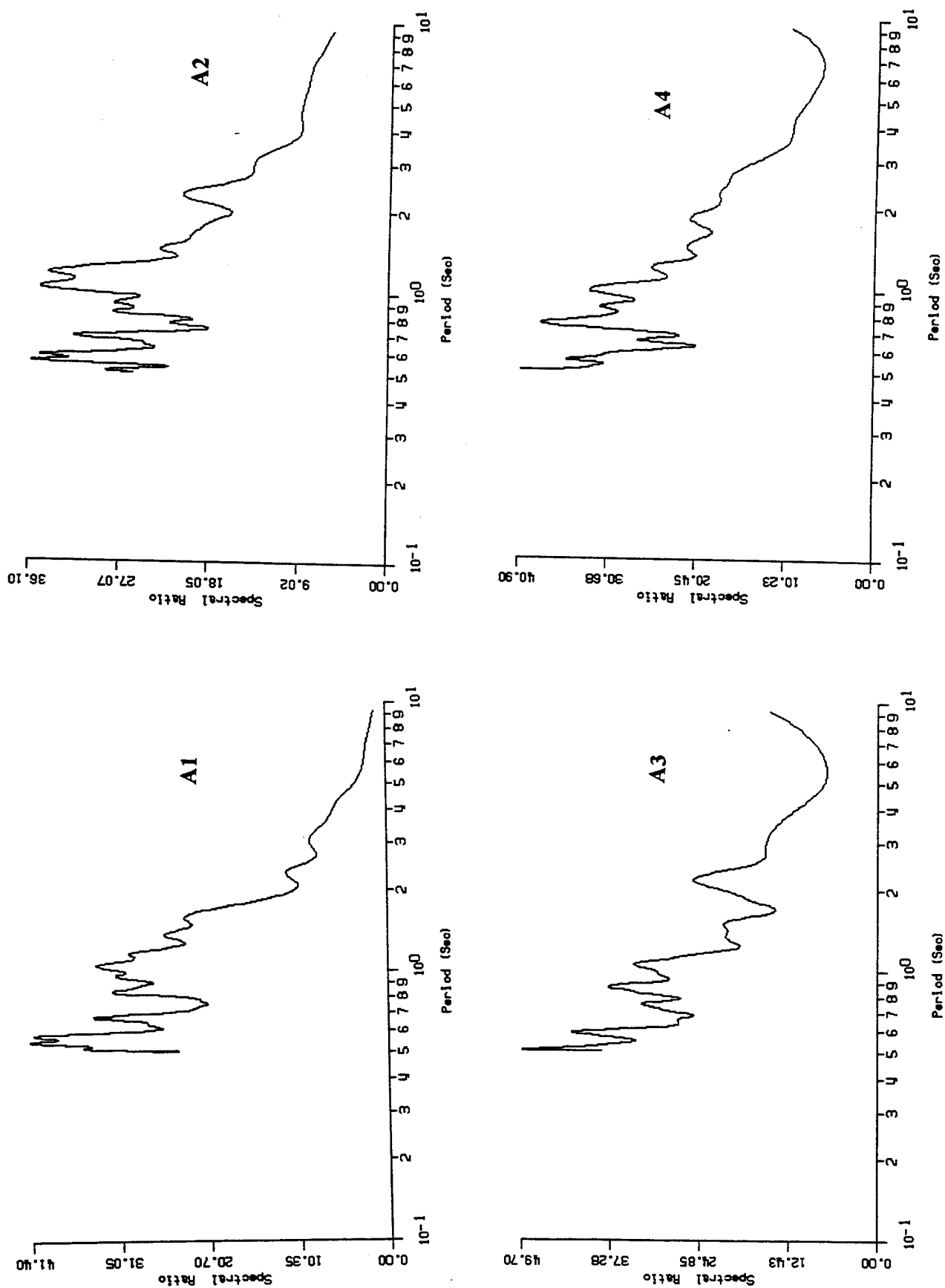
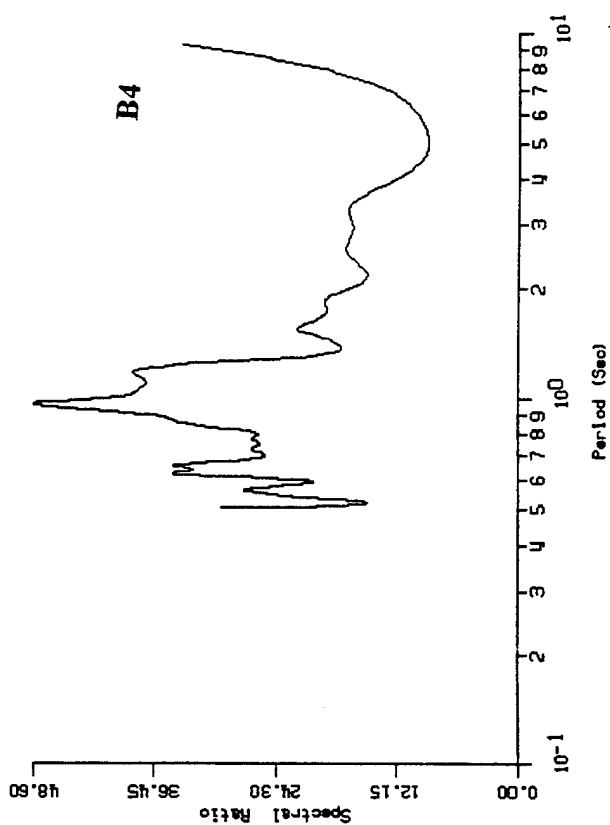
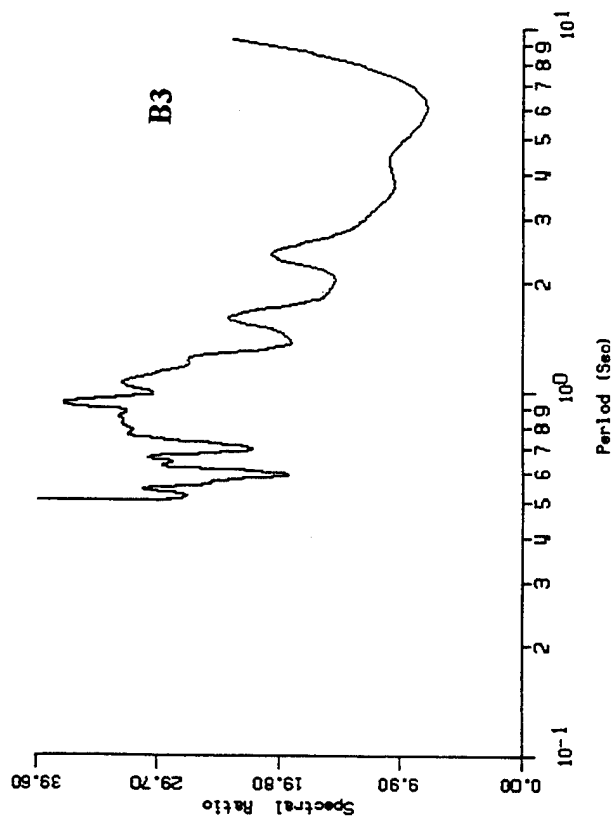
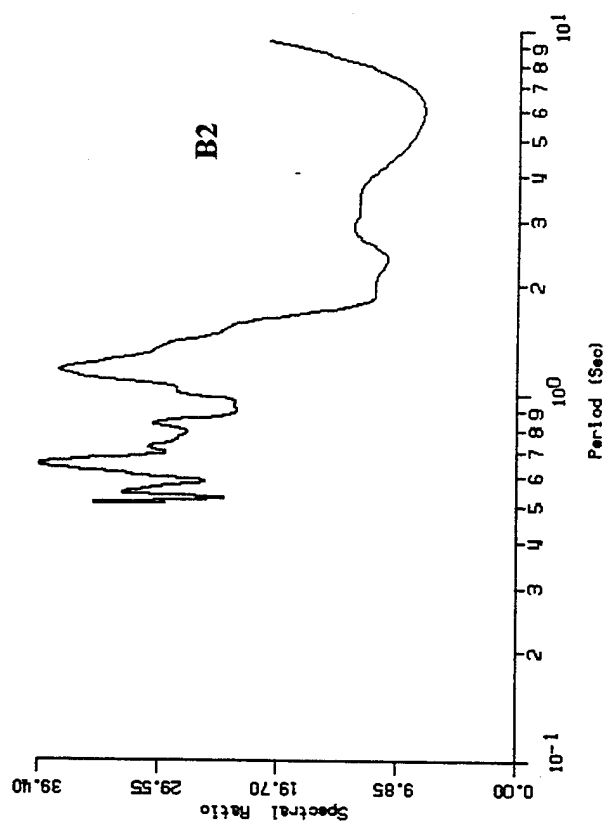
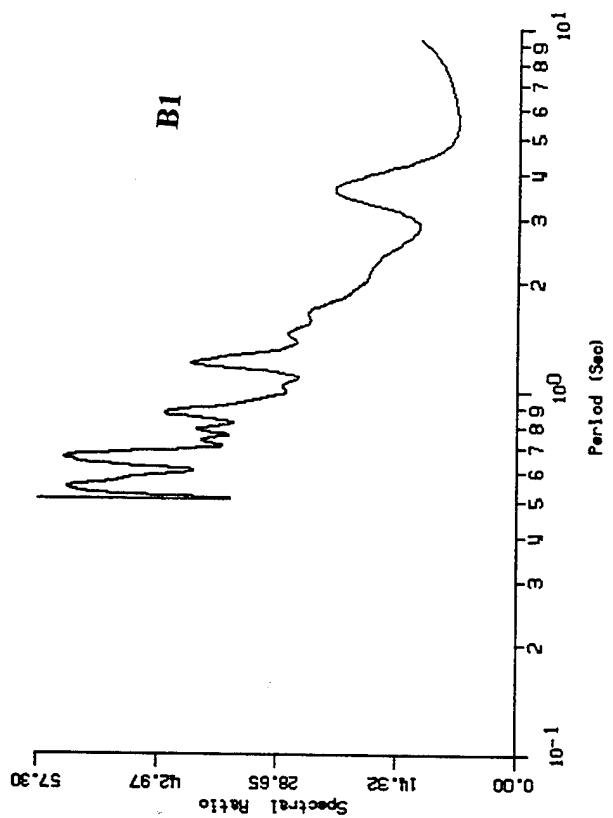


Figure 5.24.a. Spectral ratio NFESC site/ Laguna Peak, stations A1, A2, A3 and A4.



**Figure 5.24.b. Spectral ratio NFESC site/Laguna Peak, stations B1, B2, B3 and B4.**

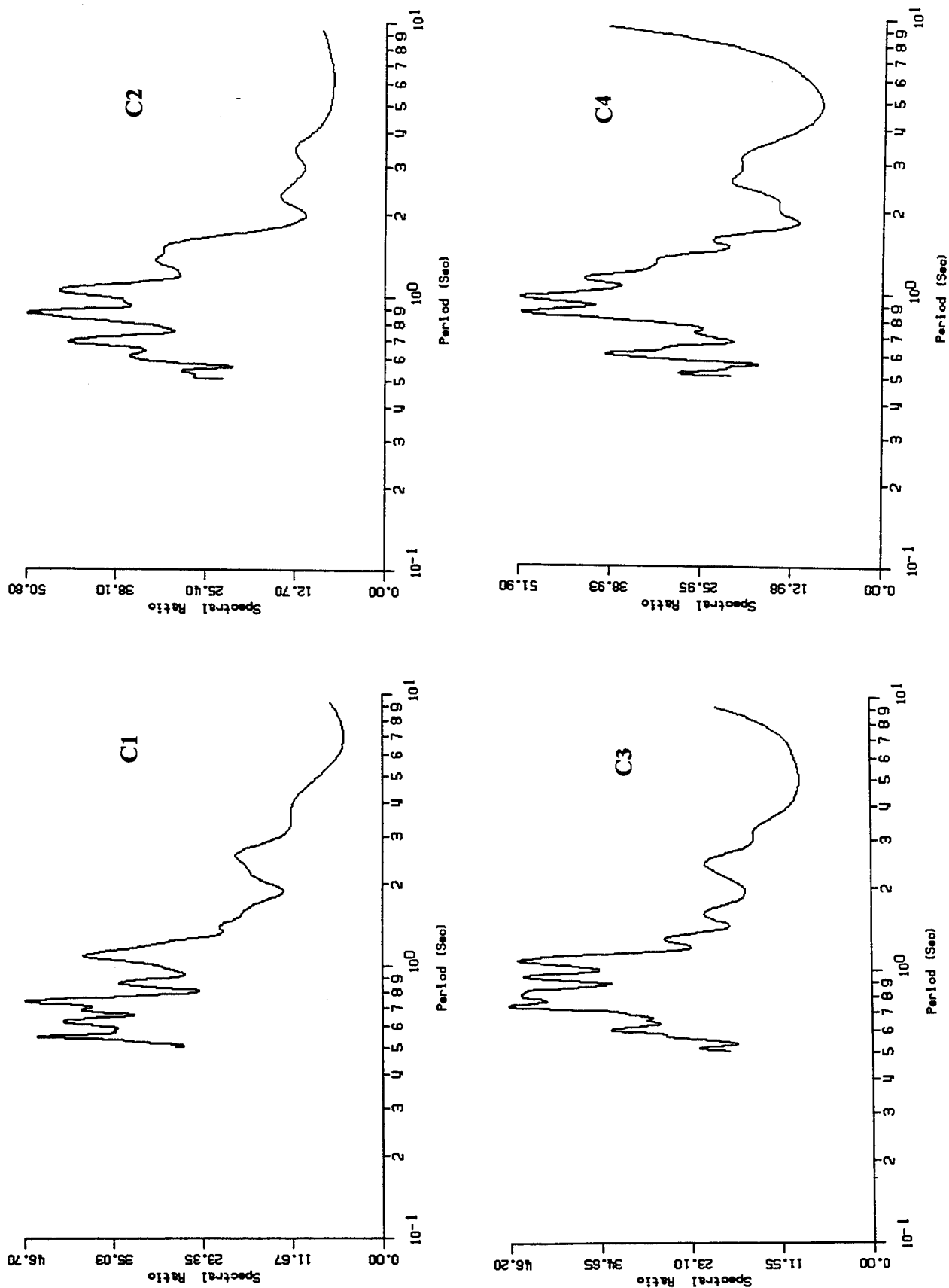


Figure 5.24.c. Spectral ratio NFESC site/Laguna Peak, stations C1, C2, C3 and C4.

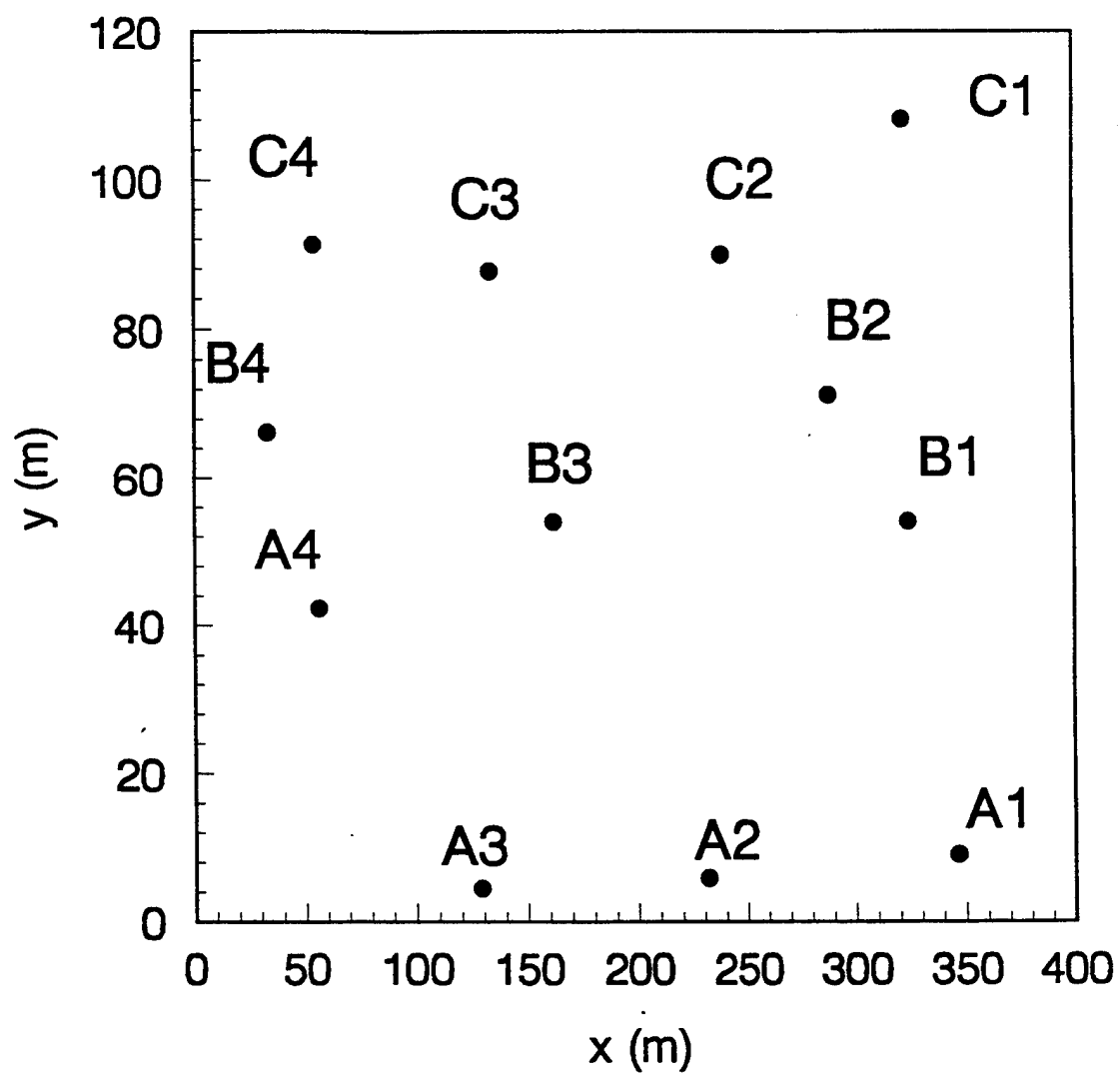


Figure 5.25a. Layout of stations NFESC site, see Figure 5.21 for site map.

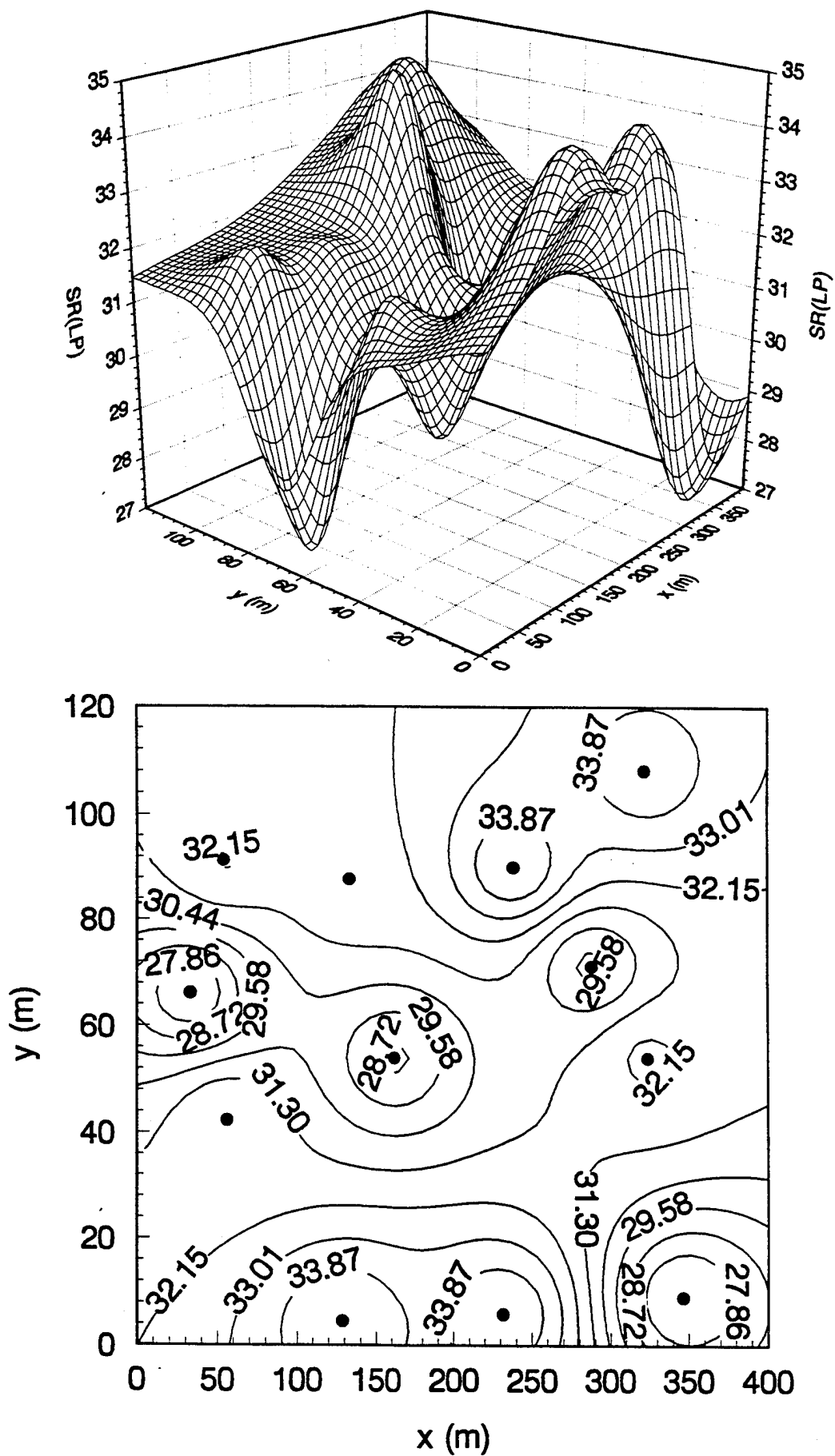


Figure 5.25b. Spectral ratio, period range 0.5 to 1.0 seconds



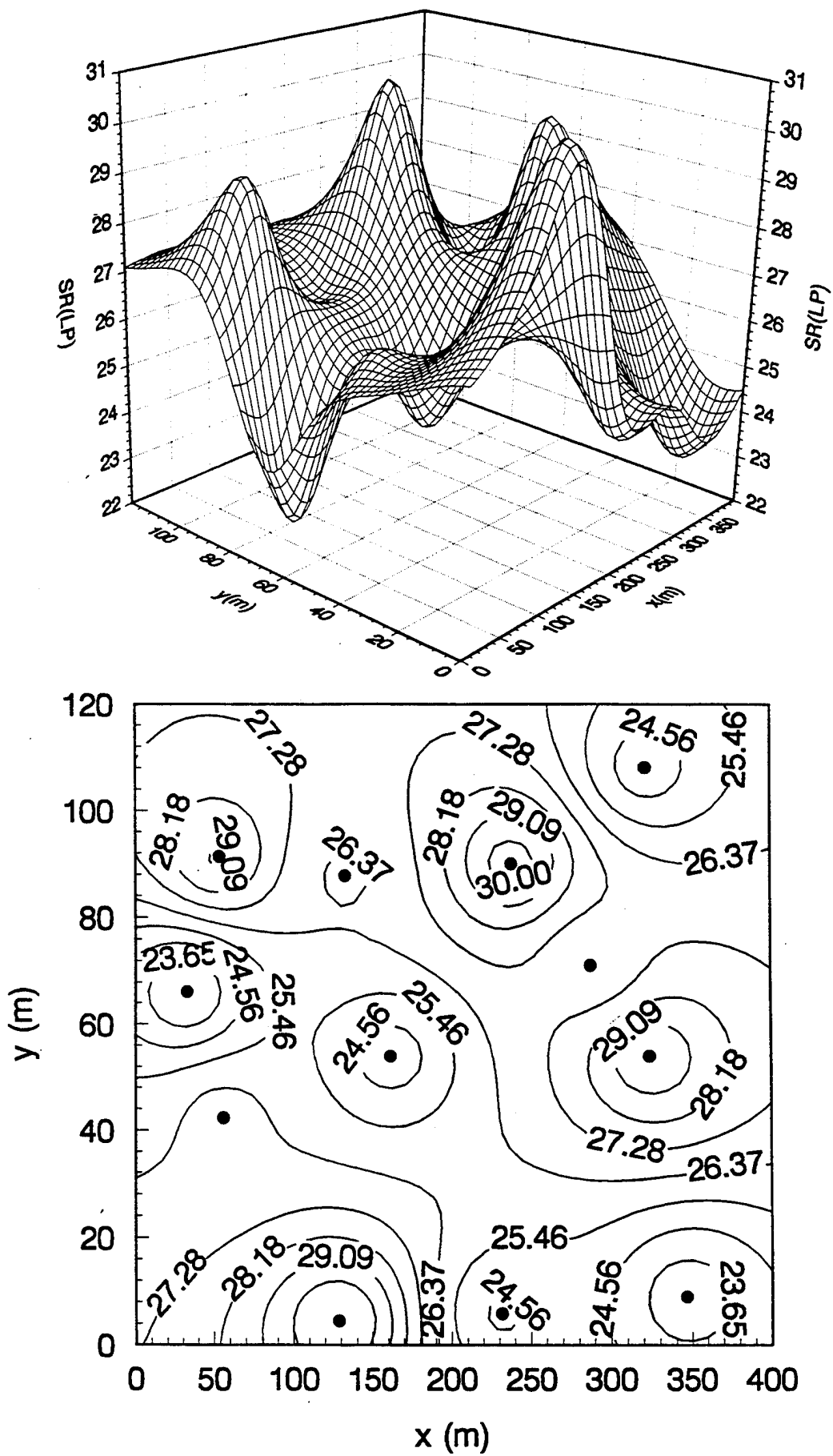


Figure 5.25c. Spectral ratio, period range 1.0 to 2.0 seconds

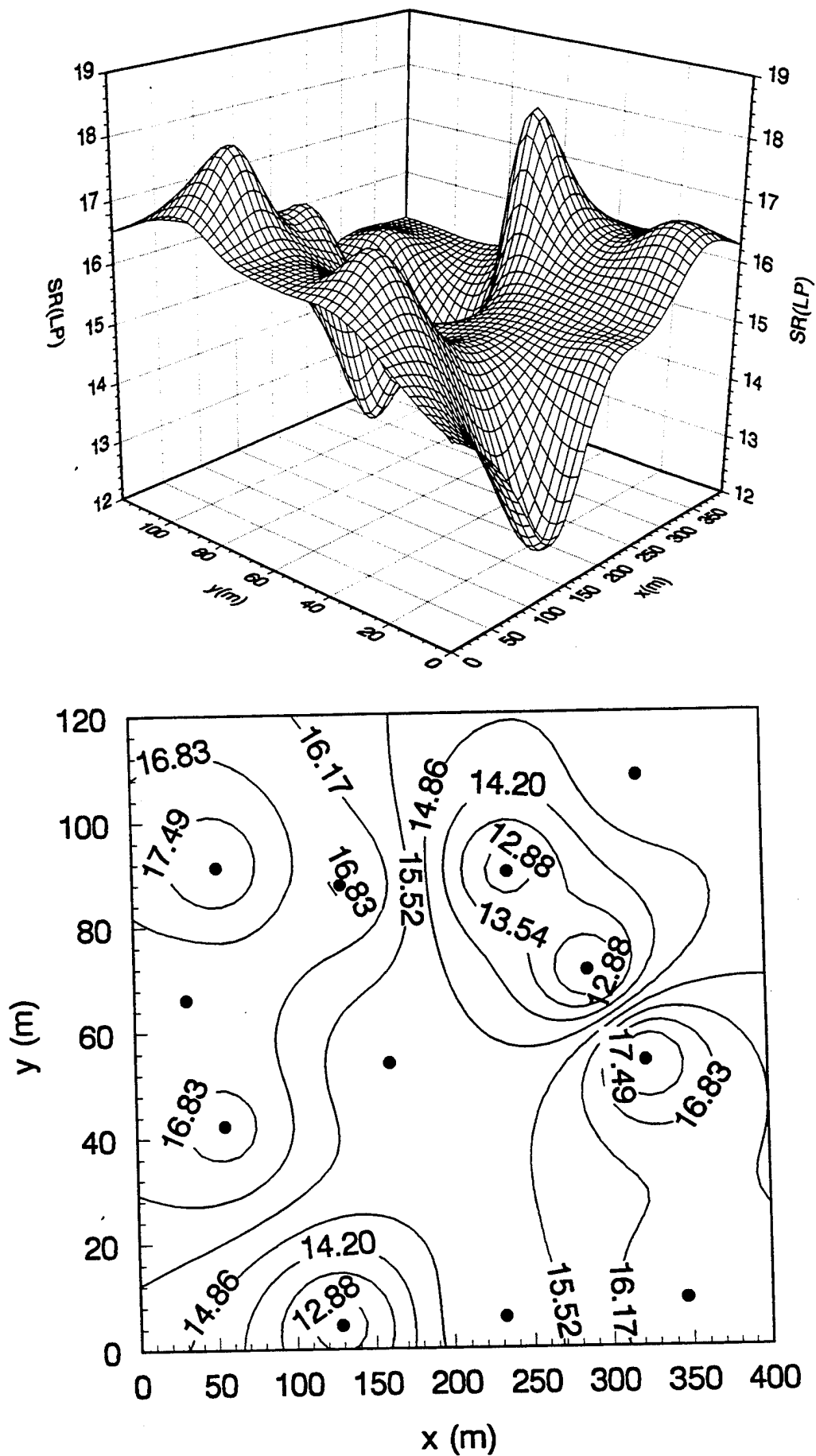


Figure 5.25d. Spectral ratio, period range 2.0 to 4.0 seconds

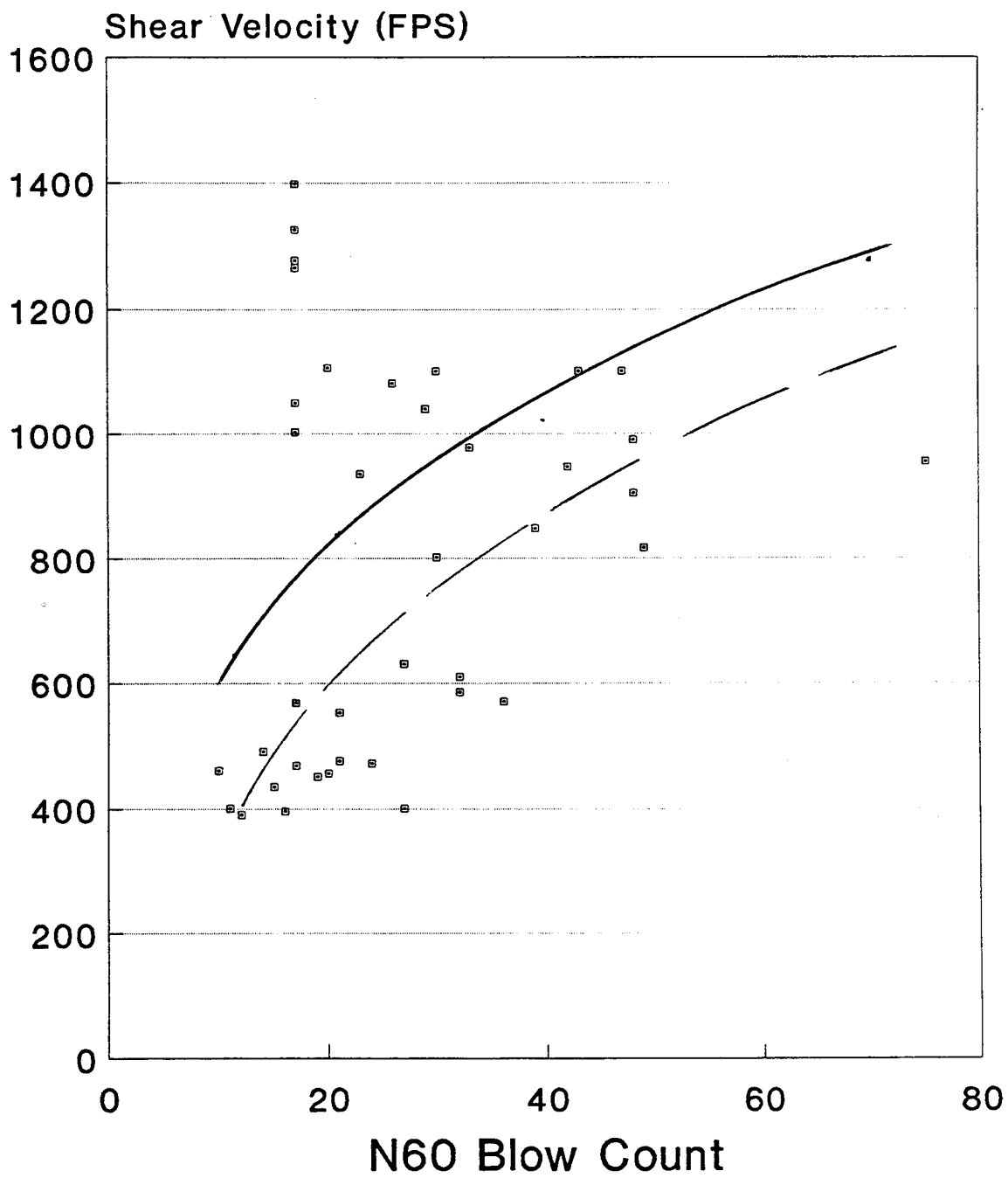


Figure 5.26. Relationship of shear velocity to blowcount.

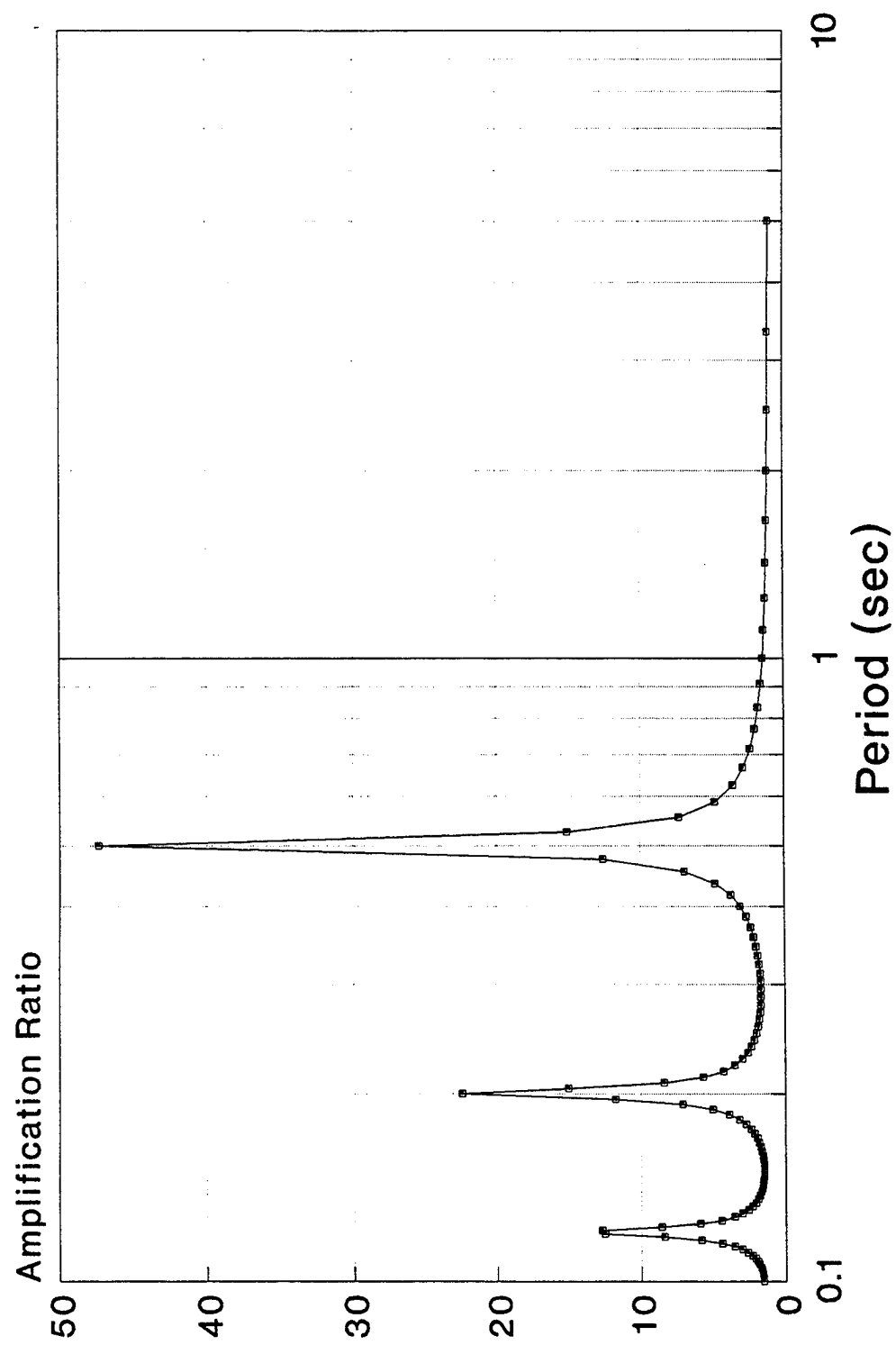


Figure 5.27. Amplification ratio computed using microseism excitation.

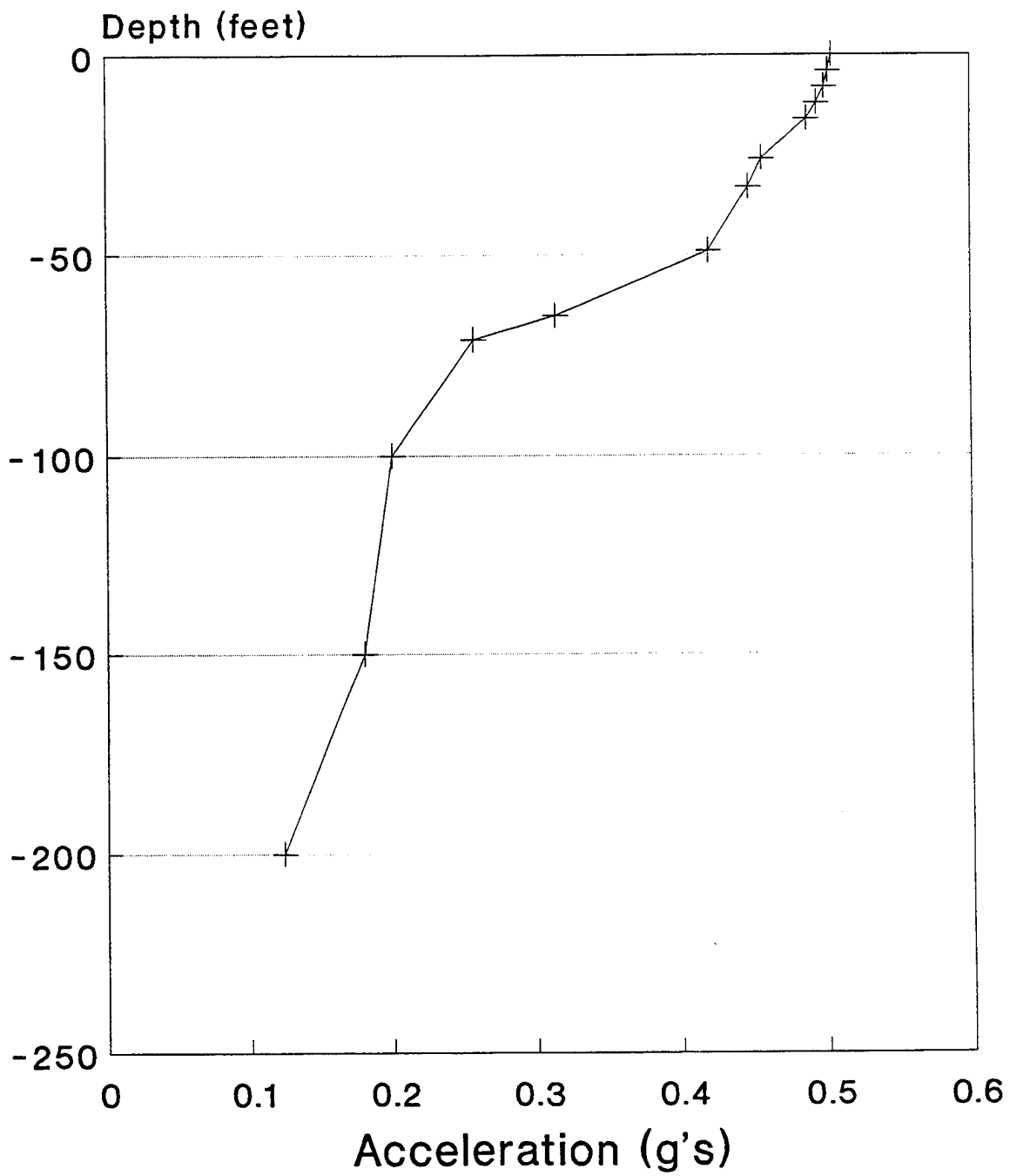


Figure 5.28 Acceleration response, 250 ft profile.

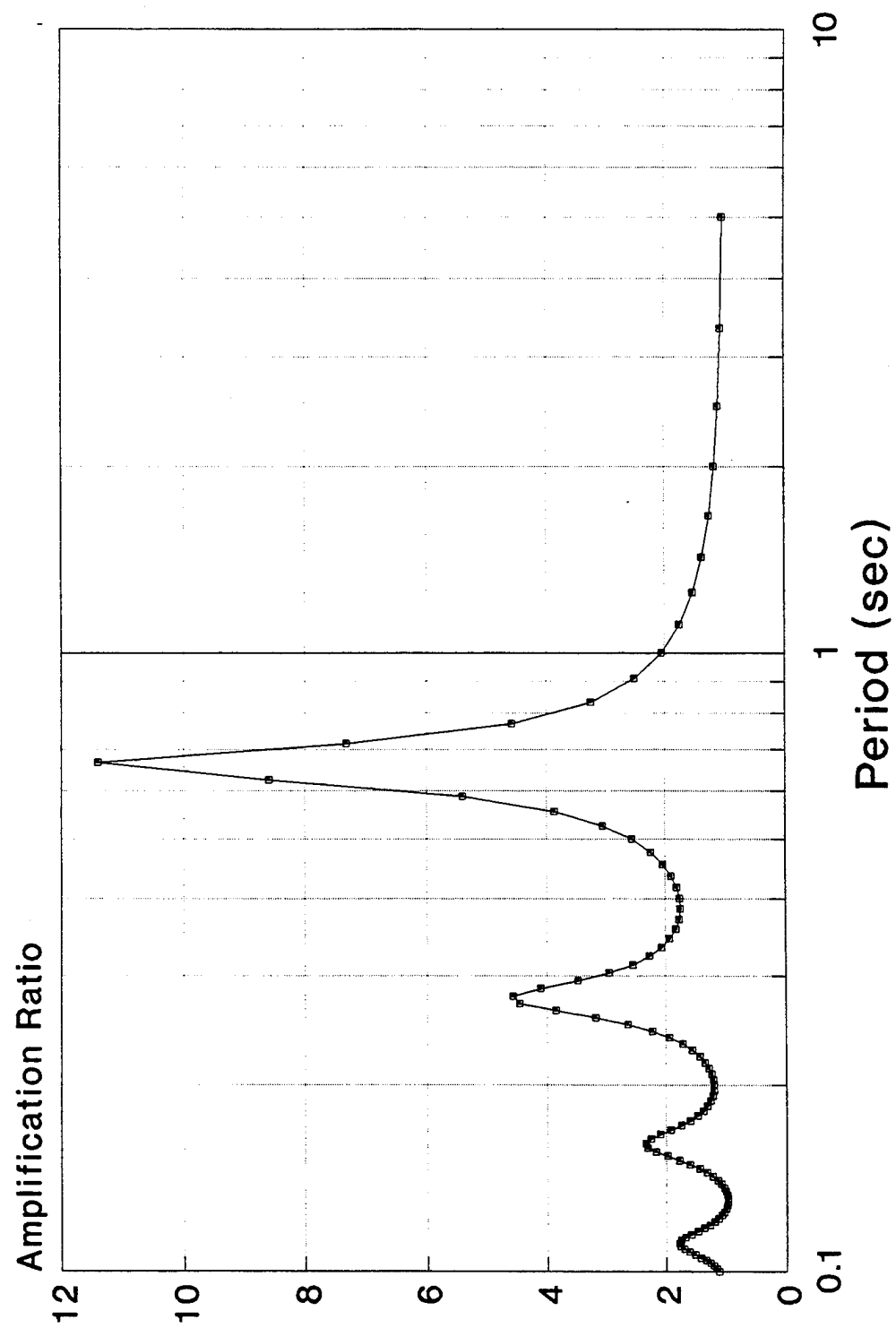


Figure 5.29 Amplification ratio, 250 ft profile.

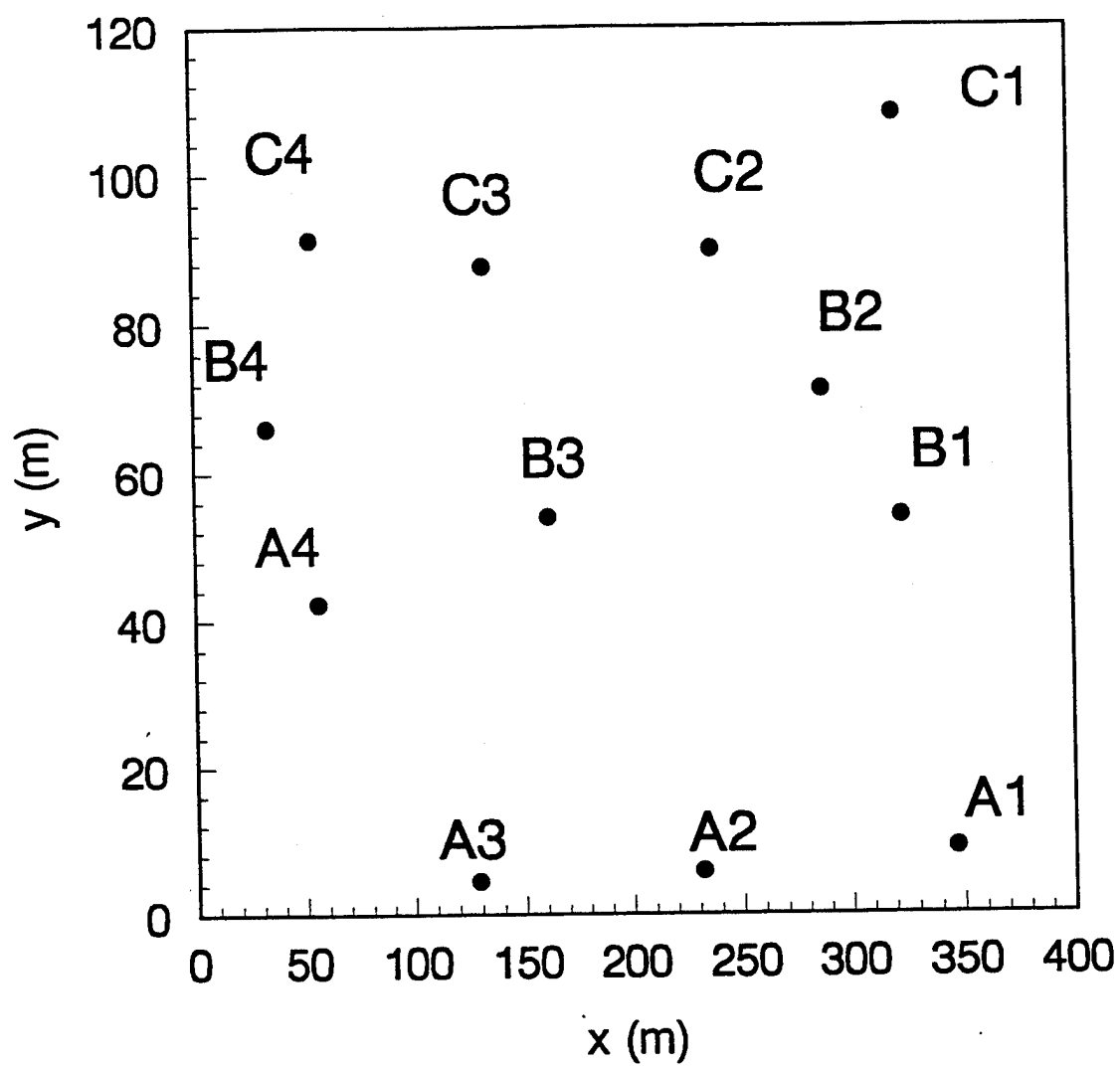


Figure 5.30a. Layout of stations, NFESC site,  
see Figure 5.21 for site map.

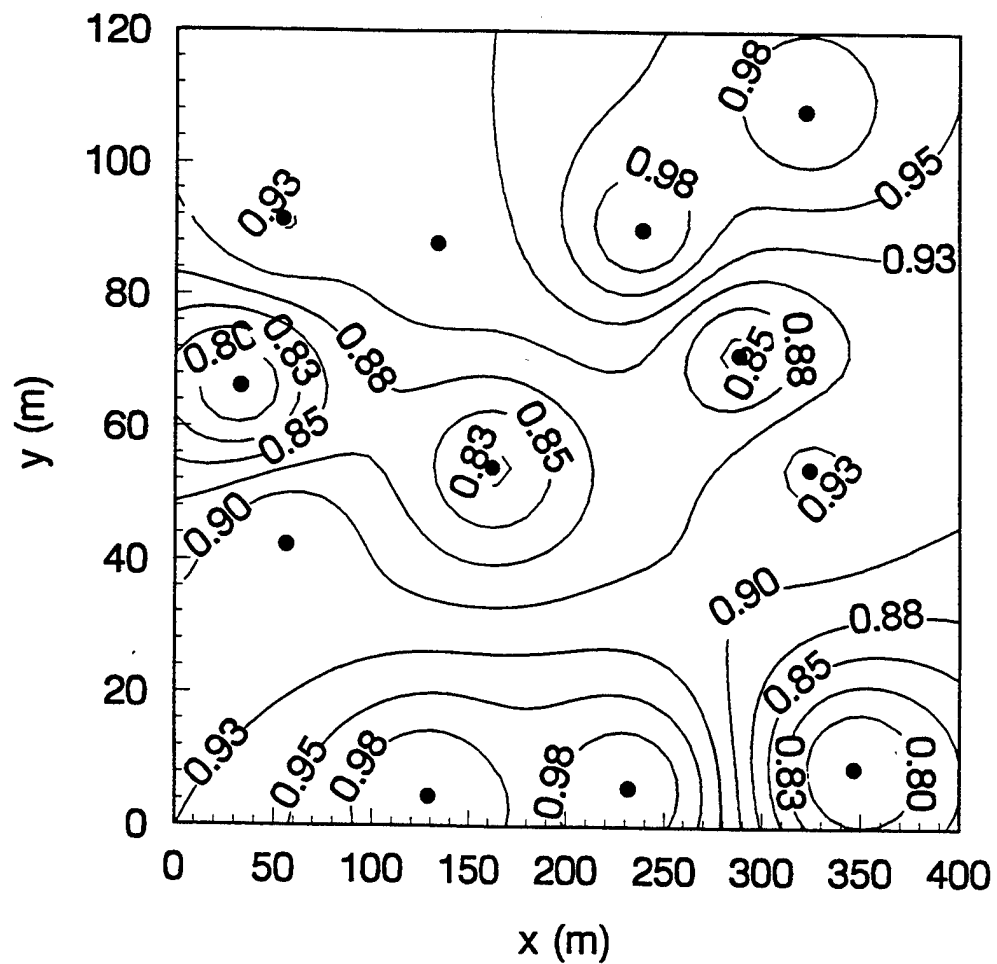
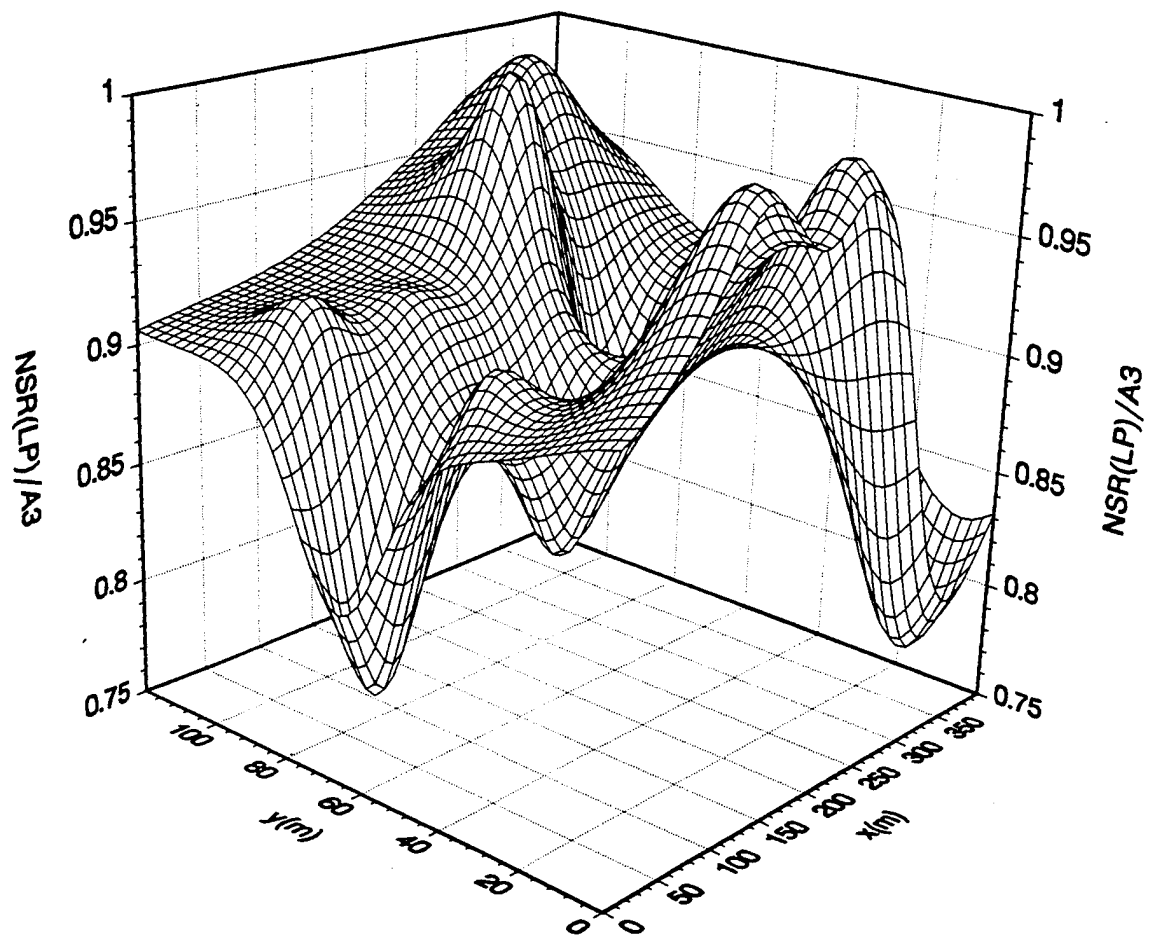


Figure 5.30b. Spectral ratio, period range 0.5 to 1.0 seconds.



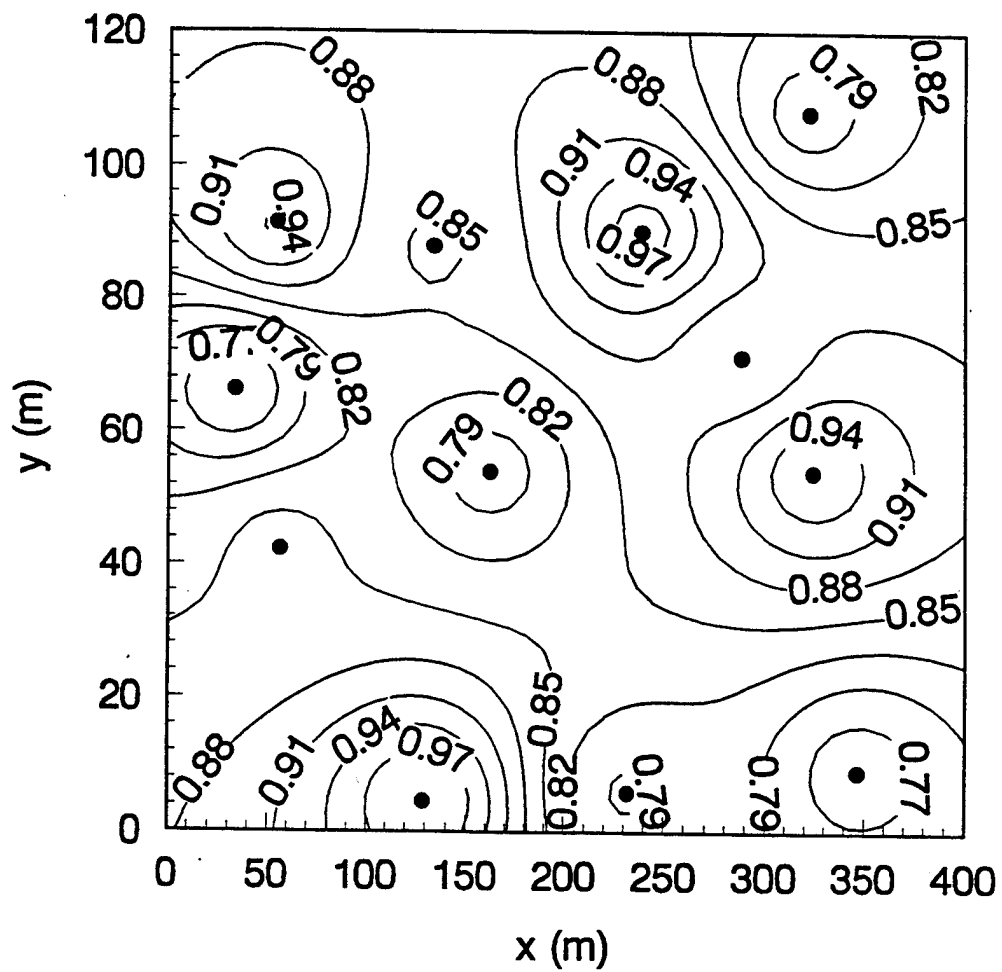
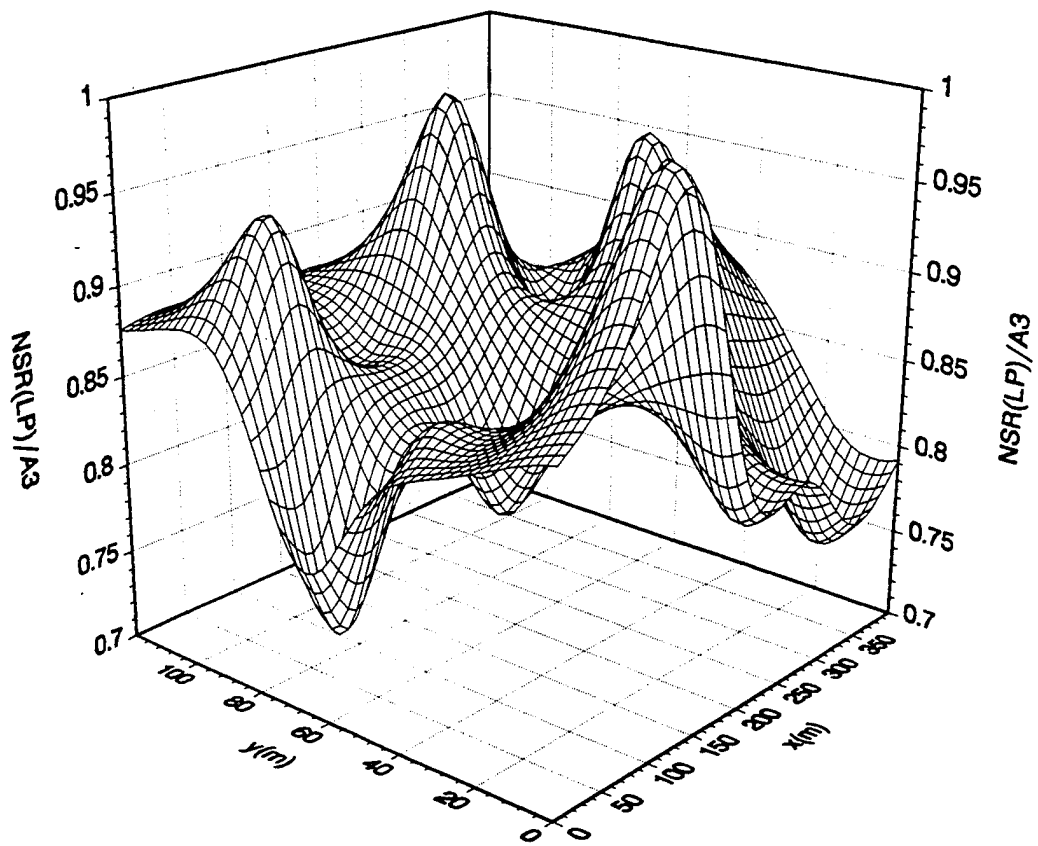


Figure 5.30c. Spectral ratio, period range 1.0 to 2.0 seconds.

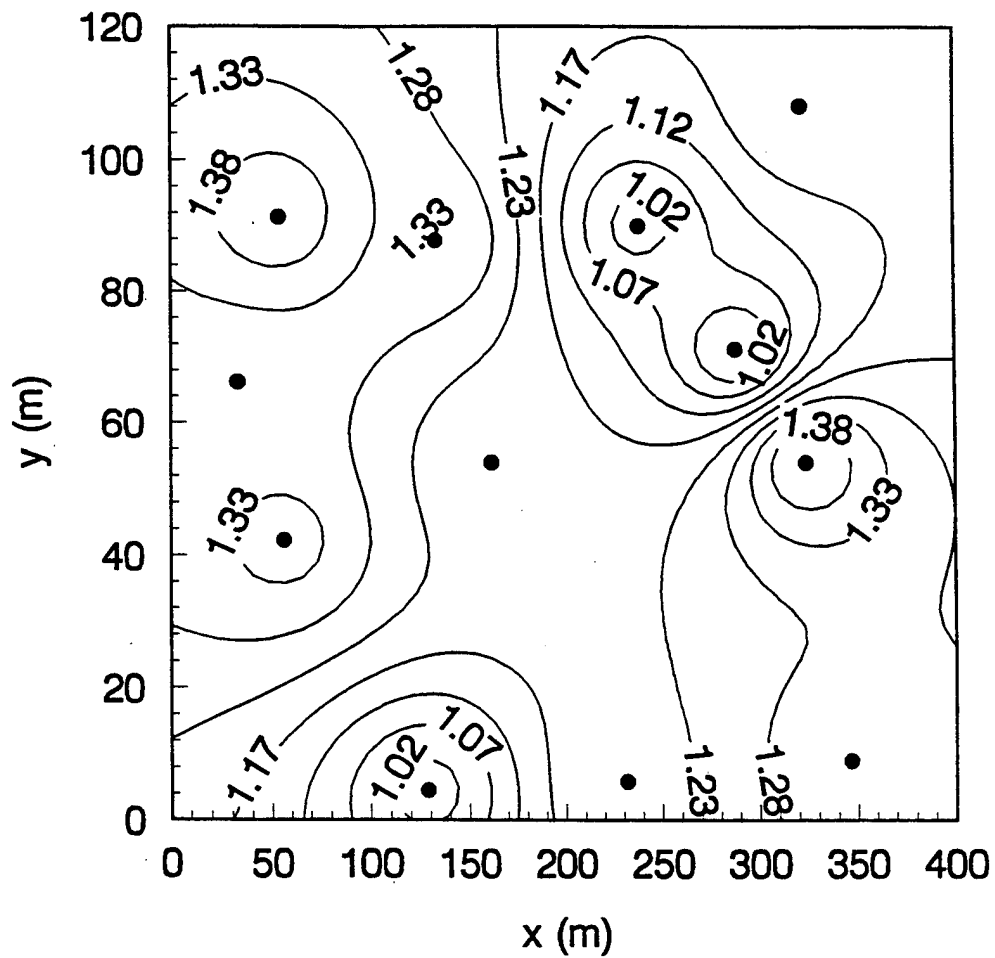
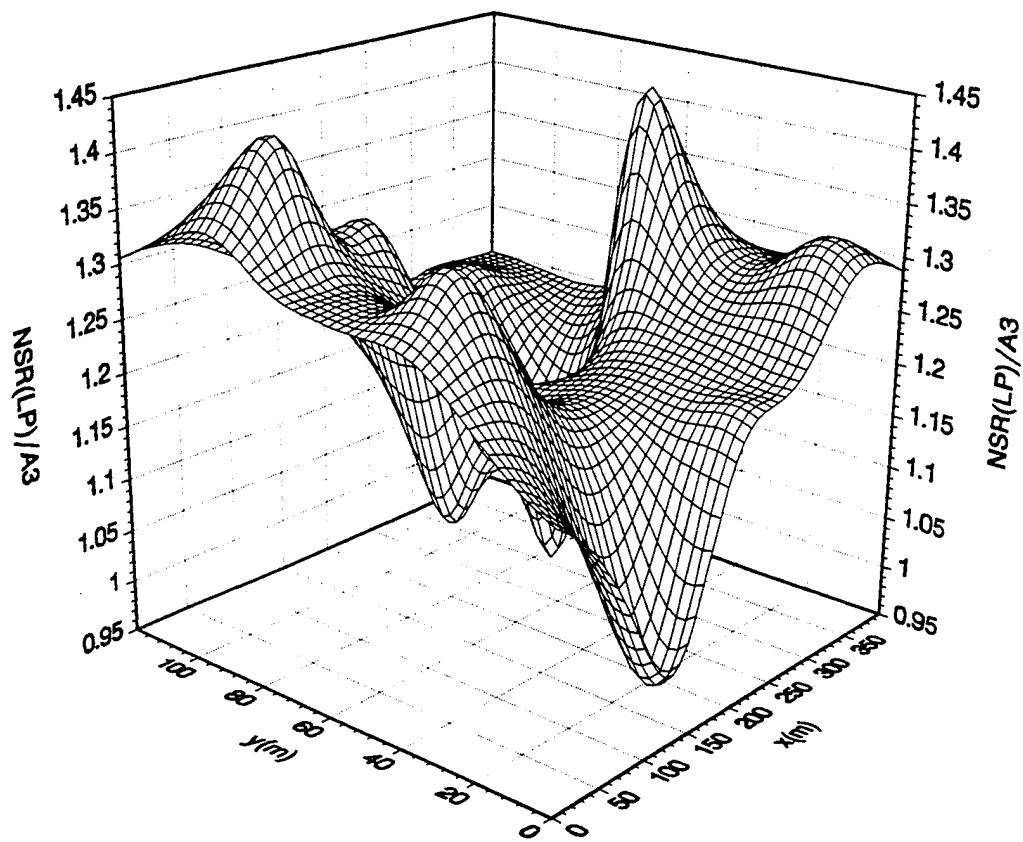
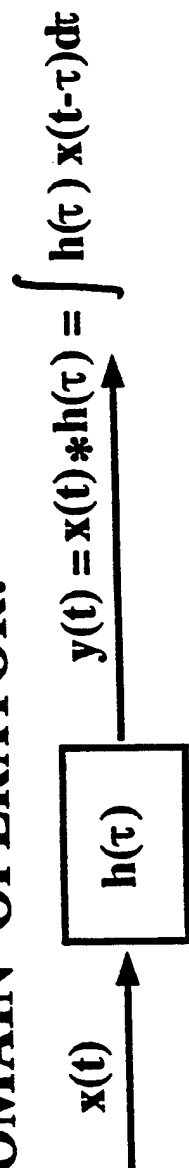
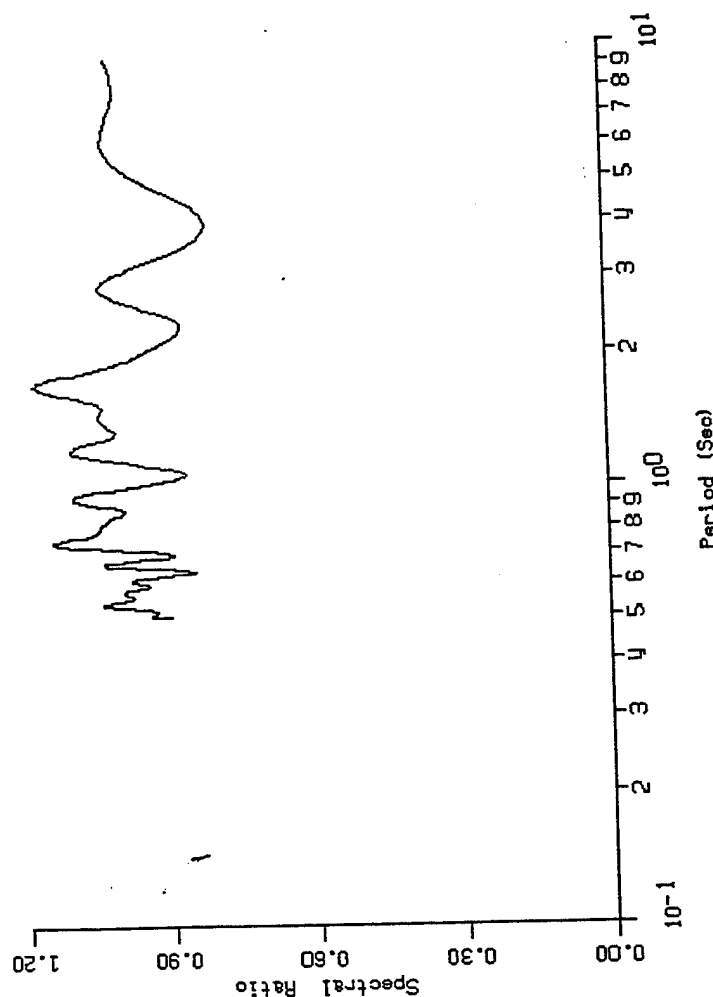
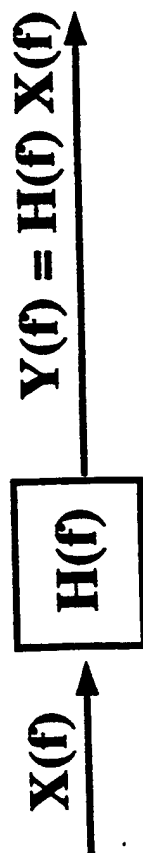


Figure 5.30d. Spectral ratio, period range 2.0 to 4.0 seconds.

## TIME DOMAIN OPERATOR:



## FREQUENCY DOMAIN OPERATOR:



$H()$  = Site A4 / Site A3

$x()$  = Earthquake Acceleration  
site A3

$y()$  = Earthquake Acceleration  
site A4

Figure 5.31. Transfer function site A4 relative to site A3.

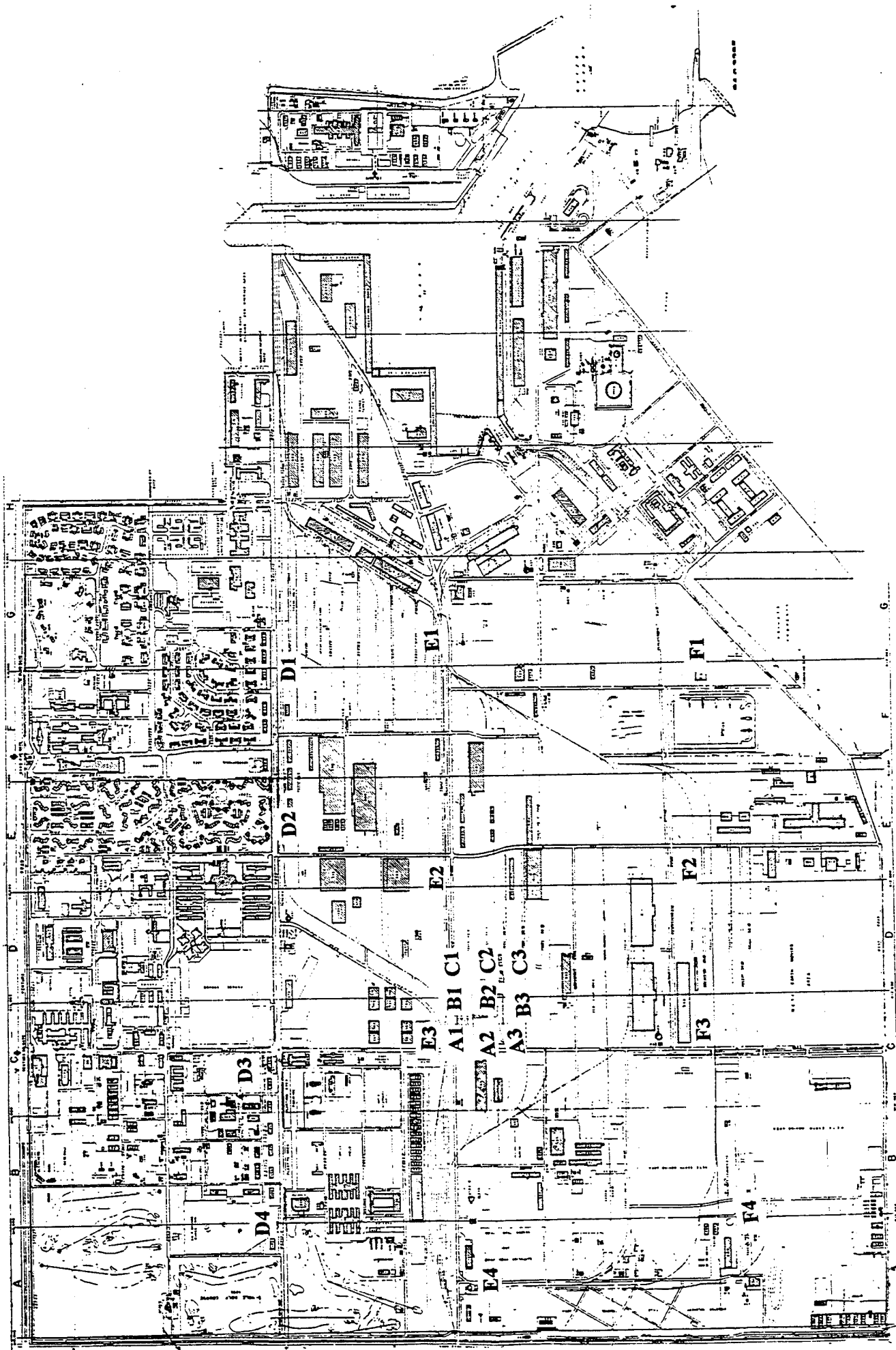


Figure 5.32. Map of NCBC showing measurement stations.

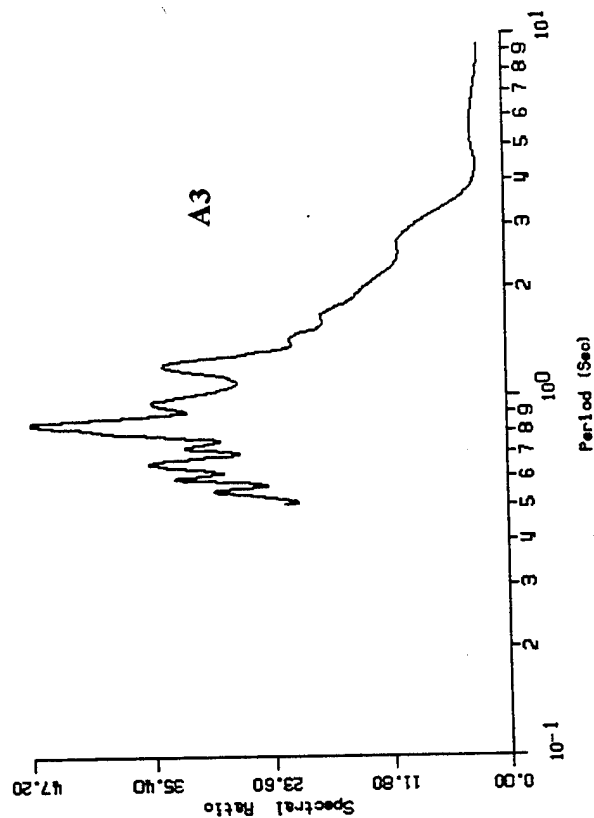
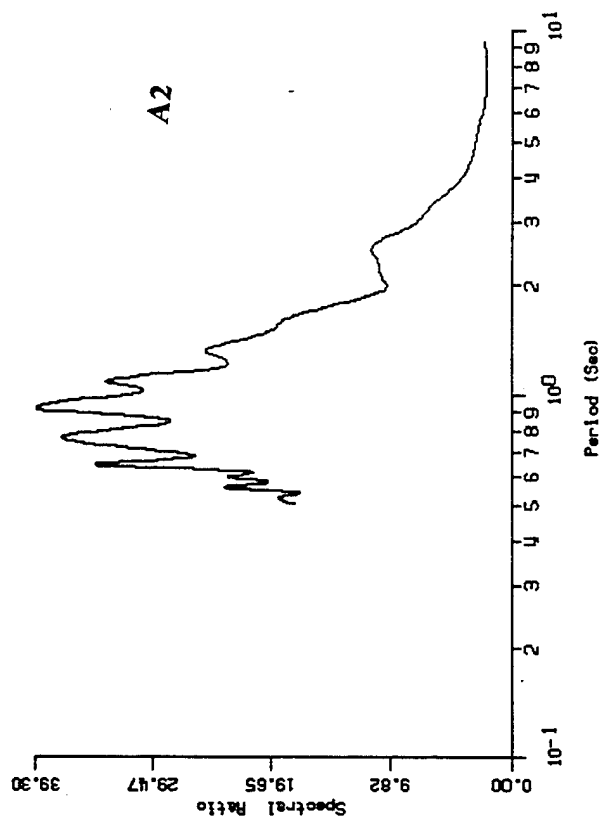
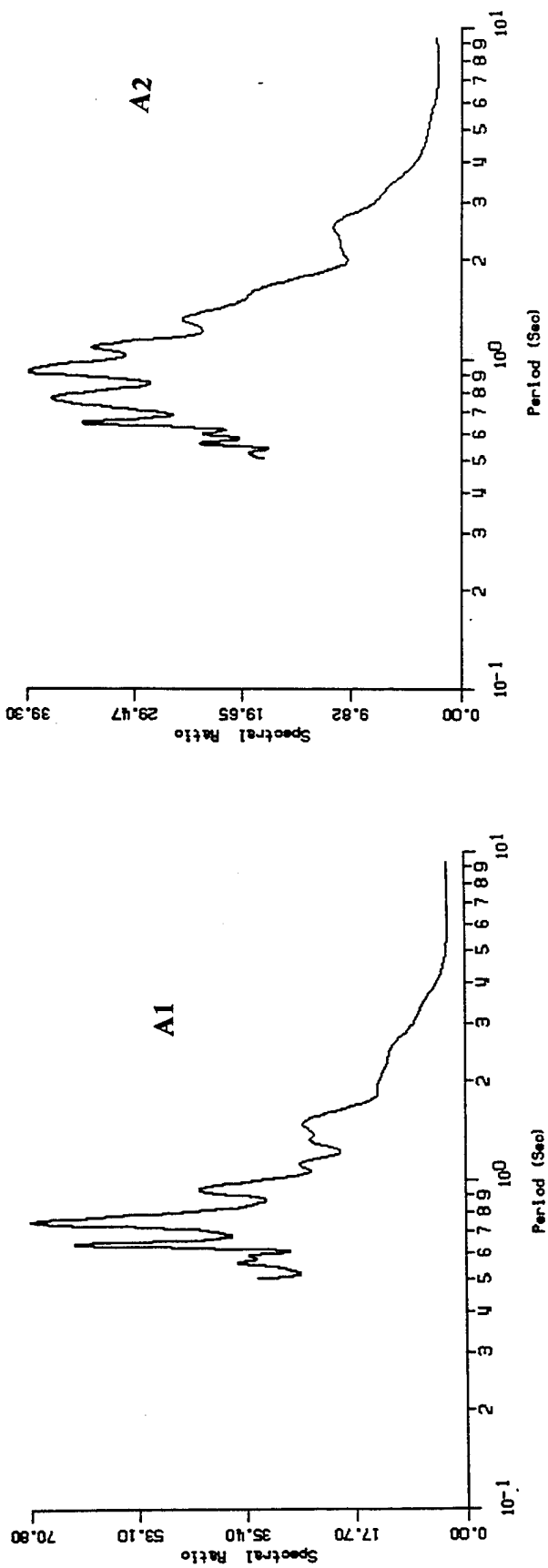


Figure 5.33a. Spectral ratio NCBC site, A1, A2, and A3.

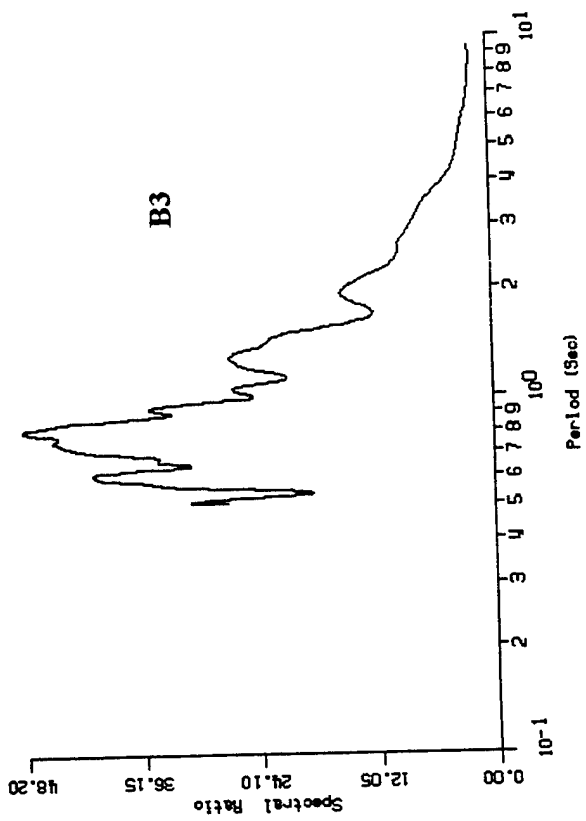
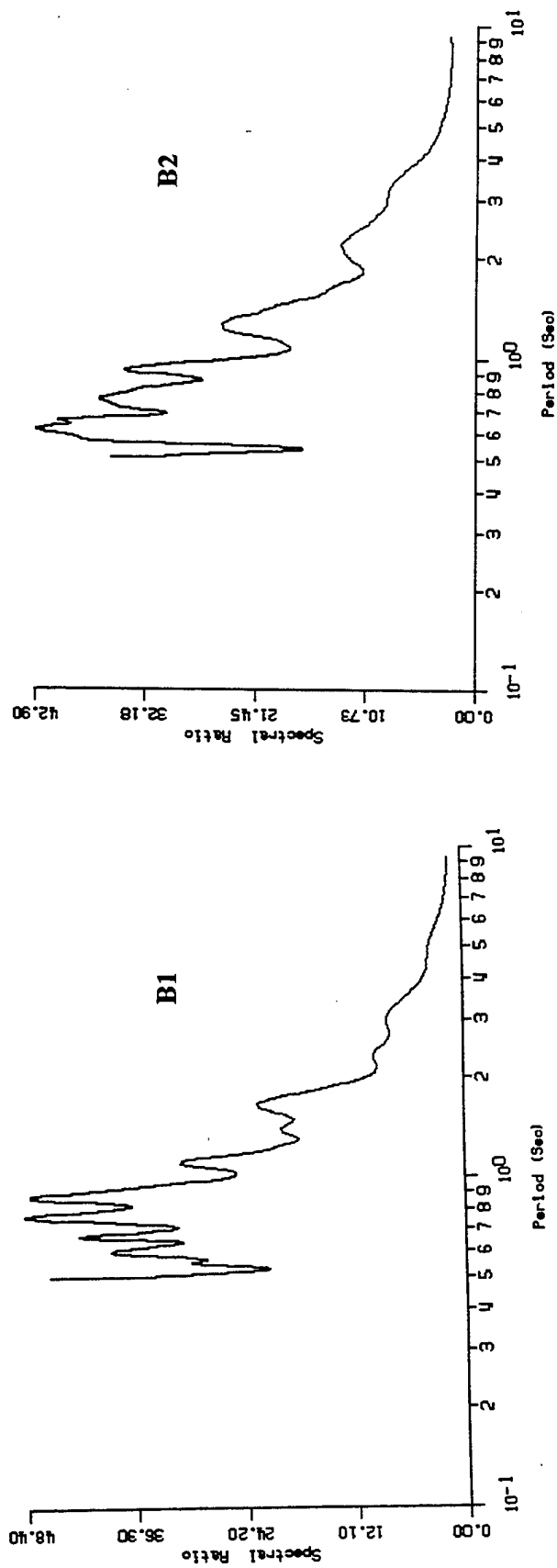


Figure 5.33b. Spectral ratio NCBC site, B1, B2, and B3.

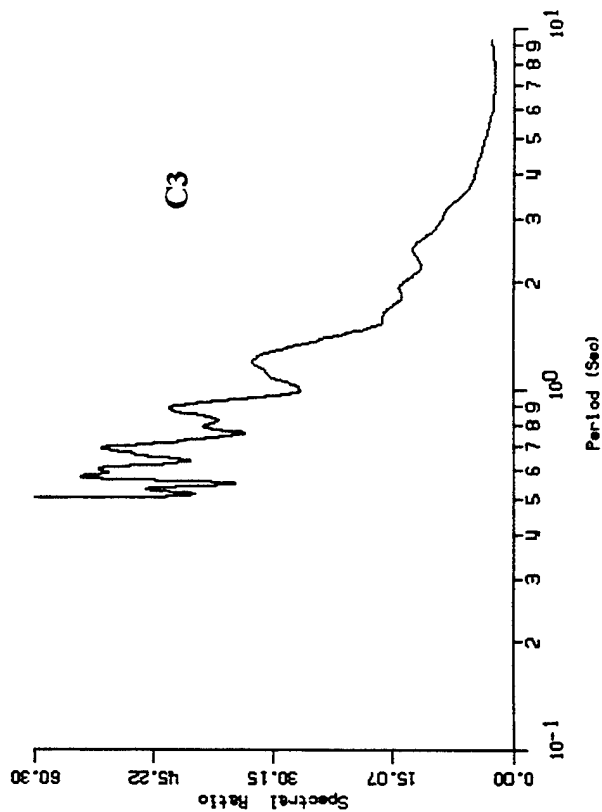
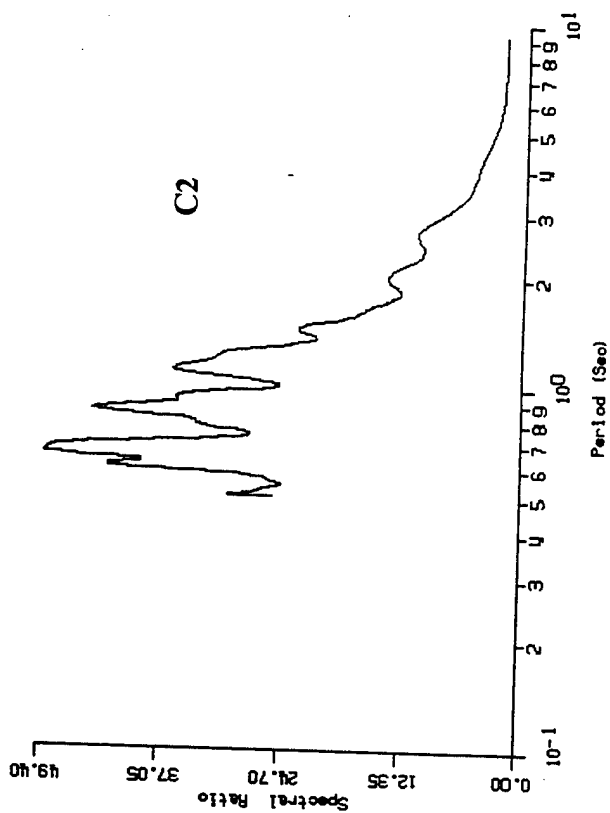
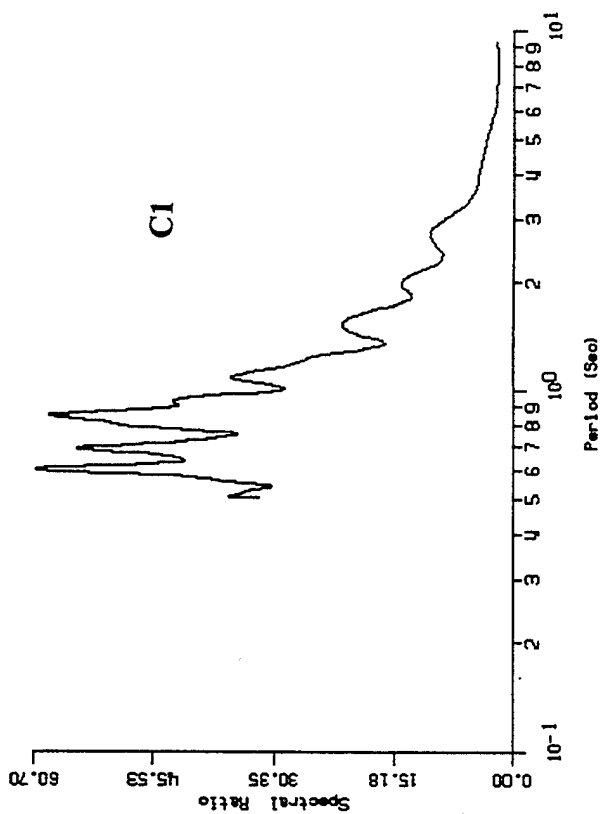


Figure 5.33c. Spectral ratio NCBC site, C1, C2, and C3.

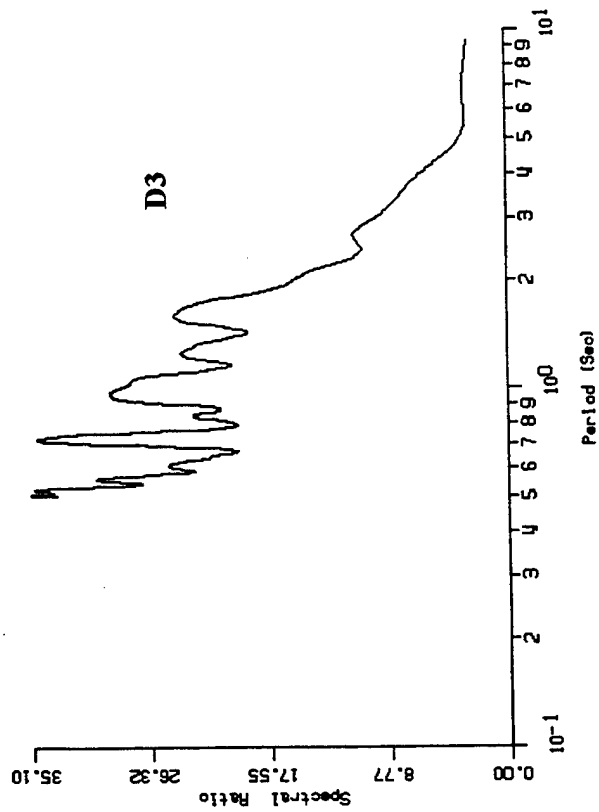
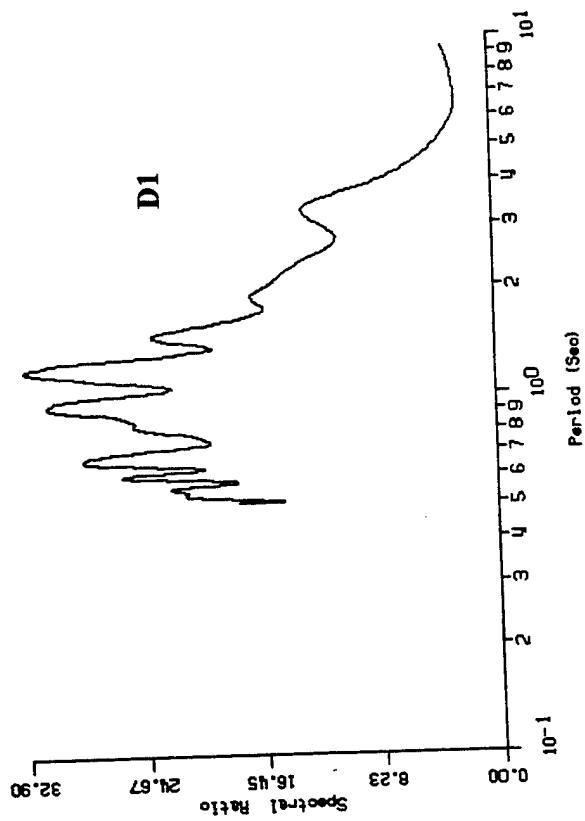
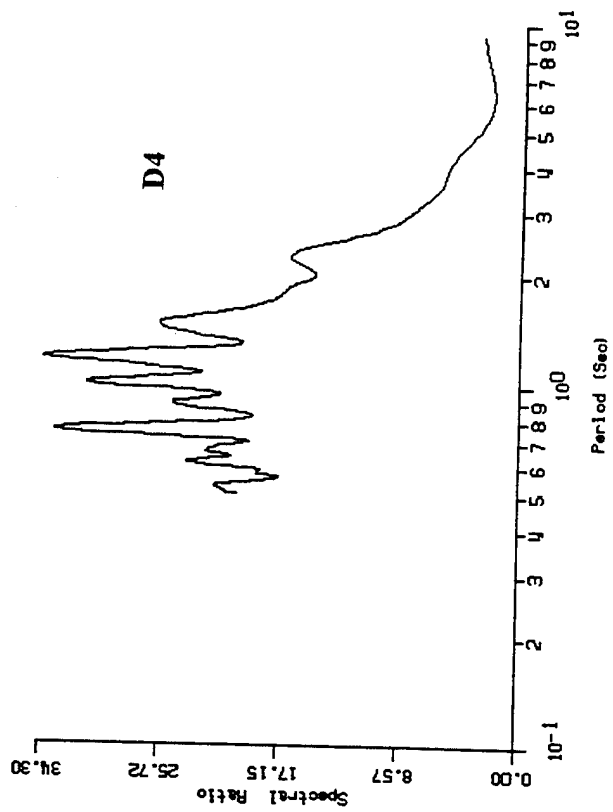
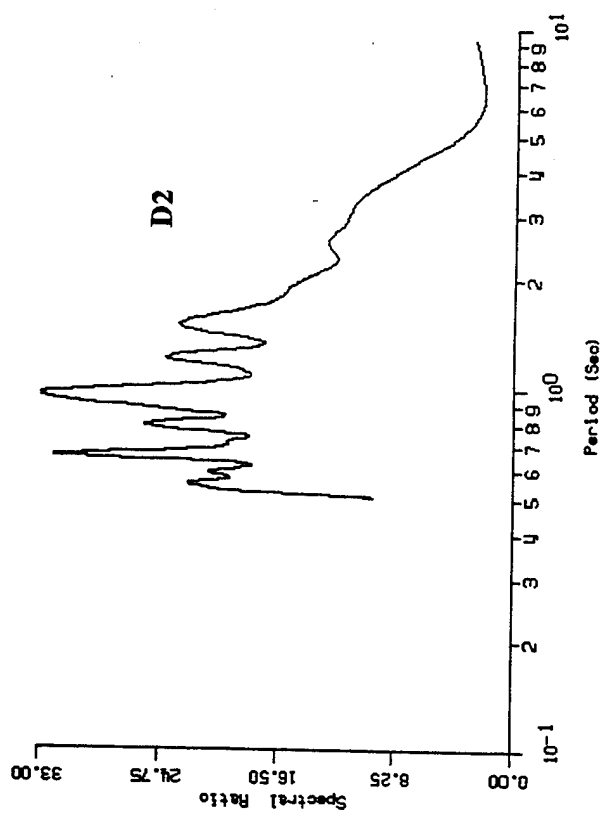
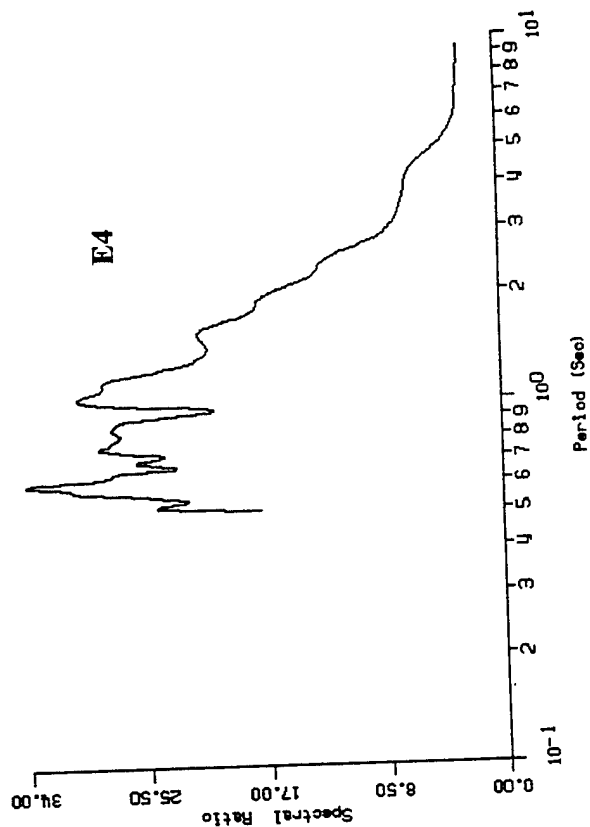
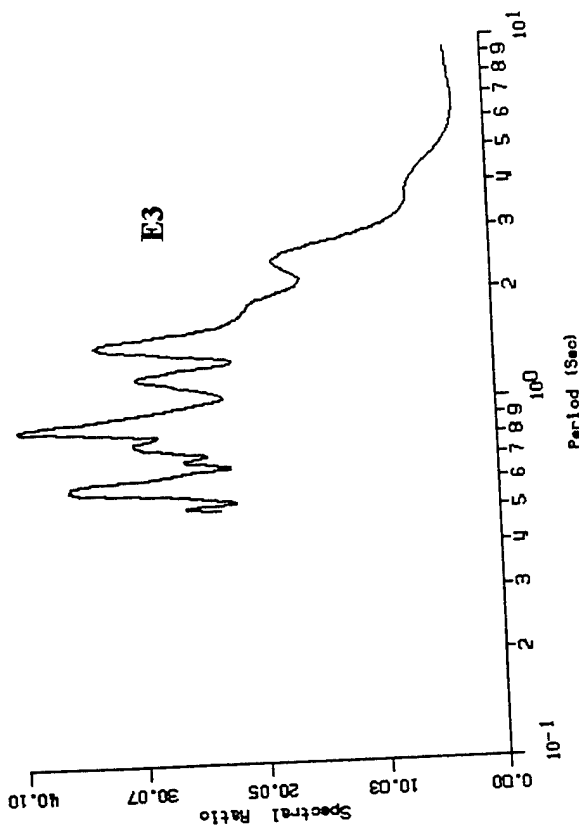
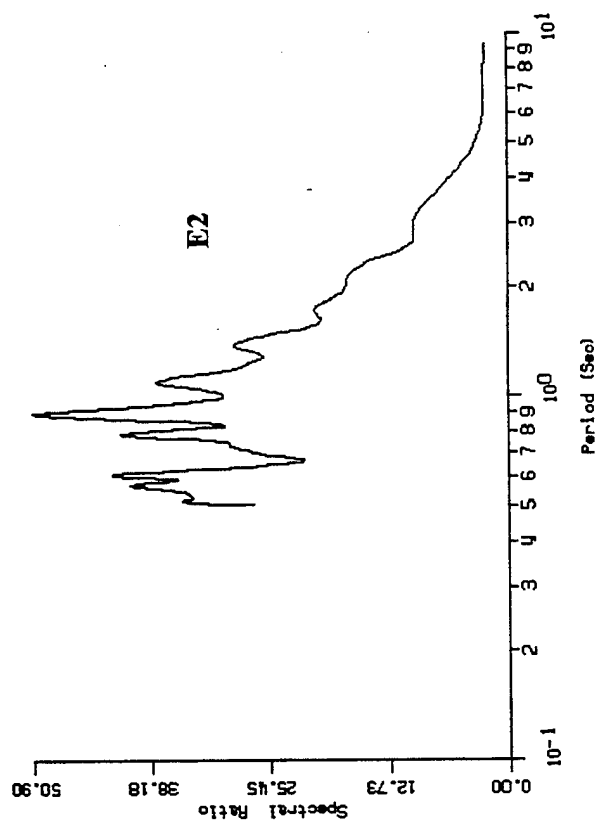
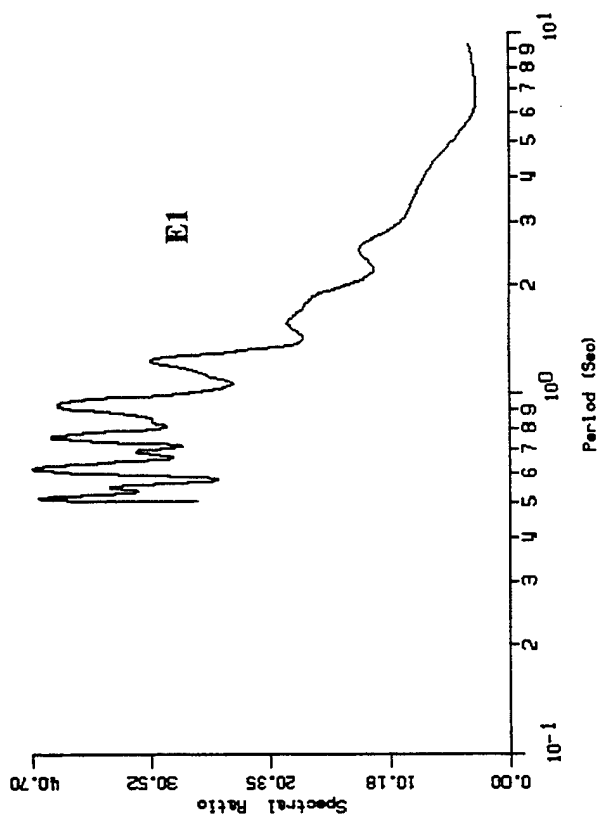


Figure 5.33d. Spectral ratio NCBC site, D1, D2, D3 and D4





**Figure 5.33e. Spectral ratio NCBC site, E, E2, E3 and E4.**

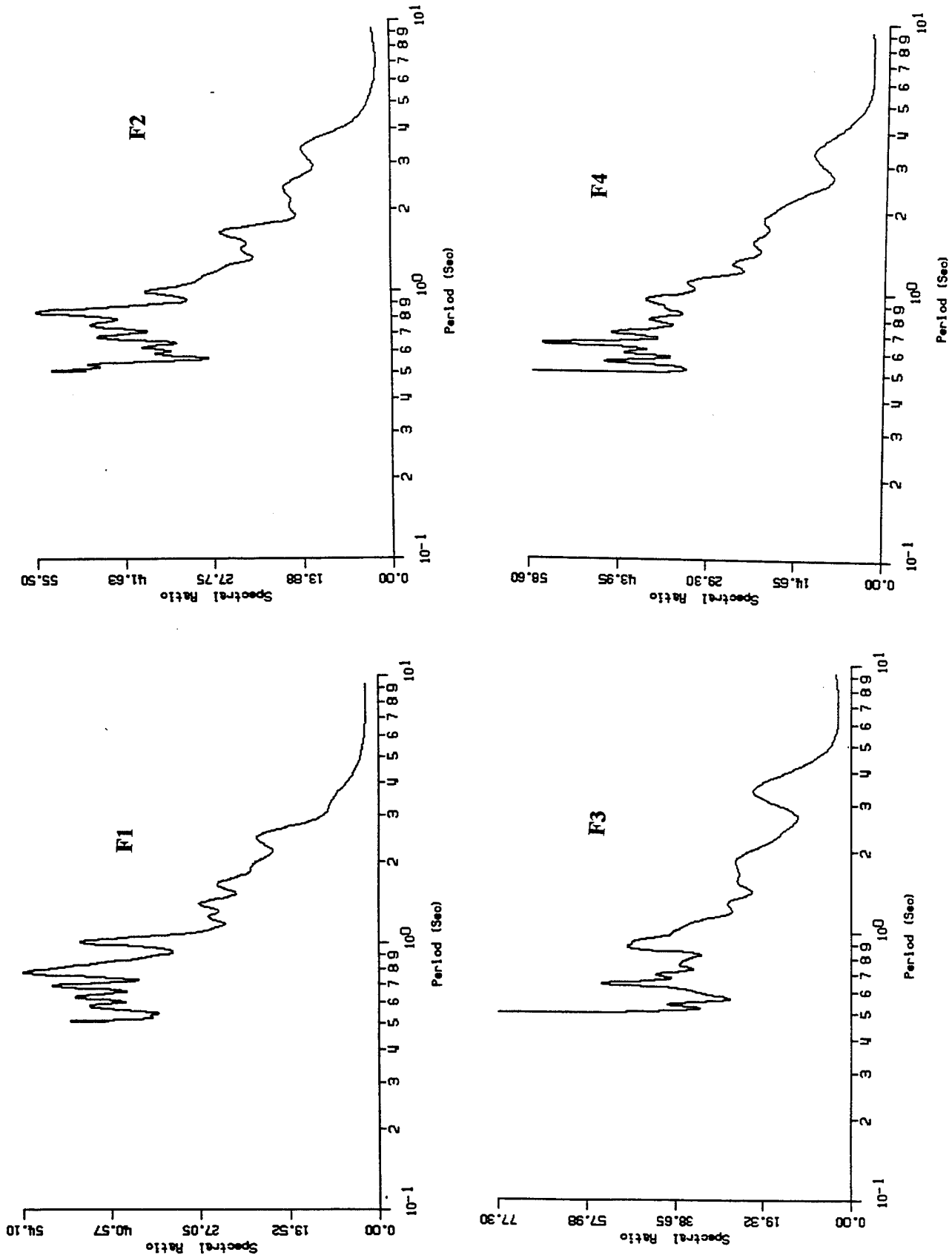


Figure 5.33f. Spectral ratio NCBC site, F1, F2, F3 and F4.

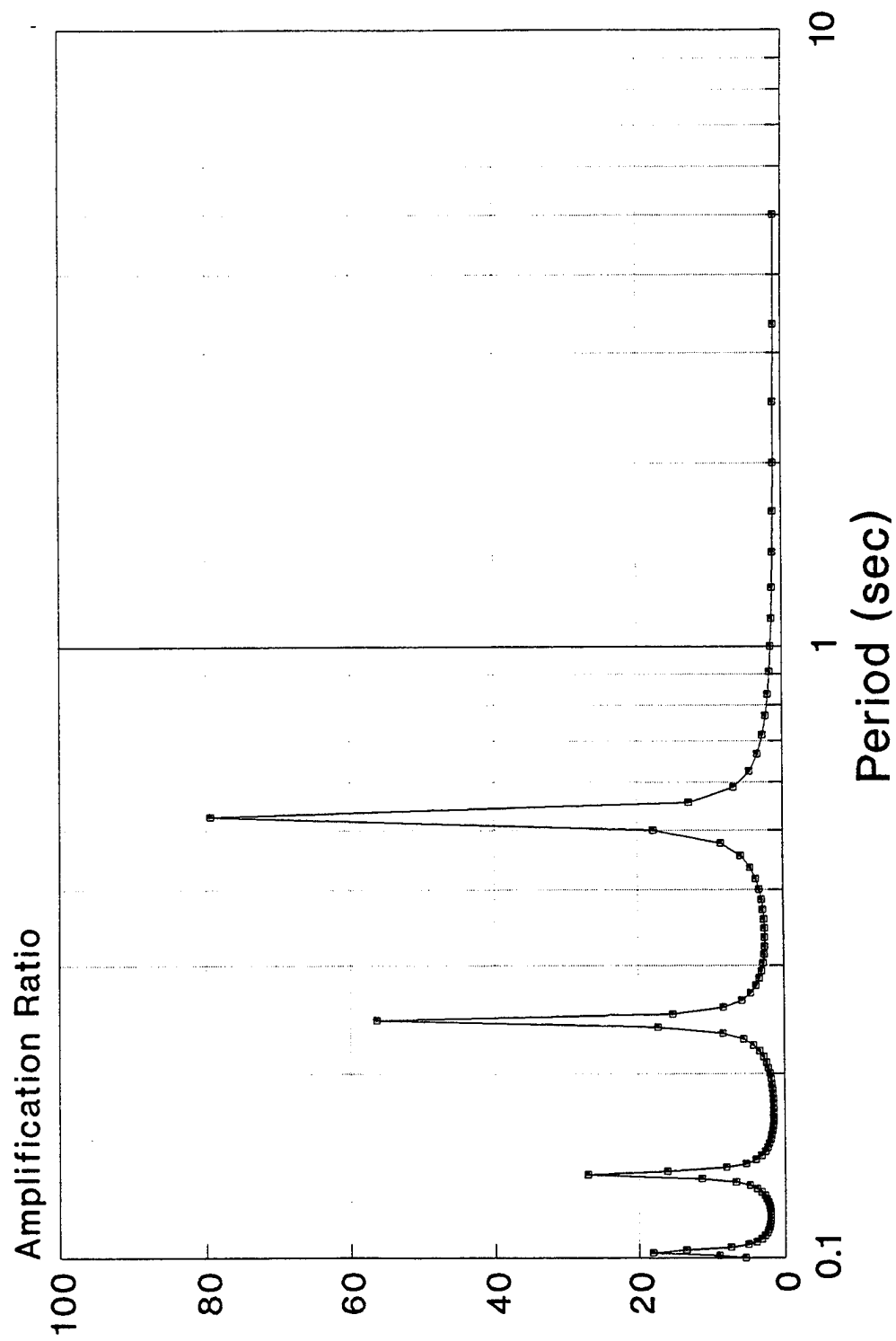


Figure 5.34. Computed spectral amplification for microseism at location A1.

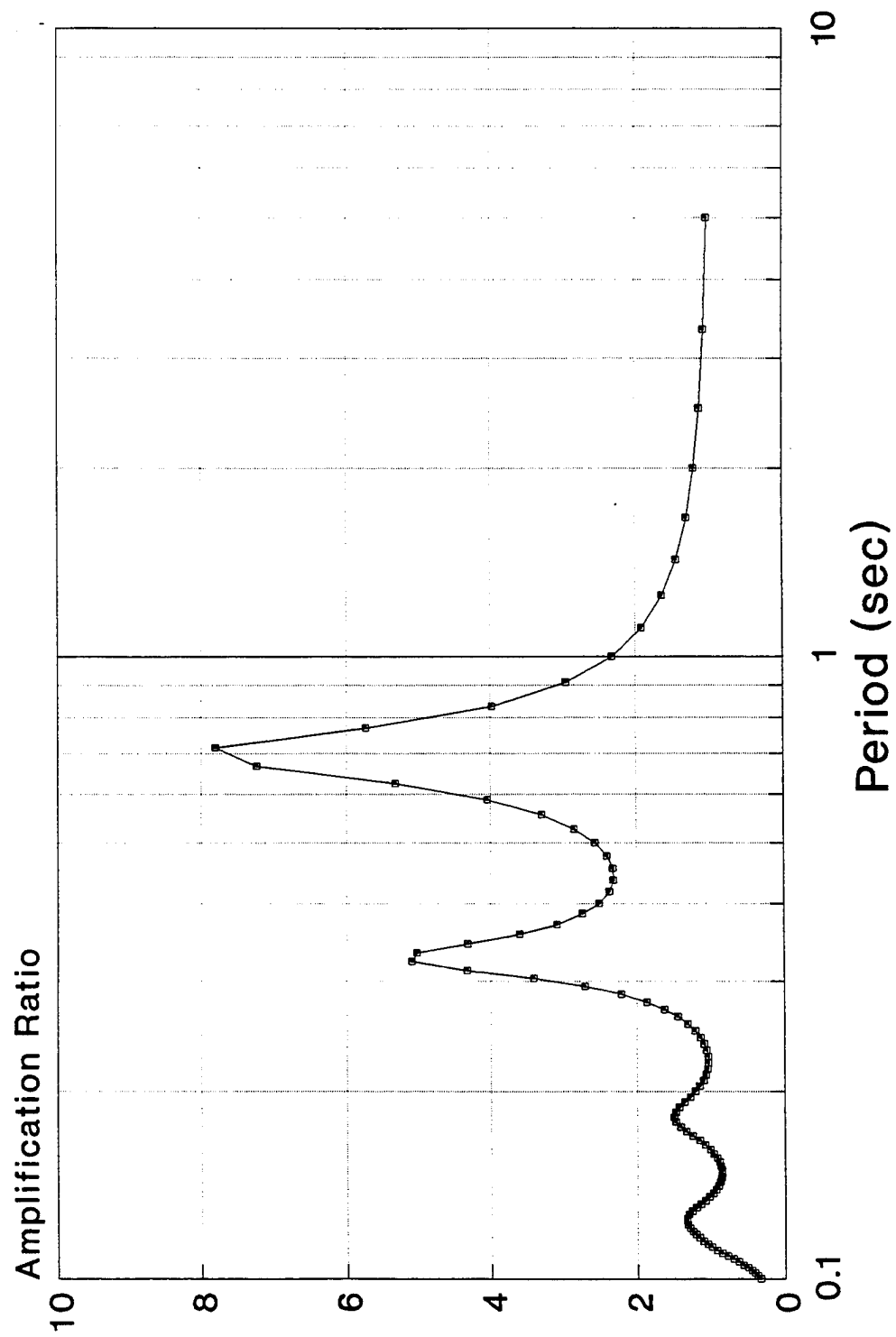


Figure 5.35. Computed spectral amplification, location A1.

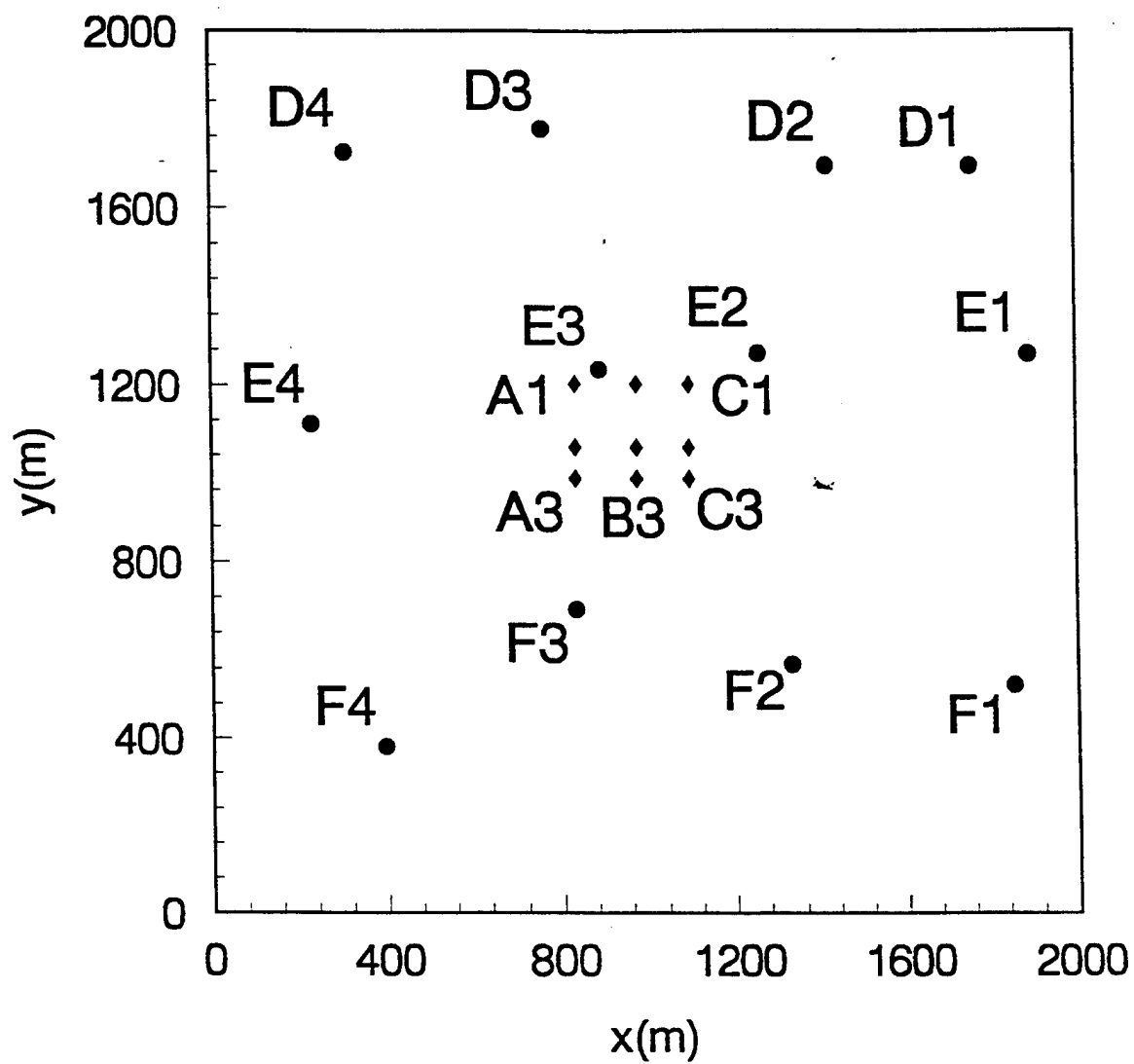


Figure 5.37a. Layout of stations NCBC site, see Figure 5.32 for site map.

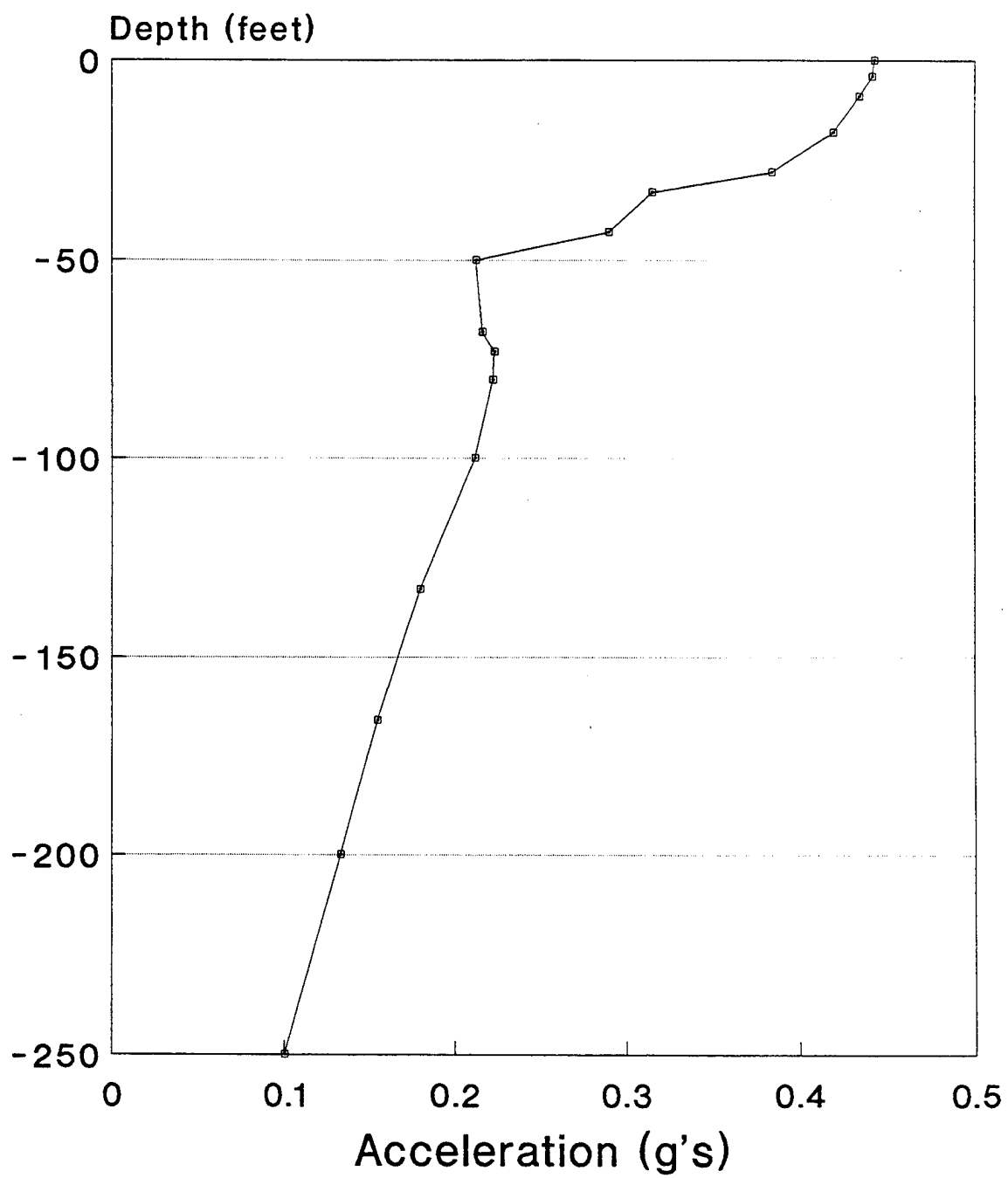


Figure 5.36. Computed site response, location A1.

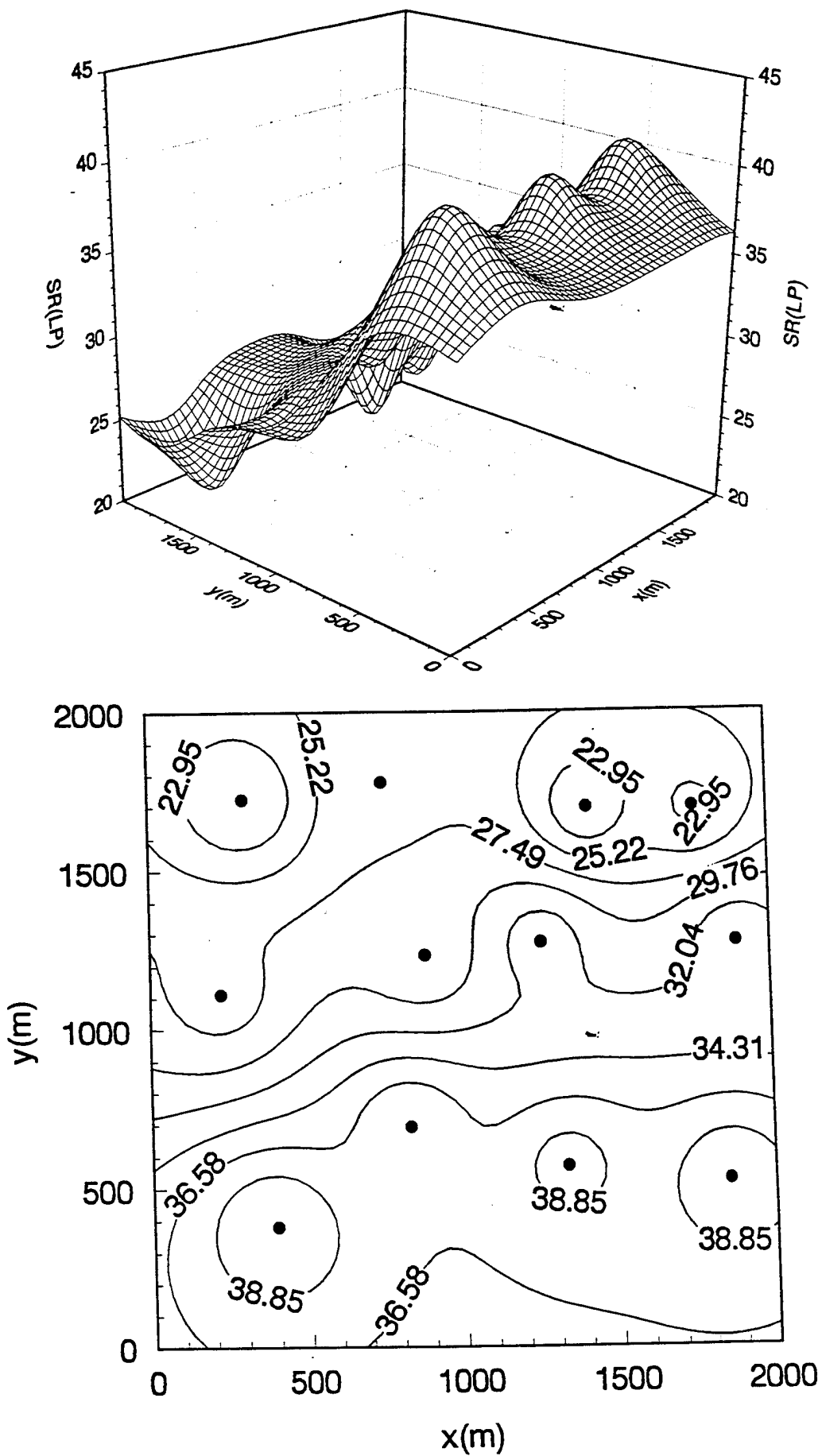


Figure 5.37b. Spectral ratio, period range 0.5 to 0.7 seconds.

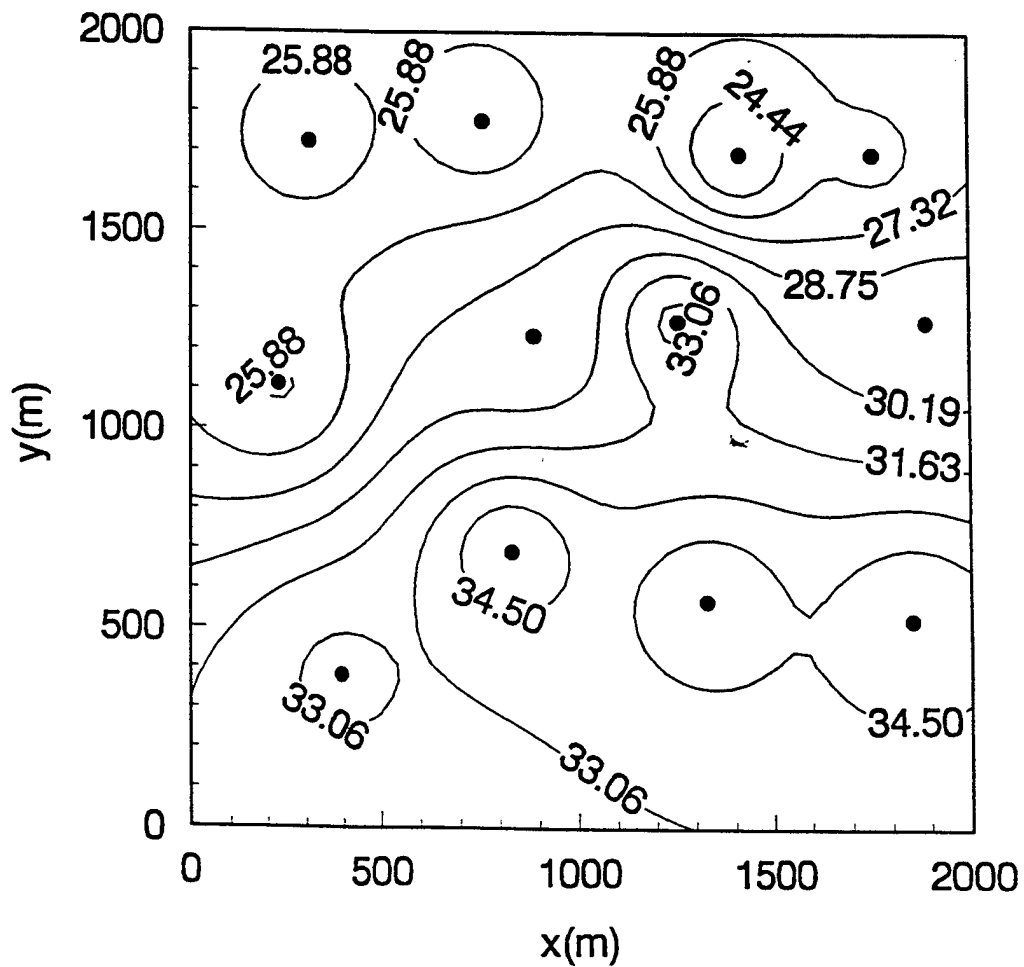
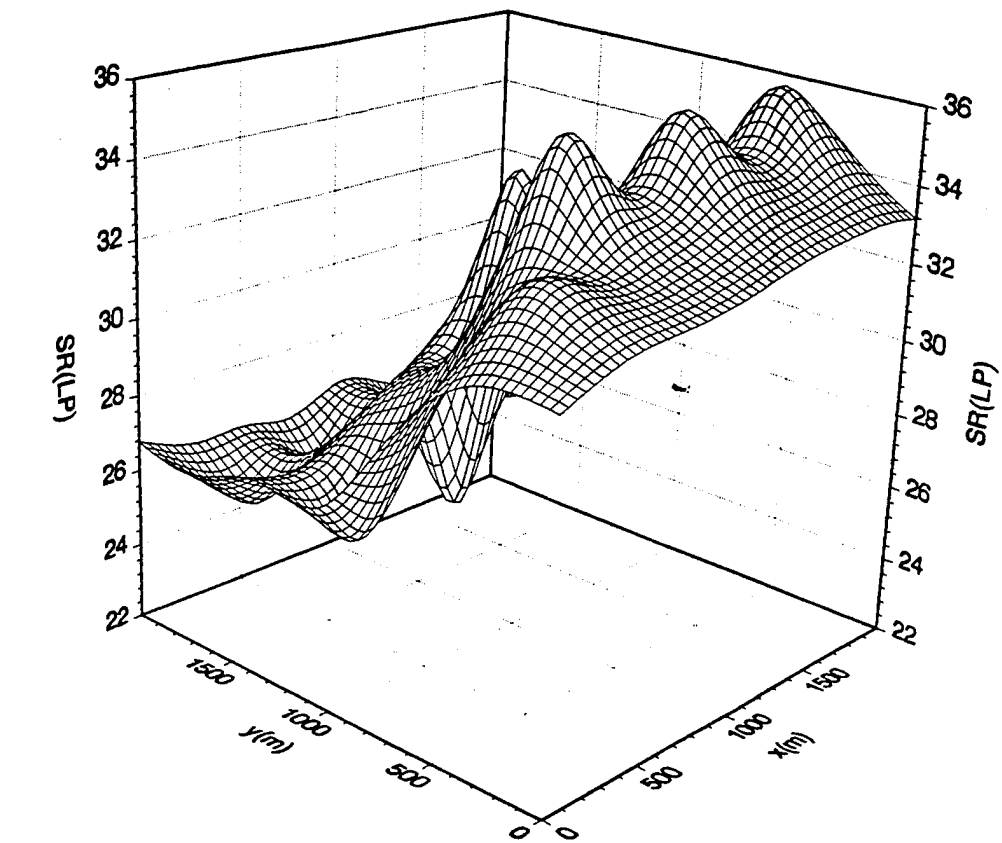


Figure 5.37c. Spectral ratio, period range 0.7 to 1.0 seconds.



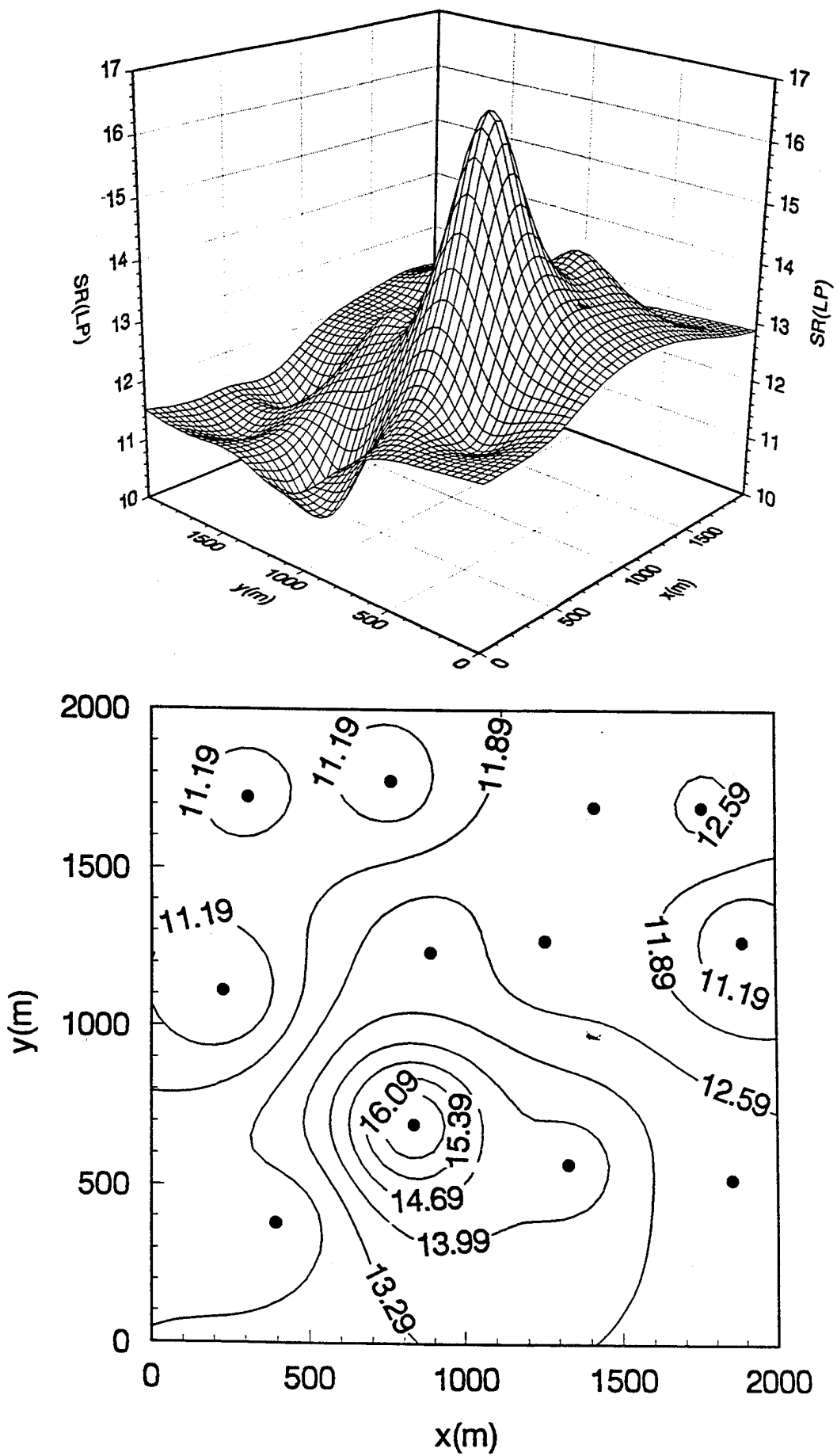


Figure 5.37c. Spectral ratio, period range 2.0 to 4.0 seconds.

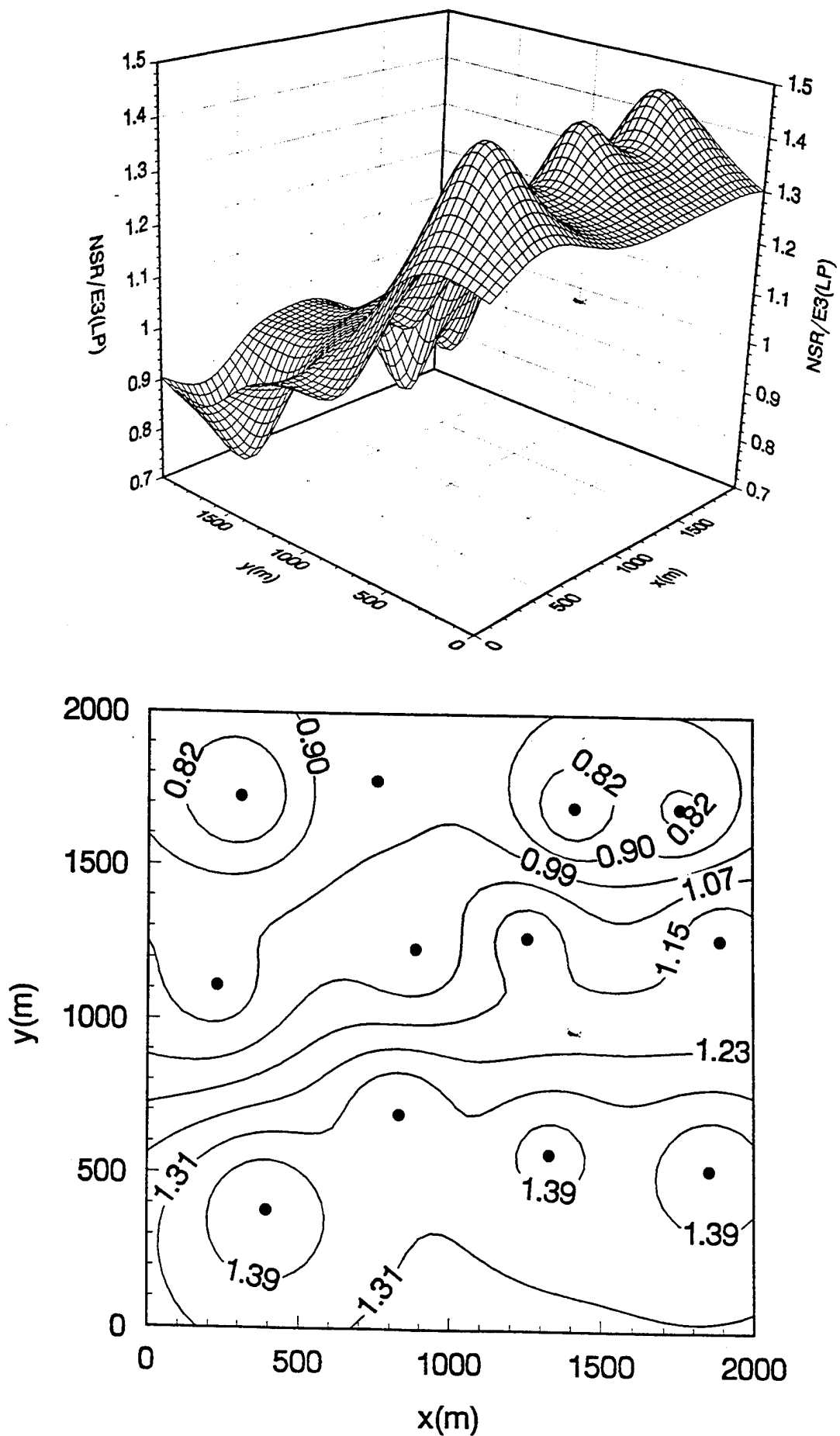


Figure 5.38a. Normalized spectral ratio, period range 0.5 to 0.7 seconds.

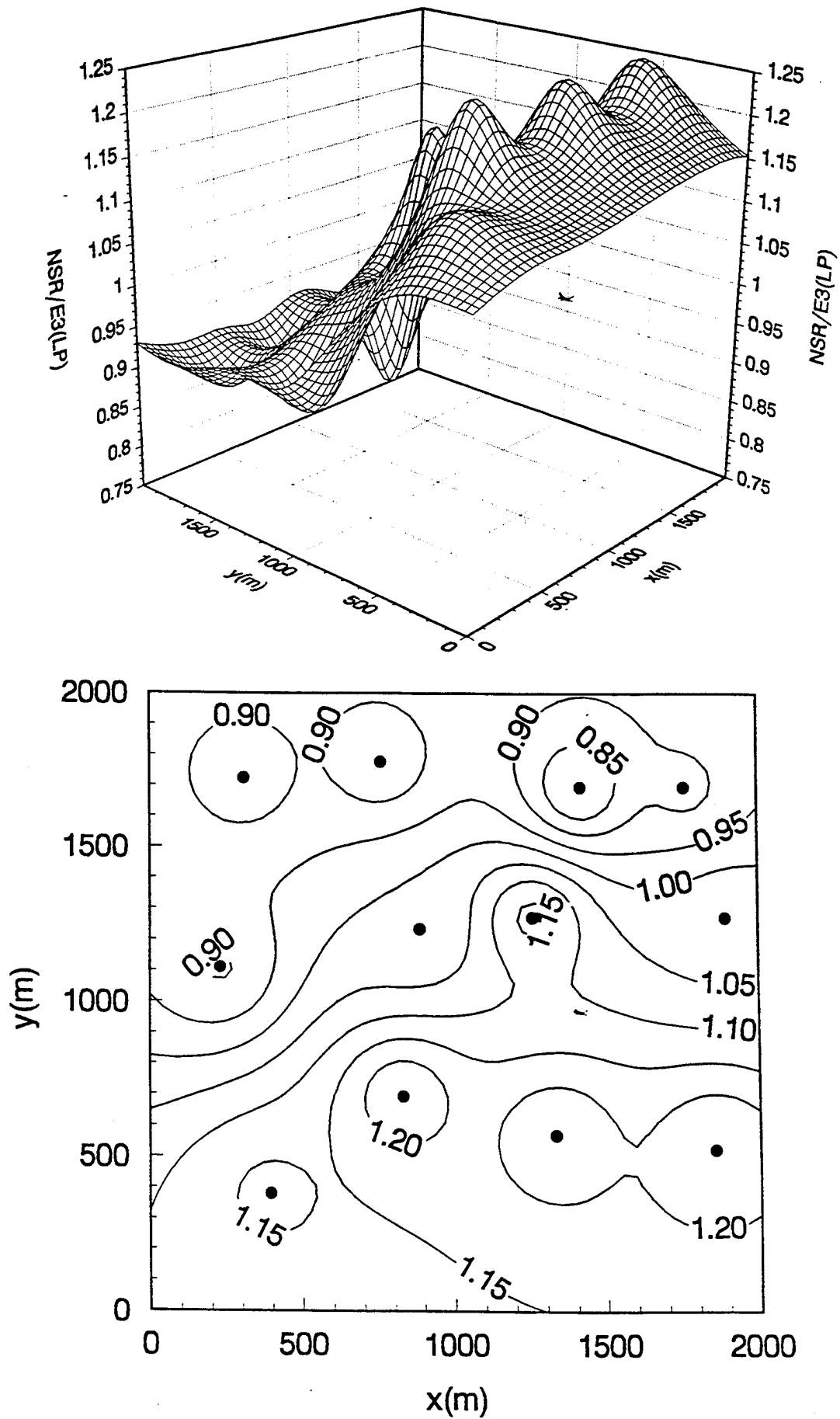


Figure 5.38b. Normalized spectral ratio, period range 0.7 to 1.0 seconds.

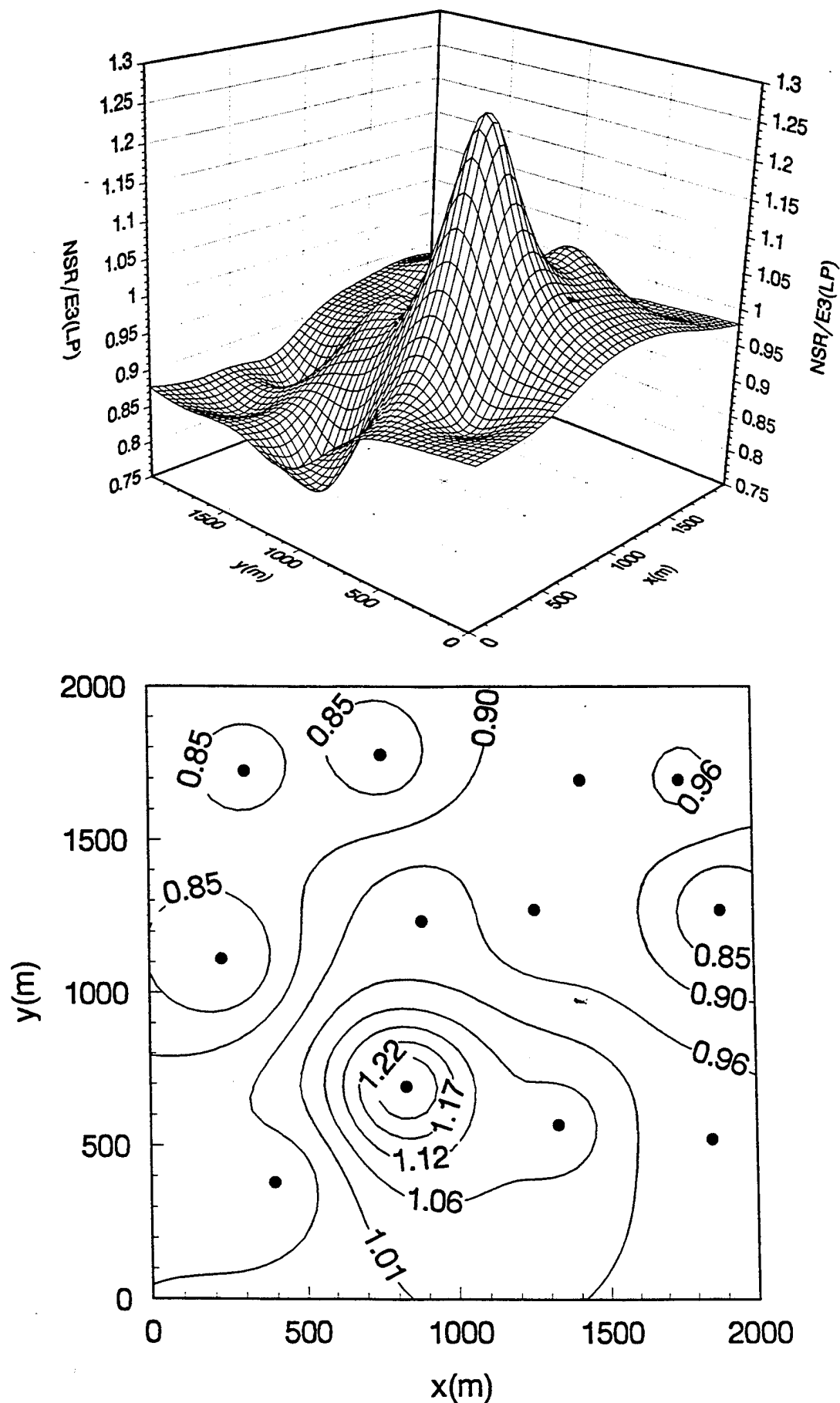


Figure 5.38c. Normalized spectral ratio, period range 2.0 to 4.0 seconds.

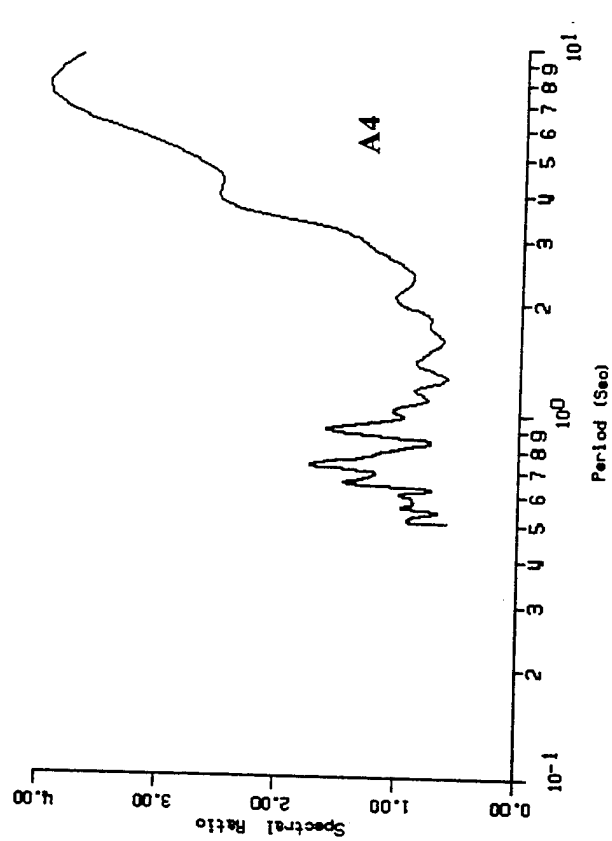
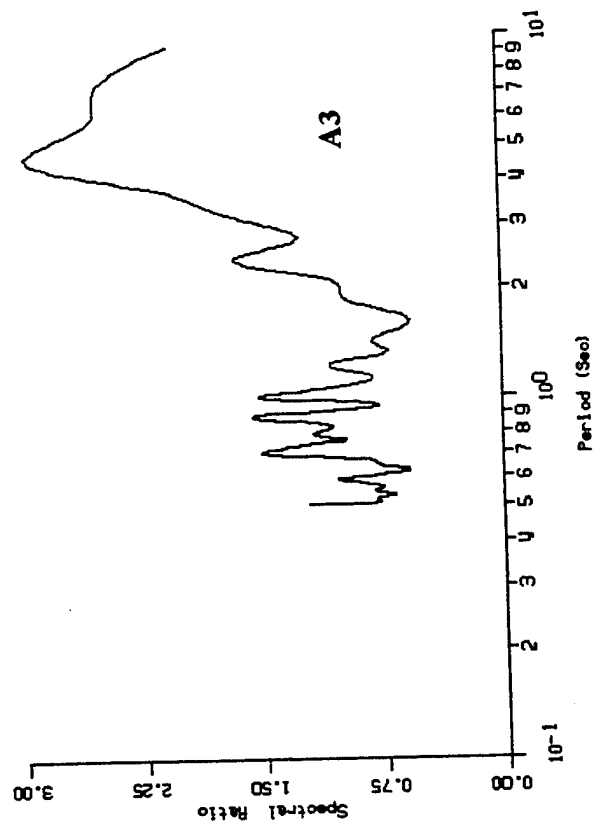
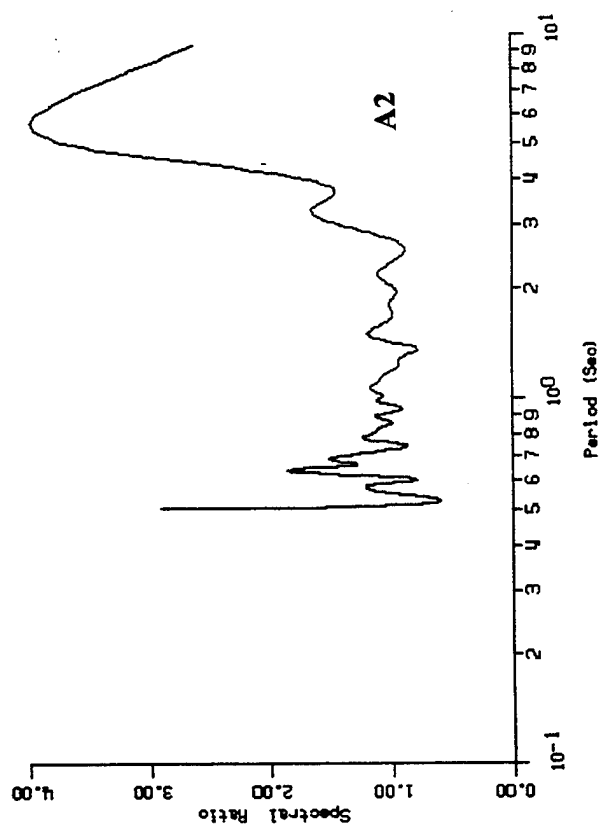
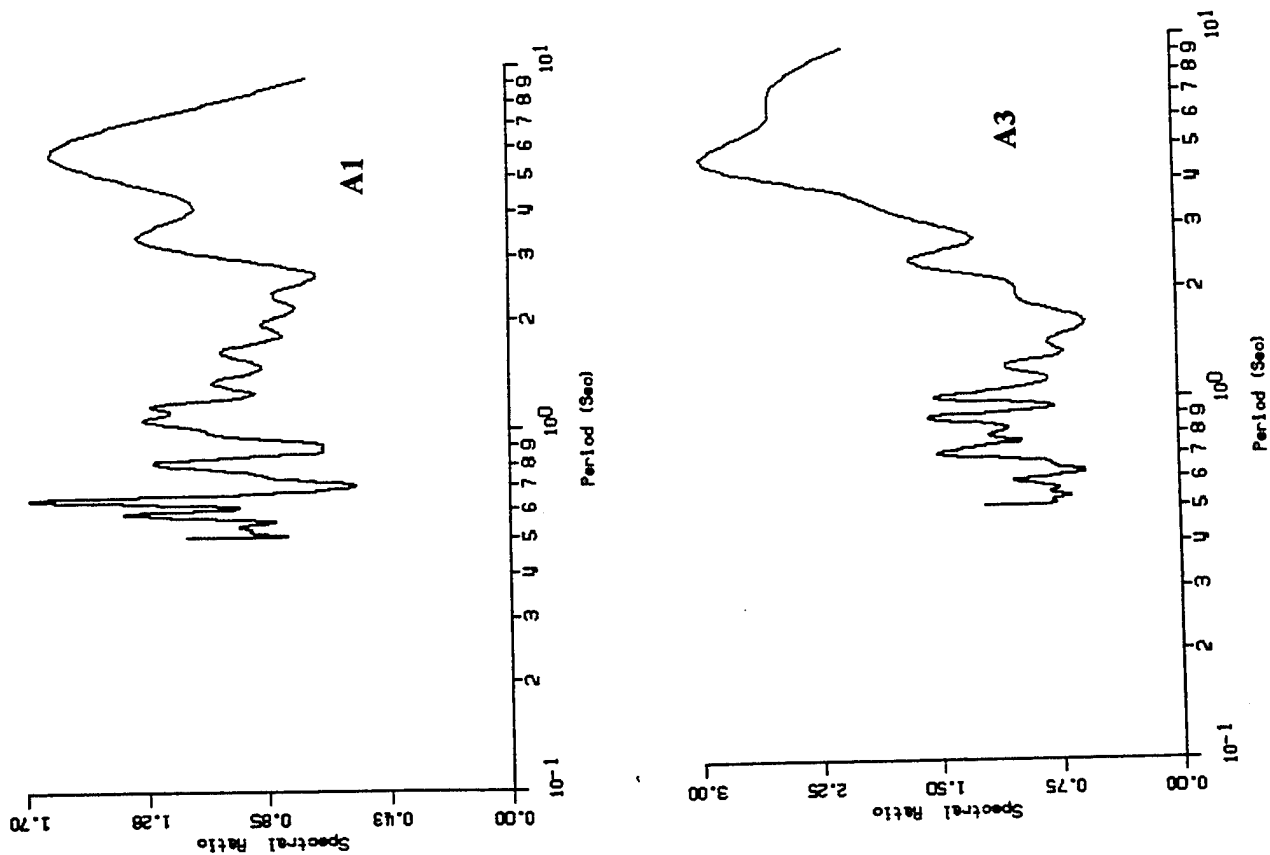


Figure 5.39a. Nakamura ratio NFESC site, A1, A2, and A3.

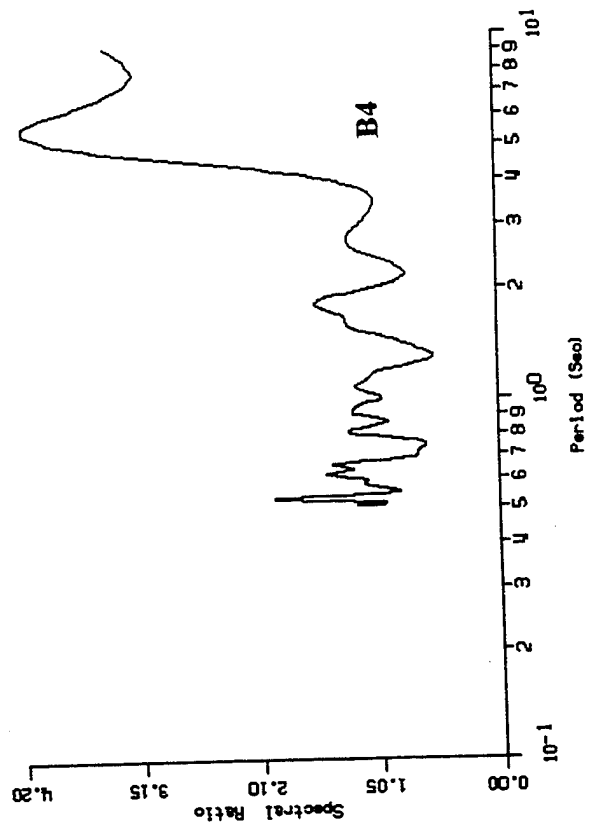
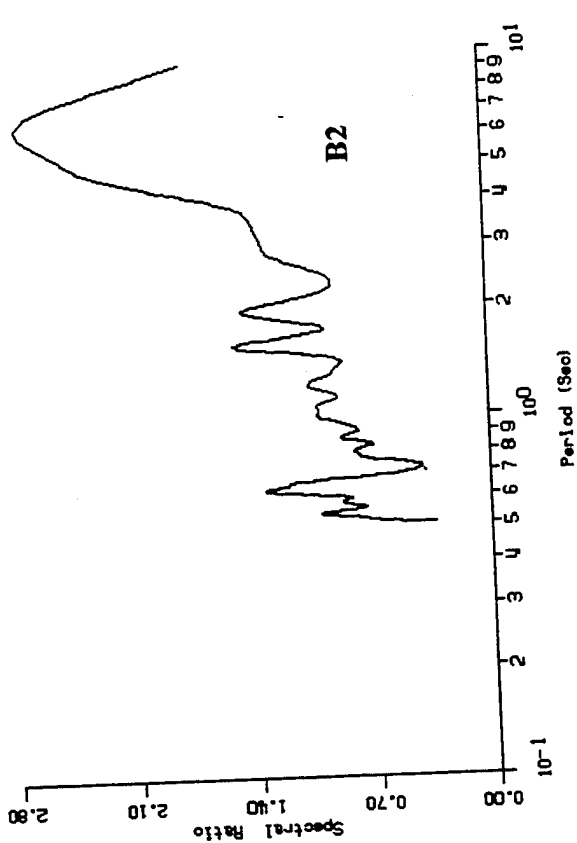
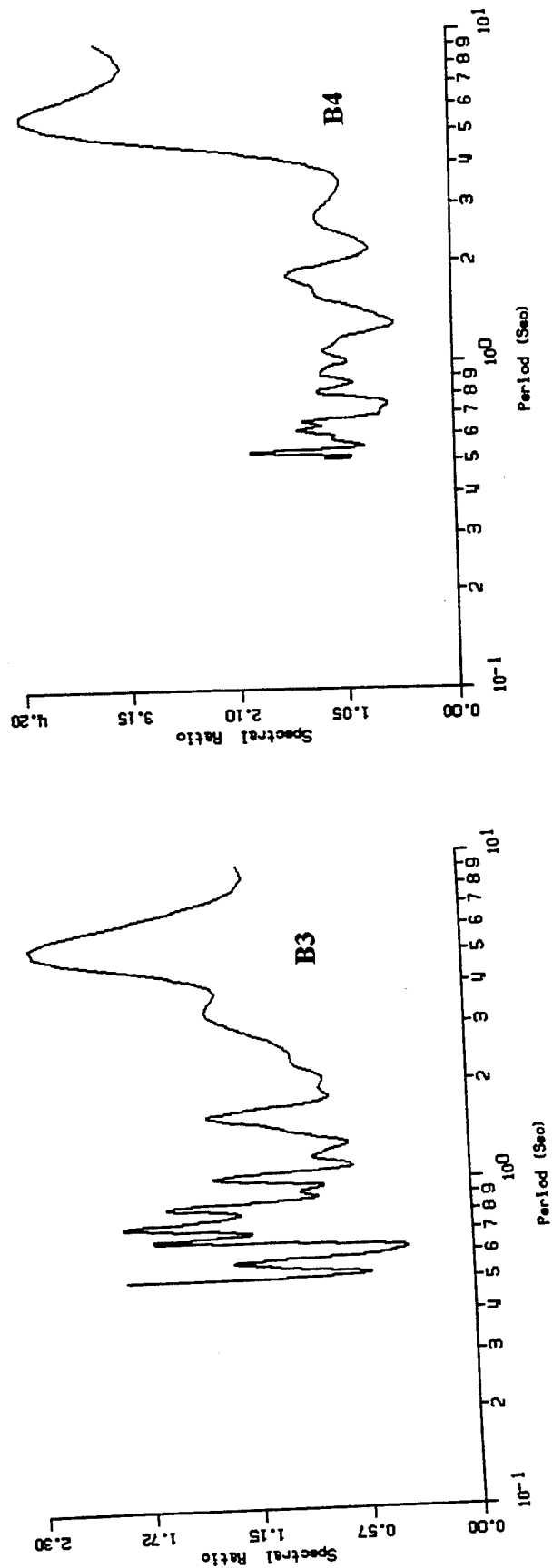
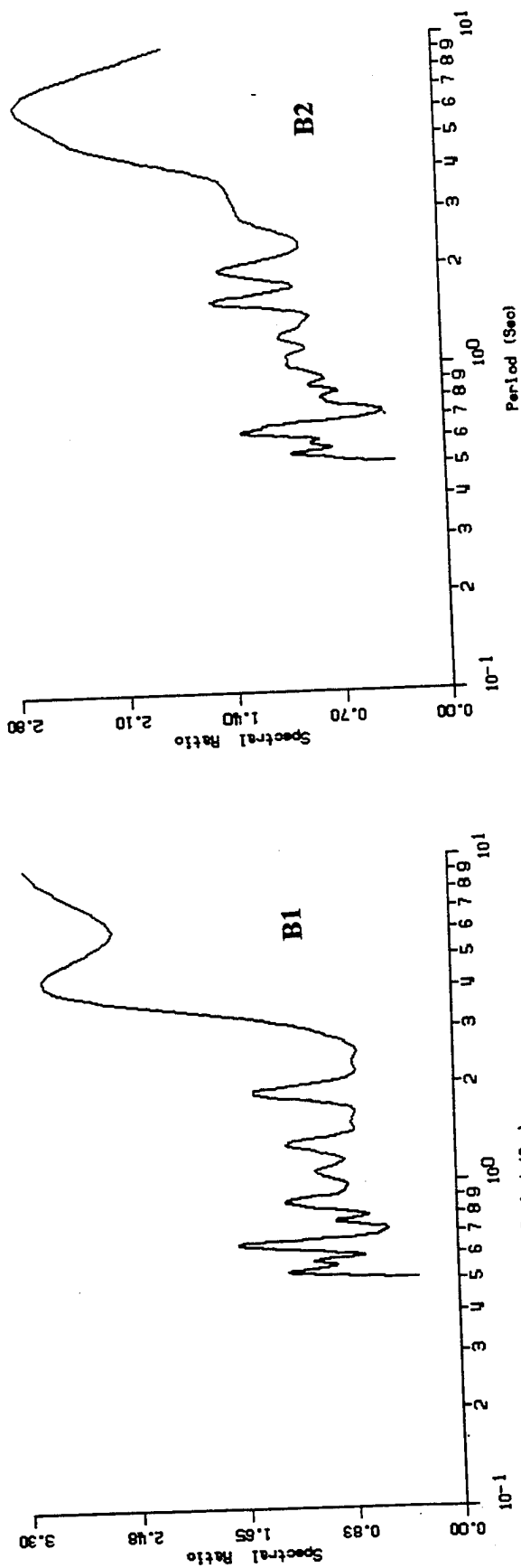


Figure 5.39b. Nakamura ratio NFESC site, B1, B2, and B3.

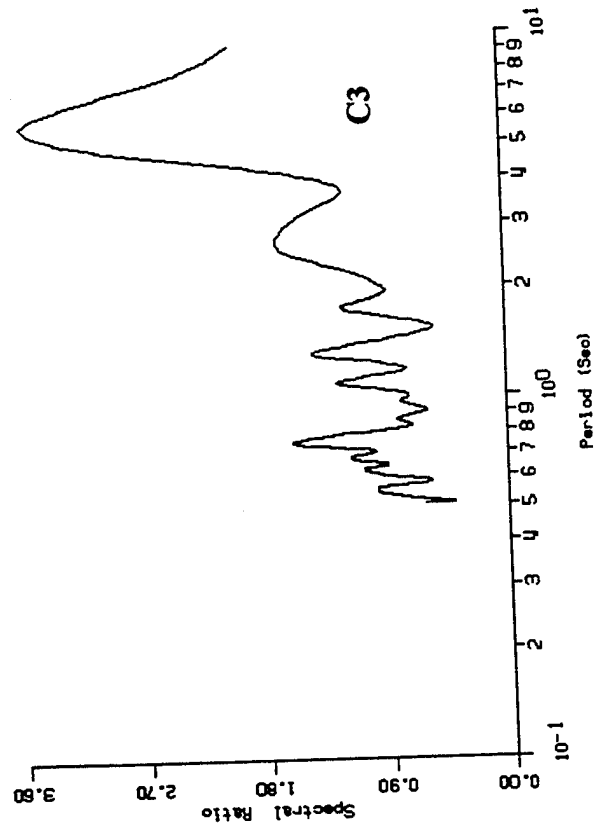
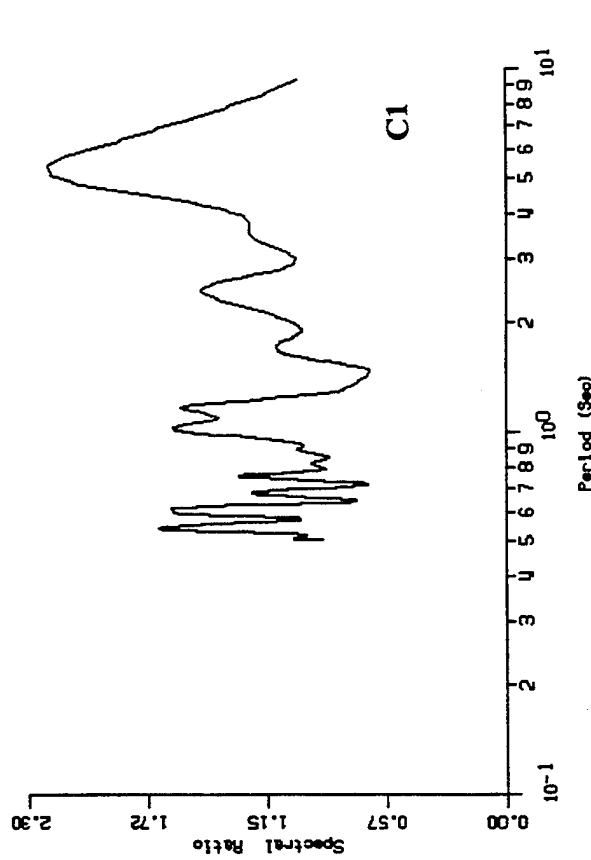
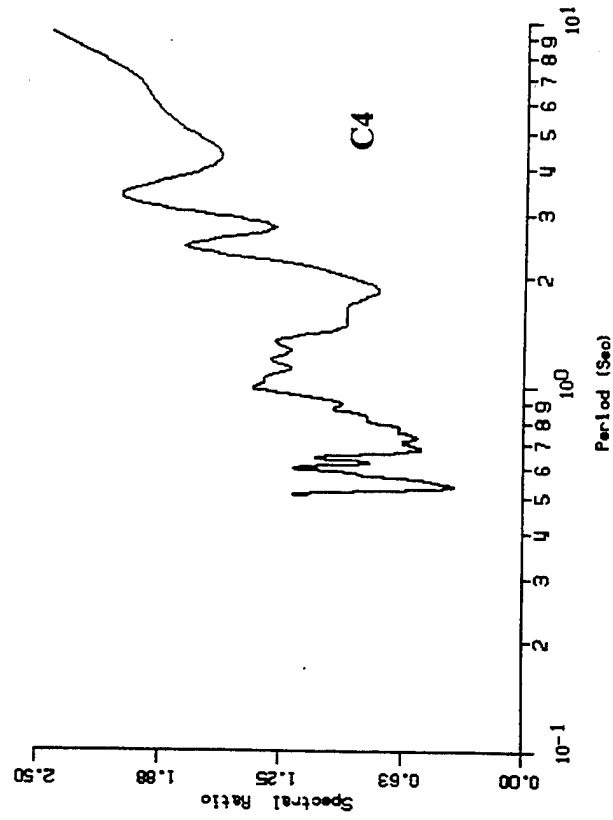
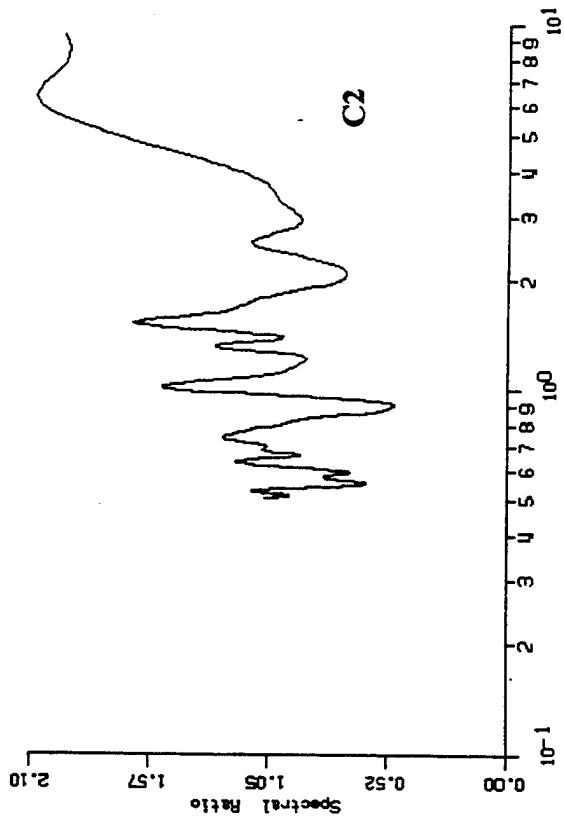


Figure 5.39c. Nakamura ratio NFESC site, C1, C2, and C3.

## CHAPTER 6 TREASURE ISLAND CASE STUDY

### Introduction

This chapter will present a case study of microseism measurements made at the Naval Station Treasure Island, a soil site and Yerba Buena Island, a rock site. This site was selected for study because the Navy experienced liquefaction at the site during the Loma Prieta earthquake of 1989. Both sites contain strong motion instrumentation and records are available. Additionally the Treasure Island site has been named a national study area and the National Science Foundation has sponsored site investigation studies to determine soil properties.

### Geology of Treasure Island and Yerba Buena Island

Treasure Island is a man-made island located near the Yerba Buena rock outcrop in San Francisco Bay, Figures 6.1 to 6.3. The island is approximately 1600 m long and 1000 m wide. Its construction was completed in 1936 as a part of the celebration of the construction of the Golden Gate and San Francisco-Oakland Bay bridges (Rollins et al., 1993). Since World War II the island has been commissioned as a Naval installation.

The soils at Treasure Island can be divided into four major groups: the sand fill, native shoal sands, recent bay mud sediments, and older bay sediments (Rollins et al., 1993). The layers of different materials exhibit significant variation in depth around the island. For example, the thickness of fill and native shoal materials range from 10.7 m at the southern end to 15.2 m in the north, Figure 6.2. Similarly, recent bay sediments begin at 10.7 m depth and extend to 15.2 m in the south. On the other hand, in the south eastern part of the island the recent bay sediments are found to a depth of 36.6 m. The bedrock depth of 85 m has been confirmed at one location only. Based on this point and the Yerba Buena rock outcrop it appears that the bedrock dips at about 2 degrees to the northwest (Rollins et al., 1993, Borchardt, 1970, Borchardt and Gibbs (1976)).

Figure 6.4 shows the surficial geology of Yerba Buena Island, Schlocker (1968) and Schlocker et. al (1958). The island is composed of the Franciscan Formation (Kj in Figure 6.4) described as follows:

“ Sandstone, arkosic to graywacke; fine to very coarse grained, with some shale beds. Sand grains consist largely of quartz, feldspar, and shale, with some chert and biotite and minor amounts of epidote, chlorite, clay and carbonaceous material. Fresh rock is medium gray; weathered or altered rock is light brown or very pale orange. Fresh rock dense, hard; altered rock may be scratched with fingernail. Sandstone varies from massive to thin bedded, is cut by veins of quartz or calcite. Rock jointed, fractured; contorted in some places; many fracture surfaces coated with iron, manganese and clay minerals, Radbruch (1957).”



The island also contains regions of shallow alluvial composed of silty, clayey sand derived from the sandstone (Qrc) and areas of artificial fill mostly sand and clay (Qaf). See Figure 6.4.

### **Yerba Buena Measurements**

Understanding the reference site geology is critical to establishment of a suitable reference location for microseism measurements. To evaluate the spatial variation of microseism signals on Yerba Buena Island an instrument was setup at the Lighthouse, a rock site part of the Franciscan Formation and the location of the strong motion instrument. Six stations as noted in Figure 6.4 were sequentially measured and the spectral ratios are shown in Figure 6.5. Noted the 6 stations are located on shallow fill. From Figure 6.5 the spectral ratio varies between 1 and 3 for 5 of the 6 sites indicating there is minimal amplification caused by the shallow surface fill. The sixth site, located at Building 40 evidences strong amplification especially in the East-West direction. Building 40 sits beneath the Oakland Bay Bridge and is straddled by its columns. This site is believed contaminated by the noise from the bridge and would make an incredibly poor choice for a reference site. The remaining sites show minimal amplification. The lighthouse station was used as the reference site for all measurements.

### **Treasure Island Measurements**

The first step in the measurement process was to establish the long term stability of the pair of sites. Measurements were made at hourly increments and are shown in Figure 6.6. Figure 6.6 indicates that there is significant fluctuation at the Treasure Island site, much more so than at Yerba Buena. This is evidence of local nonstationarity of the signal. Over the long term both sites have an average level of excitation and a fixed relationship; however over the short term fluctuation can occur. Figure 6.6 illustrates a fairly constant segment at about average intensity was used for the Treasure Island array measurements. Establishment of the long term fluctuation is critical to meaningful measurements. The limitation in the number of instruments means measurements must be made in sequence. Relative stability must be maintained from the first to the last measurement so the spectral ratios will be consistent. Should the soil site for example suddenly become more active relative to the rock reference site, a false spectral ratio would be noted. As shown in Figure 6.6 periods of constancy can be found for a number of hours permitting measurements to be made. The Treasure Island site exhibits substantially more variation than the Port Hueneme sites measured in the Chapter 5.

### **Treasure Island Array Measurements**

Microtremor measurements at Treasure Island sediment sites and Yerba Buena Island bedrock reference site were completed for all the sites within a span of 5 hours. Figure 6.7 shows the location of all the observation sites. Five sites are located along each of the three sections (A, B, and C). The sites are denoted (from left to right in

Figure 6.7) by A<sub>1</sub> to A<sub>5</sub>, B<sub>1</sub> to B<sub>5</sub>, C<sub>1</sub> to C<sub>5</sub>. A Cartesian coordinate system shown in Figure 6.7 is used with sites at about 300 m apart. Various structures precluded establishing an evenly spaced grid.

Measurement at the reference site on Yerba Buena Island was done every 30 minutes for 5 minutes. Corresponding sediment site measurements of the same duration were paired with the closest reference measurement. For all the measurements the East-West, North-South, and vertical velocity components were measured with a sampling rate of 20 Hz. Figure 6.8, 6.9 and 6.10 give the Fourier spectra. Figure 6.11 is the Yerba Buena Fourier spectra for the period during which the East-West measurements were made. The reference site records appear to be very stable throughout the measurements.

To assess ground motion amplification between the sediment sites and bedrock, spectral ratios for records at the Treasure Island sites are compared with the corresponding one observed at Yerba Buena Island. Figures 6.12 and 6.13 show the spectral ratios as a function of period for sediment sites along the Sections A, B, and C, respectively. It is evident from these results that ground motion amplification changes significantly from site to site. This demonstrates that the site amplification may change considerably over very short distances. This amplification is strongly frequency dependent as well. For these measurements, the recorded long period microtremors are caused by the action of ocean pressure waves in the far field and the assumption of the same source for Treasure Island and Yerba Buena Island is valid. Close proximity of the two islands allows the assumption that the path effects are the same. Consequently, the calculated spectral ratios should provide a good estimate of the local site effects for Treasure Island. A larger data base for the predominant period histogram which included all the local peaks in spectral ratios shows some presence of the source effects in the longer period range over 10 Hz. This is beyond the range of interest for structural dynamic response and is excluded from study.

As expected, the peak spectral amplitude for the reference site is smaller than the peak spectral amplitude at sediment sites. The velocity spectra at Treasure Island show considerable variation from site to site demonstrating the site variation and its influence on the ground motion. The peak amplification levels of 45 to 50 exhibit substantial nonlinear effects compared with those of the Loma Prieta event.

As it can be seen from the spectral ratios plots (Figures 6.12 and 6.13) the motion at certain periods is particularly amplified. The period at which the spectral ratios exhibit the sharpest peak is called the predominant period of motion. From the spectral ratios it is possible to determine predominant periods of motion and their spatial variation across Treasure Island. Figure 6.14 shows the area covered by contours and Figure 6.15 shows a contour plot of period based on excitation in the North-South direction and the East-West direction. The contours show that there is some directionality associated with the period at some sites. Table 6.1 tabulates observed period. Figure 6.16 gives contours of peak spectral ratios and Figure 6.17 gives normalized spectral ratios obtained with respect to site A2, the firehouse location of the strong motion instrument.

Table 6.1 Treasure Island Station Periods

Station	NS	EW
	sec	sec
A1	1.0	0.68
A2	0.85	0.80
A3	0.85	0.90
A4	0.82	0.90
A5	0.90	0.80
B1	0.80	0.95
B2	0.72	1.0
B3	0.70	0.90
B4	0.90	0.80
B5	0.80	0.80
C1	0.90	1.0
C2	1.0	1.0
C3	1.0	1.0
C4	0.90	0.70
C5	0.90	0.80

### Treasure Island Response to Loma Prieta Earthquake

Examination of the microtremor spectral ratio contours (Figure. 6.16) shows that qualitatively, the largest North-South amplification occurred at the North - West section of the region covered. The largest East - West amplification occurred along the West edge of the region and the center of the region. Detailed damage assessment of the perimeter retaining system at Treasure Island following the Loma Prieta earthquake was done by Sewbridge (1990). Additional information was found in Benuska, 1990, Darragh and Shakal (1991), Housner (1990) and Power (1993). Seed et al. (1990) reported on the damage in the interior of the island. Evidence of soil liquefaction was manifested by numerous large sand boils in the interior of the island. As for the perimeter of the island the following damage was reported. Along the West perimeter of the island (Figure 6.14) little or no damage was evident. Liquefaction did occur in inland central areas where settlement was greatest. East West surface motion was about 3 times greater than North-South motion. Along the North edge of the island significant damage occurred as a result of lateral spreading of the dike. Up to 9 cm of vertical settlement was observed adjacent to a building approximately 60 m inland from midpoint of the North edge of the island. . It is very difficult to correlate microseism contours with damage observations. The contours represent pure site effects while damage relates items like structural strength or structural deficiencies. Settlements tend to be greatest in areas where East-West amplification peaks are greatest.

Strong ground motion records from the Loma Prieta earthquake of October 17, 1989 were obtained at one station at Treasure Island and one site at Yerba Buena Island (see Figure 6.1). The epicentral distance from Treasure Island strong ground motion site was 98 km and for that at Yerba Buena Island 95 km. Strong ground motion acceleration traces (E-W, N-S, and UP) for the two sites are shown by Figure 6.18. Corresponding velocity components are depicted by Figure 6.19. The strongest ground motions at the two sites were in the E-W directions. Peak acceleration in this direction at Treasure Island was 0.16g and 0.03g at Yerba Buena Island. Fourier amplitude acceleration spectra for both sites are displayed by Figure 6.20.

From the microtremor period data shown in Figure 6.14 most of the island is responding with a predominant period in a range of 0.7 to 1.0 sec. For the portion of the strong ground motion spectral ratio in the range of engineering interest from 0.5 sec to 5 sec, Figure 6.20 there is a relatively flat level of amplification from 0.7 to 3 sec. As noted in the Port Hueneme study, Chapter 5, there may be a minor increase of the microseism period under strong ground shaking. Figure 6.20 shows the spectral ratio for the E-W component of the Loma Prieta earthquake at the Treasure Island/Yerba Buena sites. There is again evidence that the amplification levels under strong ground shaking at a soft site are substantially reduced compared with microseism spectral ratios.

### **Nakamura Method**

The Nakamura method described in Chapter 2 of using the vertical motion as a replacement for the rock reference site was tried. Figure 6.21 shows typical results. The results show a rather narrow spectral region around the site fundamental period. The peak amplitudes are in the range of 6 to 12 but appear to lack consistency with rock reference measurements. At this point it appears there is insufficient evidence to accept the validity of the procedure for use.

## References

- Borcherdt, R.D., (1970) Effect of local geology on ground motion near San Francisco Bay, Bulletin Seismological Society America, 29-61.
- Benuska, L., (1990) (editor) Loma Prieta Earthquake Reconnaissance Report, Earthquake Spectra, Supplement to Vol. 6.
- Borcherdt, R.D., and Gibbs, J.F., (1976) Effects of local geological conditions in the San Francisco Bay region on ground motions and the intensities of the 1906 earthquake, {\em Bulletin Seism. Society Am.}, 467-500.
- Darragh, R.B., and Shakal, A.F. (1991) The site response of two rock and soil stations pairs to strong and weak ground motion, Bulletin Seismological Society America, 1885-1899.
- Housner, G.W., (1990). Competing Against Time, Report to Governor George Dukmejian from the Governor's Board of Inquiry on the 1989 Loma Prieta Earthquake, C. Thiel Jr. (editor), State of California, Office of Planning and Research, 1990.
- Power, M.S., Egan, J.A., Schewbridge, S., deBecker, J., and Faris, J.R., (1993). Analysis of liquefaction-induced distress at Treasure Island, USGS Prof. Paper, to appear.
- Radbruch, D. (1957) "Areal and Engineering Geology of the Oakland West Quadrangle, California", US Geological Survey Miscellaneous Geologic Investigations, Map I-239, Washington D.C.
- Rollins, K.M., Hryciw, R.D., McHood, M., Homolka, M., and Shewbridge, S.E. (1993). Soil amplification at Treasure Island during the Loma Prieta earthquake, USGS Prof. Paper, to appear.
- Schlocker, J., (1968). The geology of the San Francisco Bay area and its significance in land use and planning, Association of Bay Area Governments Supplemented Report 1S-3, Regional Geology, 47.
- Schlocker, J., Bonilla, M., and Radbruc, D.H., (1958). Geology of the San Francisco north quadrangle, California, U.S. Geol. Misc. Inv. Map I-272.
- Seed, R.B., Dickenson, S.E., Riemer, M.F., Bray, J.D., Sitar, N., Mitchell, J.K., Idriss, I.M., Kayen, R.E., Kropp, A., Hrader, L.F. Jr., and Power, M.S., (1990). Preliminary Report on the Principal Geotechnical Aspects of the October 17, 1989 Loma Prieta Earthquake, Report UCB/EERC-90/05.

Sewbridge, S., Power, M.S., and Basore, C., (1990). Perimeter Dike Stability Evaluation, Naval Station Treasure Island, Report to the Western Division Naval Facilities Engineering Command, San Bruno, California.

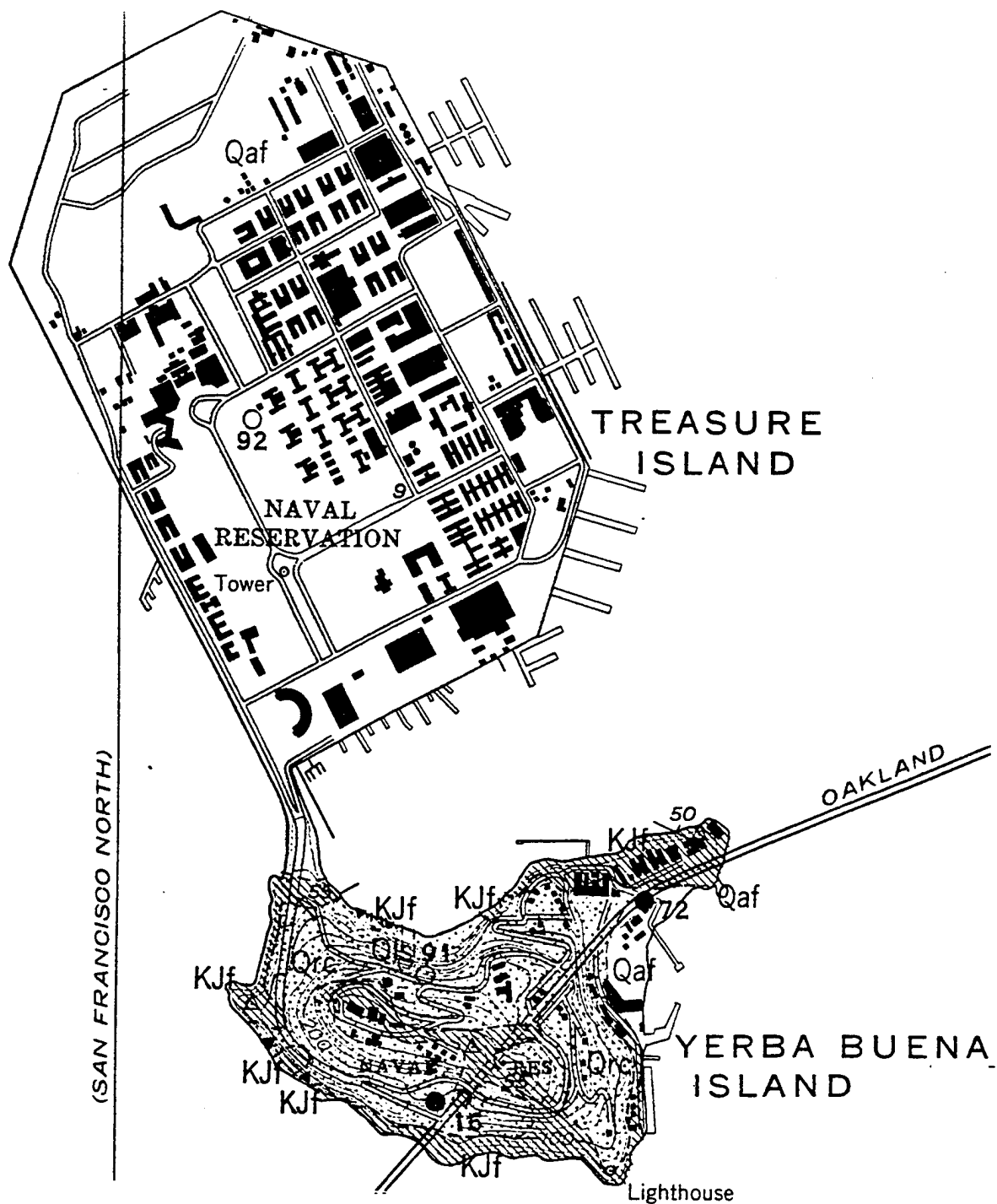
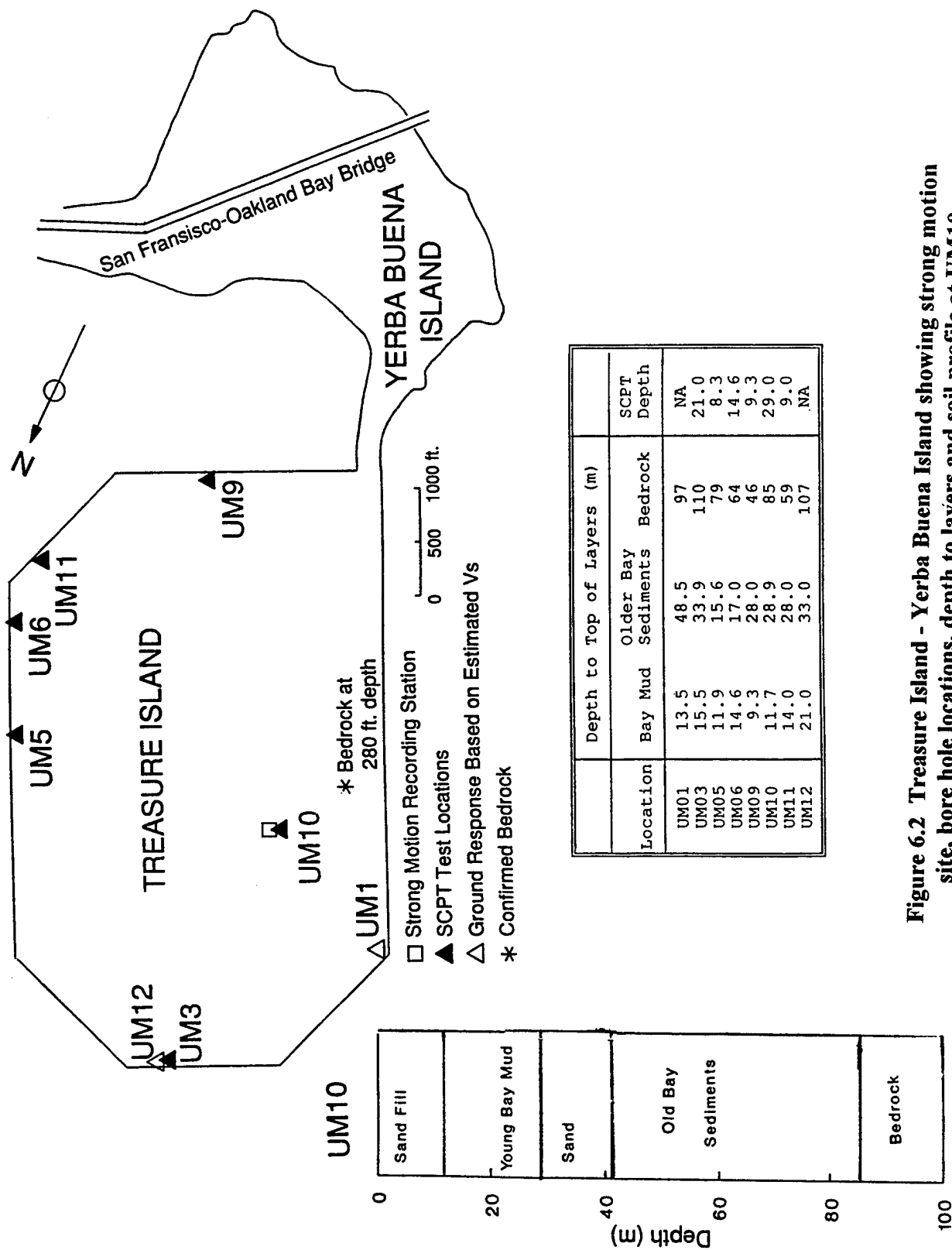


Figure 6.1. Treasure Island and Yerba Buena Island.



**Figure 6.2** Treasure Island - Yerba Buena Island showing strong motion site, bore hole locations, depth to layers and soil profile at UM10, from Hryciw et al. 1991



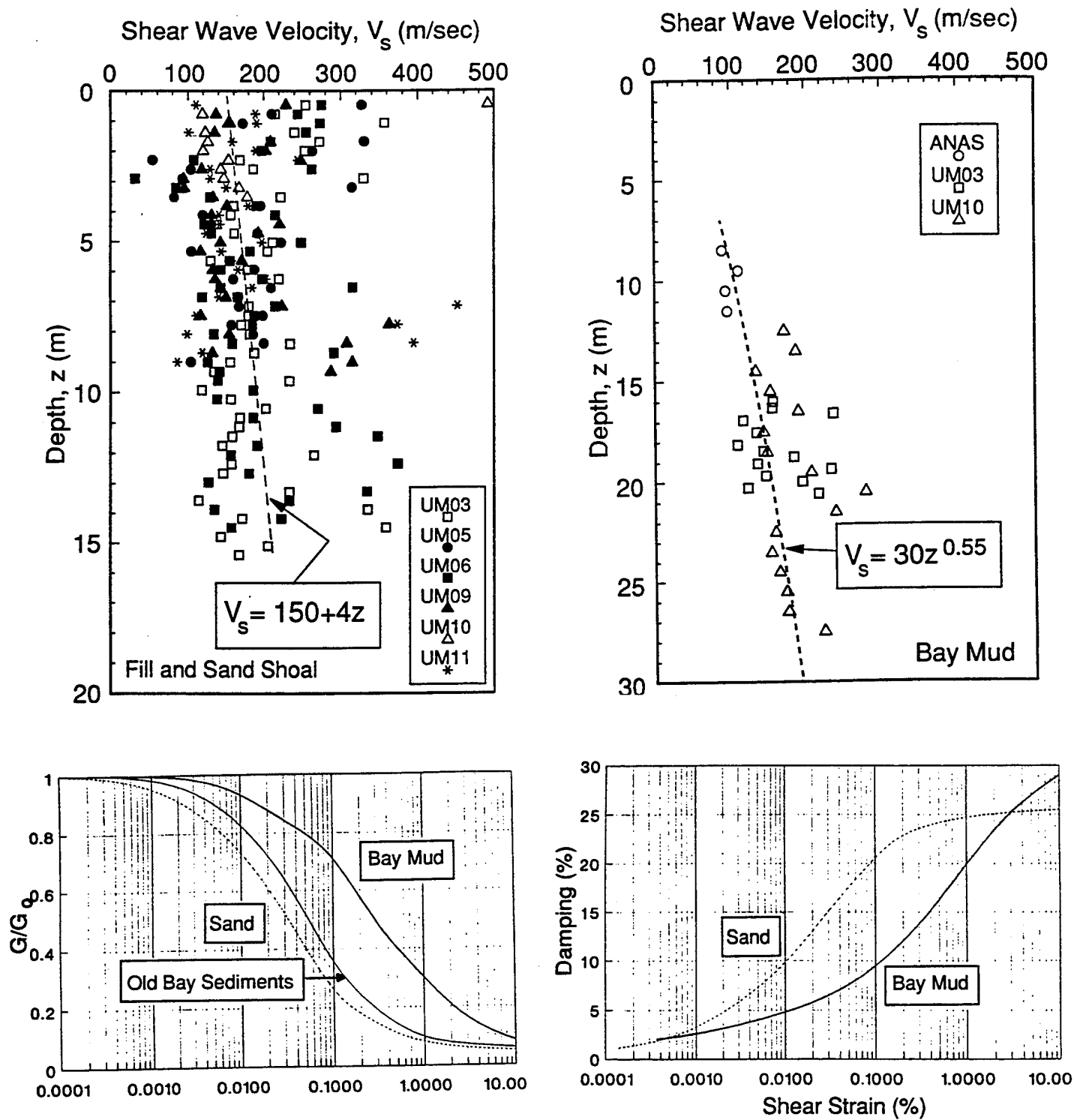
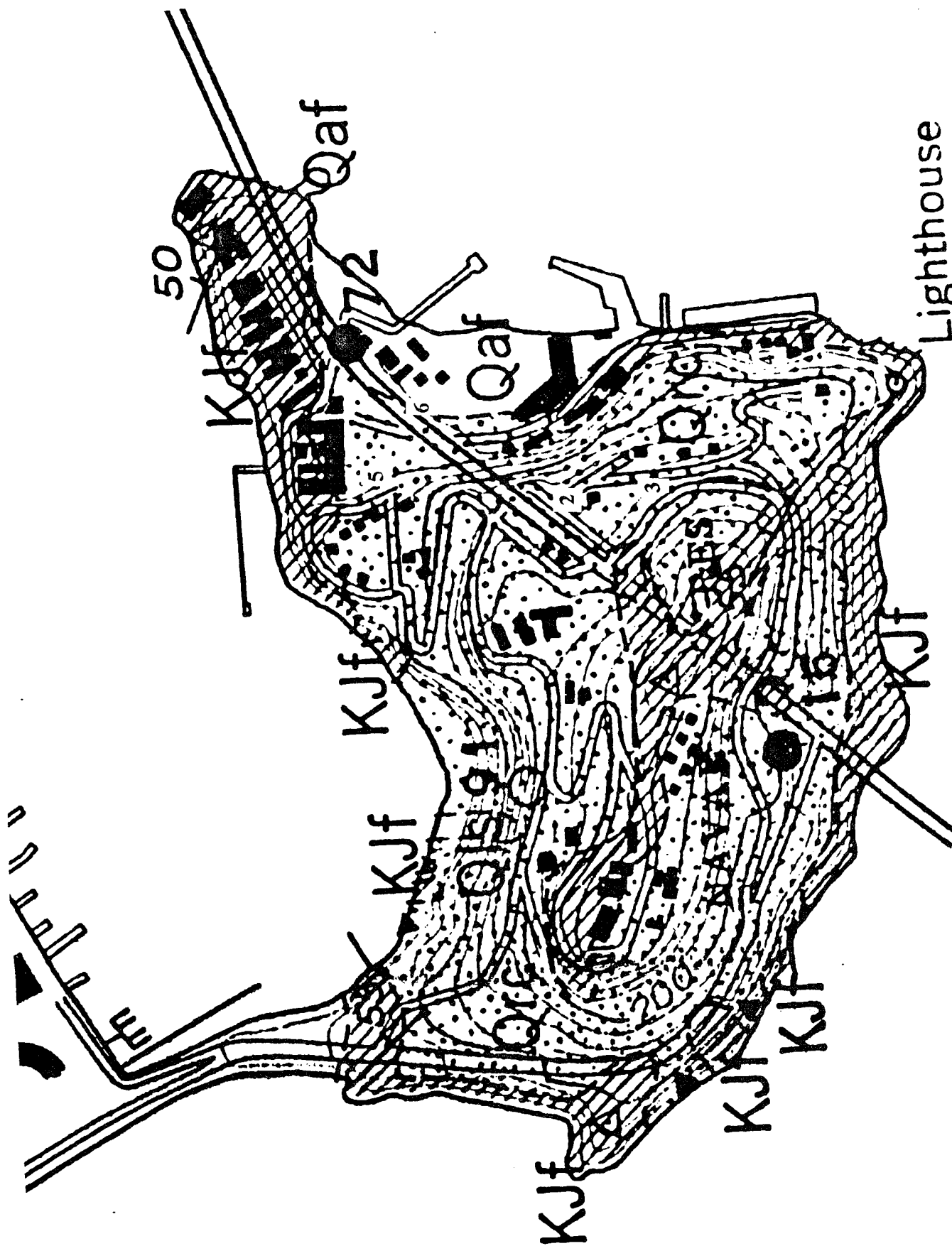


Figure 6.3 Soil data for upper layers, from Hryciw et al, 1991



Lighthouse  
Strong motion instrument

Figure 6.4 Geology of Yerba Buena Island  
and measurement locations

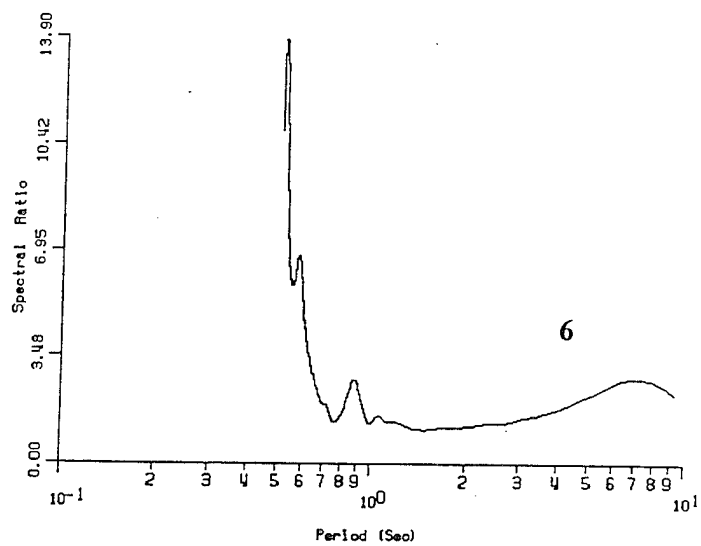
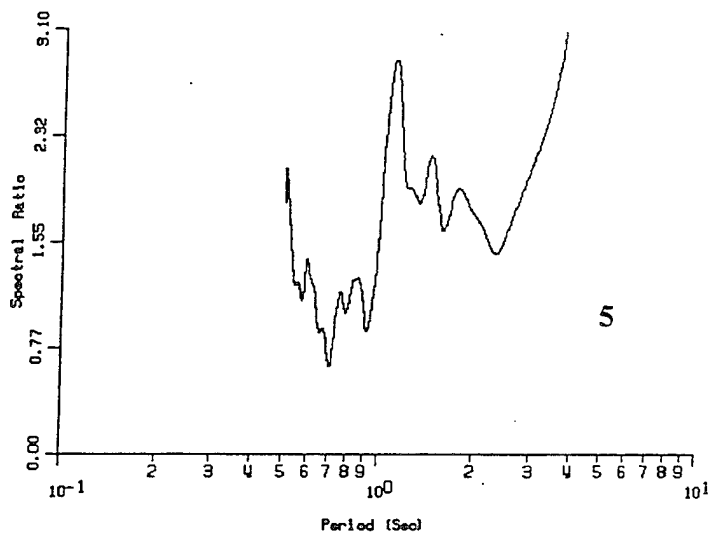
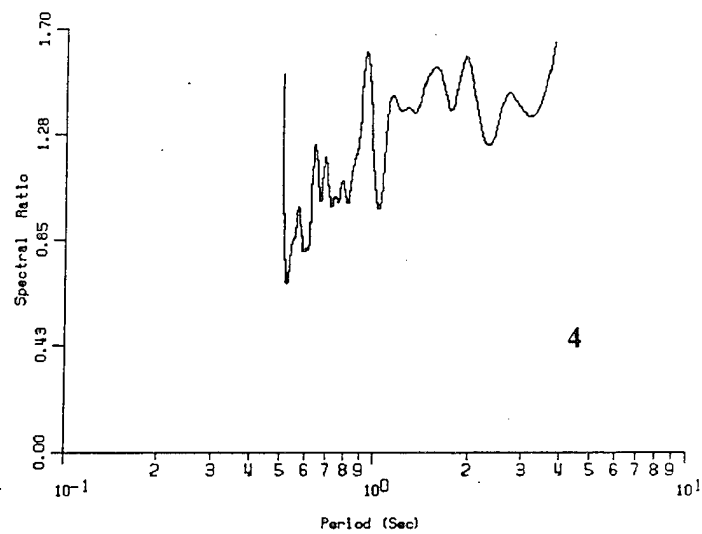
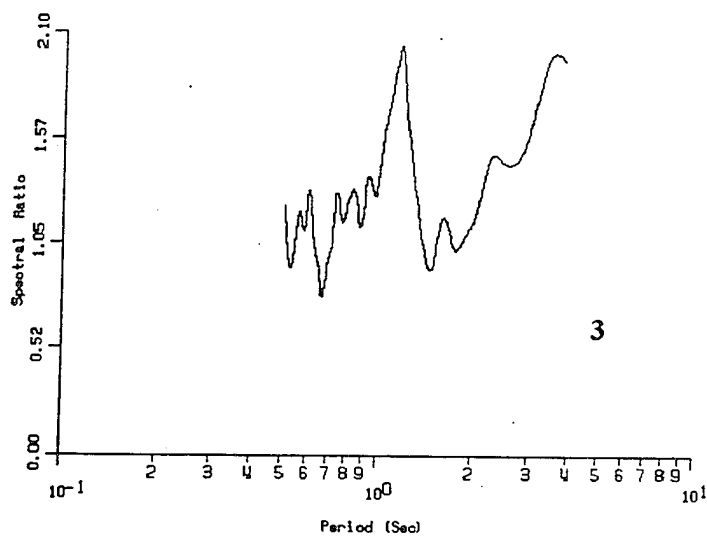
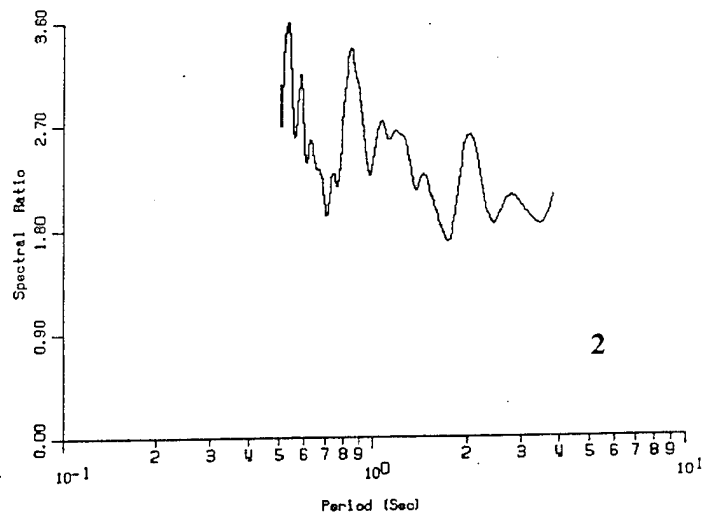
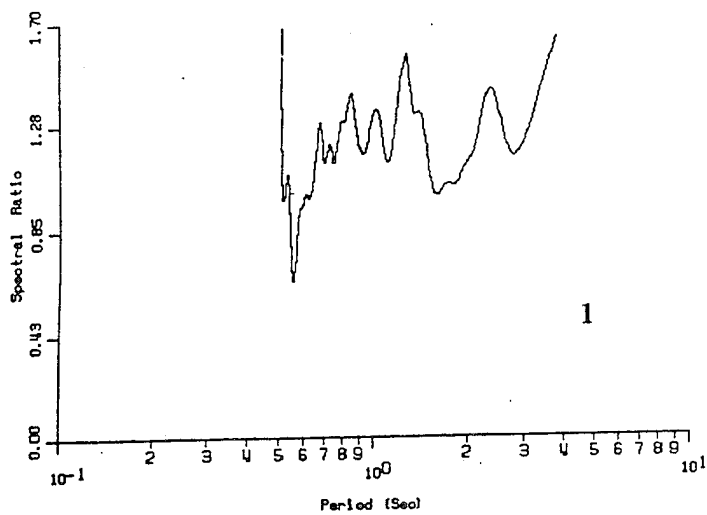


Figure 6.5a. Spectral ratios Yerba Buena Stations, East West direction.

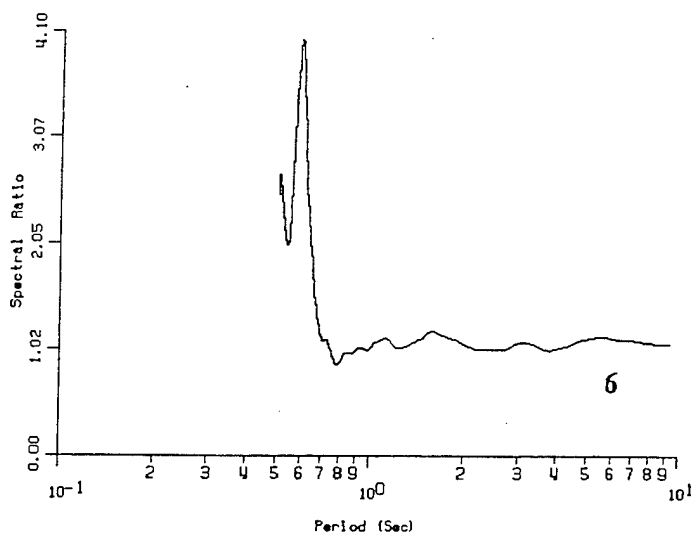
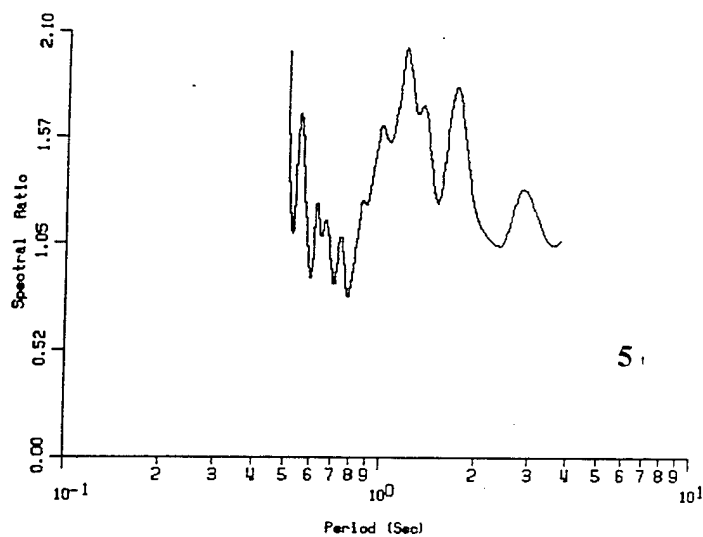
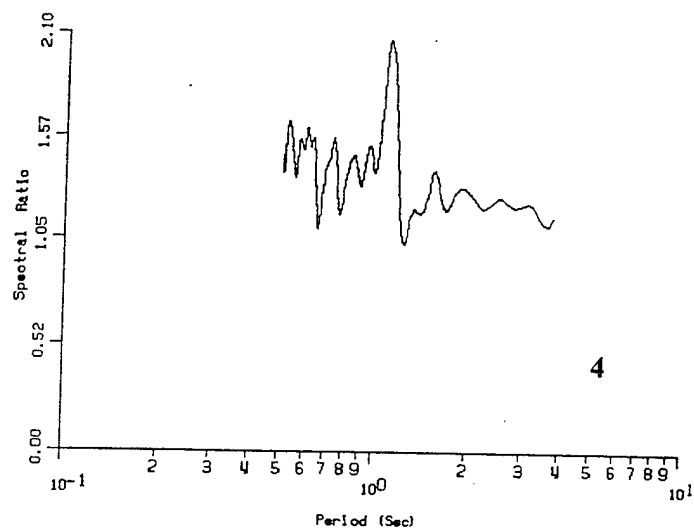
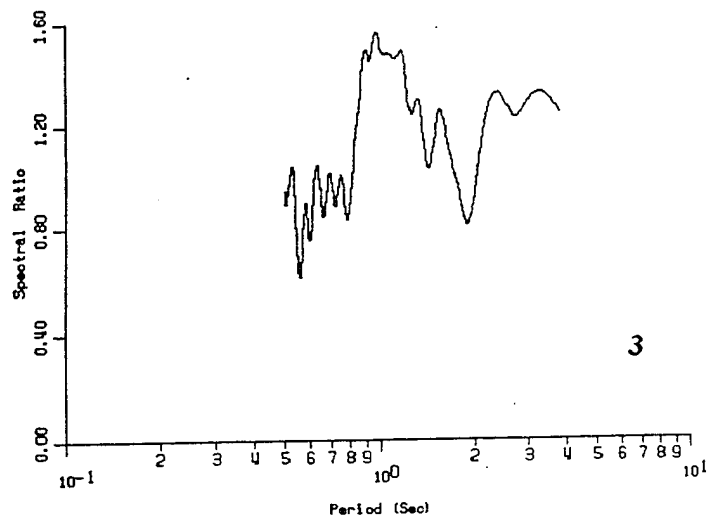
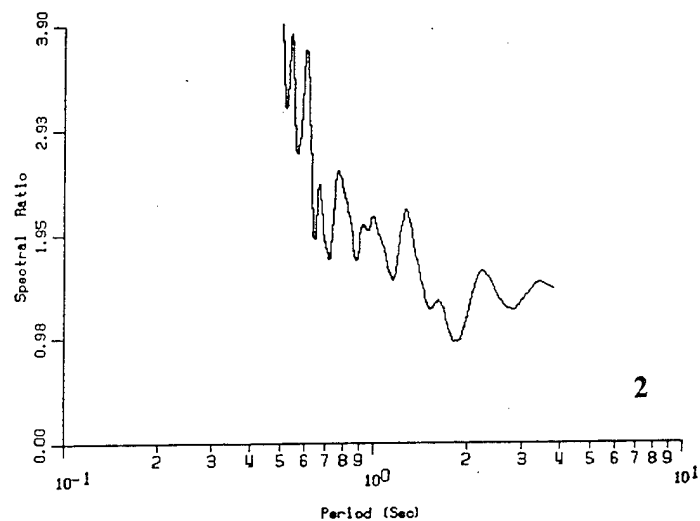
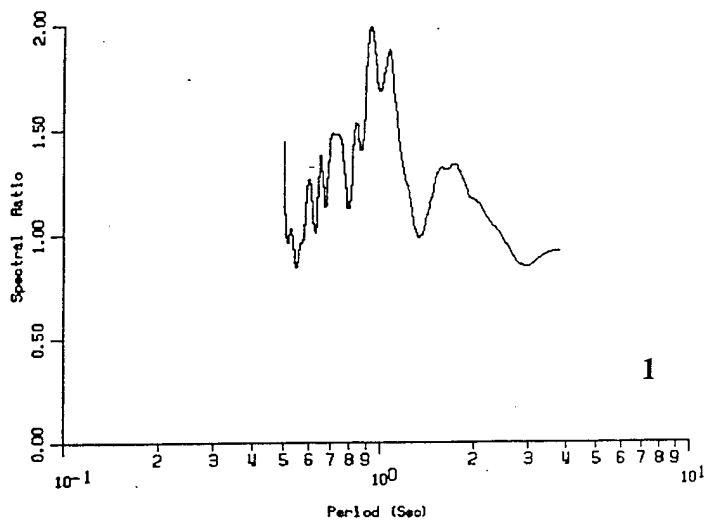


Figure 6.5b. Spectral ratios Yerba Buena Stations, North South direction.

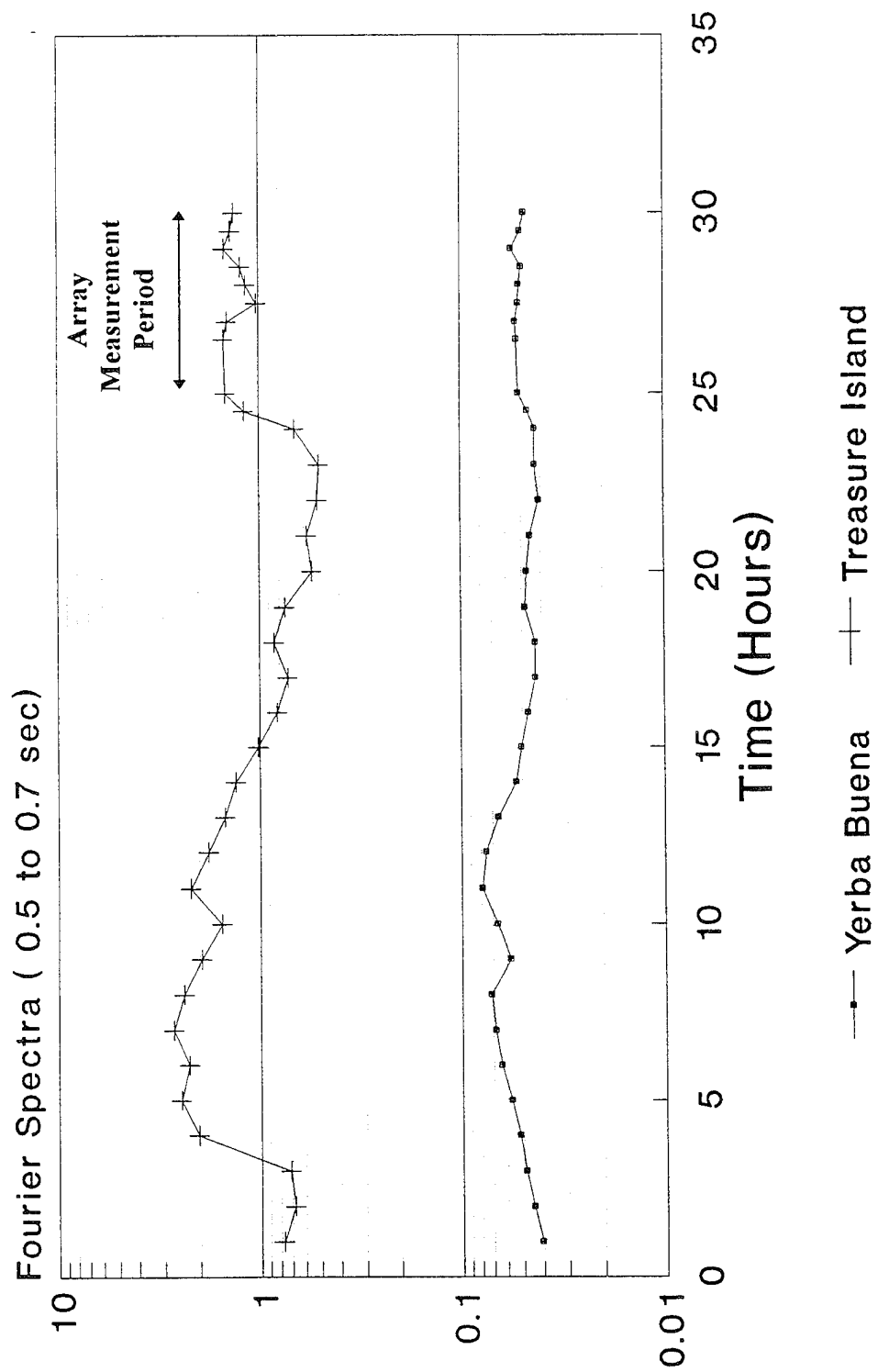


Figure 6.6. Long term measurement spectra for period 0.5 to 0.7 sec.

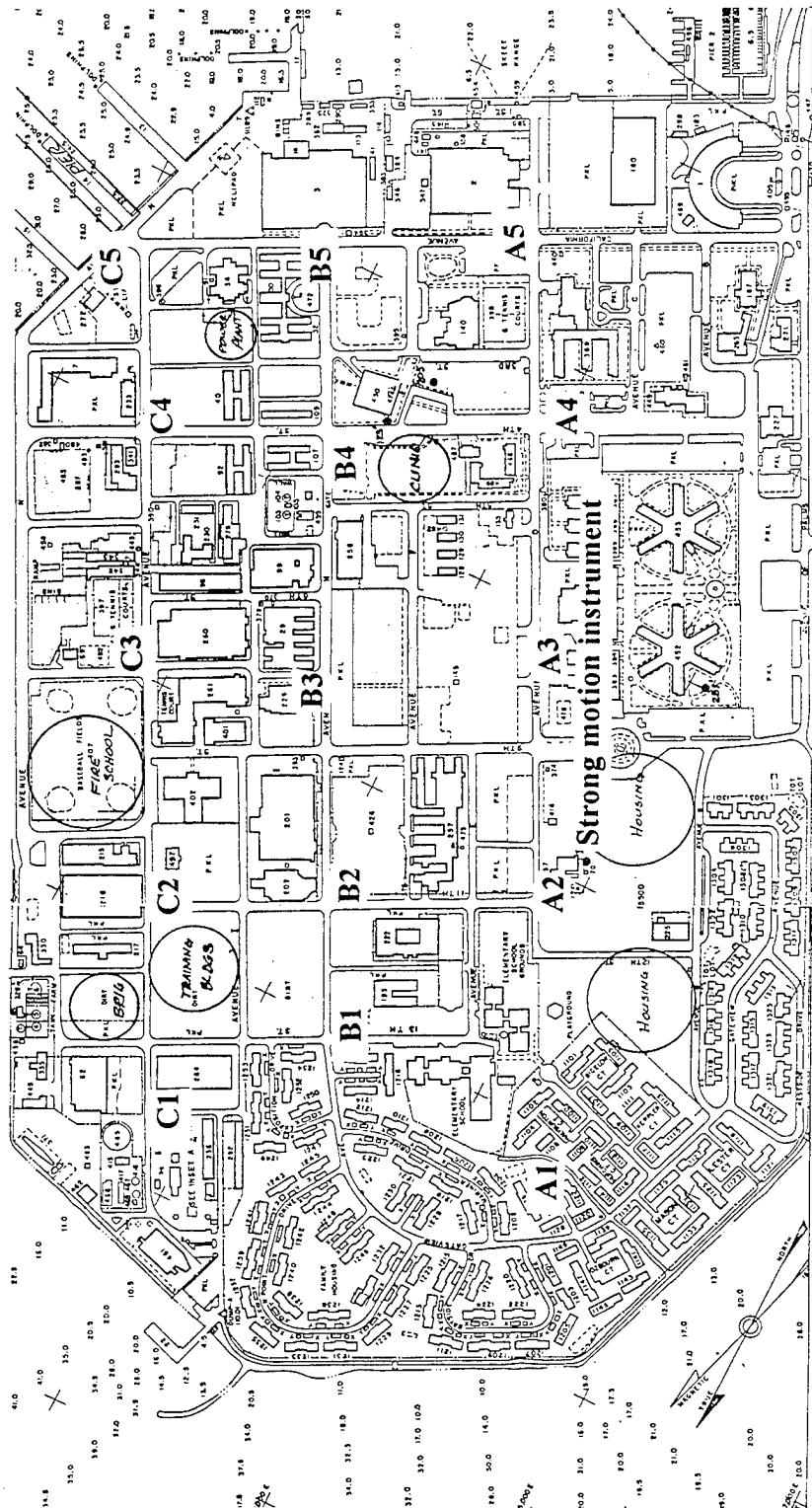
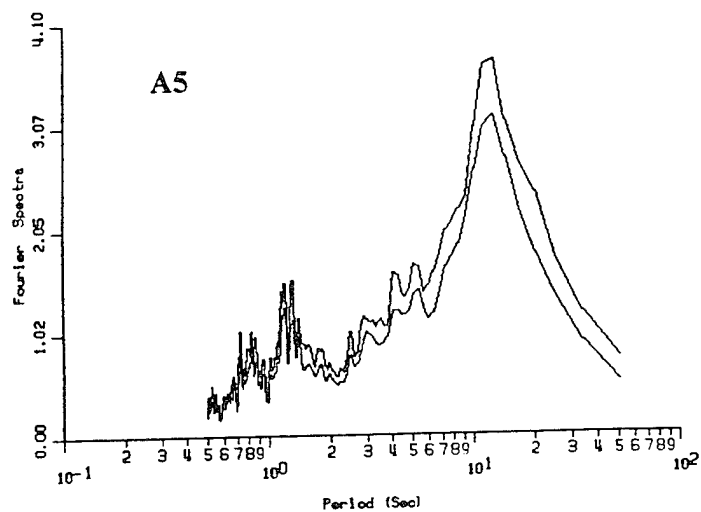
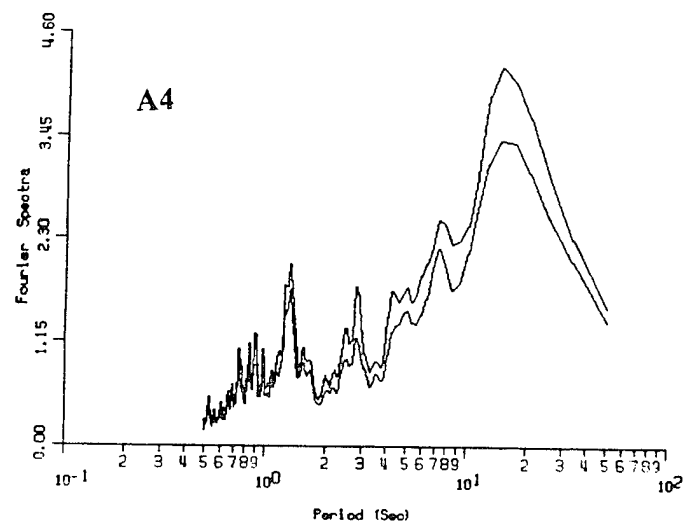
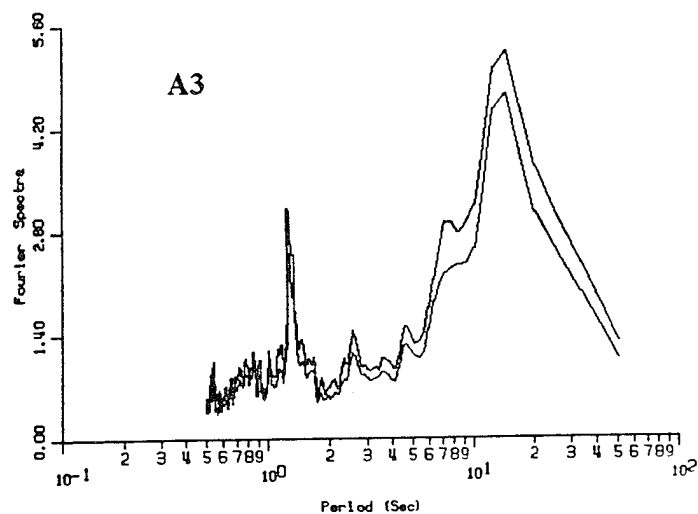
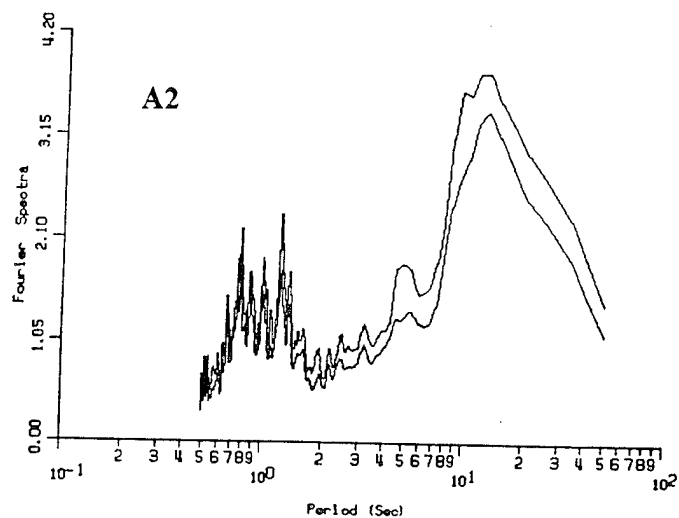
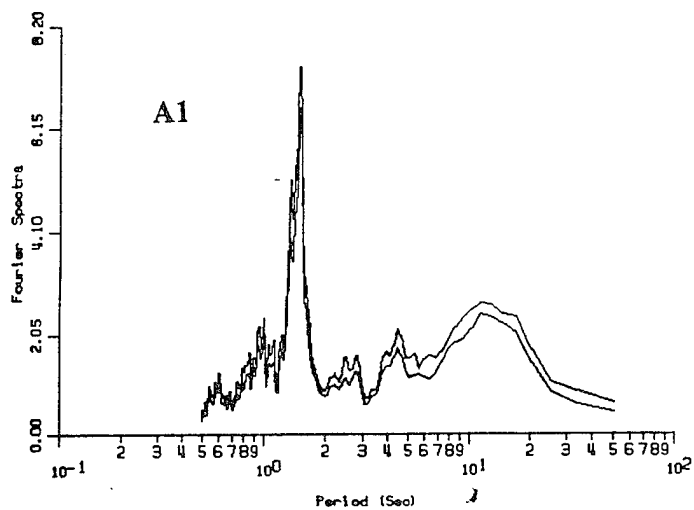
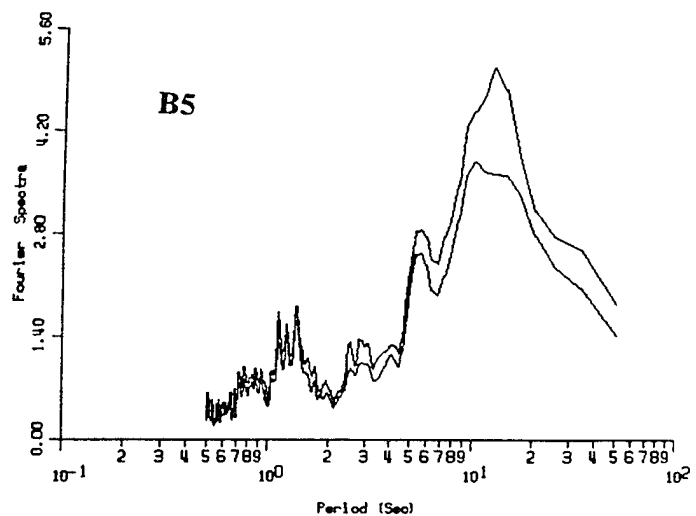
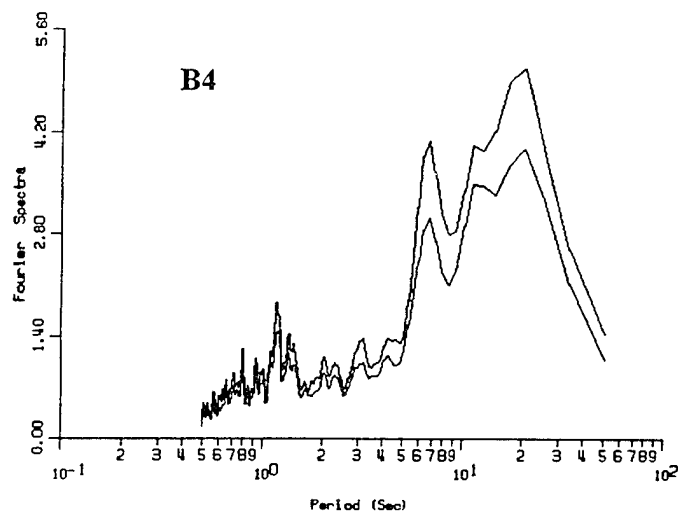
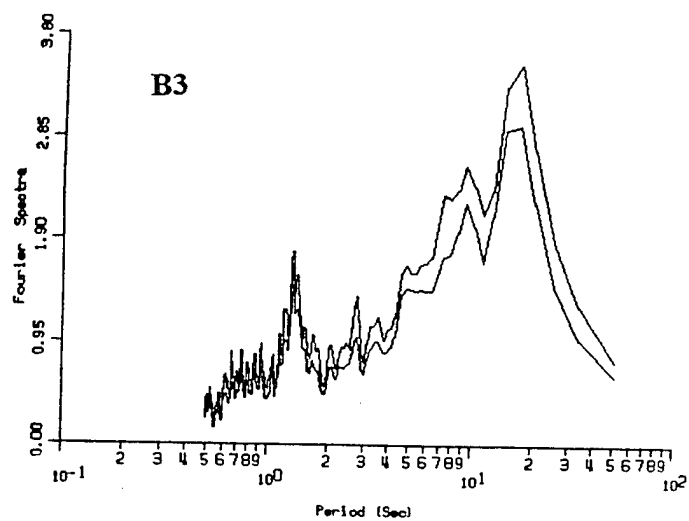
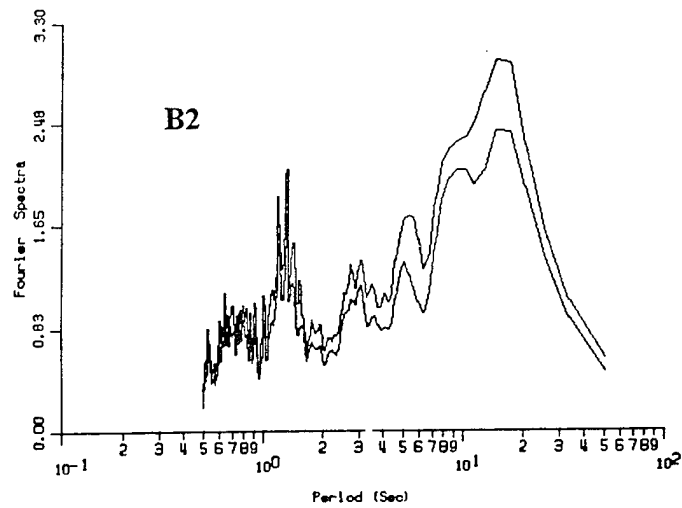
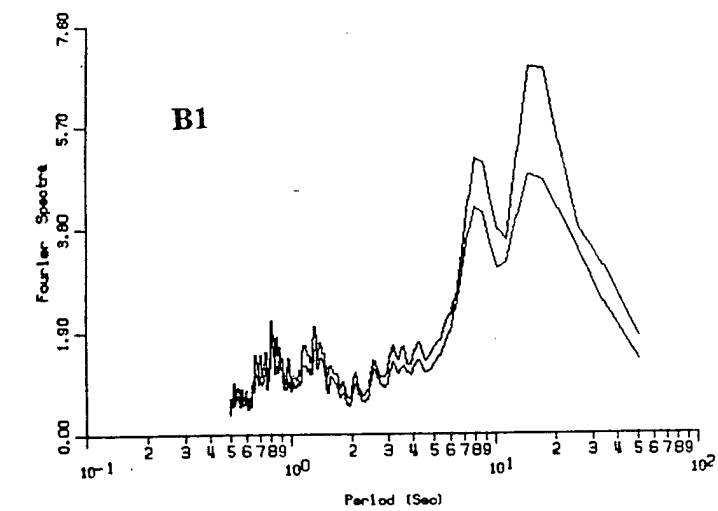


Figure 6.7 Treasure Island site plan showing measurement locations.



**Figure 6.8a. North - South Fourier velocity spectral amplitude  
for Treasure Island sites along Section A.**



**Figure 6.8b. North - South Fourier velocity spectral amplitude for Treasure Island sites along Section B.**



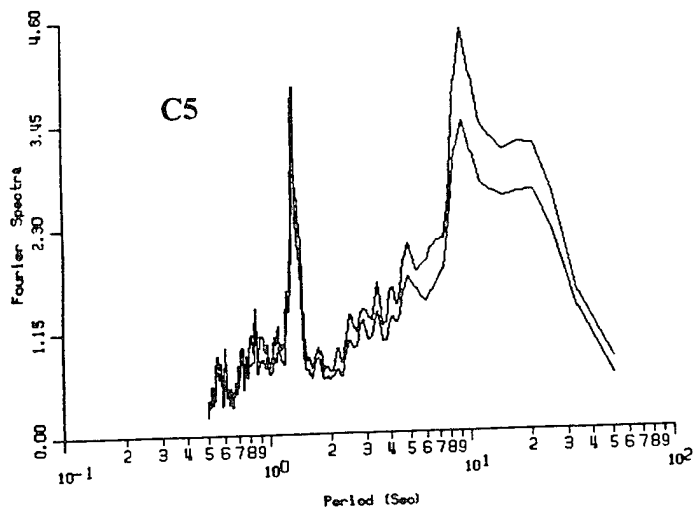
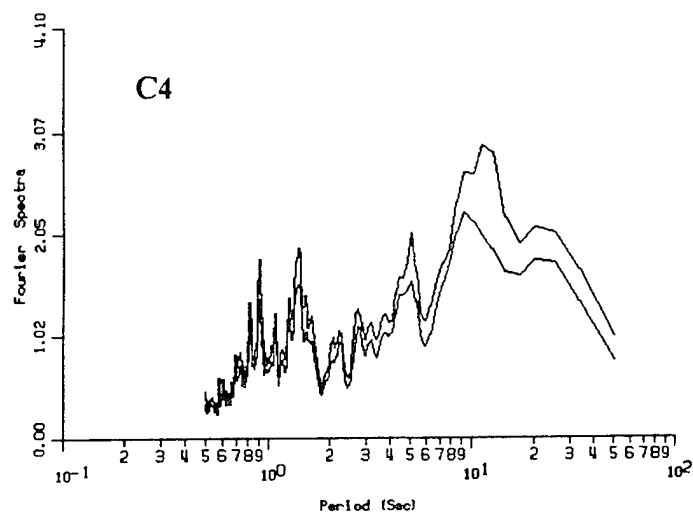
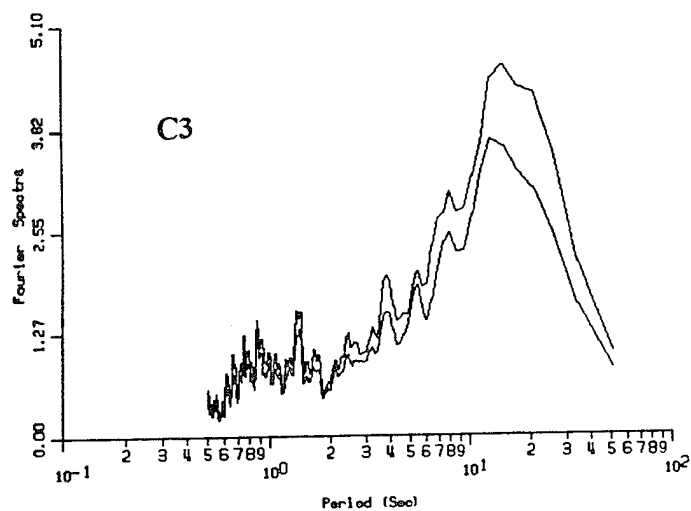
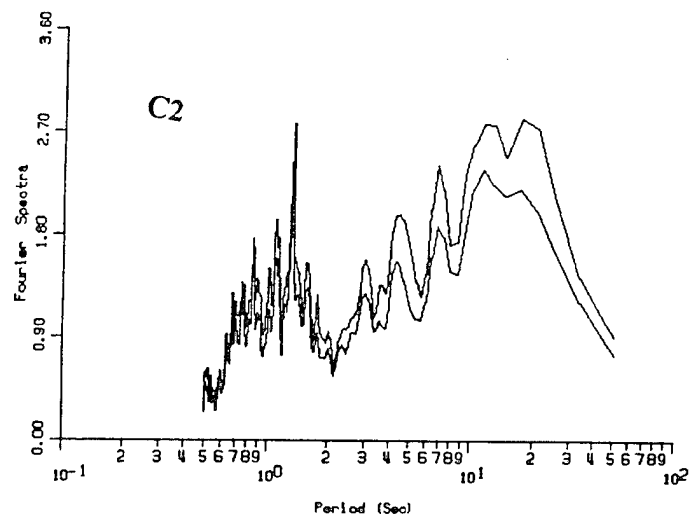
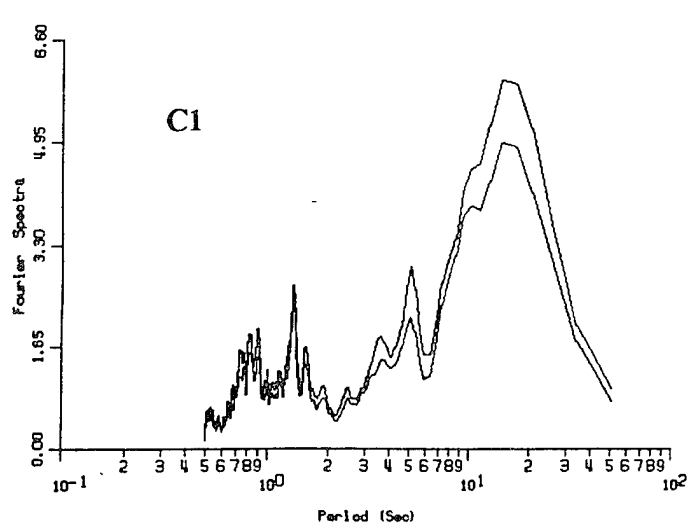


Figure 6.8c. North - South Fourier velocity spectral amplitude for Treasure Island sites along Section C.

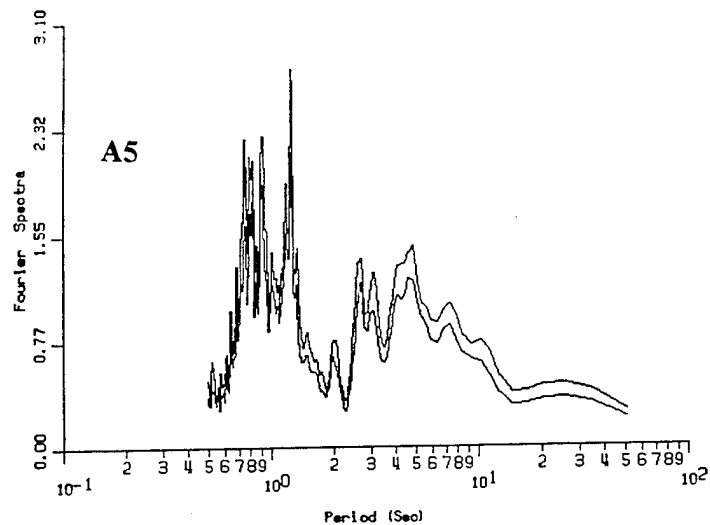
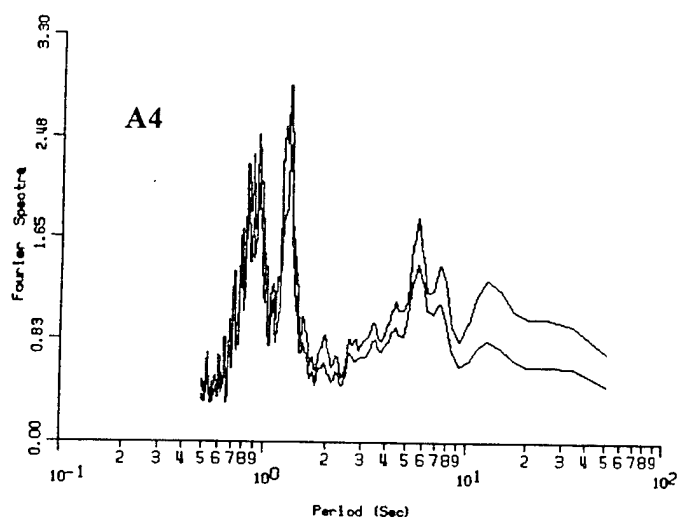
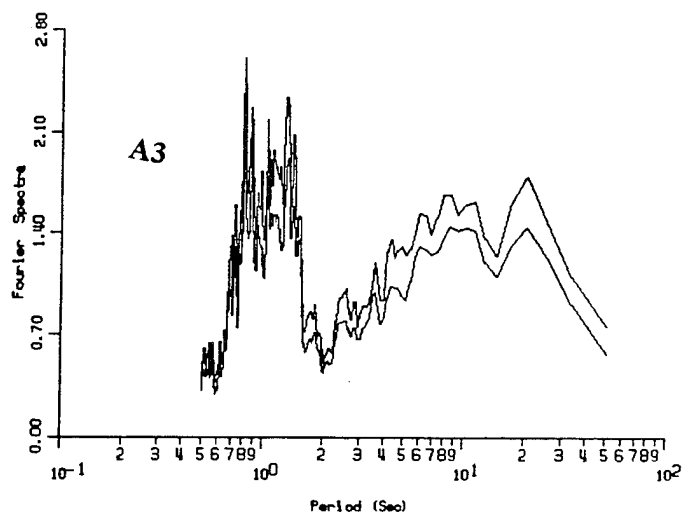
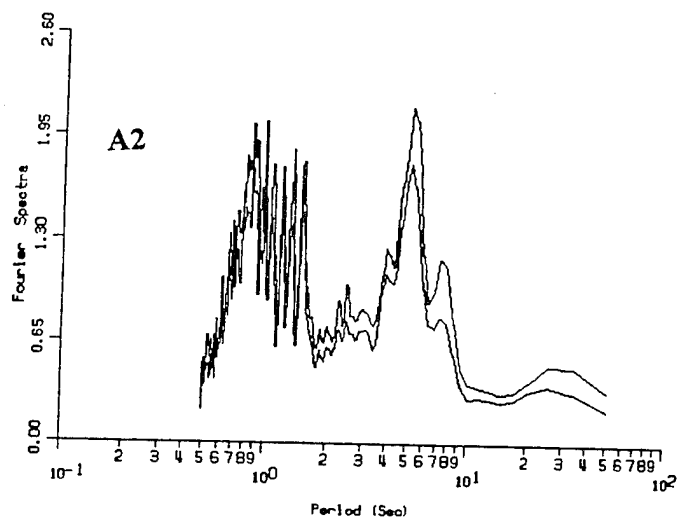
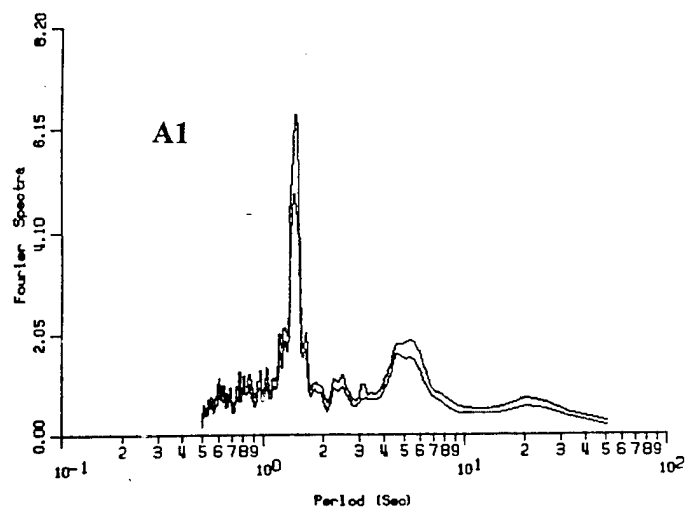
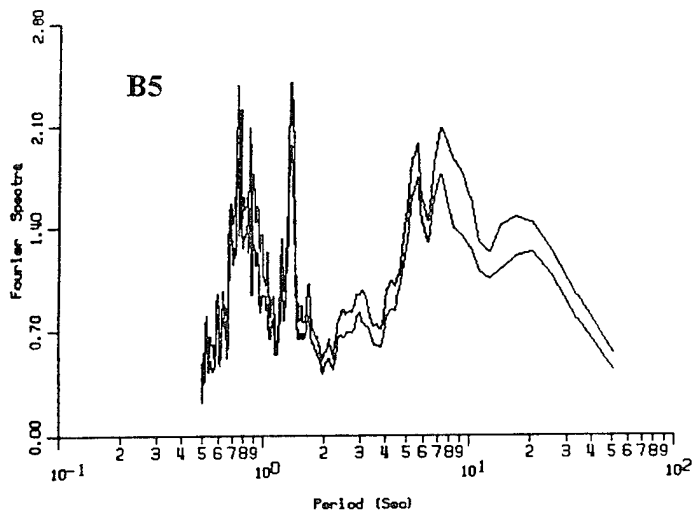
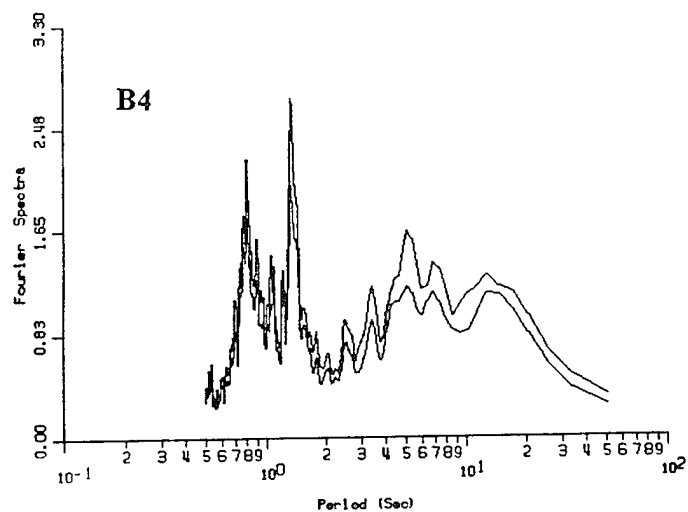
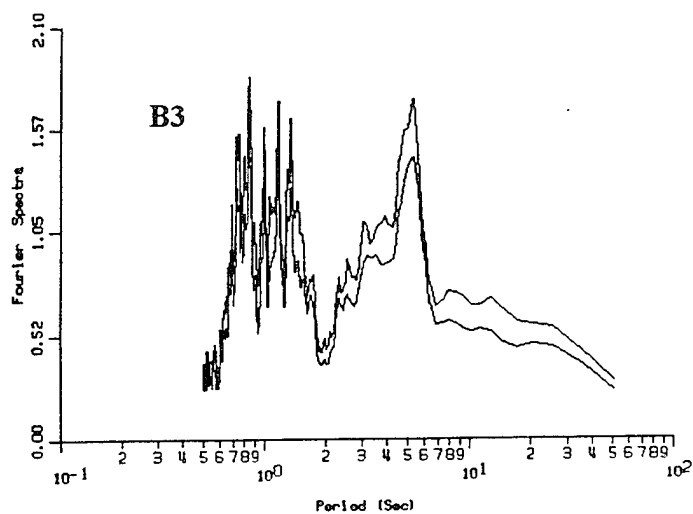
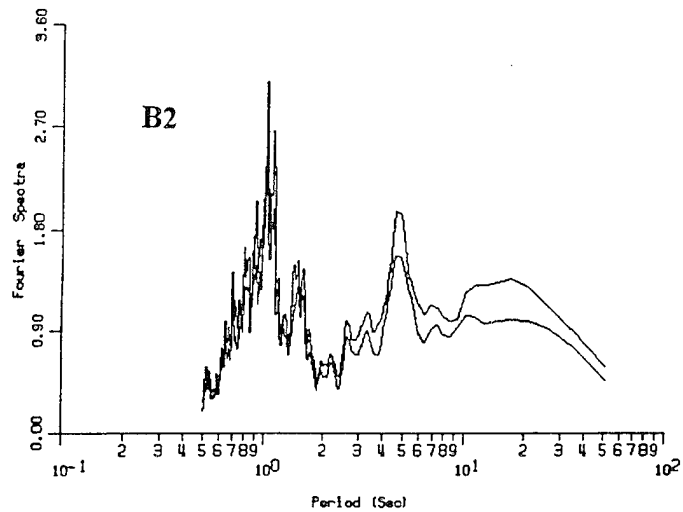
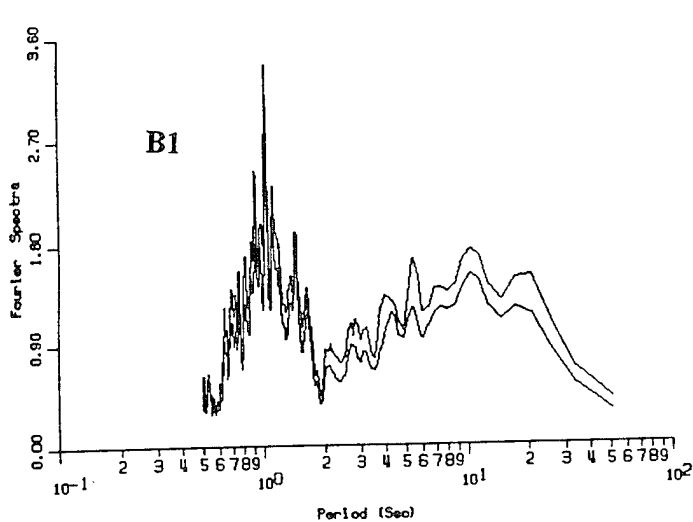


Figure 6.9a. East - West Fourier velocity spectral amplitude for Treasure Island sites along Section A.



**Figure 6.9b. East - West Fourier velocity spectral amplitude for Treasure Island sites along Section B.**

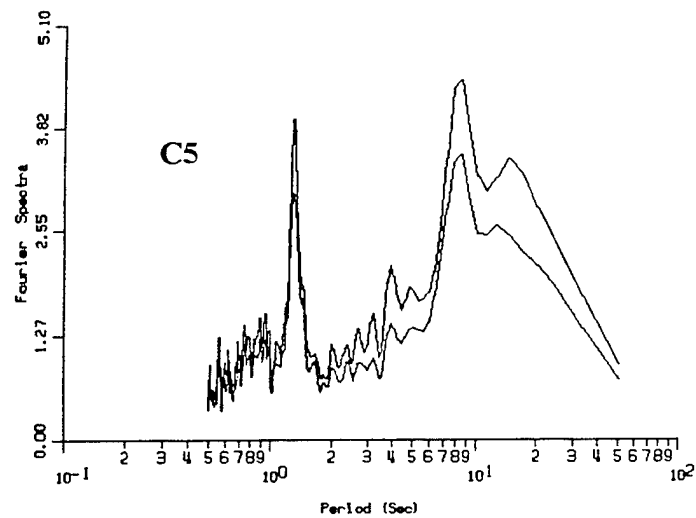
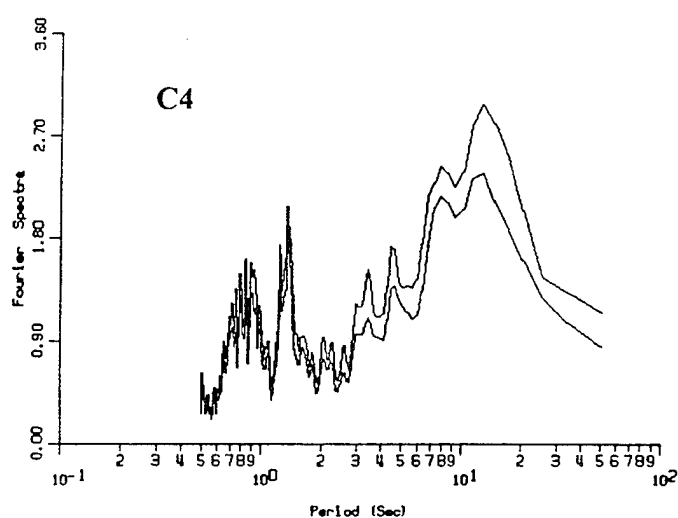
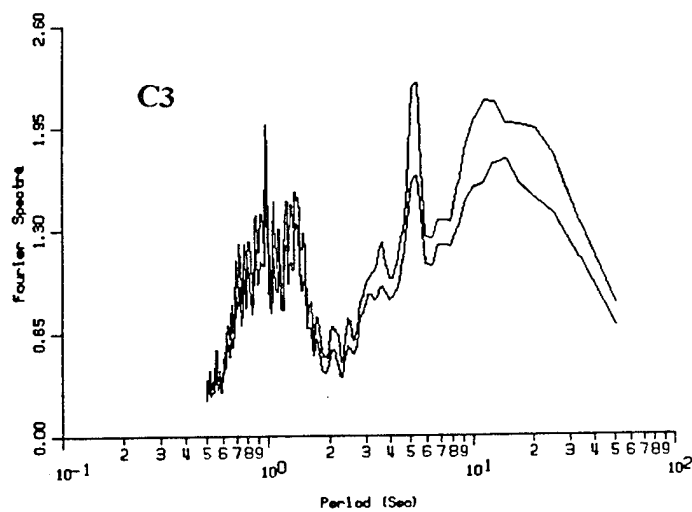
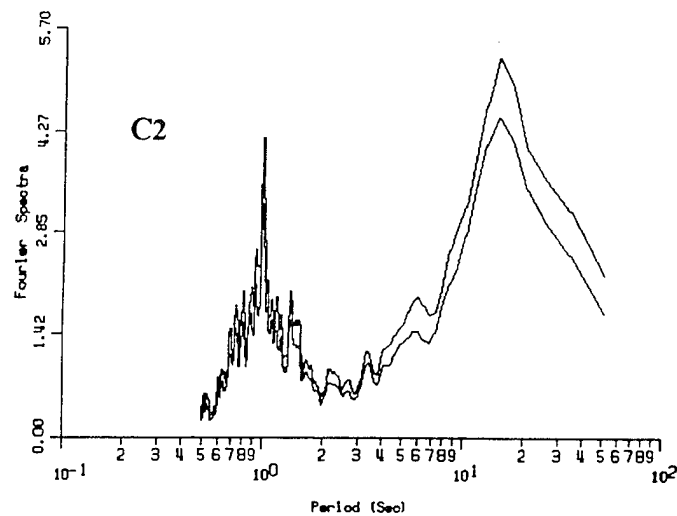
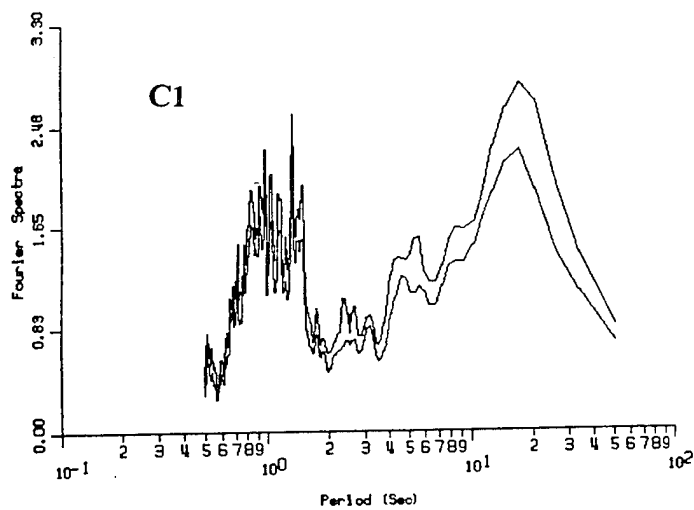


Figure 6.9c. East - West Fourier velocity spectral amplitude for Treasure Island sites along Section C.

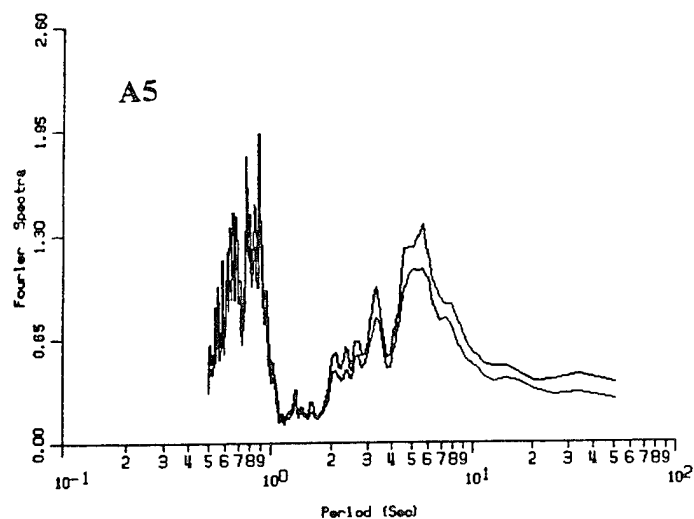
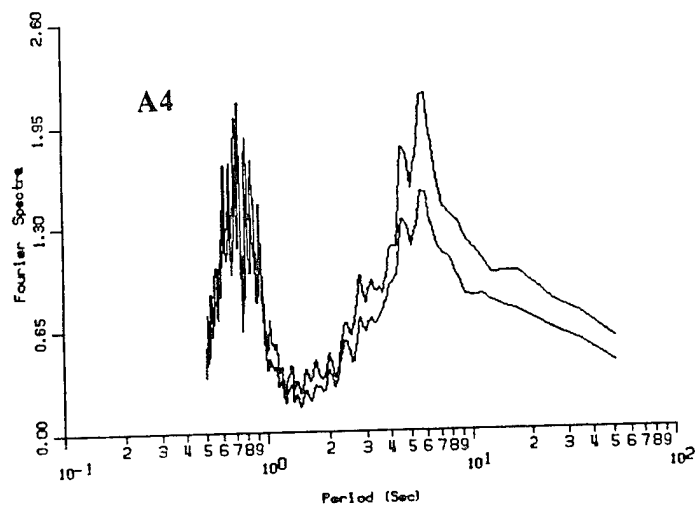
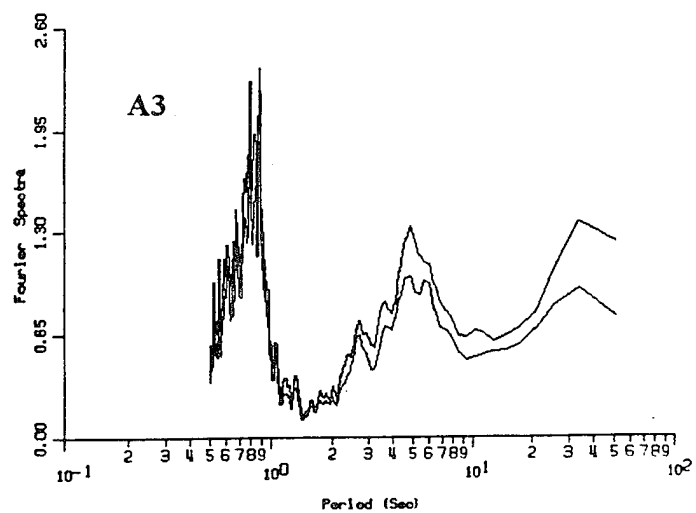
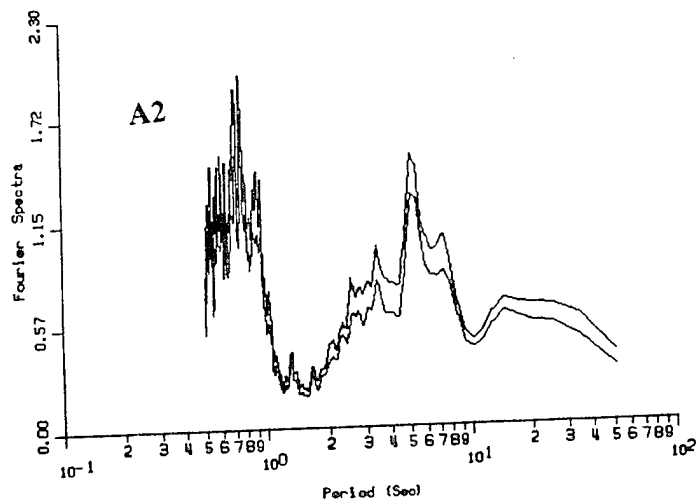
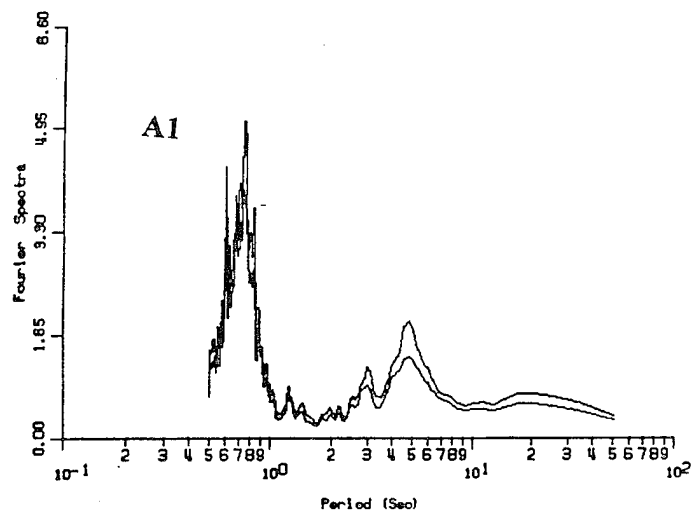


Figure 6.10a. Vertical Fourier velocity spectral amplitude for Treasure Island sites along Section A.

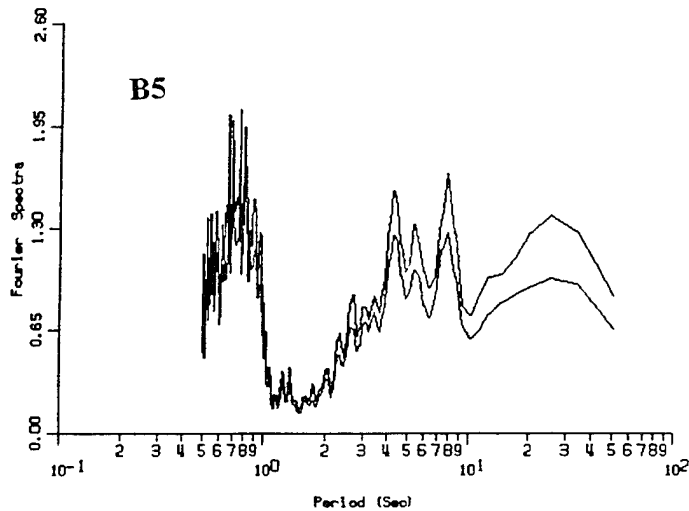
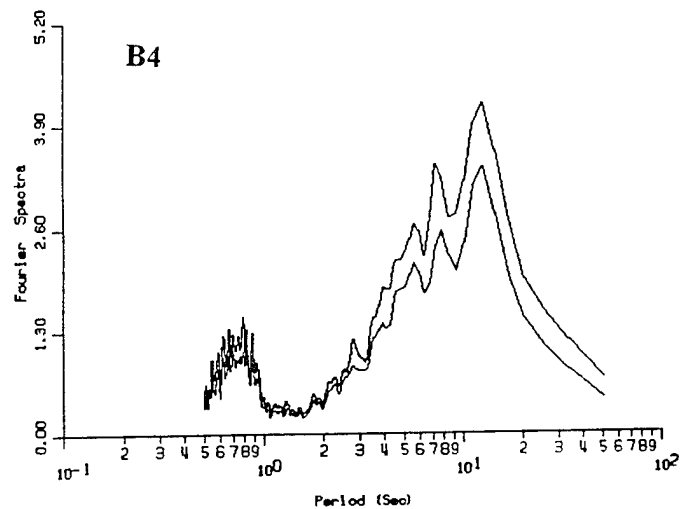
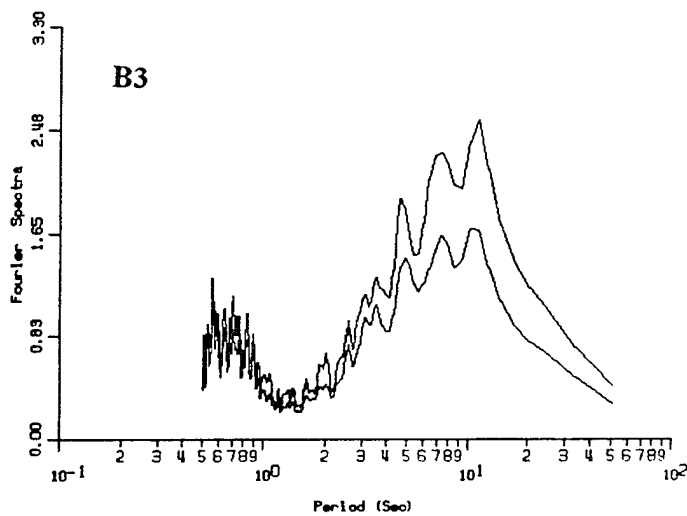
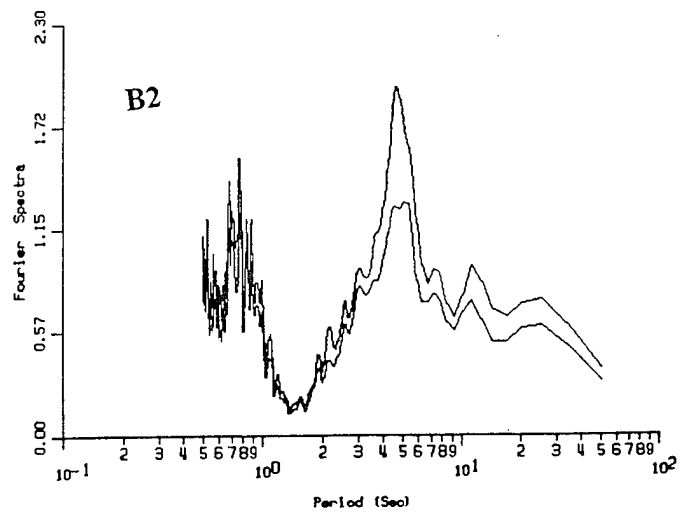
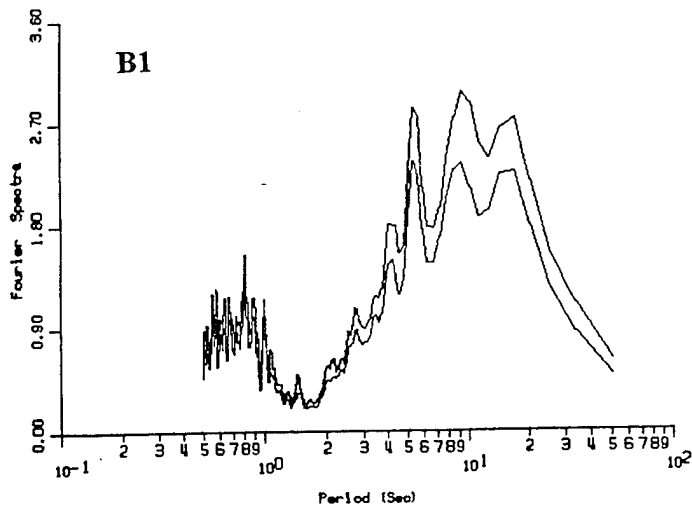


Figure 6.10b. Vertical Fourier velocity spectral amplitude for Treasure Island sites along Section B.

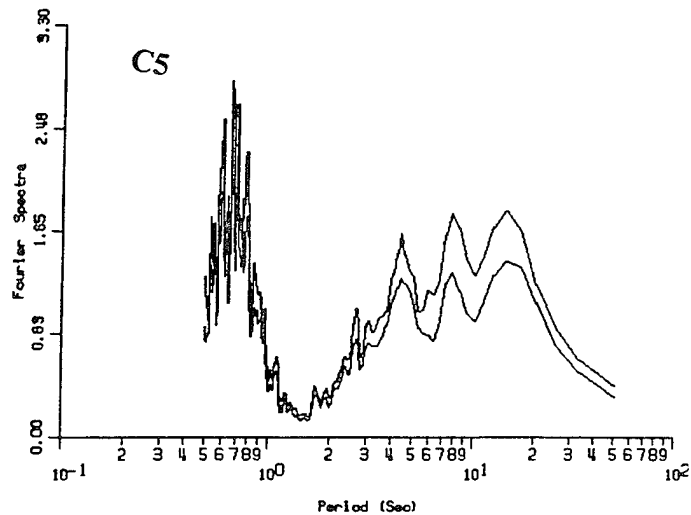
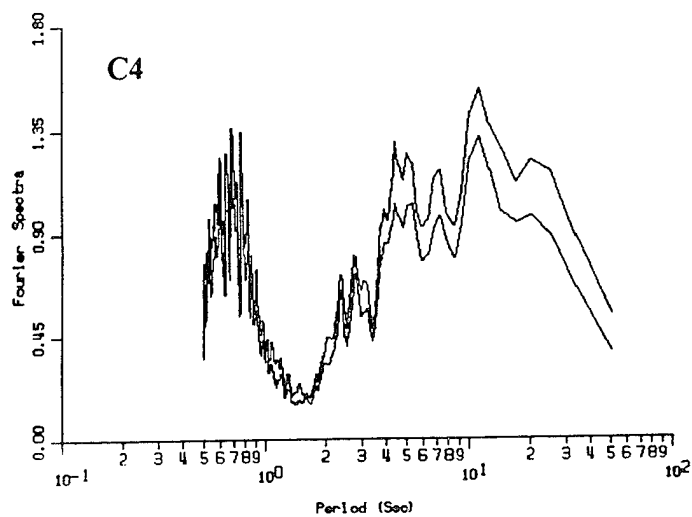
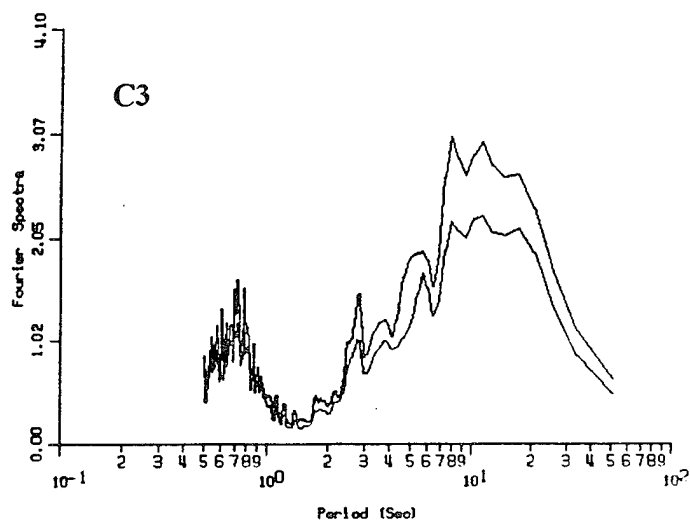
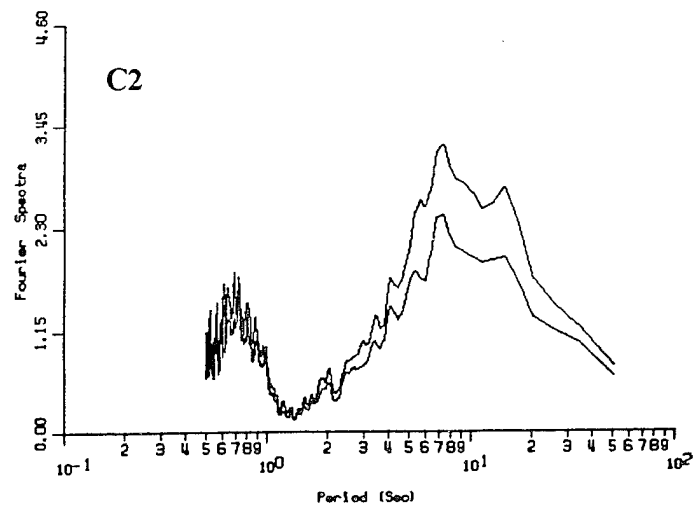
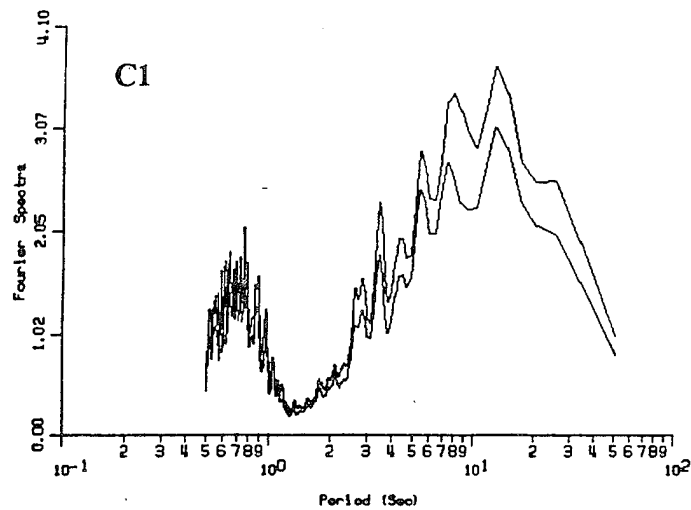


Figure 6.10c. Vertical Fourier velocity spectral amplitude for Treasure Island sites along Section C.

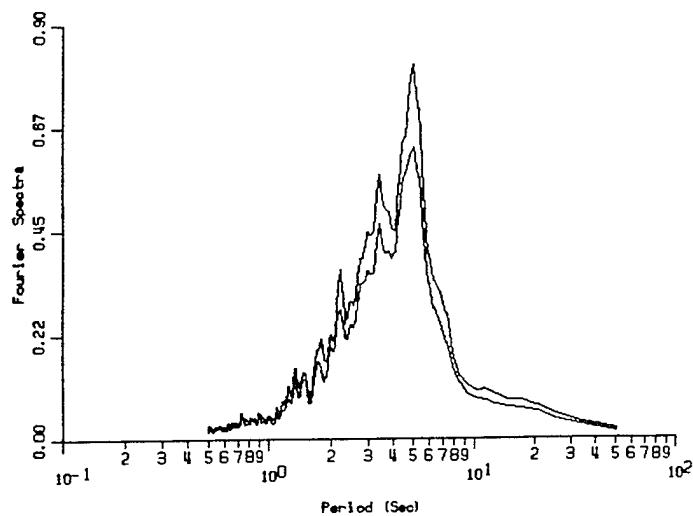
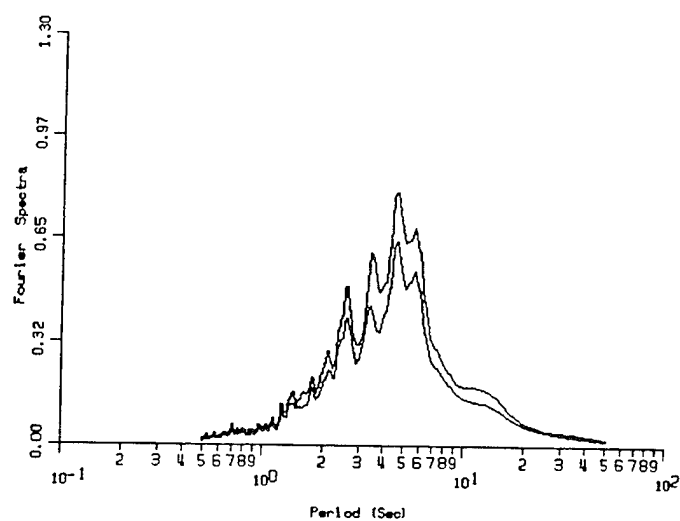
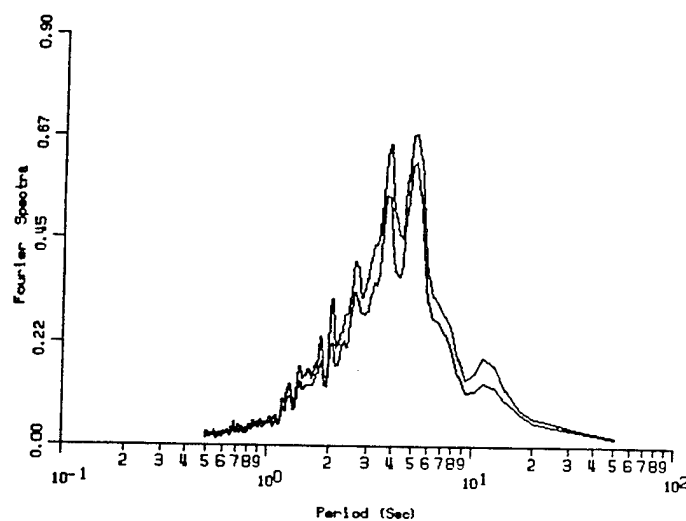
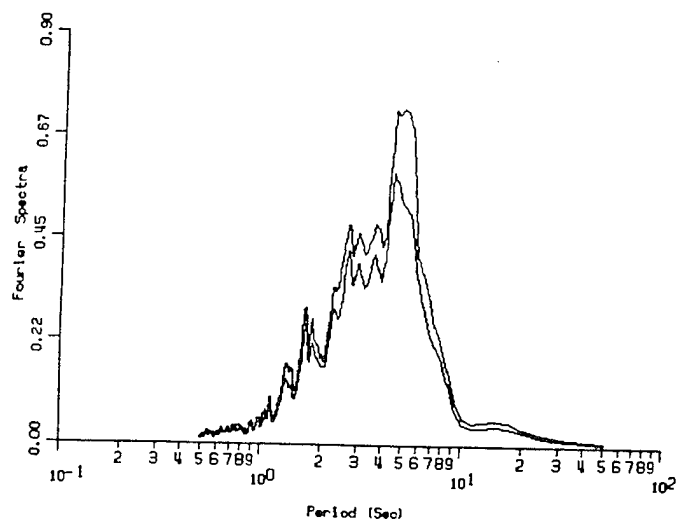
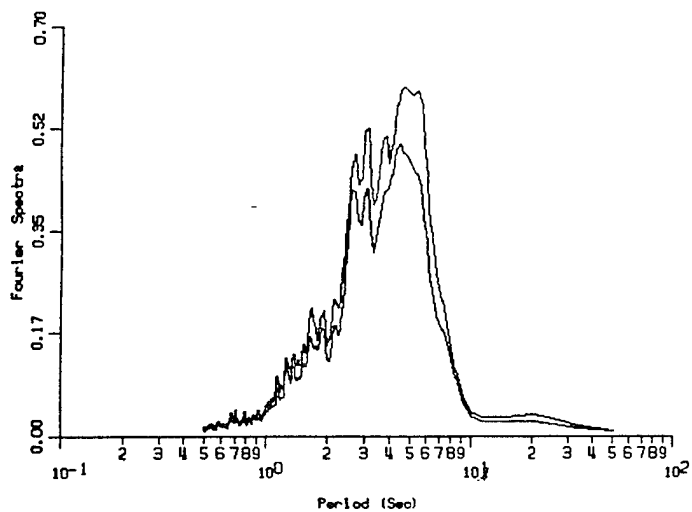


Figure 6.11 Yerba Buena reference measurements  
at half-hour increments starting at 8:00 AM.  
East - West direction



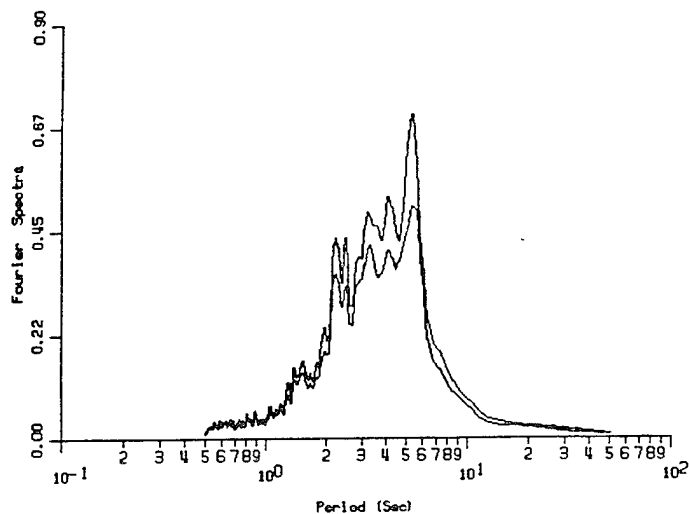
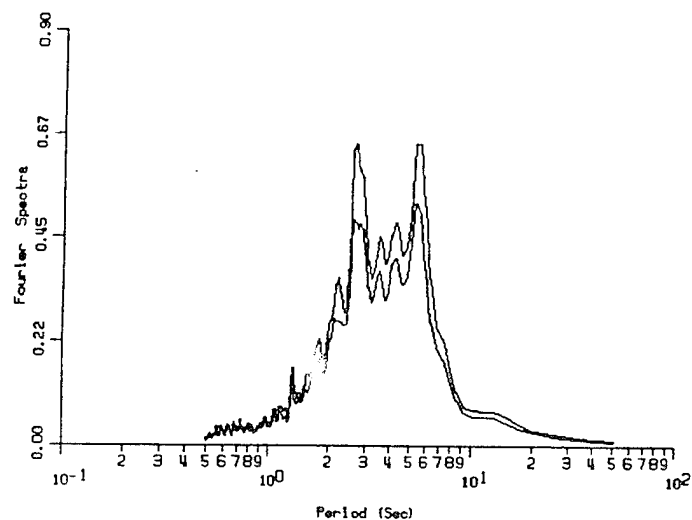
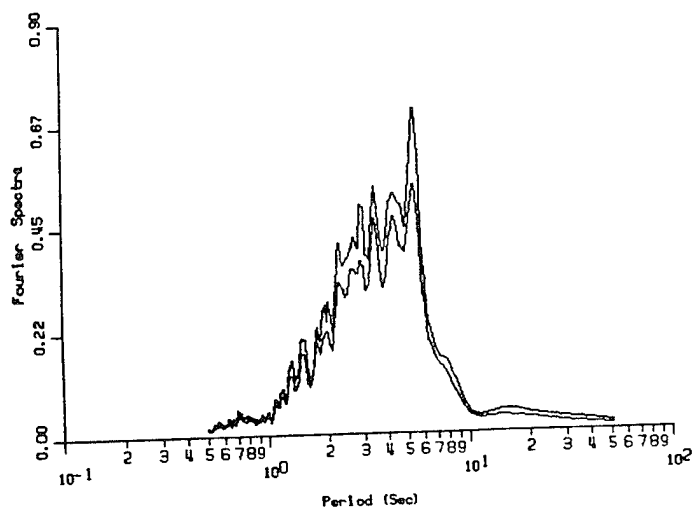
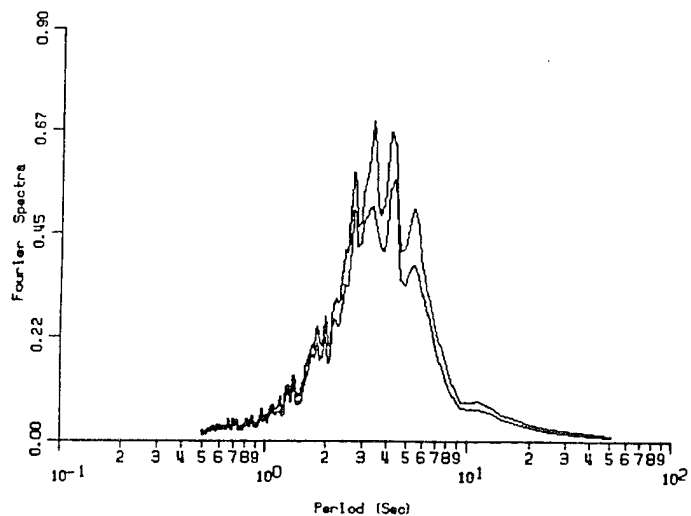
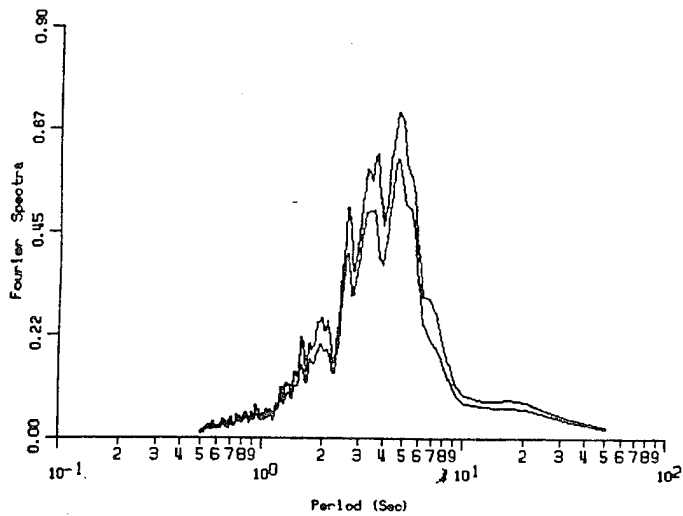


Figure 6.11. Continued

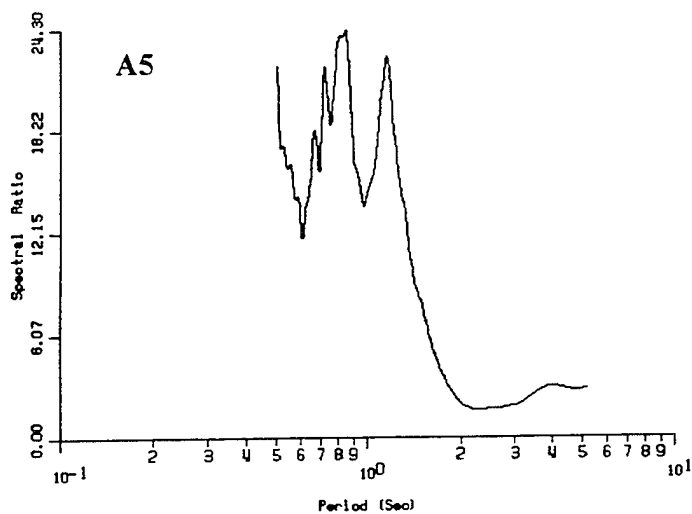
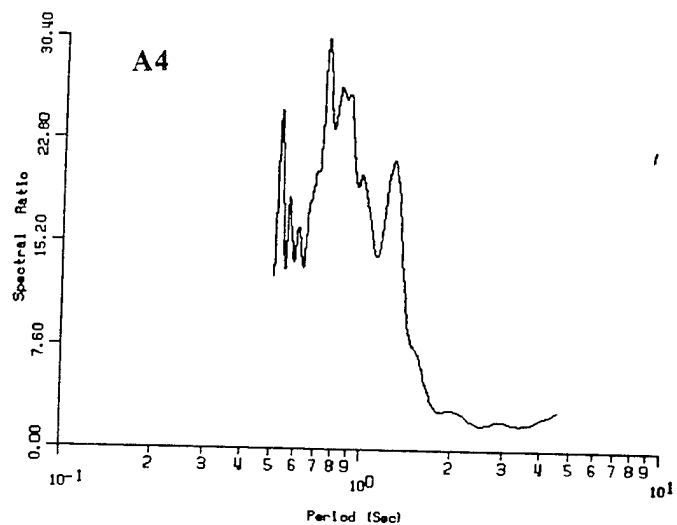
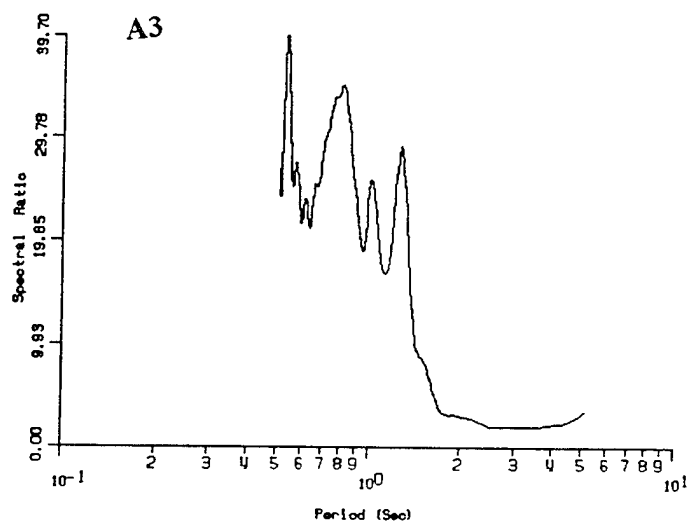
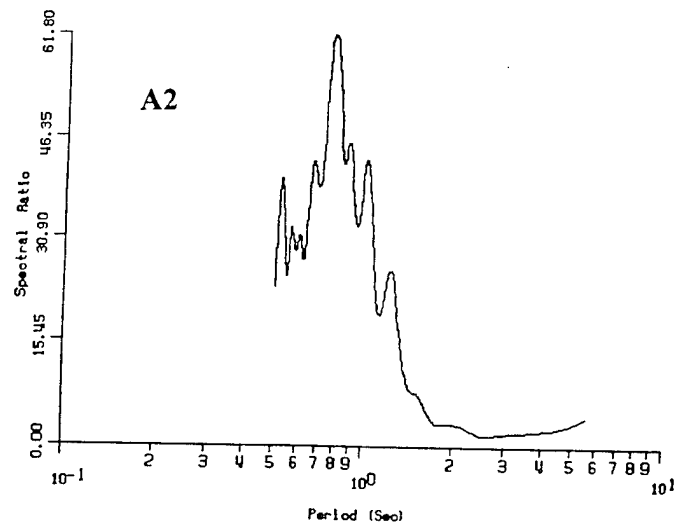
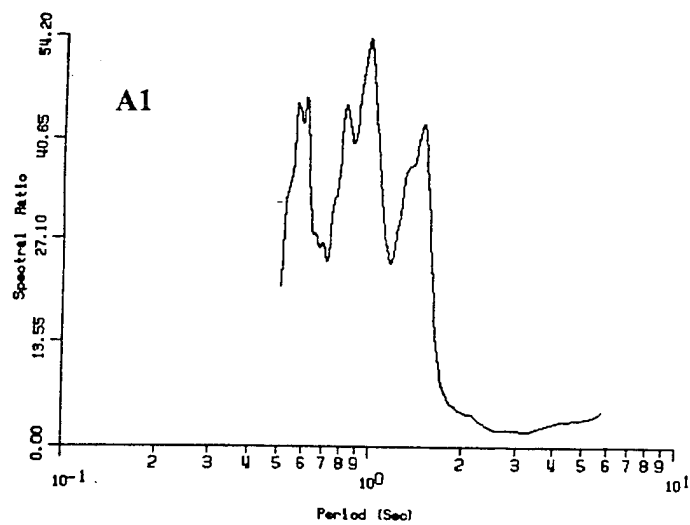
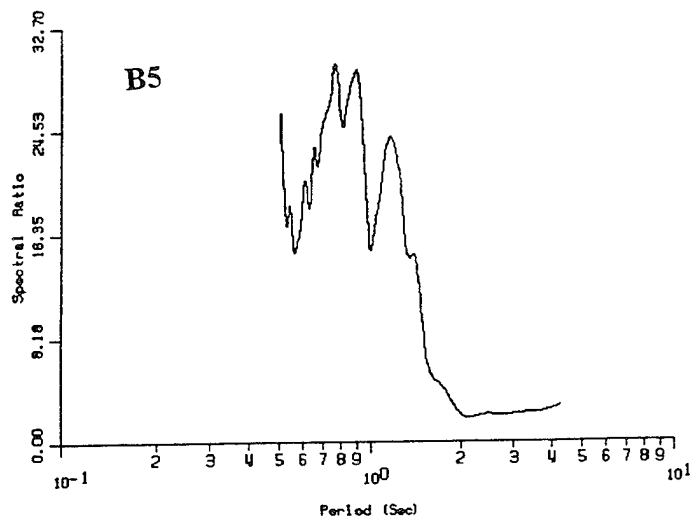
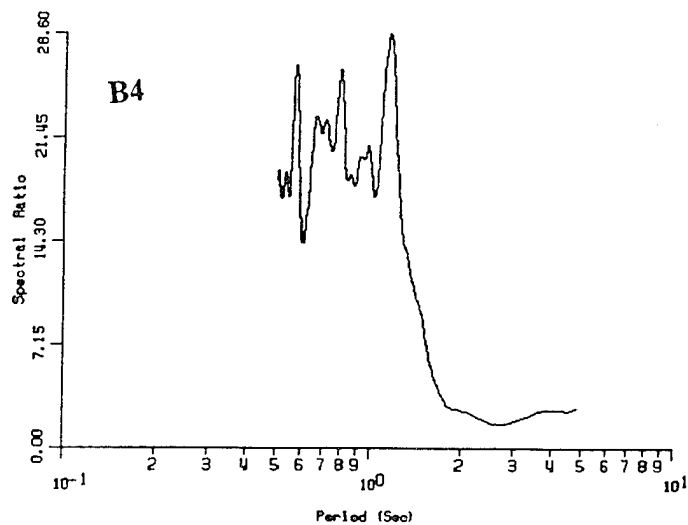
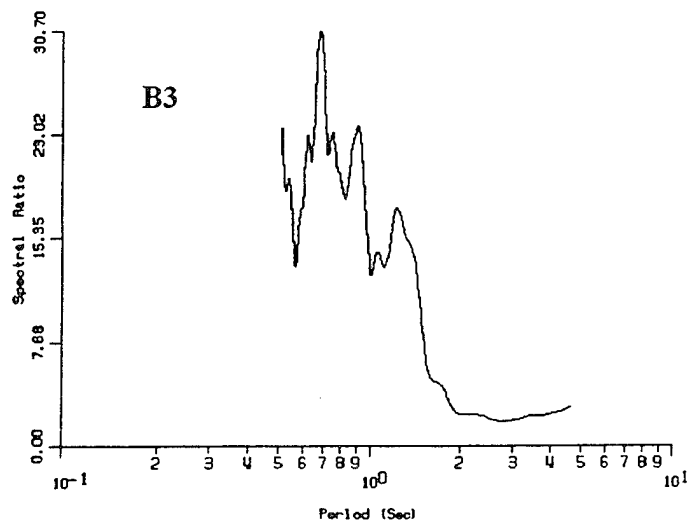
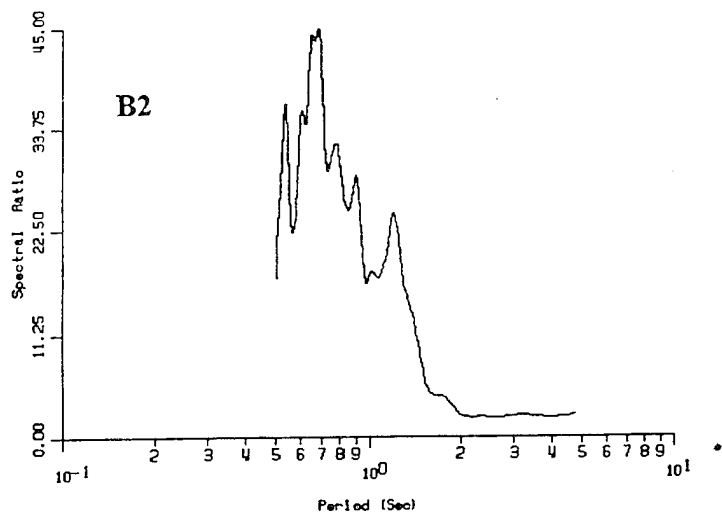
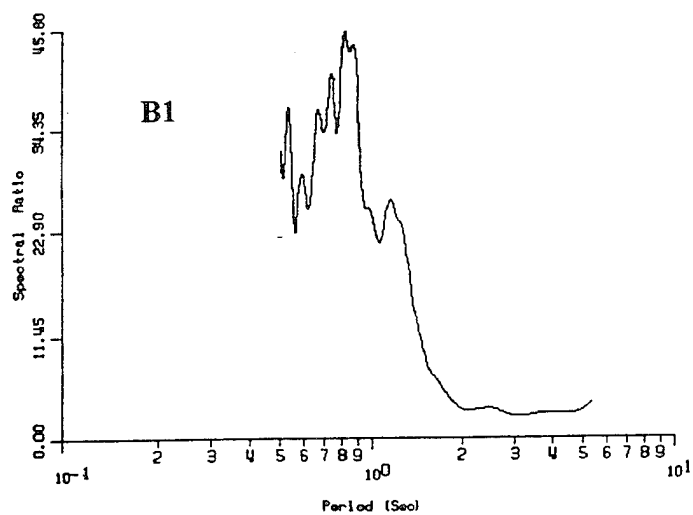
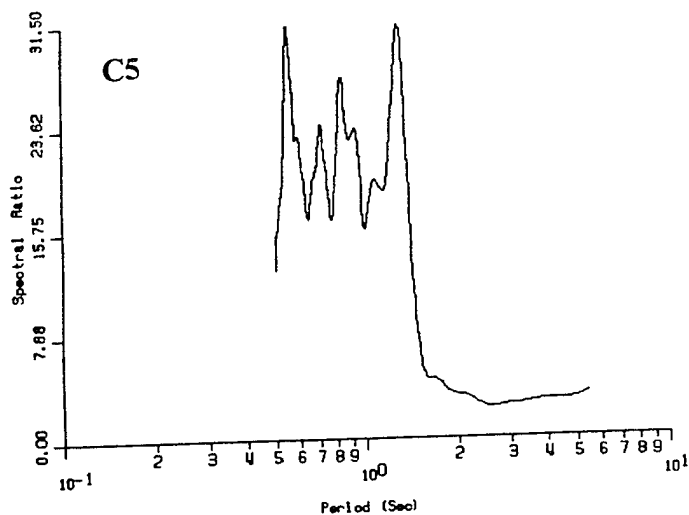
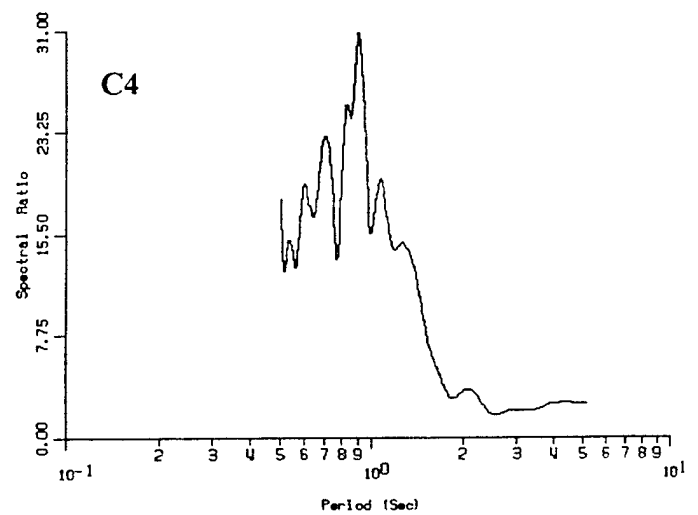
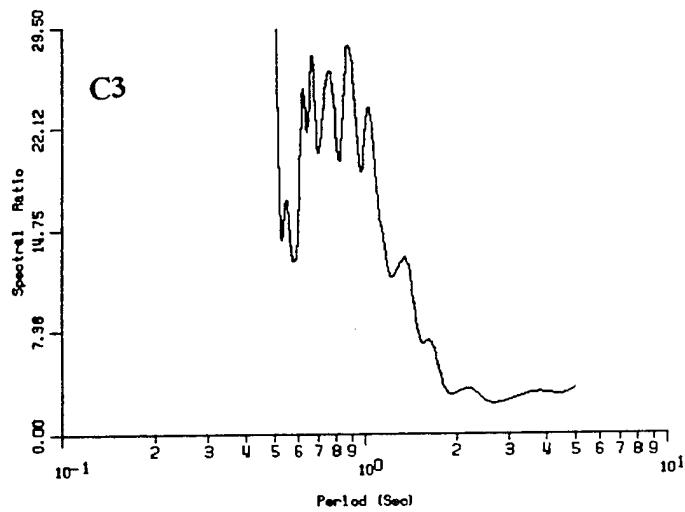
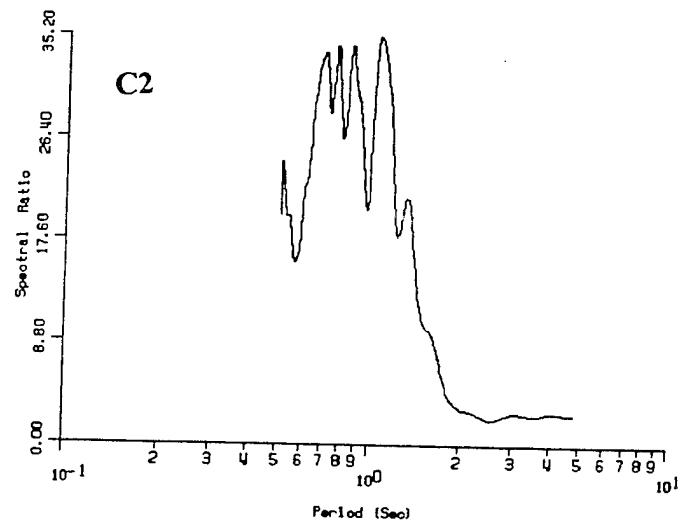
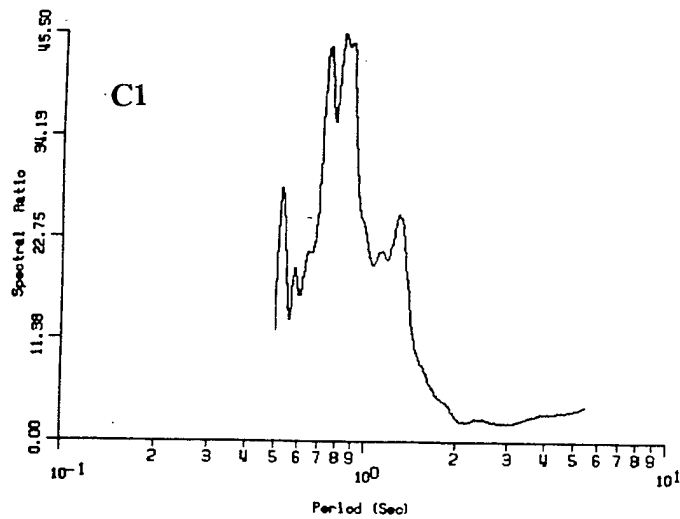


Figure 6.12a. North - South spectral ratio  
for Treasure Island sites along Section A.



**Figure 6.12b. North - South spectral ratio  
for Treasure Island sites along Section B.**



**Figure 6.12c. North - South spectral ratio  
for Treasure Island sites along Section C.**

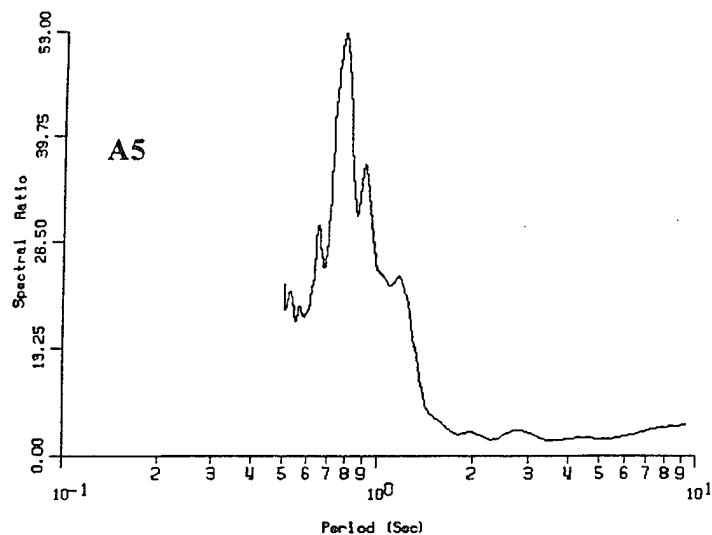
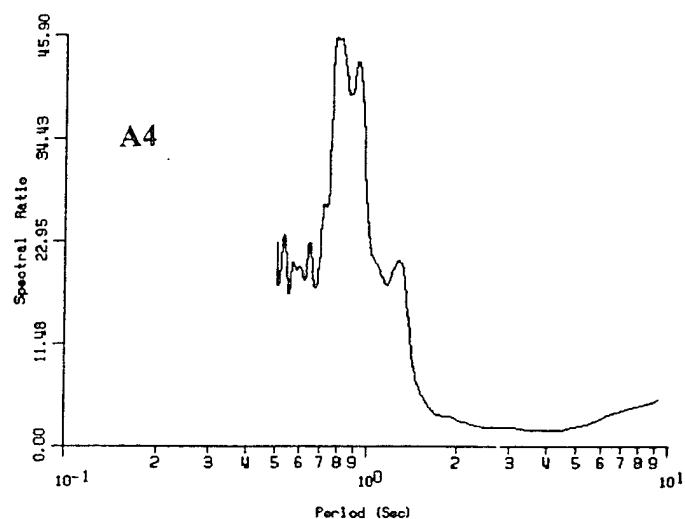
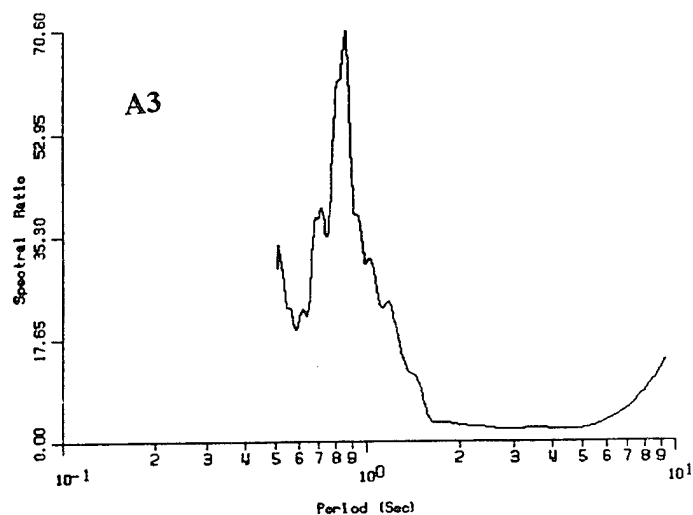
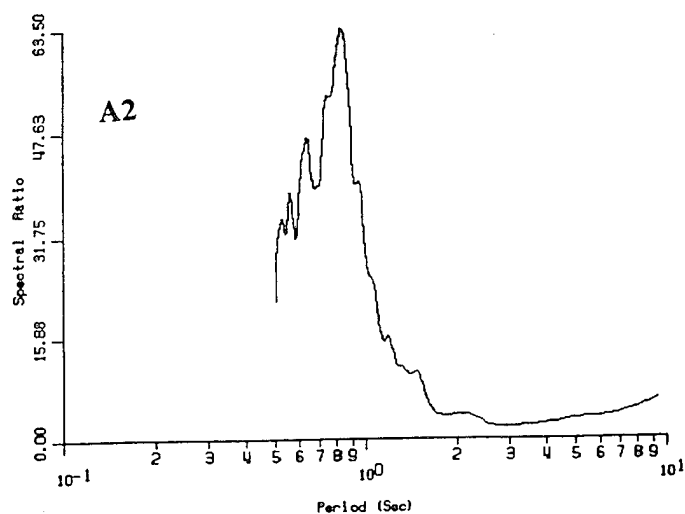
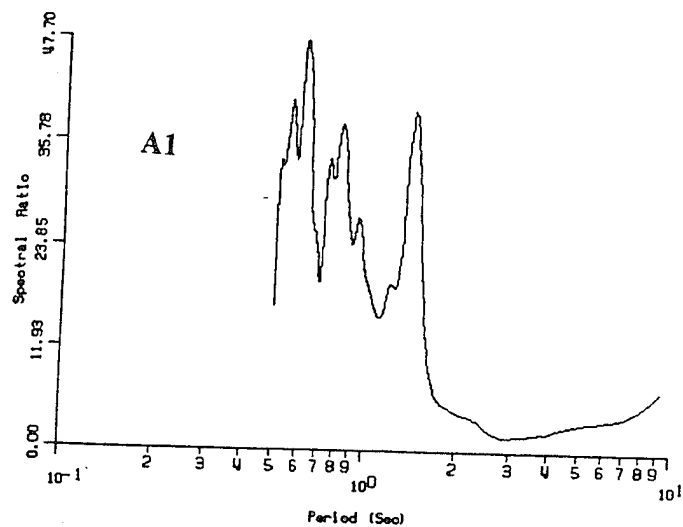
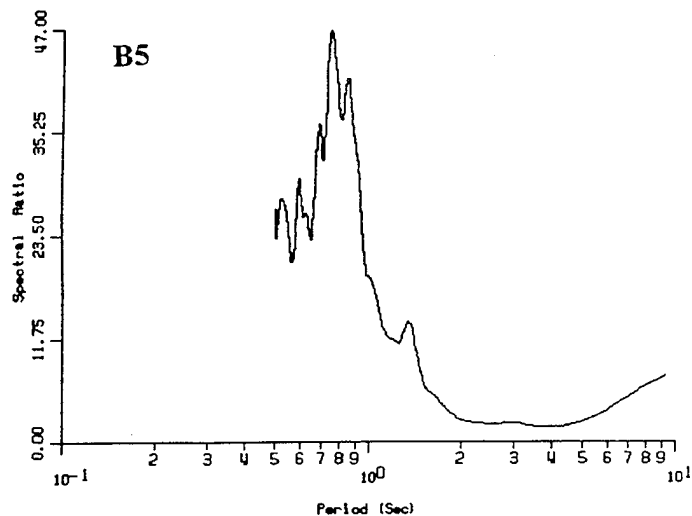
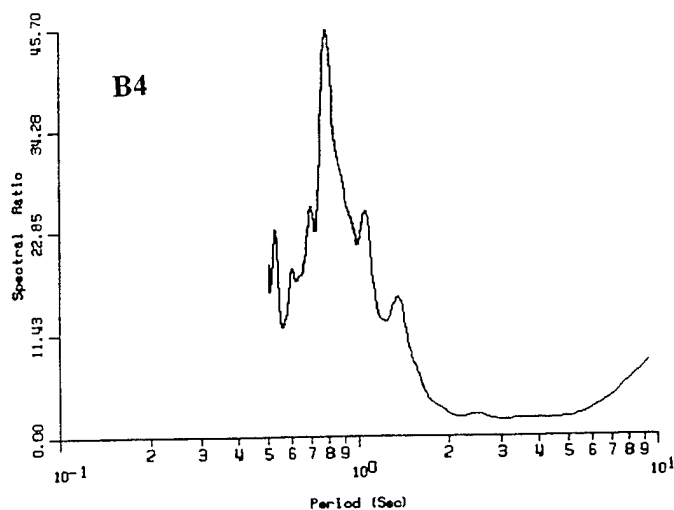
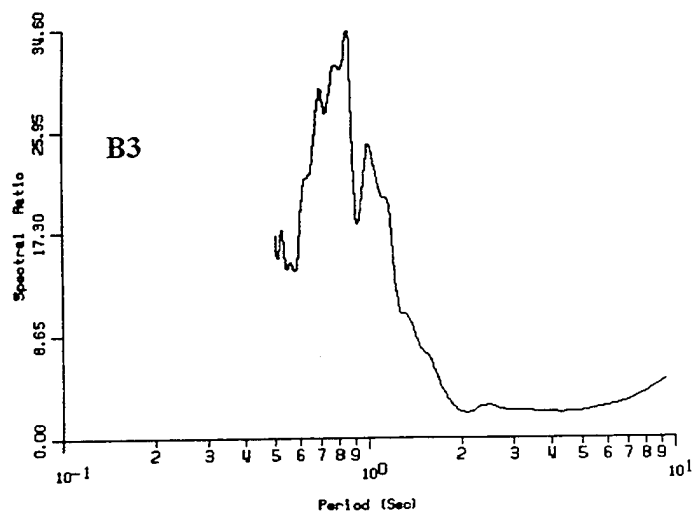
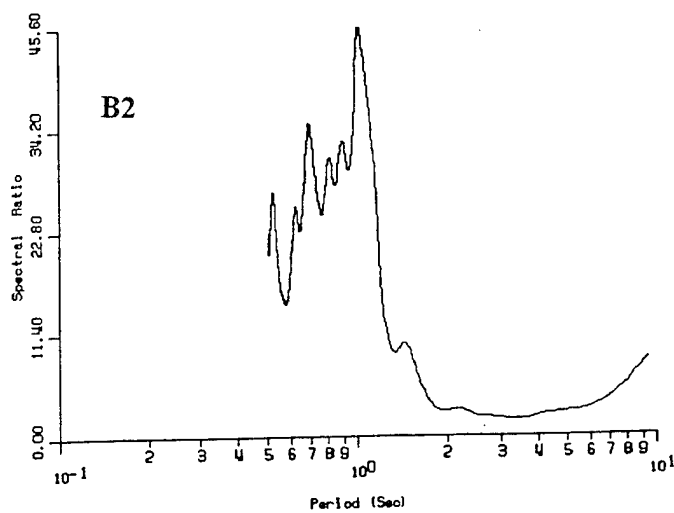
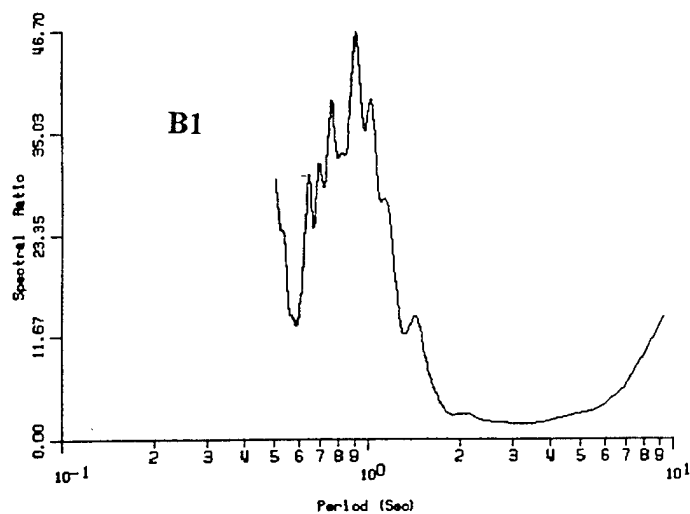
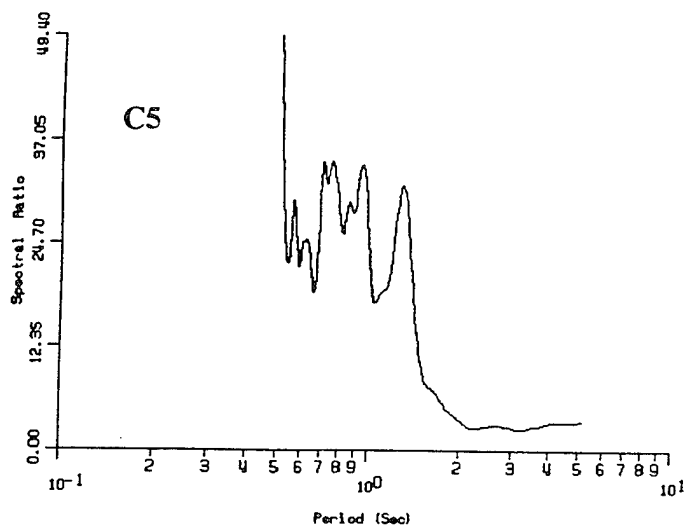
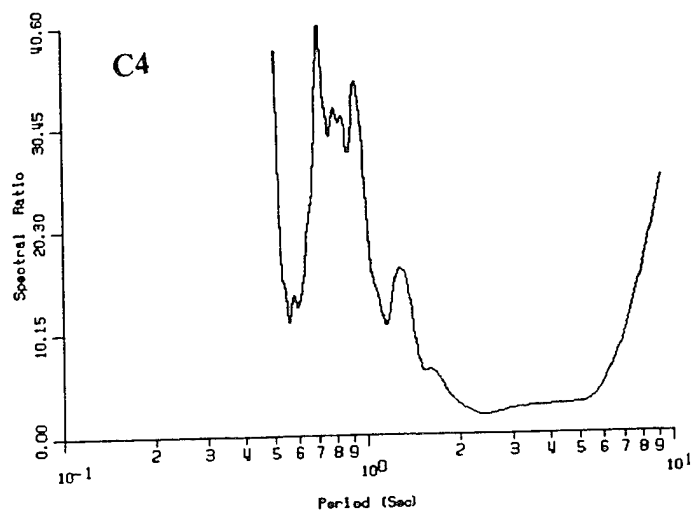
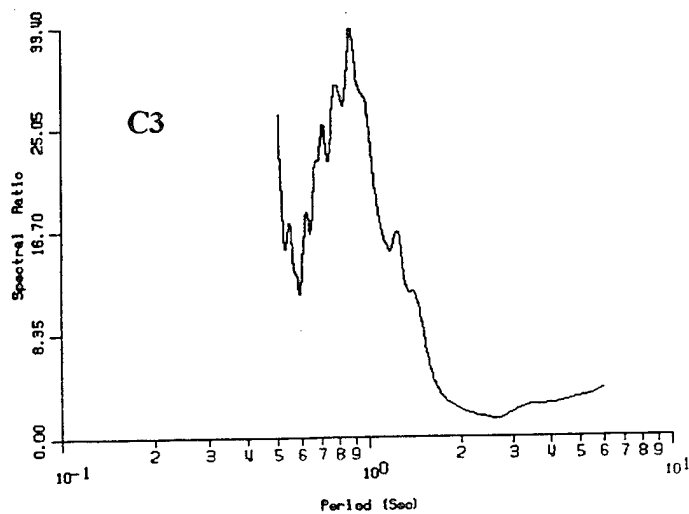
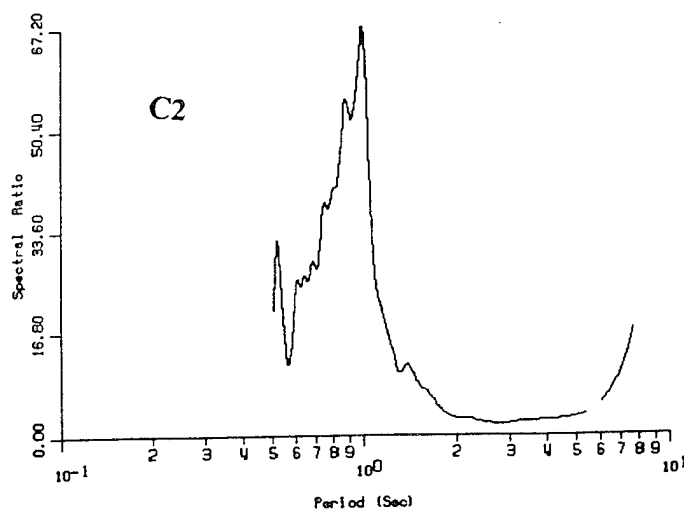
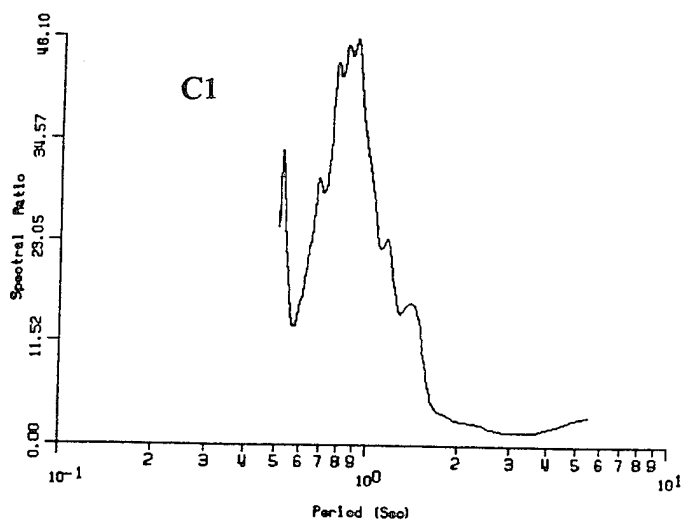


Figure 6.13a. East - West spectral ratio  
for Treasure Island sites along Section A.



**Figure 6.13b. East - West spectral ratio  
for Treasure Island sites along Section B.**



**Figure 6.13c. East - West spectral ratio  
for Treasure Island sites along Section C.**

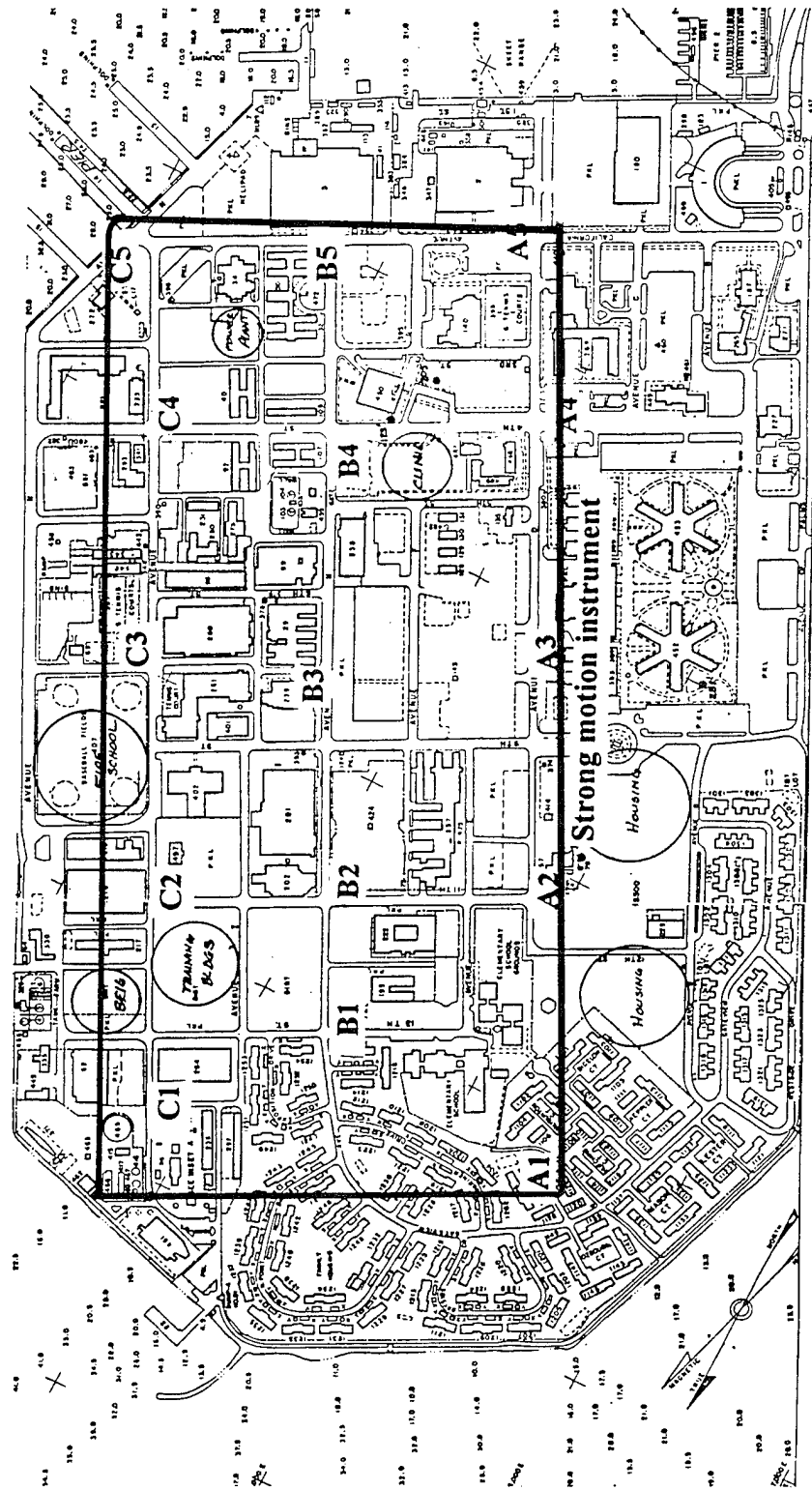


Figure 6.14. Region covered by contours.



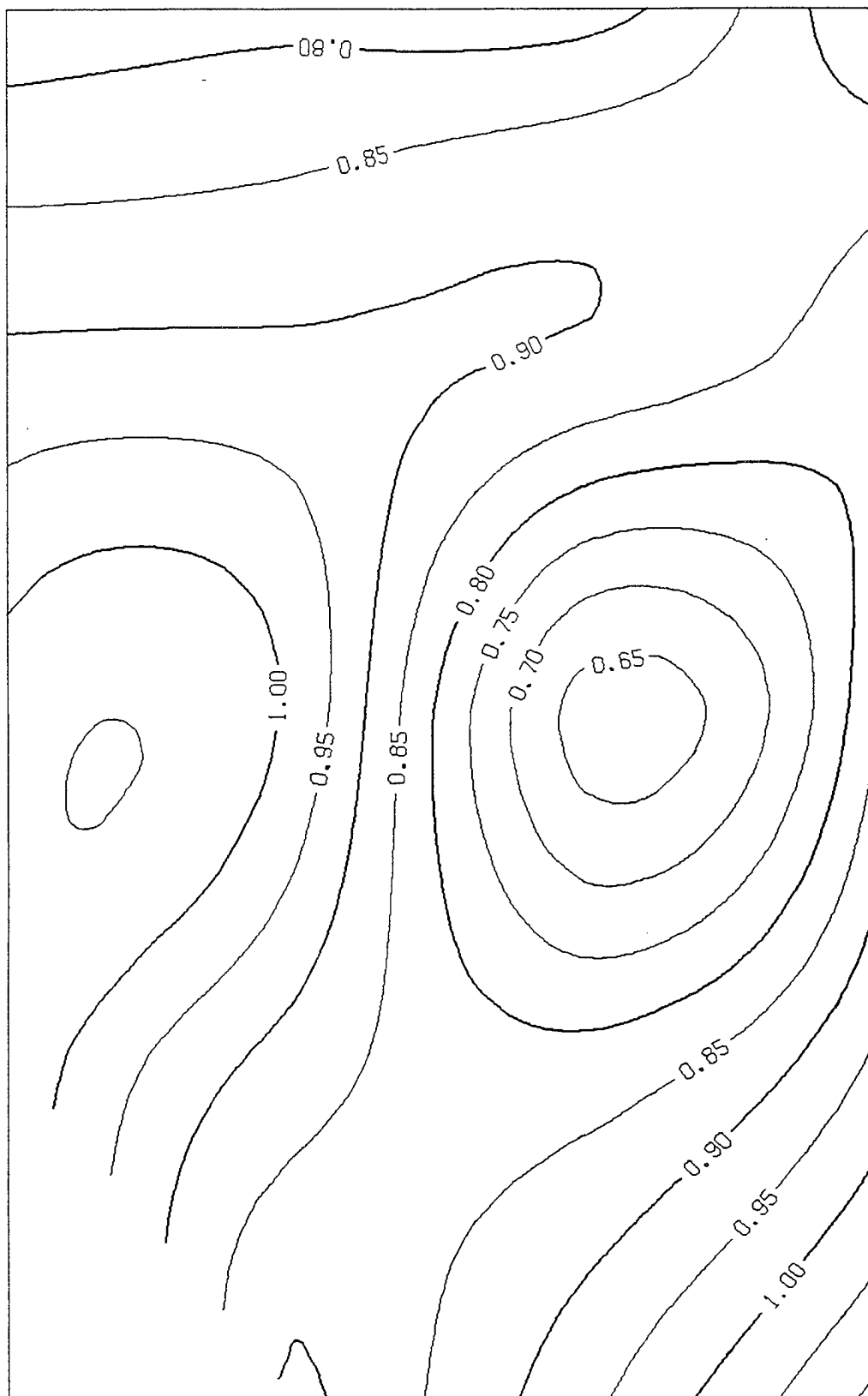


Figure 6.15a Period determined from North-South microseism measurements.

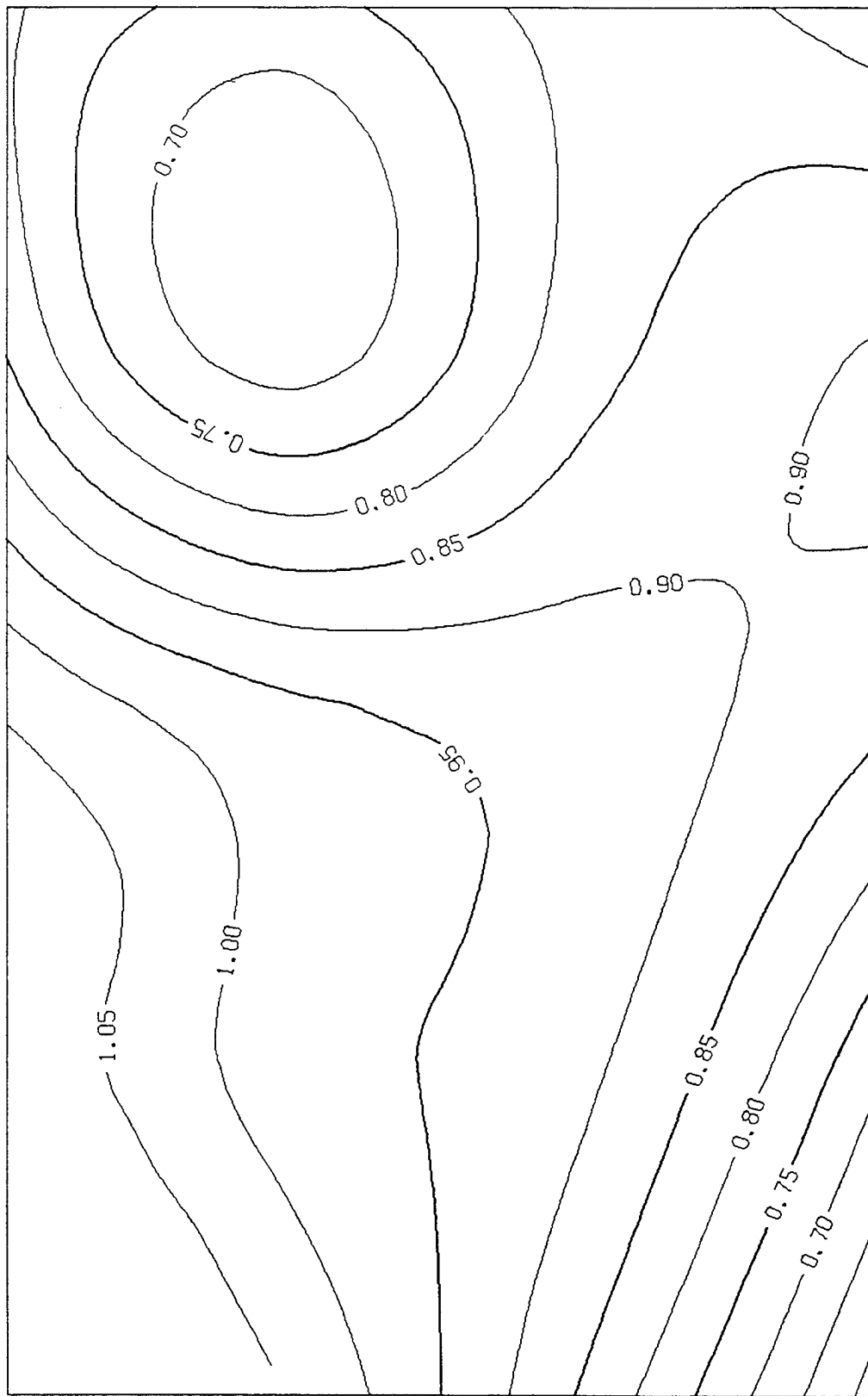


Figure 6.15b Period determined from East-West microseism measurements.

Contours of Peak Spectral Ratio

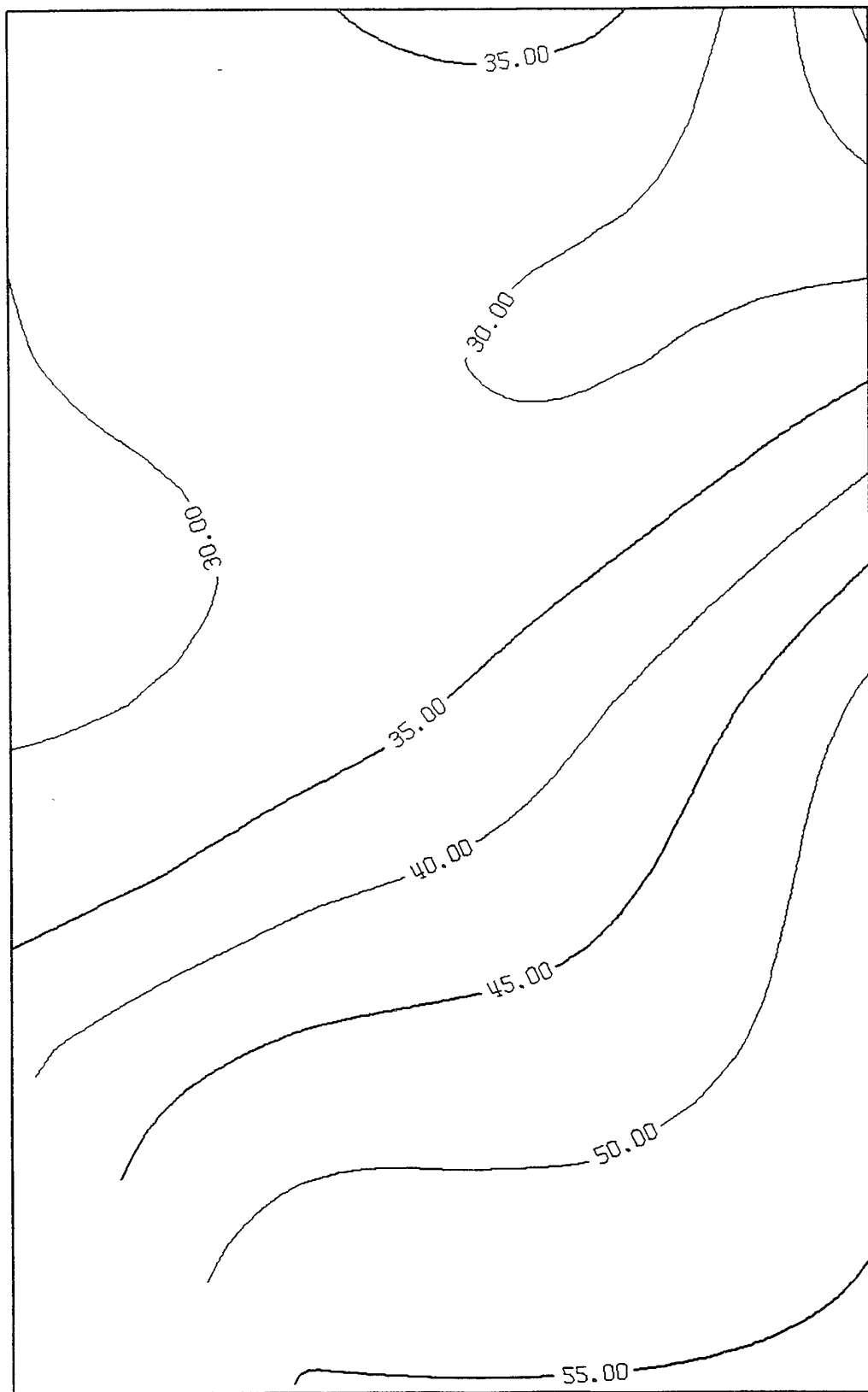
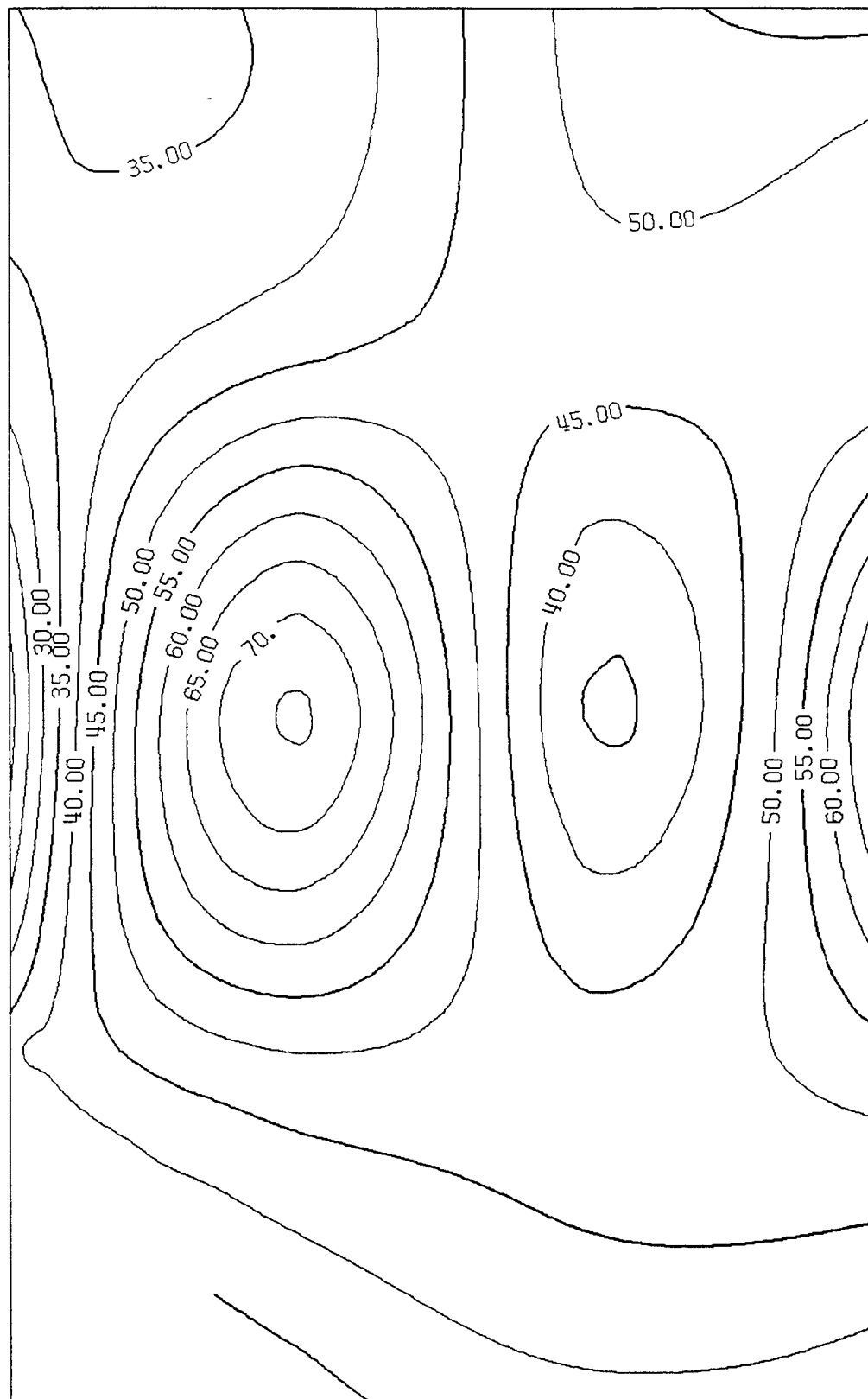


Figure 6.16a. Spectral ratios determined from North-South  
microseism measurements.

**Contours of Peak Spectral Ratio**



**Figure 6.16b. Spectral ratios determined from East-West  
microseism measurements.**

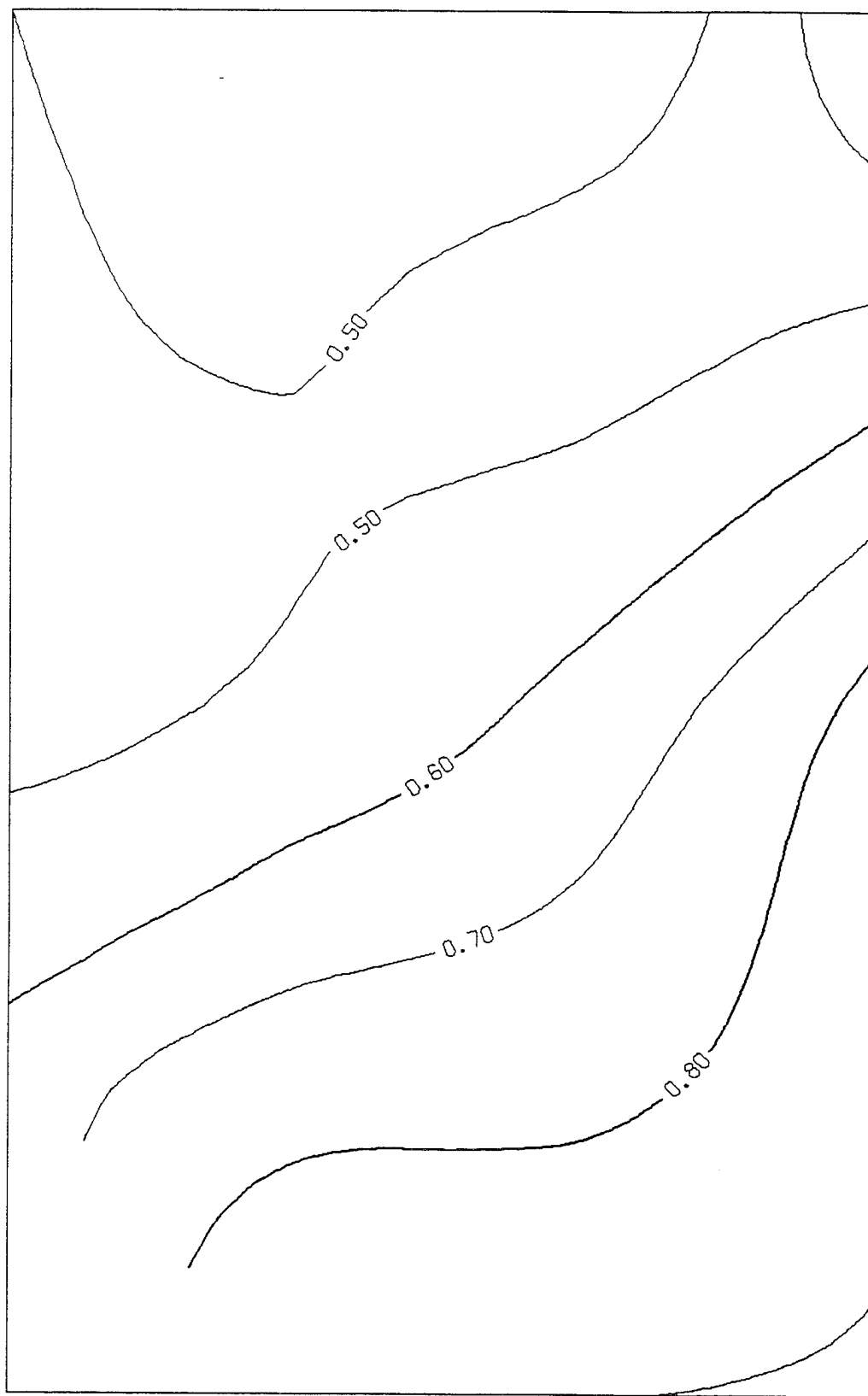


Figure 6.17a. Normalized spectral ratios determined from North-South  
microseism measurements, Station A2  $\approx$  1.

Normalized Contours of Peak Spectral Ratio

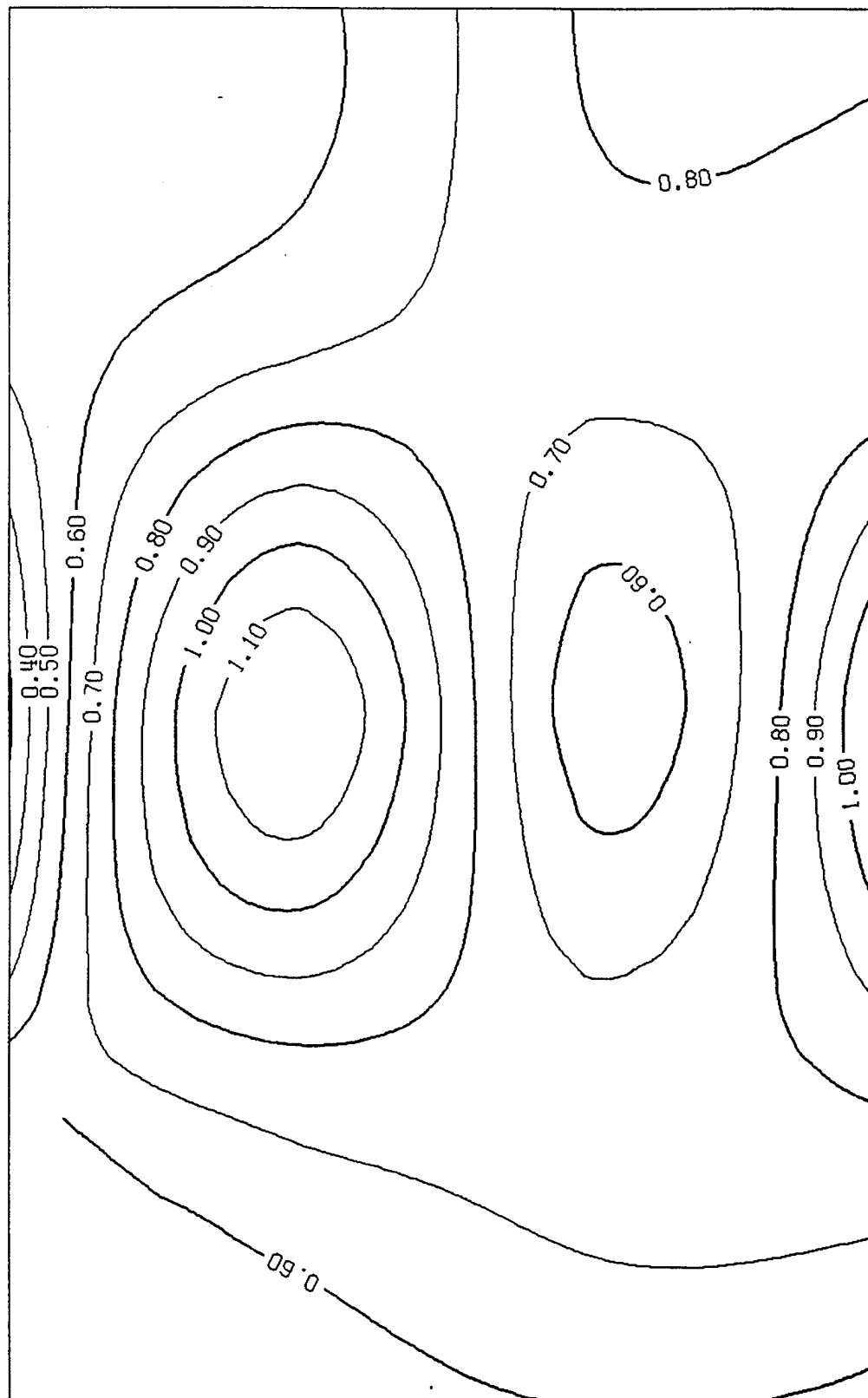
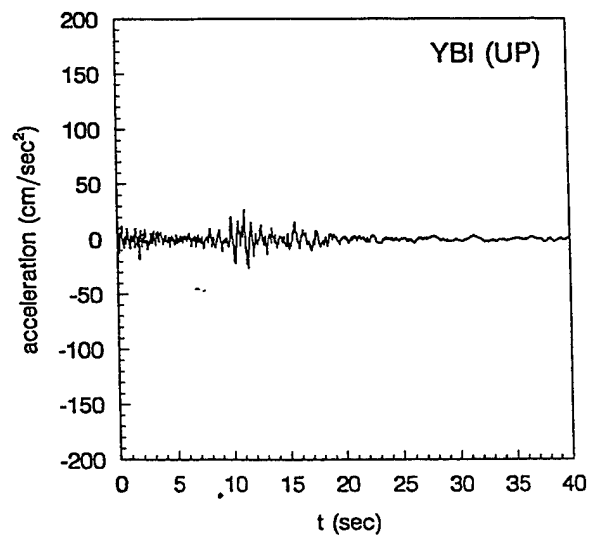
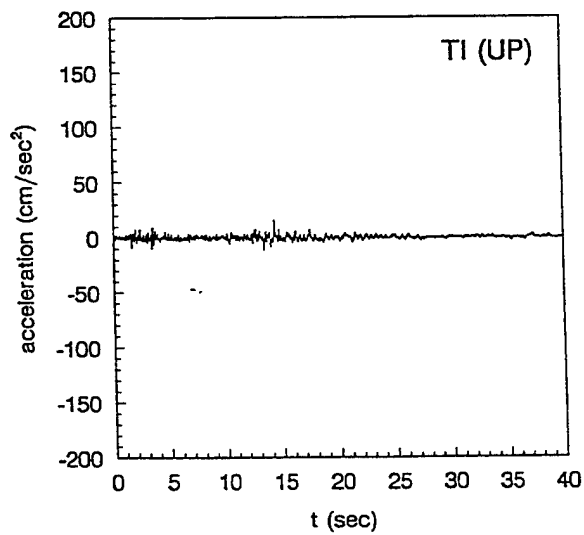
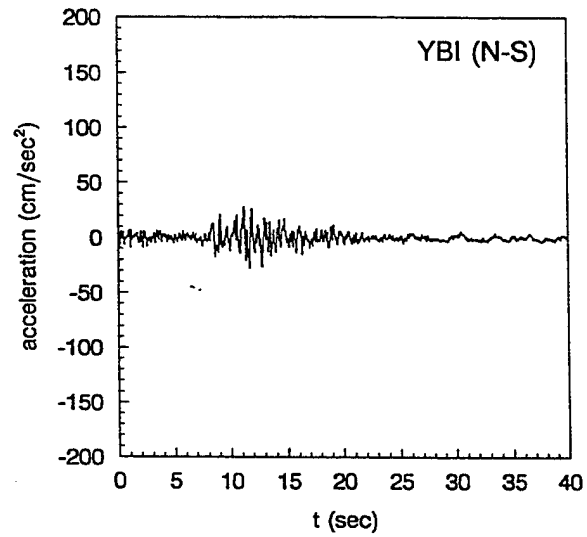
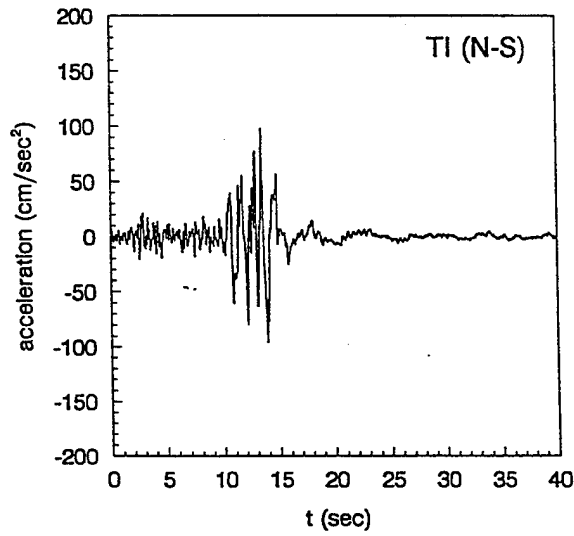
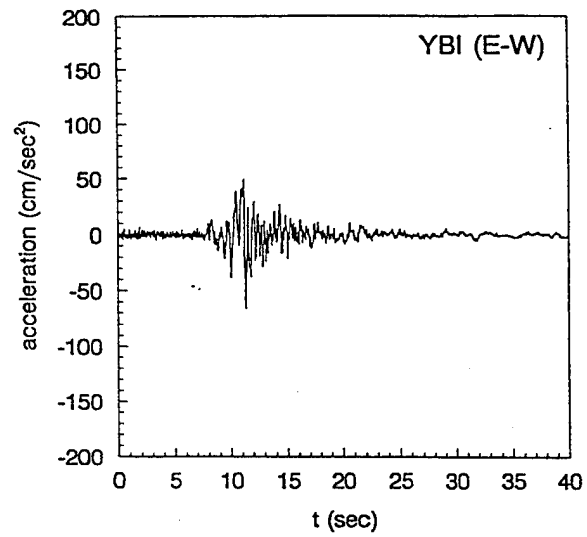
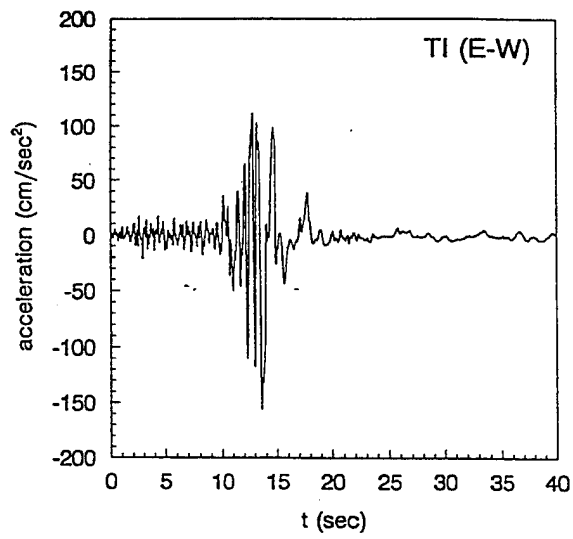
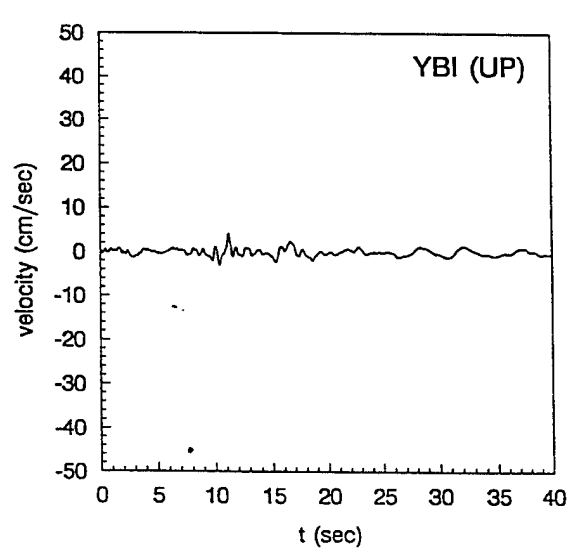
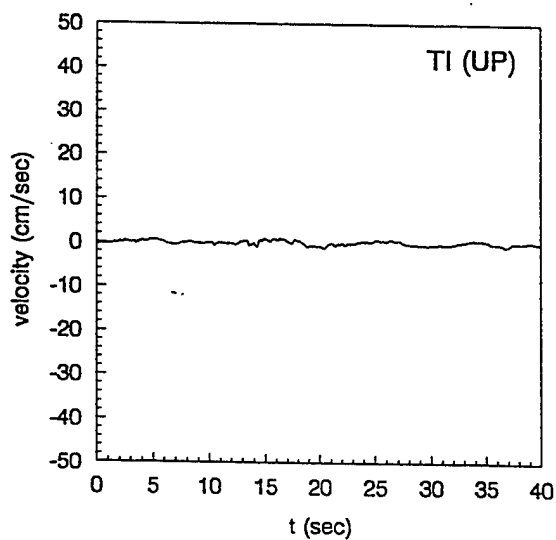
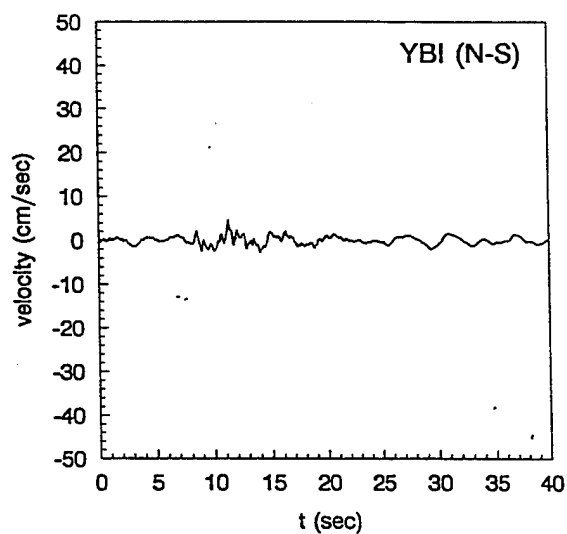
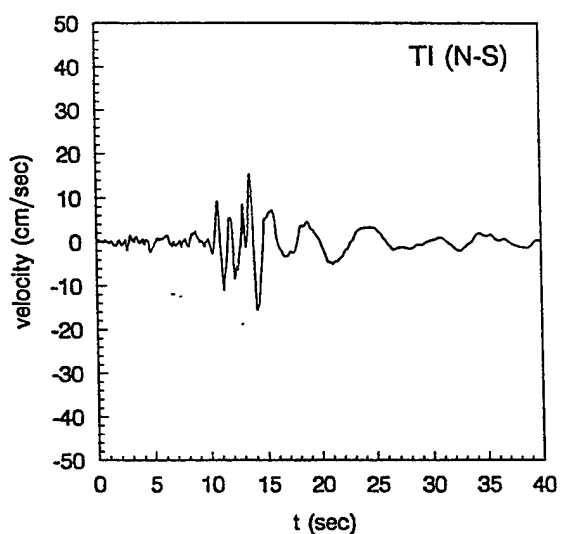
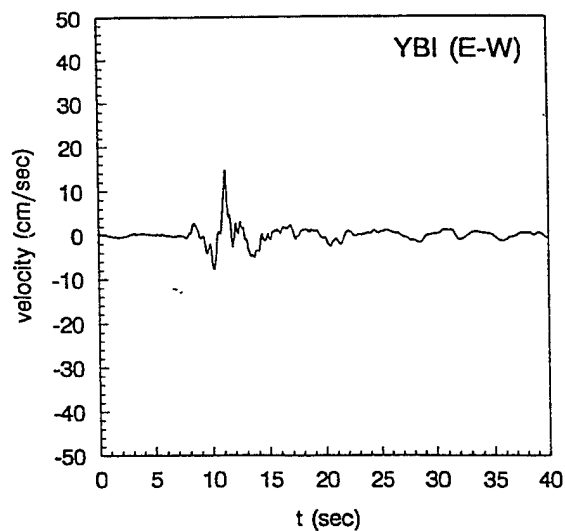
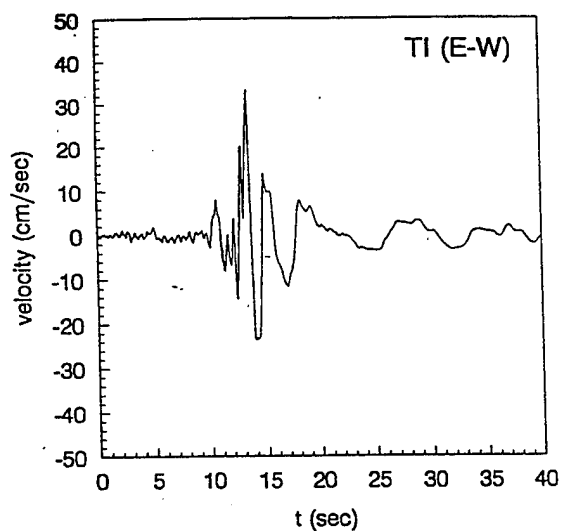


Figure 6.17b. Normalized spectral ratios determined from East-West  
microseism measurements, Station A2 = 1.



**Figure 6.18 Loma Prieta earthquake strong ground motion acceleration components at Treasure Island (TI) and Yerba Buena Island (YBI).**



**Figure 6.19 Loma Prieta earthquake strong ground motion velocity components at Treasure Island (TI) and Yerba Buena Island (YBI).**



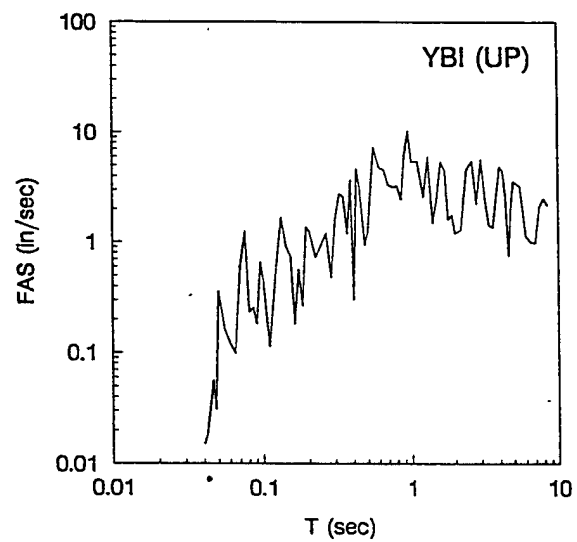
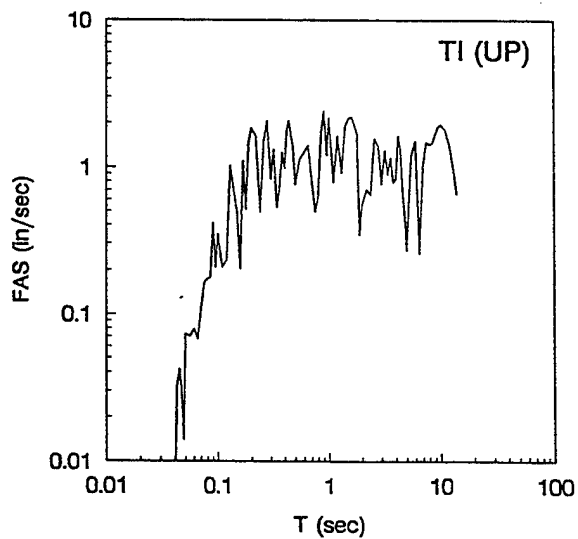
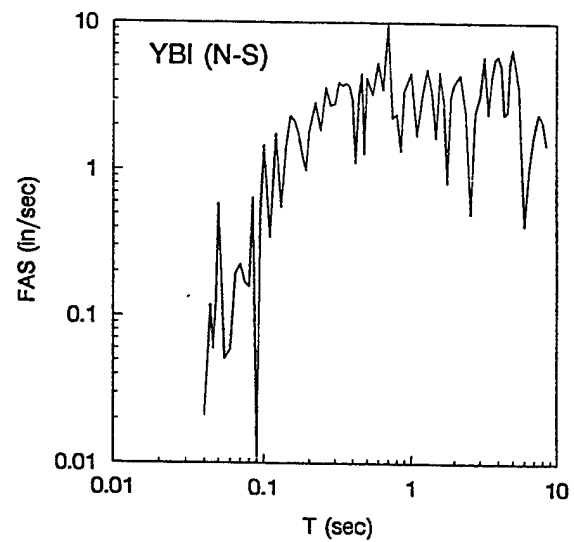
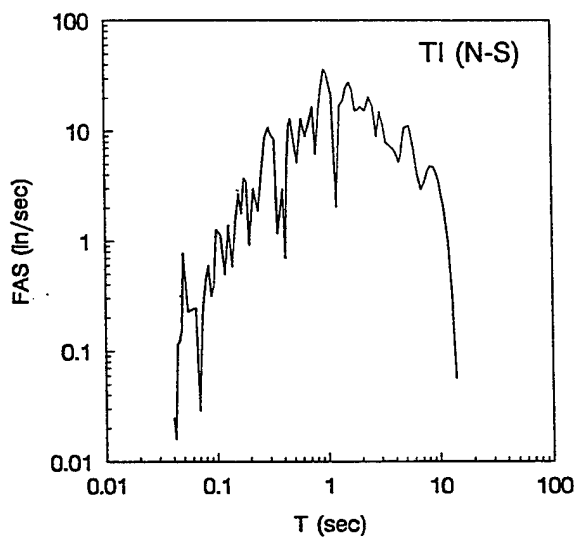
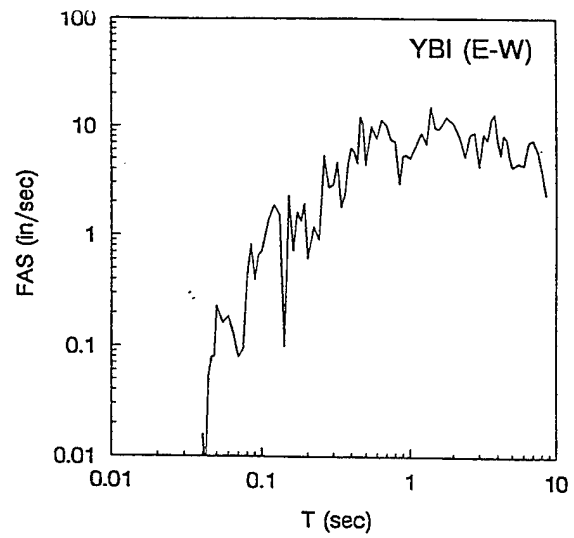
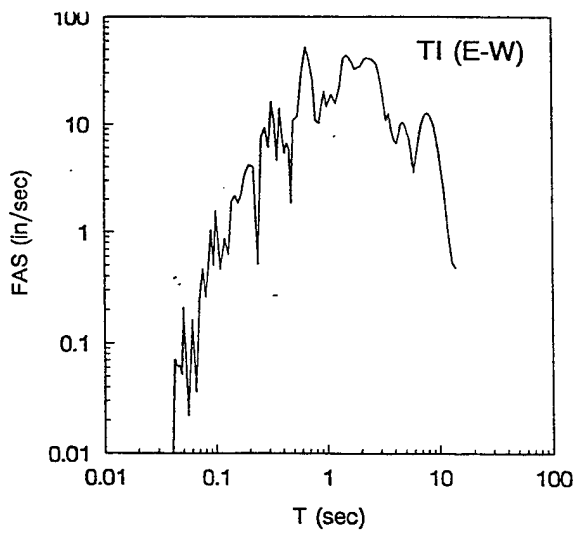


**Figure 6.20 Fourier amplitude acceleration spectra at Treasure Island (TI) and Yerba Buena Island (YBI) strong ground motion records of Loma Prieta earthquake.**

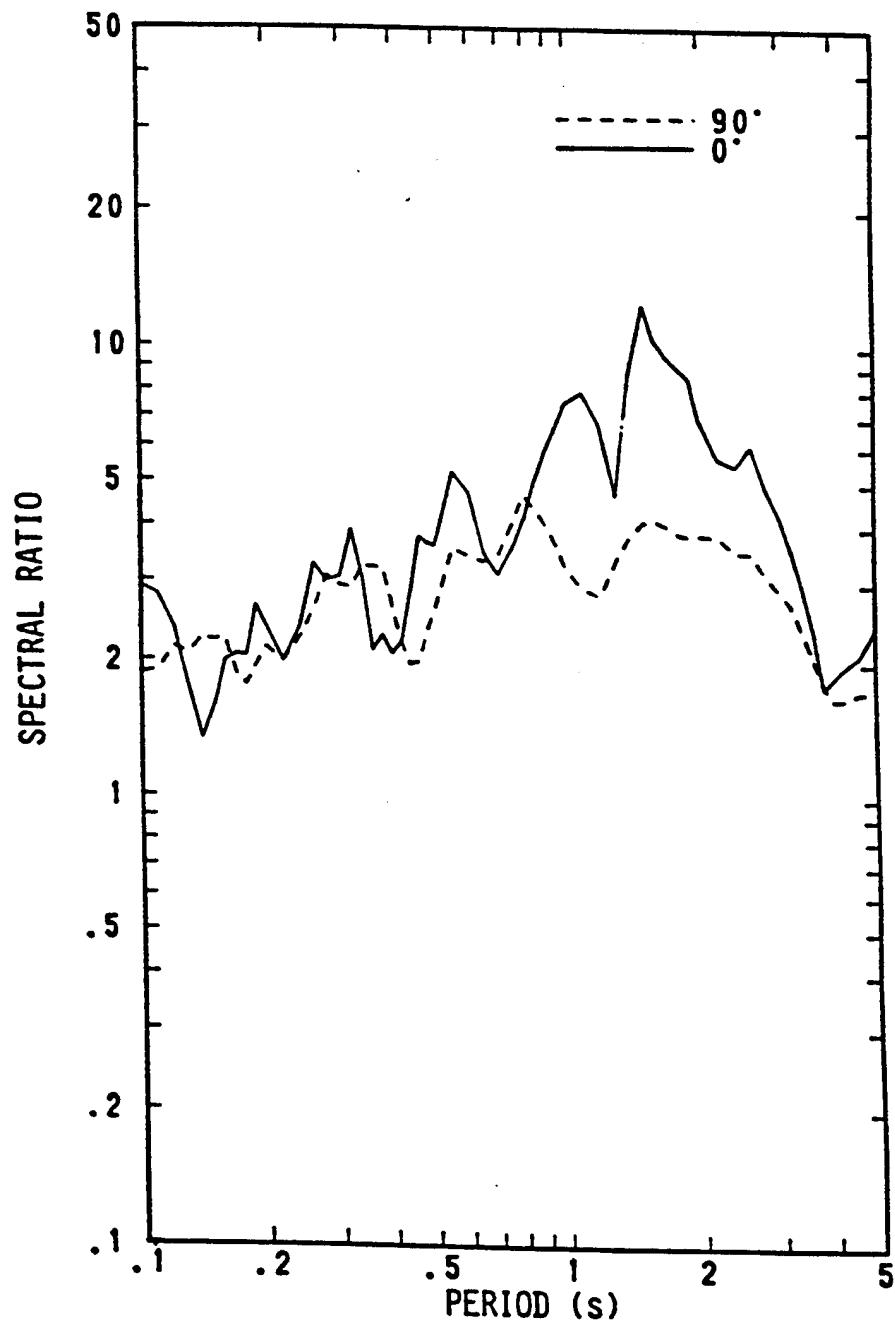


**Figure 6.20. Spectral ratios for components of strong ground motion records at Treasure Island and Yerba Buena Island for Loma Prieta earthquake.**

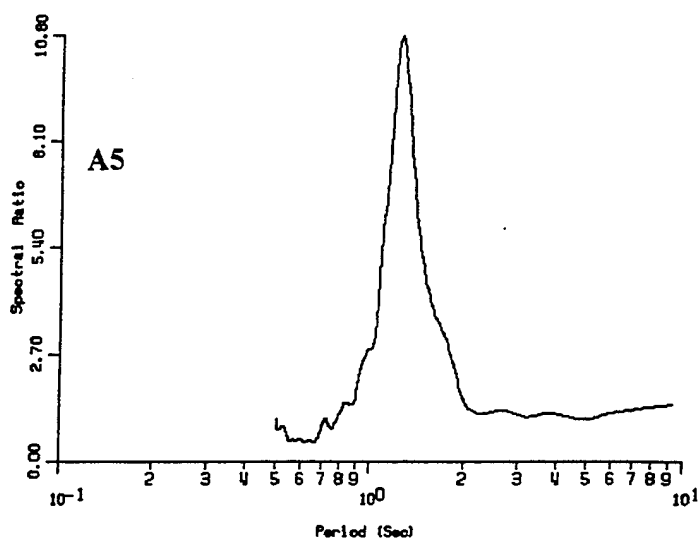
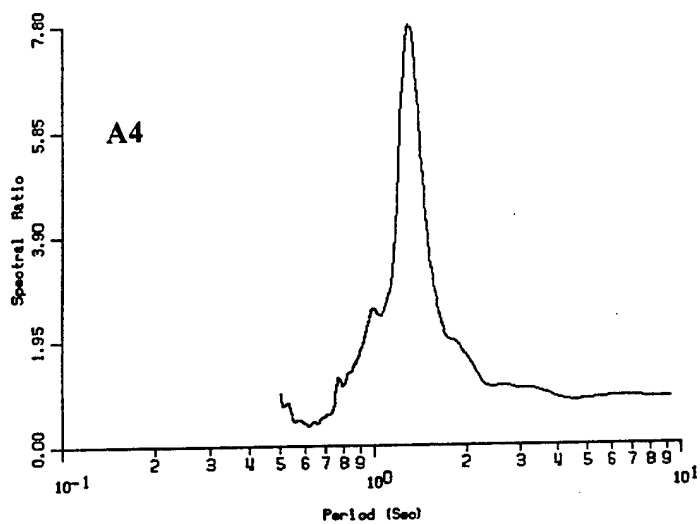
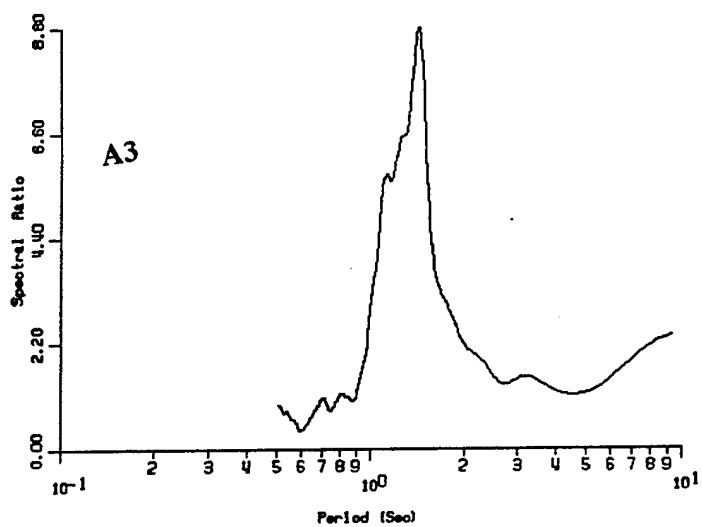
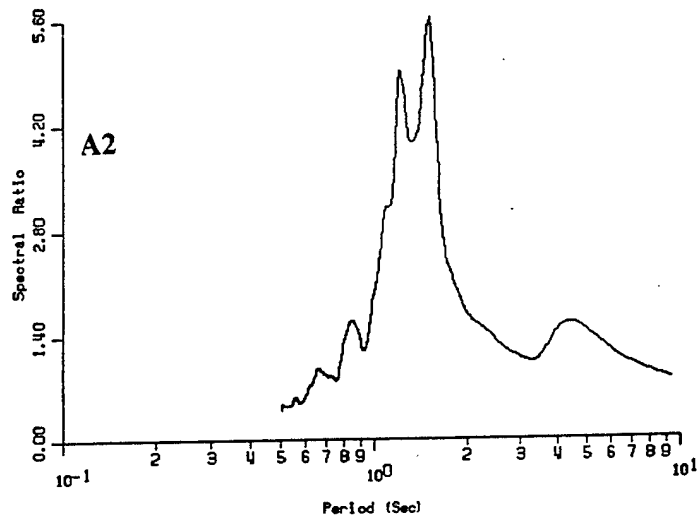
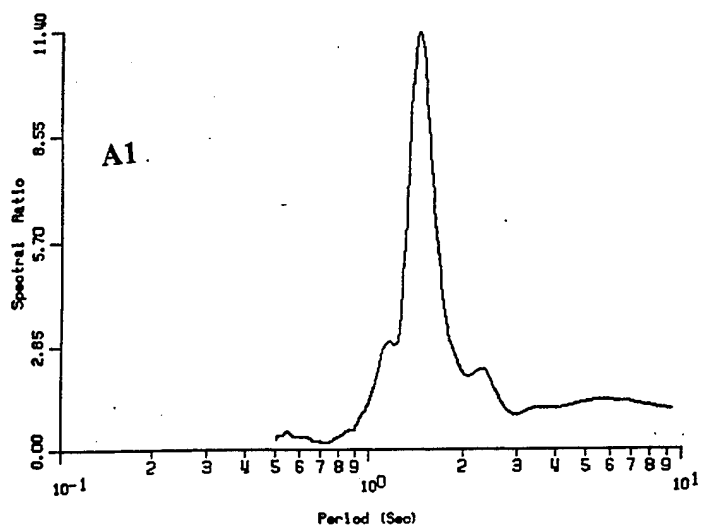


Figure 6.21 Nakamura method using vertical measurement  
East West direction typical.

## **Chapter 7 Investigation of Nonlinear Amplification.**

### **Introduction**

The Port Hueneme site and the Treasure Island site are fairly typical Navy soft sites associated with waterfront construction. Both the Port Hueneme and Treasure Island studies showed that microseism measurements produce high levels of spectral ratio amplification. These levels are much higher than would be expected during the strong ground motion shaking associated with a large earthquake. It is of major importance to the understanding of microseism usage that the phenomenon of high amplification be explored. There appears to be an inverse relationship between amplification and level of excitation.

### **Earthquake Data Treasure Island**

Data was compiled in an attempt to develop a trend to amplification at soft sites. Darragh and Shakal (1991) report data for Treasure Island and Figure 7.1 shows peak spectral ratios for the Treasure Island / Yerba Buena site pairs for the Loma Prieta earthquake and a number of aftershocks. Note that the Yerba Buena site serves as a rock reference site for the soft soil site at Treasure Island and the Y axis reflects the peak rock velocity at the reference site. Also plotted on Figure 7.1 is the microseism data discussed in Chapter 6. Note that the microseism data points are an extension of the strong motion data establishing a clear trend.

### **Earthquake Data Gilroy**

Darragh and Shakal (1991) also report data for Gilroy and Figure 7.2 shows peak spectral ratios for the Gilroy #2 / Gilroy #1 site pairs for the Loma Prieta, Morgan Hill and Coyote Lake earthquakes. As part of this research, microseism measurements were made at the Gilroy sites and the microseism spectral ratios are given in Figure 7.3 and also plotted on Figure 7.2. Gilroy #1 is a rock site and Gilroy #2 is an alluvium site whose profile and shear wave velocity is given in Figure 7.4 according to Gibbs (1992). The microseism data when taken in conjunction with data shown Figure 7.1 confirm the trend shown.

### **Earthquake Data Coalinga**

Borcherdt (1983) presents acceleration data for the Coalinga earthquake of 1983 and 18 aftershocks. The data is presented in terms of acceleration ratio of soil to rock sites rather than as spectral ratio as presented above. However the data is shown in Figure 7.5 to confirm the trend that as the peak rock velocity decreases an increase in amplification is seen on alluvial sites.

## **Discussion**

The data presented in this chapter is intended to demonstrate the inverse relationship between spectra amplification and peak rock velocity. Microseism measurements seem to be a clear extension of the data trend. The relationship supports the premise of strain dependent material properties such that as the strain levels increase an increase in damping and reduction in shear modulus is observed. Sugito (1991) presents a relationship for velocity amplification in terms of a beta factor which is a function of the site shear wave velocity and depth to bedrock. The microseism data noted here confirms this general trend. Additional microseism data is required to extend his relationship to the microseism level of velocity. The Sugito approach does however provide a framework to extend the range of a possible relationship to include both strong motion and microseisms.

## References

- Borcherdt, R. D. et. al. (1983) "Effects of local geologic conditions on strong-ground motions in the vicinity of Coalinga, California." USGS Open File Report 83-845  
Workshop on Site Effects of Soil and Rock on Ground Motion and the Implications for Earthquake-Resistant Design, July 1983
- Darragh, R.B., and Shakal, A.F. (1991) "The site response of two rock and soil stations pairs to strong and weak ground motion", Bulletin Seismological Society America, 1885-1899
- Gibbs J et. al. (1992) USGS Open File Report 92-287 "Seismic velocities and geologic logs from borehole measurements at seven strong motion stations that recorded the 1989 Loma Prieta Earthquake", Menlo Park California 1992
- Sugito M et al (1991) "Nonlinear ground motion amplification factors based on local soil parameters" Proceedings Fourth International Conference on Seismic Microzonation, Stanford California

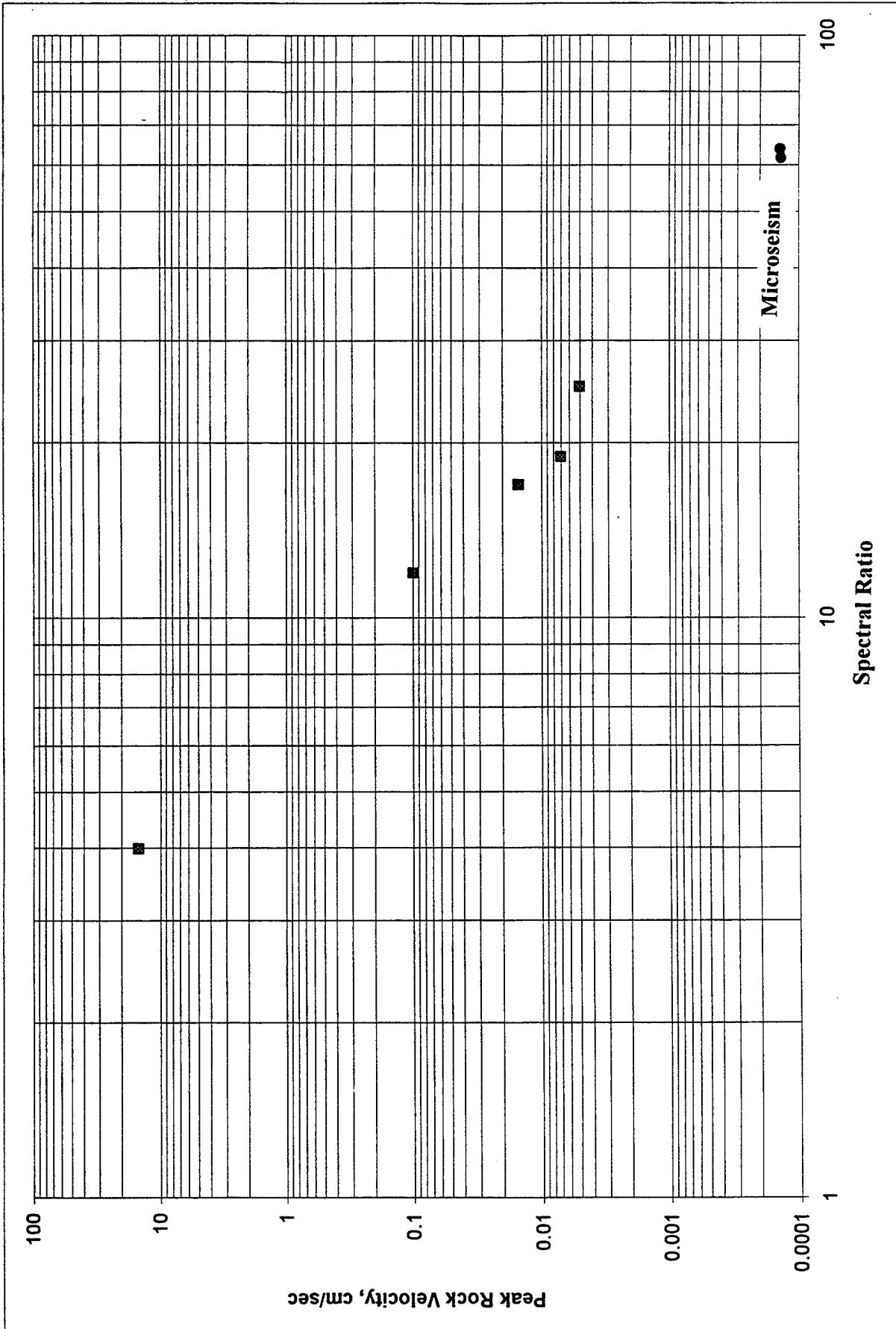


Figure 7.1. Spectral ratio for Treasure Island/Yerba Buena pairs

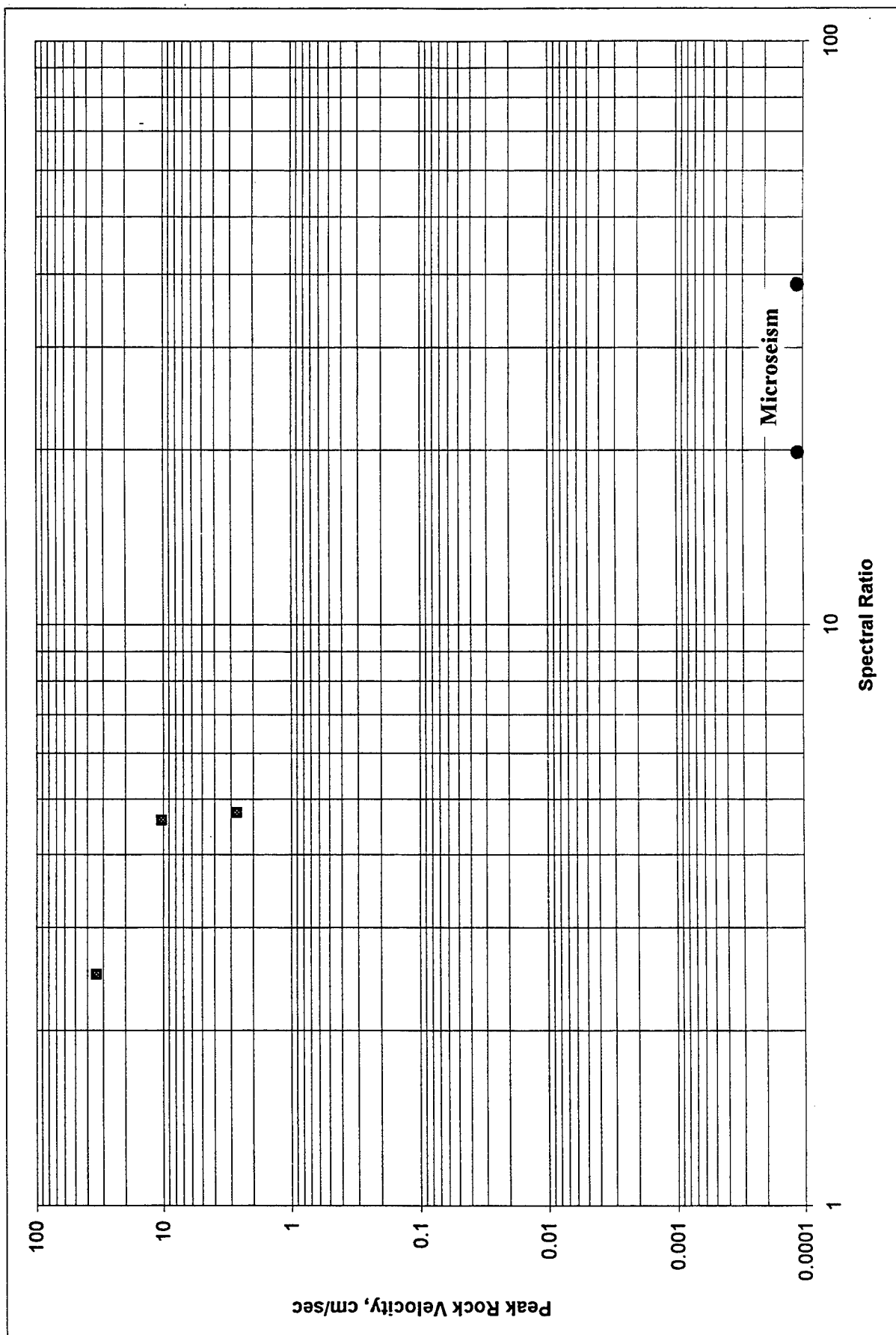


Figure 7.2. Spectral ratio for Gilroy #2/Gilroy#1 pairs



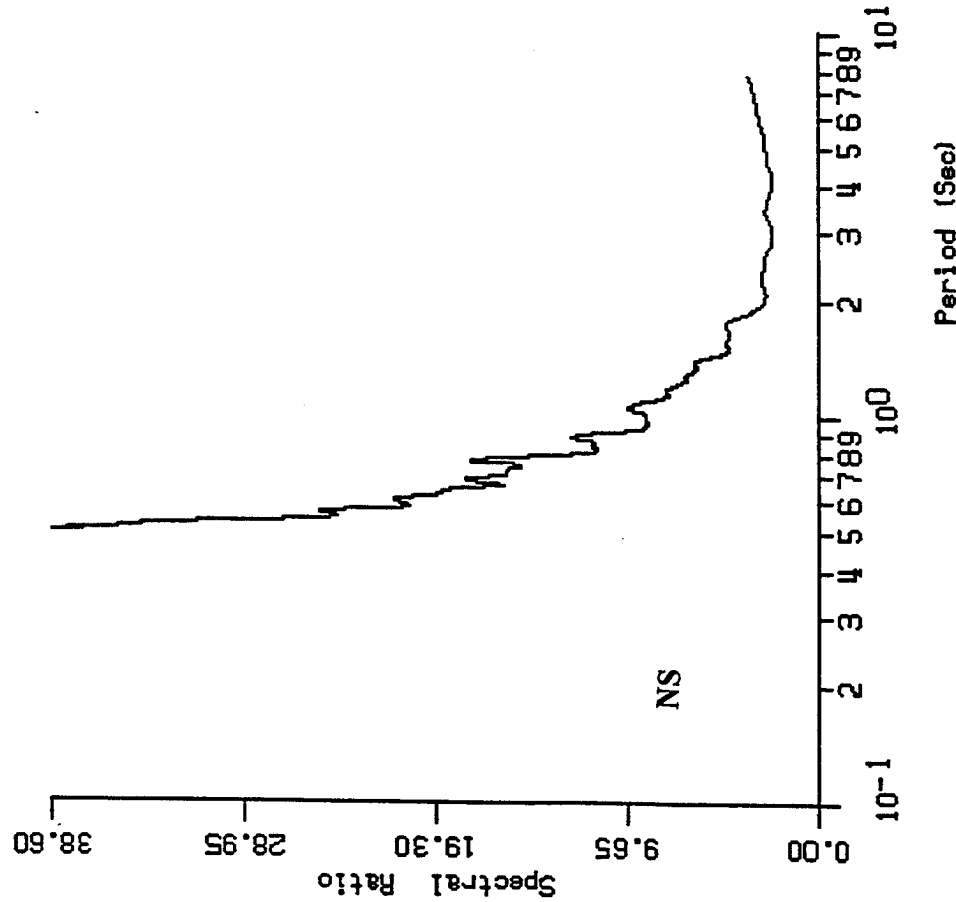
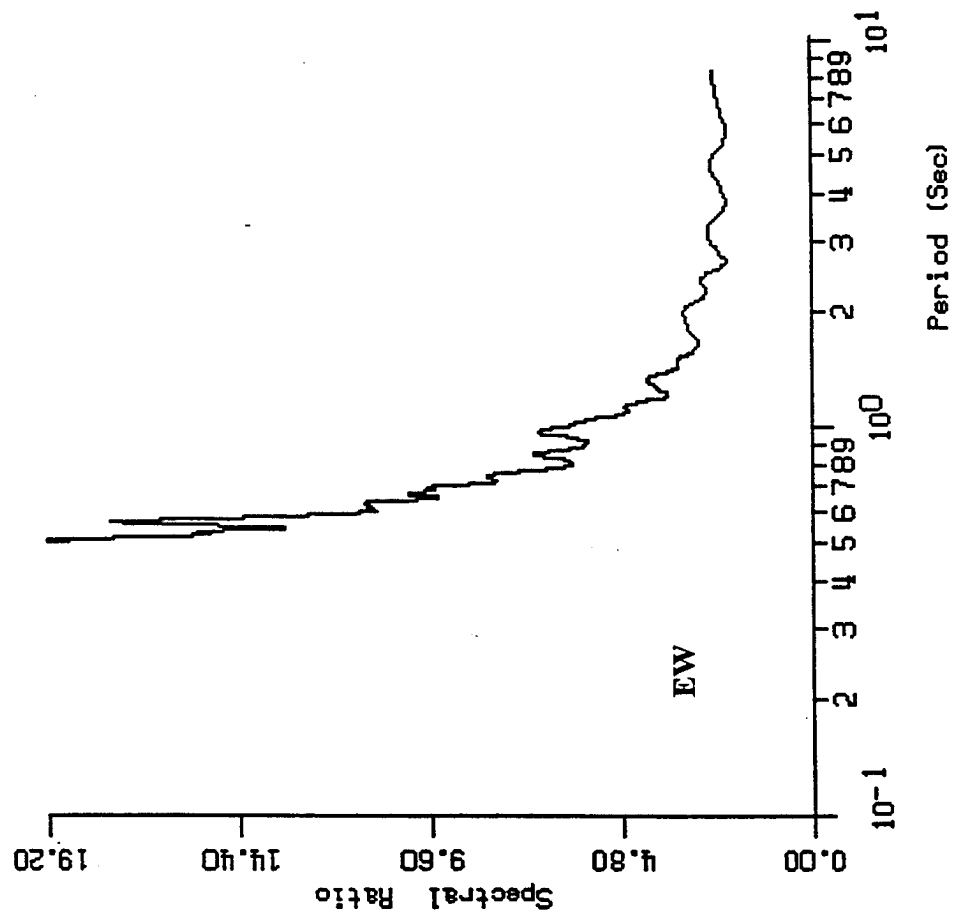


Figure 7.3. Gilroy #2/Gilroy #1 microsesm spectral ratios

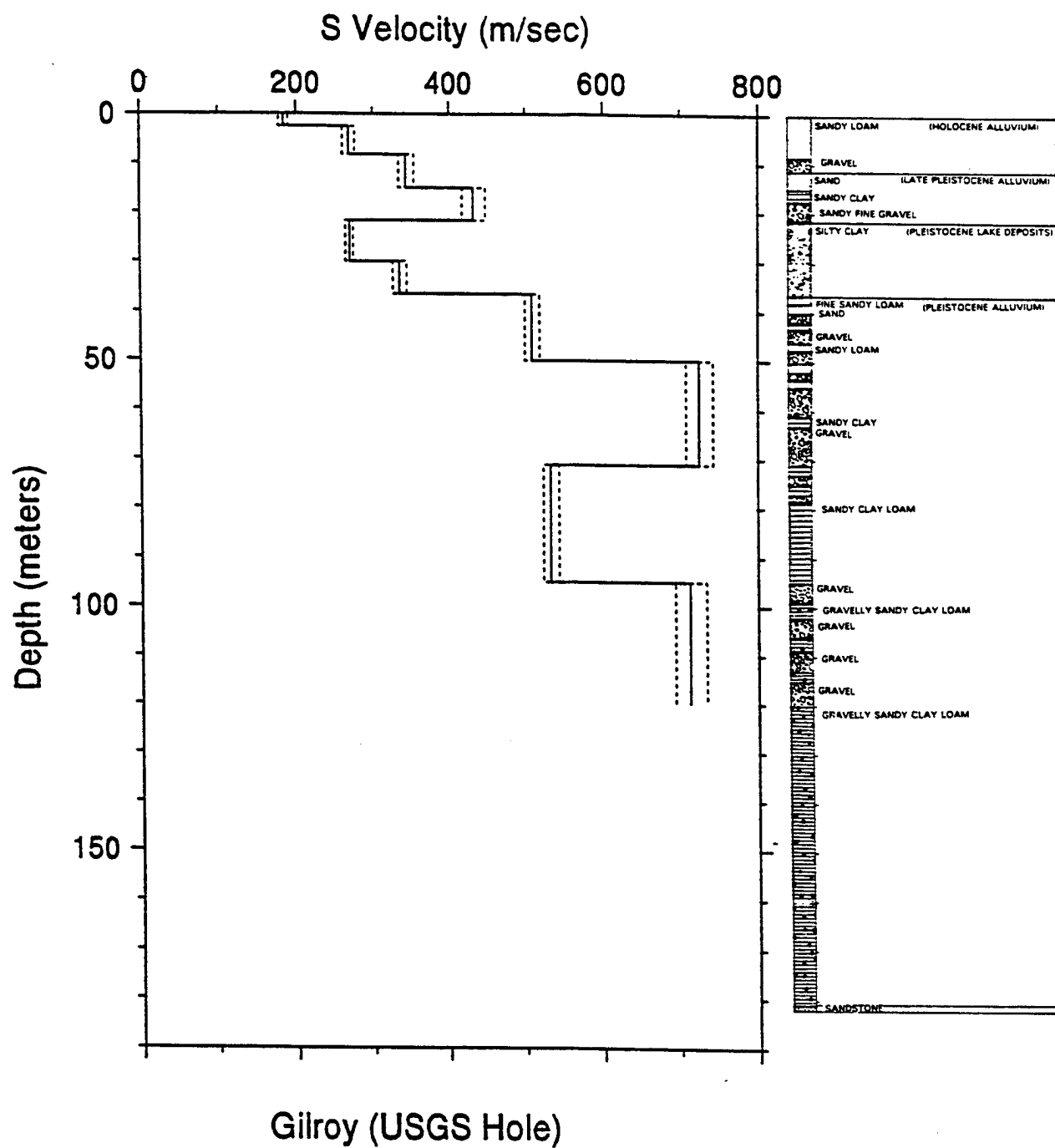


Figure 7.4. Gilroy #2 profile.

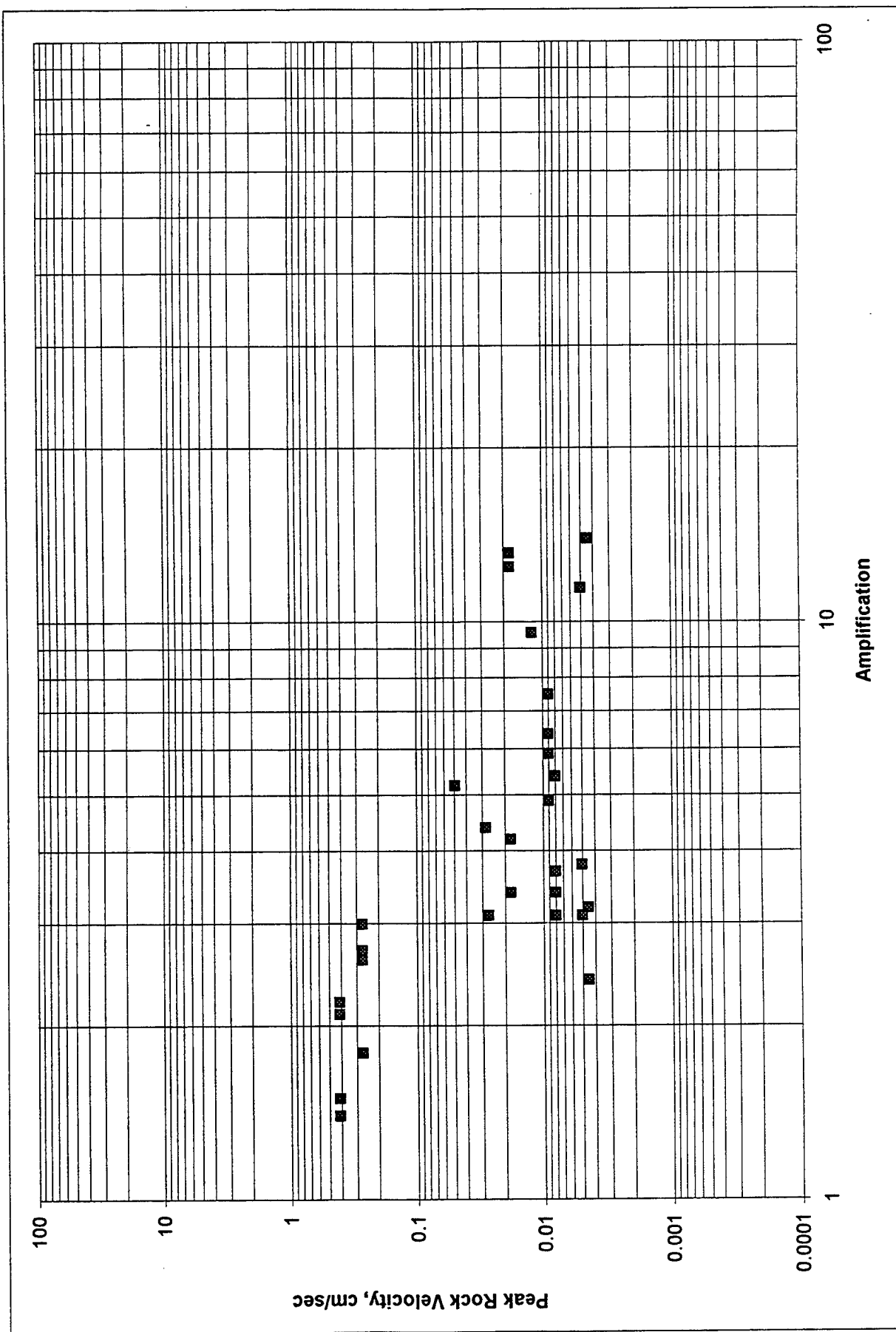


Figure 7.5. Amplification Coalinga pairs

## **Chapter 8 Summary**

### **Feasibility of Microseism Measurements**

The purpose of this study was to explore the feasibility of using microseism measurements as an extension of geophysical site properties to improve the understanding of local site response. A typical Navy application would involve soft marginal soils at the waterfront. Existing boring logs may not be available over wide areas and may lack data at depth. Often shear wave velocity is not available and must be estimated from standard penetration blowcount data. Obtaining such data can be costly and is limited to projects of such size to warrant such a detailed investigation. Strain effects on damping and shear modulus require laboratory testing and are usually not performed; several standard type curves for sand and clay are routinely used as substitutes. There is a strong need for an inexpensive field test to quantify site behavior. Microseisms seems to offer that potential.

The report has presented microseism measurements which show high levels of amplification at the low levels of excitation. Data was presented showing such a response is expected and that a relationship exists such that spectral ratio amplification is inversely related to the level of excitation. Traditional wave propagation analysis techniques for local site response were seen to be applicable to microseism measurements. Because spectral ratio obtained from microseism measurements are higher than those of strong motion shaking, normalized results can be used to provide information of the spatial variation relative to a site of known response. Microseism measurements at a soil site can be used to estimate fundamental period and damping of the site and save as a means for improving the reliability of material property data used in the wave propagation computation. A systems identification procedure was shown to lend insight to the process.

- It is concluded that microseism measurements can be used on a relative normalized basis to extend the information from a known local response to areas where additional data is lacking.
- A systems analysis procedure applied to the microseism data can be used to extend the knowledge of site material properties such as shear velocity and damping.
- Long term measurements describe overall site stability and are essential. Microseism measurements can be conducted during windows of stability

### **Development of Procedure**

A generalized procedure should consist of the following steps:

1. Careful review of site geology
2. Investigation of rock reference site and its variability
3. Selection of rock reference site
4. Selection of soil reference site having extensive borehole data
5. Long term measurements between rock and soil reference site to establish stability
6. Selection of an array plan to cover region of interest

7. Conducting measurements at rock reference site, soil reference site and at each array site.
8. Reduction of data using appropriate spectral processing

It should be noted that it is recommended that closely spaced measurements be made both at the rock and soil reference site throughout the array measurements to monitor overall stability. Generally a window of several hours is available for array measurements. Having a soil reference site, one is able to track that variation.

#### **Need for Additional Study**

There is a need for additional research to investigate long term stability of microseism measurements and their repeatability. The measurements made as part of this study need to be repeated to establish a baseline to quantify the extent of microseism variability. This work should be extended to alluvium and stiff sites in addition to the soft sites already studied. The data from the January 17 1994 Northridge earthquake should be investigated and microseism measurements made at strong motion sites to further develop the nonlinear site response data.

## **Acknowledgment**

Associate Professor M. Dravinski, University of Southern California, assisted in the data measurement and data reduction. He provided insight on procedures for microseism measurements. Dr. H. Gaberson and P. Palo, NFESC engineers, provided assistance in spectral analysis techniques. Mr. Richard Faris, Western Division Naval Facilities Engineering Command coordinated site access at Treasure Island and review comments of this report. A number of individuals provided guidance, comment and report review especially Professor Kyle Rollins, Brigham Young University, Professor George Housner, California Institute of Technology, Dr Philip Harbin, Lawrence Livermore National Laboratory, and Dr. Linda Seekins, US Geological Survey. Data was obtained from Dr. C. Mueller, USGS and Dr. R. Darragh, California Division of Mines and Geology. The assistance of all of the above is gratefully acknowledged

## **APPENDIX A:**

### **INSTRUMENTATION AND PROCEDURES FOR MICROSEISM MEASUREMENTS**

#### **Reference Site Determination**

As discussed above, the selection of the reference site is of critical importance since these measurements affect all results. The reference site must be a dense bedrock site which will minimize amplification and be of the same formation and representative of the bedrock beneath the site of interest. A careful study of site geology is critical. The reference instruments are set to record at appropriate intervals for stability of signal and record for a minimum of 5 minutes. A minimum sampling frequency of 20 Hz should be used. Amplifier gain should be set to produce a signal of appropriate level to prevent over-ranging but to insure a sufficient signal to minimize noise. Band pass filters are used to establish a signal window from 0.1 Hz to 2.5 Hz (0.4 sec to 10 sec).

#### **Site of Interest**

A soil reference site should be established where borehole data or strong ground motion can serve as a means for establishing site response. Microseism measurements should be made at the soil reference site at the same times and in the same manner as the rock reference site to track site stability. A long term program of several days or more should be undertaken to evaluate the extent of the fluctuations with time. Once a reference pair are established and a suitable window for measurement is set, a grid should be established across the site of interest covering as much of the Navy base as possible. The measurements should be made at each grid location to provide spatial variation. A precision global positioning system may be used to establish coordinates of the grid points. Signals are recorded in a similar manner to the reference site.

#### **Microseism Instruments**

Instruments used in the test consist of a seismometer, amplifier, and a recorder. The block diagram of the setup is shown by Figure A.1. A Kinemetrics Wideband Ranger I seismometer was used and found very satisfactory. This instrument is capable of horizontal or vertical measurement, one axis at a time. The seismometer produces output voltages that are proportional to both acceleration and velocity and utilizes an electronic feedback circuit for flat response over a bandwidth of 0.05 to 20 Hz (0.05 to 20 sec) or more. In addition to the seismometer, the instrument setup includes an amplifier/filter Kinemetrics model AM2 and a 12V DC power.

Data recording is accomplished by use of a 12-bit analog to digital board in a laptop computer having a docking station. The computer is powered by an inverter producing 120 volt alternating current from a 12 volt battery.

## **Setup and Recording**

Data is simultaneously made at the reference site and site of interest using two sets of instruments. The procedure used is as follows:

- The instruments are placed at the desired stations. It is essential the seismometer be level and oriented along the azimuth of interest. The level of the seismometer is established by adjusting a screw setting while reading the instrument voltage. The level position is defined by a zero voltage. Where possible orthogonal measurements should be made.
- The recording system is portable, battery operated and operates easily in a van. The data logging software is used to record the measurements. The software is capable of starting and stopping the recording at specified time intervals automatically. The power supply for the entire setup can be provided through standard car batteries. Data is recorded sequentially from site by site.

## **Data Processing**

Microtremor records are processed numerically in several steps.

- The time history of the signal is examined to determine if segments containing noise should be excluded.
- Any DC shift is removed from the data by subtracting the average amplitude.
- The data in the time domain are cosine tapered (10 percent from each end of the record). The time domain window is applied to the first and last 20.5 sec of the data.
- A series of Fourier spectra ( $N=2048$ ) are calculated with shifted starting points and averaged together. A minimum of 10 samples are made.
- The spectra are smoothed by using a 5-point Hanning window.
- Spectral ratios are then computed by multipoint averaging of soil site to reference site.



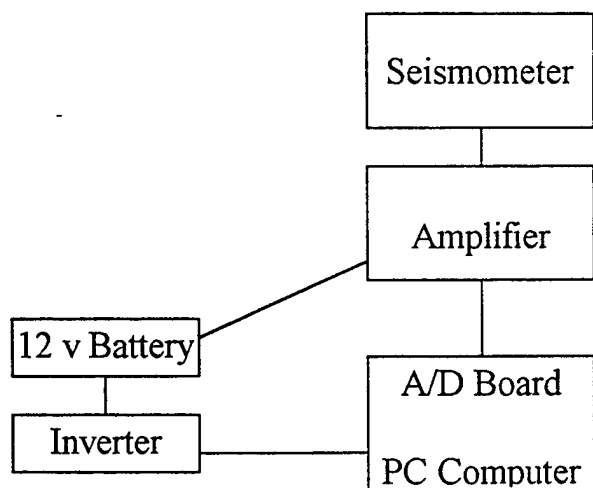


**Figure A.1 Instrumentation plan.**

## DISTRIBUTION LIST

1SG/CEEE / LT MARSH, LANGLEY AFB, VA  
AF / 438 ABG/DEE (WILSON), MCGUIRE AFB, NJ  
AF / CSR 4200 (K. DAVIDSON), PATRICK AFB, FL  
AFB / HQ TAC/DEMM (POLLARD), LANGLEY AFB, VA  
AFESC / TECH LIB, TYNDALL AFB, FL  
AMERICAN CONCRETE / LIB, DETROIT, MI  
APPLIED TECHNOLOGY AND MANAGEMENT / C. JONES, CHARLESTON, SC  
ARMSTRONG, W. / MYSTIC, CT  
ARMY / ENGR CEN, ATSE-DAC-LC, FORT LEONARD WOOD, MO; HQDA (DAEN-ZCM),  
WASHINGTON, DC  
ARMY / R&D LAB, STRNC-UE, NATICK, MA  
ARMY CECOM R&D TECH LIBRARY / ASNC-ELC-I-T, FORT MONMOUTH, NJ  
ARMY CERL / CECER-FME (HAYES), CHAMPAIGN, IL; LIB, CHAMPAIGN, IL  
ARMY CEWES / (TW RICHARDSON), VICKSBURG, MS  
ARMY CRREL / ISKANDAR, HANOVER, NH  
ARMY ENGRG DIST / CENPS-ED-SD, SEATTLE, WA; LIB, PORTLAND, OR; LIB,  
SEATTLE, WA; LIB, PHILADELPHIA, PA  
ARMY ENGRG DIV / CEEUD-ED-TA (MCVAY), FRANKFURT, GE, APO AE; CEHND-ED-CS,  
HUNTSVILLE, AL; ED-SY (LOYD), HUNTSVILLE, AL  
ARMY EWES / CEWES-CD-P, VICKSBURG, MS; CEWES-GP-N (CJ SMITH), VICKSBURG,  
MS; LIB, VICKSBURG, MS; WESCD-P (MELBY), VICKSBURG, MS; WESCW-D,  
VICKSBURG, MS  
ARMY MISSILE R&D CMD / CH, DOCS, SCI INFO CTR, REDSTONE ARSENAL, AL  
ARVID GRANT & ASSOC / OLYMPIA, WA  
ATLANTIC RICHFIELD CO / RE SMITH, DALLAS, TX  
BATTELLE / D. FRINK, COLUMBUS, OH  
BATTELLE NEW ENGLAND MARINE RSCH LAB / LIB, DUXBURY, MA  
BECHTEL CIVIL, INC / K. MARK, SAN FRANCISCO, CA  
BEN C GERWICK INC / FOTINOS, SAN FRANCISCO, CA  
BETHLEHEM STEEL CO / ENGRG DEPT, BETHLEHEM, PA  
BLAYLOCK ENGINEERING GROUP / T SPENCER, SAN DIEGO, CA  
BRITISH EMBASSY / SCI & TECH DEPT (WILKINS), WASHINGTON, DC  
BROWN, ROBERT / TUSCALOOSA, AL  
BULLOCK, TE / LA CANADA, CA  
BUREAU OF RECLAMATION / D-1512 (GS DEPUY), DENVER, CO  
CAL STATE UNIV / C.V. CHELAPATI, LONG BEACH, CA  
CALIFORNIA / DEPT BOATING AND WATERWAYS (ARMSTRONG), SACRAMENTO, CA  
CASE WESTERN RESERVE UNIV / CE DEPT (PERDIKARIS), CLEVELAND, OH  
CBC / CODE 155, PORT HUENEME, CA; CODE 82, PORT HUENEME, CA; PWO (CODE 400),  
GULFPORT, MS  
CECOS / CODE C35, PORT HUENEME, CA  
CHAO, JC / HOUSTON, TX  
CHEE, WINSTON / GRETN, LA  
CHESNAVFACENGCOM / CODE 112.1, WASHINGTON, DC; CODE 402 (FRANCIS), WASHINGTON,  
DC; CODE 407, WASHINGTON, DC; YACHNIS, WASHINGTON, DC  
CHEVRON OIL FLD RSCH CO / ALLENDER, LA HABRA, CA  
CHILDS ENGRG CORP / K.M. CHILDS, JR., MEDFIELD, MA  
CINCUSNAVEUR / LONDON, UK, FPO AE  
CITY OF MONTEREY / CONST MGR (REICHMUTH), MONTEREY, CA

CITY OF SACRAMENTO / GEN SVCS DEPT, SACRAMENTO, CA  
 CITY OF WINSTON-SALEM / RJ ROGERS, PWD, WINSTON SALEM, NC  
 CLARK, T. / SAN MATEO, CA  
 CLARKSON UNIV / CEE DEPT, POTSDAM, NY  
 CNO / DCNO, LOGS, OP-424C, WASHINGTON, DC  
 COGUARD / SUPERINTENDENT, NEW LONDON, CT  
 COLLEGE OF ENGINEERING / CE DEPT (AKINMUSURU), SOUTHFIELD, MI; CE DEPT (GRACE),  
 SOUTHFIELD, MI  
 COLLINS ENGRG, INC / M GARLICH, CHICAGO, IL  
 COLORADO STATE UNIV / CE DEPT (CRISWELL), FORT COLLINS, CO  
 COMDT COGUARD / G-ECV, WASHINGTON, DC  
 COMFAIR / MED, SCE, NAPLES, ITALY, FPO AE  
 COMFLEACT / PWO, FPO AP; SCE, FPO AP  
 COMNAVACT / PWO, LONDON, UK, FPO AE  
 COMNAVSURF / CODE N42A, NORFOLK, VA  
 COMSUBPAC / CODE 541, SCE, PEARL HARBOR, HI  
 CONRAD ASSOC / LUISONI, VAN NUYS, CA  
 CONSOER TOWNSEND & ASSOC / DEBIAK, CHICAGO, IL  
 CONSTRUCTION TECH LABS, INC / G. CORLEY, SKOKIE, IL  
 CONTINENTAL OIL CO / O. MAXSON, PONCA CITY, OK  
 CORNELL UNIV / CIVIL & ENVIRON ENGRG, ITHACA, NY; LIB, ITHACA, NY  
 DAMES & MOORE / LIB, LOS ANGELES, CA  
 DAVY DRAVO / WRIGHT, PITTSBURG, PA  
 DE PALMA, J R / LEBANON, NH  
 DELAWARE / EMERGENCY MGMT, DELAWARE CITY, DE  
 DEPT OF BOATING / ARMSTRONG, SACRAMENTO, CA  
 DEPT OF STATE / FOREIGN BLDGS OPS, BDE-ESB, ARLINGTON, VA  
 DFSC-F / ALEXANDRIA, VA  
 DOBROWOLSKI, JA / ALTADENA, CA  
 DODDS / PAC, FAC, FPO AP  
 DTRCEN / CODE 172, BETHESDA, MD  
 EASTPORT INTL, INC / VENTURA, CA  
 EDWARD K NODA & ASSOC / HONOLULU, HI  
 ENGINEERING DATA MANAGEMENT / RONALD W. ANTHONY, FORT COLLINS, CO  
 ESCO SCIENTIFIC PRODUCTS (ASIA) / PTE LTD, CHAI, SINGAPORE  
 EWI ENGINEERING ASSOCIATES / JACK COX, MIDDLETON, WI  
 FAA / ARD 200, WASHINGTON, DC  
 FACILITIES DEPT / FACILITIES OFFICER, FPO AP  
 FLORIDA ATLANTIC UNIV / OCEAN ENGRG DEPT (MARTIN), BOCA RATON, FL; OCEAN  
 ENGRG DEPT (MCALLISTER), BOCA RATON, FL; OCEAN ENGRG DEPT (SU), BOCA RATON, FL  
 FLORIDA INST OF TECH / CE DEPT (KALAJIAN), MELBOURNE, FL  
 FOWLER, J.W. / VIRGINIA BEACH, VA  
 GEI CONSULTANTS, INC. / T.C. DUNN, WINCHESTER, MA  
 GEIGER ENGINEERS / FUNSTON, BELLINGHAM, WA  
 GEOCON INC / CORLEY, SAN DIEGO, CA  
 GEORGE WASHINGTON UNIV / ENGRG & APP SCI SCHL (FOX), WASHINGTON, DC  
 GEORGIA INST OF TECH / CE SCHL (KAHN), ATLANTA, GA; CE SCHL (SWANGER), ATLANTA, GA;  
 CE SCHL (ZURUCK), ATLANTA, GA; DR. J. DAVID FROST, ATLANTA, GA  
 GEOTECHNICAL ENGRS, INC / MURDOCK, WINCHESTER, MA  
 GERWICK, BEN / SAN FRANCISCO, CA  
 GIORDANO, A.J. / SEWELL, NJ  
 GLIDDEN CO / RSCH LIB, STRONGSVILLE, OH  
 GRUMMAN AEROSPACE CORP / TECH INFO CENTER, BETHPAGE, NY  
 GSA / HALL, WASHINGTON, DC

HAN-PADRON ASSOCIATES / DENNIS PADRON, NEW YORK, NY  
 HANDLEY, DM / GULF BREEZE, FL  
 HARDY, S.P. / SAN RAMON, CA  
 HARTFORD STEAM BOILER INSP & INS CO / SPINELLI, HARTFORD, CT  
 HAYNES & ASSOC / H. HAYNES, PE, OAKLAND, CA  
 HAYNES, B / LYNDEN, WA  
 HEUZE, F / ALAMO, CA  
 HJ DEGENKOLB ASSOC / W. MURDOUGH, SAN FRANCISCO, CA  
 HOIDRA / NEW YORK, NY  
 HOPE ARCHTS & ENGRS / SAN DIEGO, CA  
 HQ AFLC / CAPT SCHMIDT, WRIGHT PATTERSON AFB, OH  
 HUGHES AIRCRAFT CO / TECH DOC CEN, EL SEGUNDO, CA  
 INFOTEAM INC / M. ALLEN, PLANTATION, FL  
 INST OF MARINE SCIENCES / LIB, PORT ARANSAS, TX; LUETTICH, MOREHEAD CITY, NC  
 INTL MARITIME, INC / D. WALSH, SAN PEDRO, CA  
 JOHN HOPKINS UNIV / CE DEPT, JONES, BALTIMORE, MD  
 JOHN J MC MULLEN ASSOC / LIB, NEW YORK, NY  
 KAISER PERMANENTE MEDICAL CARE PROGRAM / OAKLAND, CA  
 KLIEGER, PAUL / CE, NORTHBROOK, IL  
 KTA-TATOR, INC / PITTSBURG, PA  
 LAWRENCE LIVERMORE NATL LAB / FJ TOKARZ, LIVERMORE, CA; PLANT ENGRG LIB (L-654),  
 LIVERMORE, CA  
 LAYTON & SELL, INC, P.S. / REDMOND, WA  
 LBNSY / CODE 106.3, LONG BEACH, CA  
 LEHIGH UNIV / CE DEPT, HYDRAULICS LAB, BETHLEHAM, PA; MARINE GEOTECH LAB,  
 BETHLEHAM, PA  
 LEO A DALY CO / HONOLULU, HI  
 LIN OFFSHORE ENGRG / P. CHOW, SAN FRANCISCO, CA  
 LONG BEACH PORT / ENGRG DIR (ALLEN), LONG BEACH, CA; ENGRG DIR (LUZZI),  
 LONG BEACH, CA  
 MAINE MARITIME ACADEMY / LIB, CASTINE, ME  
 MARATHON OIL CO / GAMBLE, HOUSTON, TX  
 MARCORBASE / CODE 4.01, CAMP PENDLETON, CA; CODE 406, CAMP LEJEUNE, NC;  
 PAC, PWO, FPO AP  
 MARCORPS / FIRST FSSG, ENGR SUPP OFFR, CAMP PENDLETON, CA  
 MARINE CONCRETE STRUCTURES, INC / W.A. INGRAHAM, METAIRIE, LA  
 MARITECH ENGRG / DONOGHUE, AUSTIN, TX  
 MARITIME ADMIN / MAR-840, WASHINGTON, DC; MMA, LIB, KINGS POINT, NY  
 MCAS / CODE 1JD-31 (HUANG), SANTA ANA, CA; CODE 1JE.50 (ISAACS), SANTA ANA, CA; CODE  
 6EDD, FPO AP; CODE LE, CHERRY POINT, NC; PWO, KANEOHE BAY, HI  
 MCRD / PWO, SAN DIEGO, CA  
 MCRDAC / AROICC, QUANTICO, VA  
 MERMEL, TW / WASHINGTON, DC  
 MICHIGAN TECH UNIV / CO DEPT (HAAS), HOUGHTON, MI  
 MOBIL R&D CORP / OFFSHORE ENGRG LIB, DALLAS, TX  
 MT DAVISSON / CE, SAVOY, IL  
 NAF / ENGRG DIV, PWD, FPO AP  
 NALF / OIC, SAN DIEGO, CA  
 NAS / CHASE FLD, PWO, BEEVILLE, TX; CODE 421, SAN DIEGO, CA; CODE 8, PATUXENT RIVER,  
 MD; CODE 83, PATUXENT RIVER, MD; CODE 85GC, GLENVIEW, IL; DIR, ENGRG DIV, PWD,  
 KEFLAVIK, ICELAND, FPO AE; FAC MGMT OFFC, ALAMEDA, CA; MIRAMAR, PWO, SAN DIEGO,  
 CA; NI, SCE, SAN DIEGO, CA; PW ENGRG, PATUXENT RIVER, MD; PWO, KEY WEST, FL; PWO,  
 CECIL FIELD, FL; PWO, MOFFETT FIELD, CA; PWO, SIGONELLA, ITALY, FPO AE; SCE, BARBERS  
 POINT, HI; WHITING FLD, PWO, MILTON, FL

NAS ADAK / CODE 114, FPO AP  
NAS MEMPHIS / CODE N-81, MILLINGTON, TN  
NAS NPWC / CODE 102 (J. ARESTO), SAN DIEGO, CA  
NAS OCEANA / ADAMETZ, VIRGINIA BEACH, VA  
NATL ACADEMY OF ENGRY / ALEXANDRIA, VA  
NAVAIRDEVCCEN / CODE 832, WARMINSTER, PA  
NAVAVNDEPOT / CODE 640, PENSACOLA, FL  
NAVCAMS / PWO, NORFOLK, VA  
NAVCOASTSYSCEN / CO, PANAMA CITY, FL; CODE 715 (J. MITTLEMAN), PANAMA CITY, FL; PWO  
(CODE 740), PANAMA CITY, FL  
NAVCOMMSTA / PWO, FPO AP  
NAVCONSTRACEN / CODE D2A, PORT HUENEME, CA; CODE S24, GULFPORT, MS; TECH LIB, INDIAN  
HEAD, MD  
NAVFACENGCOM / CODE 04A3, ALEXANDRIA, VA; CODE 04A3A, ALEXANDRIA, VA; CODE 07,  
ALEXANDRIA, VA; CODE 07M (BENDER), ALEXANDRIA, VA; CODE 163, ALEXANDRIA, VA; CODE  
1632B, ALEXANDRIA, VA  
NAVHOSP / SCE, NEWPORT, RI  
NAVMAG / SCE, FPO AP  
NAVMEDCOM / NWREG, FAC ENGR, PWD, OAKLAND, CA  
NAVOCEANO / CODE 6200 (M PAIGE), NSTL, MS; LIB, NSTL, MS  
NAVPGSCOL / CODE 68WY (WYLAND), MONTEREY, CA; PWO, MONTEREY, CA  
NAVPHIBASE / PWO, NORFOLK, VA; SCE, SAN DIEGO, CA  
NAVSCSCOL / PWO, ATHENS, GA  
NAVSEASYSKOM / CODE 56W23, WASHINGTON, DC  
NAVSECGRUACT / CODE 31 PWO, FPO AA; PWO, FPO AP  
NAVSHIPREFAC / SCE, FPO AP  
NAVSHIPYD / CARR INLET ACOUSTIC RANGE, BREMERTON, WA; CODE 134, PEARL HARBOR, HI;  
CODE 244.13, LONG BEACH, CA; CODE 308.3, PEARL HARBOR, HI; CODE 380, PORTSMOUTH, VA;  
CODE 440, PORTSMOUTH, VA; CODE 441, PORTSMOUTH, NH; CODE 903, LONG BEACH, CA; MARE  
IS, CODE 106.3, VALLEJO, CA; MARE IS, CODE 401, VALLEJO, CA; MARE IS, CODE 421, VALLEJO,  
CA; MARE IS, CODE 440, VALLEJO, CA; MARE IS, CODE 457, VALLEJO, CA; MARE IS, PWO,  
VALLEJO, CA; TECH LIB, PORTSMOUTH, NH  
NAVSTA / CODE N4214, MAYPORT, FL; DIR, ENGR DIV, PWD, GUANTANAMO BAY, CUBA, FPO AE;  
ENGR DIV, PWD, FPO AA; ENGRG DIR, PWD, ROTA, SPAIN, FPO AE; PWO, MAYPORT, FL; PWO,  
GUANTANAMO BAY, CUBA, FPO AE; PWO, ROTA, SPAIN, FPO AE; SCE PEARL HARBOR, HI  
NAVSTA PANAMA CANAL / CODE 54, FPO AA  
NAVSUBBASE / AMES, NEW LONDON, CT  
NAVSUPACT / CODE 430, NEW ORLEANS, LA  
NAVSUPACT / PWO, NAPLES, ITALY, FPO AE  
NAVSUPSYSCOM / CODE 0622, WASHINGTON, DC  
NAVSWC / CODE U48, FORT LAUDERDALE, FL  
NAVSWC / CODE W41C1, DAHLGREN, VA  
NAVSWC / CODE W42 (GS HAGA), DAHLGREN, VA; DET, WHITE OAK LAB, PWO, SILVER SPRING,  
MD; PWO, DAHLGREN, VA  
NAVWPNCEN / PWO (CODE 266), CHINA LAKE, CA  
NAVWPNSTA / CODE 092B (HUNT), YORKTOWN, VA; CODE 093, YORKTOWN, VA; CODE 104,  
CHARLESTON, SC; PWO, YORKTOWN, VA  
NAVWPNSTA EARLE / CODE 092, COLTS NECK, NJ; PWO (CODE 09B), COLTS NECK, NJ  
NAWC / CODE 1018, POINT MUGU, CA; CODE 5041, POINT MUGU, CA; CODE P4234 (G. NUSSEAR),  
POINT MUGU, CA  
NBS / BLDG MAT DIV, MATHEY, GAITHERSBURG, MD  
NCBC / PWO, DAVISVILLE, RI  
NCCOSC / CODE 9642, SAN DIEGO, CA  
NETPMSA / TECH LIB, PENSACOLA, FL

NEW MEXICO SOLAR ENERGY INST / LAS CRUCES, NM  
 NEW ZEALAND CONCRETE RSCH ASSN / LIB, PORIRUA, NEW ZEALAND  
 NIEDORODA, AW / GAINESVILLE, FL  
 NOAA / JOSEPH VADUS, ROCKVILLE, MD  
 NOARL / CODE 440, NSTL, MS  
 NORDA / CODE 440, NSTL, MS  
 NORTHDIV / CODE 164, LESTER, PA; CO, LESTER, PA; CODE 408AF, LESTER, PA  
 NORTHWEST ENGRG CO / GRIMM, BELLEVUE, WA  
 NRL / CODE 4670, WASHINGTON, DC; CODE 6127, WASHINGTON, DC  
 NSC / SCE, NORFOLK, VA; SCE, CHARLESTON, SC; SCE, PEARL HARBOR, HI  
 NSWG / CODE 09RA, INDIAN HEAD, MD  
 NSY / CODE 214.3 (WEBER), PORTSMOUTH, VA  
 NUHN & ASSOC / A.C. NUHN, WAYZATA, NM  
 NUSC DET / CODE 2143 (VARLEY), NEW LONDON, CT; CODE 44 (MUNN), NEW LONDON, CT; CODE  
 TA131, NEW LONDON, CT; LIB, NEWPORT, RI; PWO, NEW LONDON, CT  
 NY CITY COMMUNITY COLLEGE / LIB, BROOKLYN, NY  
 OCNR / CODE 1121 (EA SILVA), ARLINGTON, VA  
 OMEGA MARINE, INC. / SCHULZE, LIBRARIAN, HOUSTON, TX  
 OREGON STATE UNIV / CE DEPT (HICKS), CORVALLIS, OR  
 OREGON STATE UNIV / CE DEPT (YIM), CORVALLIS, OR; OCEANOGRAPHY SCOL, CORVALLIS, OR  
 PACIFIC MARINE TECH / M. WAGNER, DUVALL, WA  
 PACNAVFACENGCOM / CODE 102, PEARL HARBOR, HI; CODE 2011, PEARL HARBOR, HI  
 PAULI, DC / SILVER SPRING, MD  
 PAYE-KOSANOWSKY, S / POND EDDY, NY  
 PENNSYLVANIA STATE UNIV / GOTOLSKI, UNIVERSITY PARK, PA; RSCH LAB, STATE COLLEGE, PA  
 PERKOWSKI, MICHAEL T. / TIPPECANOE, OH  
 PHILADELPHIA ELEC CO / E. D. FREAS, WESTCHESTER, PA  
 PIKE, L / SAN ANTONIO, TX  
 PILE BUCK, INC / SMOOT, JUPITER, FL  
 PMB ENGRG / LUNDBERG, SAN FRANCISCO, CA  
 PORTLAND CEMENT ASSOC / AE FIORATO, SKOKIE, IL  
 PORTLAND STATE UNIV / ENGRG DEPT (MIGLIORI), PORTLAND, OR  
 PUGET SOUND / REUNINE, BREMERTON, WA  
 PURDUE UNIV / CE SCOL (ALTSCHAEFFL), WEST LAFAYETTE, IN; CE SCOL (CHEN), WEST  
 LAFAYETTE, IN; CE SCOL (LEONARDS), WEST LAFAYETTE, IN  
 PWC / CO, OAKLAND, CA; CODE 101, GREAT LAKES, IL; CODE 102, OAKLAND, CA; CODE 123C, SAN  
 DIEGO, CA; CODE 400, OAKLAND, CA; CODE 400A.3, FPO AP; CODE 420, OAKLAND, CA; CODE 421  
 (KAYA), PEARL HARBOR, HI; CODE 421 (QUIN), SAN DIEGO, CA; CODE 421 (REYNOLDS), SAN  
 DIEGO, CA; CODE 421, NORFOLK, VA; CODE 422, SAN DIEGO, CA; CODE 423, SAN DIEGO, CA;  
 CODE 430 (KYT), PEARL HARBOR, HI; CODE 500, NORFOLK, VA; CODE 505A, OAKLAND, CA; CODE  
 590, SAN DIEGO, CA; SAN DIEGO (WAID), SAN DIEGO, CA  
 Q ASSOCIATES / QUIRK, J PANAMA CITY, FL  
 SAN DIEGO PORT / PORT FAC, PROJ ENGR, SAN DIEGO, CA  
 SAN DIEGO STATE UNIV / CE DEPT (KRISHNAMOORTHY), SAN DIEGO, CA  
 SANDIA LABS / LIB, LIVERMORE, CA  
 SARGENT & HERKES, INC / JP PIERCE, JR, NEW ORLEANS, LA  
 SEATECH CORP / PERONI, MIAMI, FL  
 SEATTLE PORT / DAVE VAN VLEET, SEATTLE, WA; DAVID TORSETH, SEATTLE, WA  
 SEATTLE UNIV / CE DEPT (SCHWAEGLER), SEATTLE, WA  
 SHELL OIL CO / E. DOYLE, HOUSTON, TX  
 SIMPSON, GUMPERTZ & HEGER, INC / HILL, ARLINGTON, MA  
 SMELSER, D / SEVIERVILLE, TN  
 SOUTHNAVFACENGCOM / CODE 04A, CHARLESTON, SC; CODE 1622, CHARLESTON, SC

SOUTHWEST RSCH INST / ENERGETIC SYS DEPT (ESPARZA), SAN ANTONIO, TX; KING, SAN ANTONIO, TX; M. POLCYN, SAN ANTONIO, TX; MARCHAND, SAN ANTONIO, TX; THACKER, SAN ANTONIO, TX  
 SOWESTNAVFACENGCOM / CODE 101.1, SAN DIEGO, CA; LANGSTRAAT, SAN DIEGO, CA  
 SPCC / PWO, MECHANICSBURG, PA  
 STATE UNIV OF NEW YORK / CE DEPT, BUFFALO, NY; CE DEPT, REINHORN, BUFFALO, NY  
 SUBASE / PWO (CODE 8323), BREMERTON, WA; SCE, PEARL HARBOR, HI  
 SUPSHIP / CODE 190, NEWPORT, VA; TECH LIB, NEWPORT, VA  
 TECHNOLOGY UTILIZATION / K WILLINGER, WASHINGTON, DC  
 TEXAS A&M UNIV / CE DEPT (HERBICH), COLLEGE STATION, TX; CE DEPT (MACHEMEHL), COLLEGE STATION, TX; CE DEPT (NIEDZWECKI), COLLEGE STATION, TX; OCEAN ENGR PROJ, COLLEGE STATION, TX  
 THE WORLD BANK / ARMSTRONG, WASHINGTON, DC  
 TRW INC / ENGR LIB, CLEVELAND, OH  
 TUDOR ENGRG CO / ELLEGOOD, PHOENIX, AZ  
 UNIV OF ALASKA / BIOMED & MARINE SCI LIB, FAIRBANKS, AK  
 UNIV OF CALIFORNIA / CE DEPT (FENVES), BERKELEY, CA; CE DEPT (FOURNEY), LOS ANGELES, CA; CE DEPT (TAYLOR), DAVIS, CA; CE DEPT (WILLIAMSON), BERKELEY, CA; NAVAL ARCHT DEPT, BERKELEY, CA  
 UNIV OF HAWAII / CE DEPT (CHIU), HONOLULU, HI; MANOA, LIB, HONOLULU, HI; OCEAN ENGRG DEPT (ERTEKIN), HONOLULU, HI; RIGGS, HONOLULU, HI  
 UNIV OF ILLINOIS / METZ REF RM, URBANA, IL  
 UNIV OF MARYLAND / CE DEPT, COLLEGE PARK, MD  
 UNIV OF MICHIGAN / CE DEPT (RICHART), ANN ARBOR, MI  
 UNIV OF N CAROLINA / CE DEPT (AHMAD), RALEIGH, NC  
 UNIV OF NEW MEXICO / NMERI (BEAN), ALBUQUERQUE, NM; NMERI, HL SCHREYER, ALBUQUERQUE, NM  
 UNIV OF PENNSYLVANIA / DEPT OF ARCH, PHILADELPHIA, PA  
 UNIV OF RHODE ISLAND / CE DEPT (KARAMANLIDIS), KINGSTON, RI; CE DEPT (KOVACS), KINGSTON, RI; CE DEPT (TSIATAS), KINGSTON, RI; DR. VEYERA, KINGSTON, RI  
 UNIV OF TEXAS / CONSTRUCTION INDUSTRY INST, AUSTIN, TX; ECJ 4.8 (BREEN), AUSTIN, TX; ECJ 5.402 (TUCKER), AUSTIN, TX  
 UNIV OF WASHINGTON / APP PHYS LAB (SANDWITH), SEATTLE, WA  
 UNIV OF WASHINGTON / CE DEPT (HARTZ), SEATTLE, WA; CE DEPT (MATTOCK), SEATTLE, WA  
 UNIV OF WISCONSIN / GREAT LAKES STUDIES CEN, MILWAUKEE, WI  
 UNIV OF WYOMING / SCHMIDT, LARAMIE, WY  
 US GEOLOGICAL SURVEY / MARINE GEOLOGICAL OFFC, RESTON, VA  
 US NUCLEAR REGULATORY COMMISSION / KIM, WASHINGTON, DC  
 USACOE / CESPD-CO-EQ, SAN FRANCISCO, CA  
 USAE / CEWES-IM-MI-R, VICKSBURG, MS  
 USCG / G-ECV-4B, WASHINGTON, DC  
 USCINCPAC / CODE J44, CAMP HM SMITH, HI  
 USDA / FOR SVC, REG BRIDGE ENGR, ALOHA, OR; FOREST PROD LAB (DEGROOT), MADISON, WI; FOREST PROD LAB (JOHNSON), MADISON, WI  
 USN / CAPT COLIN M JONES, HONOLULU, HI  
 USNA / CH, MECH ENGRG DEPT (C WU), ANNAPOLIS, MD; OCEAN ENGRG DEPT, ANNAPOLIS, MD; PWO, ANNAPOLIS, MD  
 USPS / BILL POWELL, WASHINGTON, DC  
 VALLEY FORGE CORPORATE CENTER / FRANKLIN RESEARCH CENTER, NORRISTOWN, PA  
 VAN ALLEN, B / KINGSTON, NY  
 VENTURA COUNTY / DEPUTY PW DIR, VENTURA, CA  
 VIATEUR DE CHAMPLAIN / INST OF MARITIME ENGRG, MATANE, QUEBEC  
 VSE / OCEAN ENGRG GROUP (MURTON), ALEXANDRIA, VA  
 VSE CORP / LOWER, ALEXANDRIA, VA

VULCAN IRON WORKS, INC / DC WARRINGTON, CLEVELAND, TN  
WESCR-P / HALES, VICKSBURG, MS  
WESTINGHOUSE ELECTRIC CORP / LIB, PITTSBURG, PA  
WESTNAVFACENGCOM / CODE 162, SAN BRUNO, CA; CODE 1833, SAN BRUNO, CA; CODE 401, SAN  
BRUNO, CA; CODE 407, SAN BRUNO, CA; PAC NW BR OFFC, CODE C/42, SILVERDALE, WA;  
VALDEMORO, SAN BRUNO, CA  
WISS, JANNEY, ELSTNER, & ASSOC / DW PFEIFER, NORTHBROOK, IL  
WISWELL, INC. / SOUTHPORT, CT  
WOODWARD-CLYDE CONSULTANTS / R. CROSS, OAKLAND, CA; WEST REG, LIB, OAKLAND, CA